



HAL
open science

Mécanisme du magmatisme mésozoïque supérieur (jurassique-crétacé inférieur) en Chine du Sud et les implications en géodynamique

Hongsheng Liu

► **To cite this version:**

Hongsheng Liu. Mécanisme du magmatisme mésozoïque supérieur (jurassique-crétacé inférieur) en Chine du Sud et les implications en géodynamique. Sciences de la Terre. Université d'Orléans, 2017. Français. NNT : 2017ORLE2071 . tel-02096395

HAL Id: tel-02096395

<https://theses.hal.science/tel-02096395v1>

Submitted on 11 Apr 2019

HAL is a multi-disciplinary open access archive for the deposit and dissemination of scientific research documents, whether they are published or not. The documents may come from teaching and research institutions in France or abroad, or from public or private research centers.

L'archive ouverte pluridisciplinaire **HAL**, est destinée au dépôt et à la diffusion de documents scientifiques de niveau recherche, publiés ou non, émanant des établissements d'enseignement et de recherche français ou étrangers, des laboratoires publics ou privés.

ÉCOLE DOCTORALE
ENERGIE, MATERIAUX, SCIENCES DE LA TERRE ET DE L'UNIVERS

Institut des Sciences de la Terre d'Orléans

THÈSE présentée par :

LIU Hongsheng

Soutenue le **24 Octobre, 2017**

Pour obtenir le grade de: **Docteur de l'université d'Orléans**

Discipline/ Spécialité: Sciences de la Terre et de l'Univers

**Mécanisme du magmatisme mésozoïque supérieur
(jurassique-crétacé inférieur) en Chine du Sud et les implications en
géodynamique**

THÈSE dirigée par :

Chen Yan

Professeur, Université d'Orléans

Faure Michel

Professeur, Université d'Orléans

Wang Bo

Professeur, Université de Nanjing

RAPPORTEURS :

De Saint Blanquat Michel

Directeur de Recherche, CNRS

Jin Zhenmin

Professeur, China University of Geoscience, China

JURY (*y reporter tous les membres de jury présents à la soutenance*) :

Jin Zhenmin

Professeur, China University of Geoscience

De Saint Blanquat Michel

Directeur de Recherche, CNRS

Xing Tianfu

Professeur, Institute of Geology and Mineral Resources

Faure Michel

Professeur, Université d'Orléans

Wang Bo

Professeur, Université de Nanjing

Chen Yan

Professeur, Université d'Orléans

LIU Hongsheng

Mécanisme du magmatisme mésozoïque supérieur (jurassique-crétacé inférieur) en Chine du Sud et les implications en géodynamique

La géologie du bloc de Chine du Sud se caractérise par un important magmatisme mésozoïque dont la genèse des magmas, la mise en place des plutons et les contextes tectoniques et géodynamiques restent très disputés. Dans ce travail, 41 plutons d'âge Jurassique ont été visités. Ceux de Qitianling et Shibeï ont été choisis pour des études détaillées.

Les textures des granites sont magmatiques et dépourvues de déformation post-solidus. La modélisation gravimétrique révèle que le pluton de Qitianling est un lopolithe mis en place dans l'interface que représente la discordance dévonienne. Le pluton de Shibeï est formé par accréation de dykes le long d'une faille verticale. Les mesures des fabriques dans différents plutons montrent que la tectonique régionale ne contrôle pas leur mise en place. La mise en place du magma est contrôlée par sa viscosité et des structures héritées.

L'étude paléomagnétique de deux plutons du même âge indique des mouvements relatifs ce qui implique que ce bloc ne peut pas être considéré comme rigide. Nos résultats montrent que le Jurassique était une époque de calme tectonique dans le secteur d'étude. Ces granites sont issus de la fusion de la croûte inférieure. Au Trias, les événements tectoniques qui ont épaissi la croûte continentale sont responsables du magmatisme jurassique. L'important contraste de rigidité du bloc de Chine du Sud est responsable de la localisation de la déformation dans sa partie SE. L'épaississement crustal contribue aussi à élever le flux de chaleur mais les magmas issus du manteau sont rares. Ainsi, les modèles de subduction océanique ou de rifting continental ne s'accordent pas avec nos résultats.

Mots clés: SCB; magmatisme Jurassique; mécanisme de mise en place; ASM; modélisation gravimétrique; paléomagnétisme

Mechanism of the late Mesozoic magmatism (Jurassic-early Cretaceous) in South China and its implications for the geodynamic

The Mesozoic geology of the South China Block (SCB) is marked by widespread magmatism. Disputes exist on magma genesis, tectonic and geodynamic contexts. The tectonic setting of the Jurassic magmatism is poorly investigated. 41 Jurassic plutons were investigated and the Qitianling and Shibeï plutons were selected for detailed studies.

Our study shows that the emplacement of J plutons is not related to regional tectonics. The granite textures are magmatic, devoid of post-solidus deformation. The magma emplacement is controlled by its buoyancy and the inherited structures or stratigraphic interfaces of country rocks. Gravity modeling reveals that the Qitianling pluton is a lopolith intruded in the stratigraphic uniformity and the Shibeï pluton formed by dike-accretion intruded in a vertical tectonic structure. The fabric measurements on different Jurassic plutons show that the regional tectonics do not control their emplacement. Paleomagnetic results from the two contemporaneous plutons show a relative movement, implying that this block cannot be considered as a rigid one.

Our results show that the Jurassic was a tectonically quiet epoch in our study area. These granites are mainly derived from partial melting of lower crust. The Triassic subduction-collision events that have thickened the continental crust are responsible for the Jurassic magmatism. Due to the high rigidity contrast of the SCB, the deformation was localized on its SE part. The crustal thickening may increase the thermal contribution of the mantle, but few mantle materials are observed. So, the slab subduction or intracontinental rifting models are not supported by our studies.

Mots clés: SCB, Jurassic magmatism, emplacement mechanism, AMS, gravity modeling, paleomagnetism



*Institut des Sciences de la Terre d'Orléans, 45067
Orléans, France*

Université de Nanjing, 210046 Nanjing, Chine



Remerciments

I would like to express sincere gratitude to my supervisors and everyone else who has supported me in my PhD studies and in my life. It has been at times a hard but always a rewarding period.

Seven years ago, I have enrolled as a Master and Ph.D. degree candidate in geology at the School of Earth Sciences and Engineering, Nanjing University, under the supervision of Professor Wang Bo. I became his first Ph.D. student, which is a great honour. For one year and a half, Prof. Wang shared his office with me, an opportunity for me to benefit from Prof. Wang's subject knowledge and to learn how to do research and how to efficiently present it. These are things I have learned for life. All his time, ideas, and support through connections and funding are greatly appreciated. I am especially grateful for his support to pursue my studies in France.

Sincere thanks equally go to my supervisor, Prof. Yan Chen from the Unisversité d'Orléans. I appreciate that he gave me the opportunity to pursue my studies under his guidance, supported through a scholarship of l'Ecole Doctorale Energie Matériaux Sciences de la Terre of the Université d'Orleans. His enthusiasm for geosciences has been contagious; I have met few people who approach his endless passions for geology and our study. Through continued and intense discussions, we have arrived at an intriguing interpretation of the phenomena that we have observed. Prof. Chen's approach and passion have for science have "infected" me and benefited me a lot. I have been touched by his sharing of life philosophy, and experiences, it has helped me through tough periods and to finish my thesis.

I would like to express my sincere gratitude to Prof. Liangshu Shu, for his impressive teaching, field instruction and continuous encouragement and support of my Ph.D study and research. His immense knowledge of the geology of our study area inspired me and lead me to overcome this hard journey.

I would also like to sincerely thank all of my co-supervisors: Prof. Michel Faure, Bruno Scaillet, and Nicole Le Breton from the Université d'Orléans. I would like to thank them for their sharing of ideas in many discussions and for their encouragement throughout all stages of my thesis. I also thank Prof. Guillaume Martelet from the Bureau de Recherches Géologiques et Minières for his kind teaching in gravity modelling, which has become a pillar of understanding in our study. I further thank him for their suggestions and corrections in manuscript writing.

I am also grateful to other members of our team. Many heartfelt thanks go to Ph.D. candidate Fangfang Huang, for her help in planning and organizing fieldwork, in sharing samples, and for discussions and new insights from her experimental and petrological work. I am particularly indebted to Saskia Erdmann for her help in the field and for constructive suggestions and corrections of our manuscripts. Encouragement from Fangfang and Saskia also helped. Funding

support and instructions in the field from Profs. Rucheng Wang and Jinchu Zhu are also truly appreciated.

I thank my colleagues Xin Zhu and Chaolei Yan for their help in drilling and sample collection in the field in 2014 and 2015, respectively. The AMS and paleomagnetism sample measurements by three master students from Michaël Pons, Laurine Dissard and Alexane Legeay (the Université d'Orléans) are much appreciated. The support from Ms. France Lagroix of IPGP in the hysteresis loop measurements are also greatly appreciated. The help of Ida Di Carlo in training of microprobe measurements also appreciated.

Many other teachers have also helped me in my studies and in my life. I thank Dr. Stéphane Scaillet, Dr. Hugues Raimbourg and Dr. Augier Romain for their teaching in the field and for their help during my studies at ISTO. Profs. Wenbin Zhu, Dong Jia, Liangshu Wang, Yongxiang Li, Qin Wang and Guoai Xie at Nanjing University have also helped me a lot with their teachings and suggestions for my study.

I am grateful for the time spent with all my colleagues and friends both in Nanjing and in Orléans, the students of our group, Kongsheng Li, Yazhong Zhai, Linglin Zhong, Xin Zhu, Yuchuang Cao, Guzalnur Wali, Ting Fang, Zhiyuan He, Yong Zhou and Xiaoyan Zhu; my roommates and colleagues Jianqiang Liu, Xiang Cui, Xianqing Jing, Xiaoyong Chen, Kai Wang, Wei Zhou, Weiming Zhou, Jinlong Yao, Chuang Sun, Wei wei, Huang Xudong, Xiang Lu, Xia Wenjing, Xue Zhenhua, Chen Jinyu, Yan Chaolei, Rabillard, Aurélien and Mohammed AL-JUHAISHI. And I am especially grateful for the bureaucratic but also moral support from Mrs. Wang Shujun, Tang Xiaoqian, Zhang Xiaoqing in Nanjing University and Marie-Noëlle Pailhès, our secretary at ISTO.

Lats but not least, I would like to thank the thesis evaluation members for their time and interest to read my thesis, and thanks for their helpful suggestions on the content and format of my thesis.

In addition, I acknowledge financial support from the Centre National de la Recherche Scientifique, the National Basic Research Program of China (973 Program, 2012CB416701), and the Open Fund of State Key Laboratory for Mineral Deposits Research of Nanjing University (ZZKT-201603).

Finally, I would like to thank my family for all their love and encouragement. My parents who raised me and supported me to study abroad. My sister for all her spiritually support. Thank you!

2017.10

LIU Hongsheng

Table of Contents

| | |
|---|------------|
| Abstract in English..... | XII |
| Remerciments | III |
| Chapter 1. General introduction | 1 |
| 1.1 State-of-the-art of magmatism: relationship with the tectonic-geodynamic settings and overview of magma emplacement mechanisms..... | 1 |
| 1.1.1 Tectonic and geodynamic settings of magmatism | 1 |
| 1.1.1.1 <i>Magmatism developed at an active plate margin setting</i> | 2 |
| 1.1.1.2 <i>Magmatism under an intraplate setting</i> | 2 |
| 1.1.2 Overview of the magma emplacement mechanisms | 4 |
| 1.1.2.1 <i>Introduction of the emplacement mechanism</i> | 4 |
| 1.1.2.2 <i>Diapirism and ballooning</i> | 5 |
| 1.1.2.3 <i>Dykes and sills</i> | 6 |
| 1.1.2.4 <i>Laccolith and lopolith</i> | 7 |
| 1.1.2.5 <i>Stoping</i> | 7 |
| 1.1.2.6 <i>Syntectonic magma emplacement</i> | 8 |
| 1.2 Overview of the study..... | 11 |
| 1.2.1 Research background..... | 11 |
| 1.2.1.1 <i>Mesozoic magmatism of the South China Block</i> | 11 |
| 1.2.1.2 <i>Previous opinions on the tectonic and geodynamic settings of the Mesozoic magmatism in South China</i> | 13 |
| 1.2.2 Research purpose and contents | 16 |
| 1.2.3 Research design and methodology | 16 |
| 1.2.4 Workload of the study..... | 18 |
| 1.2.5 Major findings and innovations..... | 18 |
| Chapter 2. Regional geological setting | 22 |
| 2.1. The components and basements of the South China Block..... | 22 |
| 2.2. Tectonic framework and evolution of the South China Block..... | 23 |
| 2.2.1 Pre-Triassic tectonic evolution of the South China Block..... | 24 |
| 2.2.2 The Qinling-Dabie orogen..... | 25 |
| 2.2.3 The Longmenshan thrust belt | 25 |

| | |
|--|-----------|
| 2.2.4 The Indochina - South China Block collision | 25 |
| 2.2.5 Triassic intracontinental deformation | 25 |
| 2.2.6 Mesozoic magmatism in the South China Block..... | 26 |
| | |
| Chapter 3. Incremental emplacement of the late Jurassic mid-crustal, lopolith-like Qitianling pluton, South China, revealed by AMS and Bouguer gravity data | 28 |
| 3.1 Introduction..... | 28 |
| 3.2 Geological setting | 30 |
| 2.1 The South China Block | 30 |
| 2.2 The Qitianling pluton..... | 31 |
| 3.3 Field observations and sampling..... | 32 |
| 3.4 Methodology and results..... | 34 |
| 4. 1. Microscopic observations..... | 34 |
| 4. 2. Magnetic mineralogical analysis | 36 |
| 4. 3. AMS parameters | 38 |
| 4. 4. AMS results | 39 |
| 4.5. Gravity modelling..... | 40 |
| 3.5 Discussion..... | 43 |
| 5.1. Origin of the magnetic fabrics..... | 43 |
| 5.2. Emplacement into ductile crust..... | 43 |
| 5.3. Sill- to lopolith-like emplacement..... | 44 |
| 5.4. Incremental magma emplacement..... | 45 |
| 5.4.1. <i>Model 1-Large-sheet emplacement, in situ fractionation</i> | 46 |
| 5.4.2. <i>Model 2- Small-sheet emplacement, deep-level fractionation</i> | 48 |
| 5.5. Magma feeder zone(s) | 49 |
| 3.6. Conclusions | 49 |
| | |
| Chapter 4. The emplacement mechanism of the late Jurassic Shibeï pluton in the Wuyishan area, South China Block..... | 51 |
| 4.1 Introduction of the reserch | 51 |
| 4.2 Geological setting of the Shibeï pluton and its surrounding area | 52 |
| 4.3 Field observations and sampling | 54 |
| 4.4 Petrofabrics of the Shibeï pluton | 55 |

| | |
|--|-----------|
| 4.4.1 Petrographic features of the granite | 55 |
| 4.4.2 AMS of the Shibeï pluton | 55 |
| 4.4.2.1 Magnetic mineral analysis..... | 55 |
| 4.4.2.2 Magnetic fabric parameters..... | 57 |
| 4.4.2.3 AMS results of the Shibeï pluton..... | 58 |
| 4.5 Gravity modelling | 60 |
| 4.6 The emplacement mechanism of the Shibeï pluton | 62 |
| 4.6.1 The acquisition and the implication of the magnetic fabrics of the granite | 62 |
| 4.6.1.1 The acquisition of the magnetic fabric..... | 62 |
| 4.6.1.2 The implication of the magnetic fabrics..... | 63 |
| 4.6.2 The construction of the Shibeï pluton | 64 |
| 4.6.2.1 The geometry of the Shibeï pluton | 64 |
| 4.6.2.2 The magma supply channel and space for emplacement..... | 64 |
| 4.6.2.3 The mechanism of the magma emplacement | 66 |
| 4.7 Conclusions | 66 |
| | |
| Chapter 5. A rigidity test of the southeastern part of the South China Block (the ancient Cathaysia Block): insights from paleomagnetic studies on Jurassic plutons | 68 |
| 5.1 Introduction of the research content..... | 68 |
| 5.2 Regional geological context..... | 69 |
| 5.2.1 The Qitianling pluton | 70 |
| 5.2.2 The Shibeï pluton..... | 71 |
| 5.3 Sampling and laboratory analyses..... | 72 |
| 5.3.1 Sampling and specimen preparation | 72 |
| 5.3.2 Magnetic mineralogical investigation | 73 |
| 5.3.3 Demagnetization of specimens and calculation of paleomagnetic direction | 74 |
| 5.4 Discussion of the paleomagnetic results and its implications..... | 77 |
| 5.4.1 The Shibeï pluton as the target of study | 77 |
| 5.4.2 Origin of the magnetic remanence..... | 78 |
| 5.4.3 Age of the magnetic remanence..... | 78 |
| 5.4.4 Comparison of paleomagnetic poles and rigidity test | 79 |
| 5.5 Conclusions and perspectives | 80 |

Chapter 6. Understanding of the Jurassic Large Granitic Province of SE China

| | |
|---|------------|
| | 81 |
| 6.1 Introduction of the research of Large Granitic Provinces | 81 |
| 6.2 Geological setting of the Mesozoic magmatism | 82 |
| 6.3 Field and experimental results | 84 |
| 6.3.1 Overview of the Jurassic plutons and their country rocks in the SCFB | 84 |
| 6.3.2 Field observation and experimental analysis of the Jurassic Qitianling pluton | 85 |
| 6.4 Discussion of the formation and geodynamic model of the Jurassic LGP in South China | 86 |
| 6.4.1 Major geological features of Jurassic plutons and their incompatibilities with those predicted by the slab subduction model..... | 86 |
| 6.4.2 The genesis of the Jurassic magmatism of the LGP..... | 89 |
| 6.4.3 A tentative geodynamic model for the formation of the Jurassic LGP in the SCFB | 92 |
| 6.5 Conclusions | 92 |
| Chapter 7. Discussion..... | 94 |
| 7.1 The relationship between granite petrofabrics-pluton emplacement-tectonics | 94 |
| 7.1.1 Emplacement under a crustal shortening setting..... | 96 |
| 7.1.2 Emplacement under extensional setting | 96 |
| 7.1.3 Emplacement under transpressional setting | 97 |
| 7.2 Structural Characteristics of the Jurassic plutonism in South China | 97 |
| 7.3 New understanding on the Jurassic magmatism in South China | 99 |
| 7.3.1 The source of the Jurassic magmatism in the South China Block | 99 |
| 7.3.2 The emplacement mechanism of Jurassic plutons..... | 102 |
| 7.3.3 Tectonic and geodynamic contexts of the Jurassic magmatism..... | 103 |
| Chapter 8. Conclusions and perspectives..... | 106 |
| 8.1 Conclusions | 106 |
| 8.2 Perspectives | 107 |
| References | 108 |
| Supplementary materials..... | 132 |

Chapter 1. General introduction

1.1 State-of-the-art of magmatism: relationship with the tectonic-geodynamic settings and overview of magma emplacement mechanisms

1.1.1 Tectonic and geodynamic settings of magmatism

Magmatic rock is one of the most important components of the continental crust, and records the processes of crust growth and recycling. Therefore, the study of magmatism, especially in the large zones or provinces where occurred numerous magmatism, can help to understand not only the magma evolution but also the crust evolution.

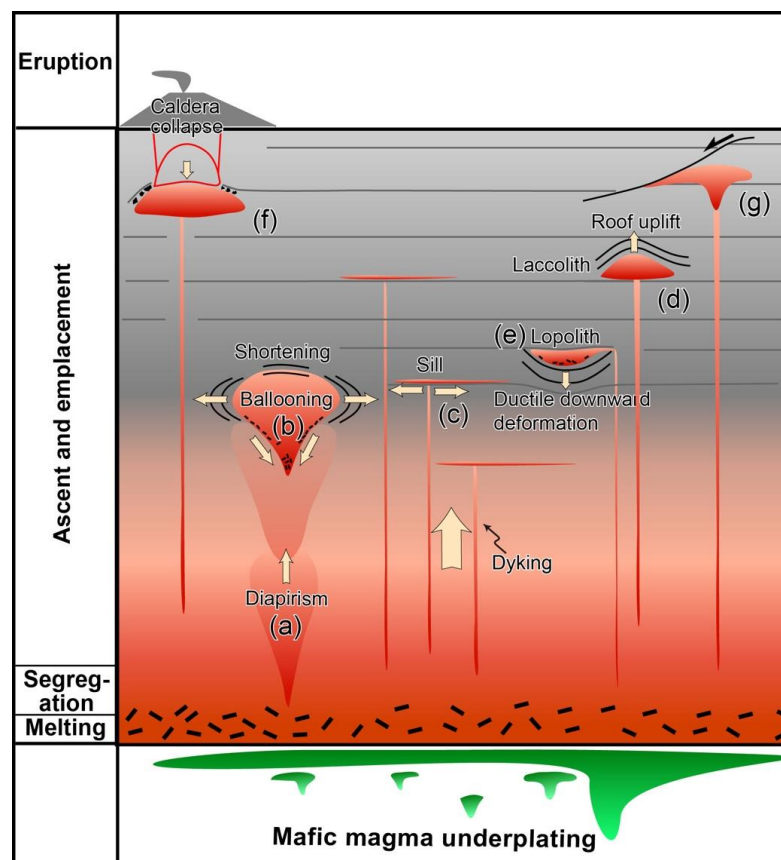


Figure 1-1. Simplified diagram of the magma evolution system (according to Huppert and Sparks, 1988; Petford et al., 2000, Burchardt, 2009; Annen et al., 2015).

The entire magma evolution system, including the magma generation, segregation, transport and emplacement (Fig. 1-1), is usually controlled by the geodynamic and regional tectonic settings (Maniar and Piccoli, 1989; Pearce and Peate, 1995; Wilson, 2007). Previous studies have principally classified the magmatism into two groups, according to the geodynamic and tectonic settings. One concerns the magmatism developed at an active plate margin setting, and another is the magmatism developed in an intraplate setting (Fig. 1-2; Wilson, 2007) and different features of these two groups of magmatism will be recorded due to the different natures of magma and overlying crust.

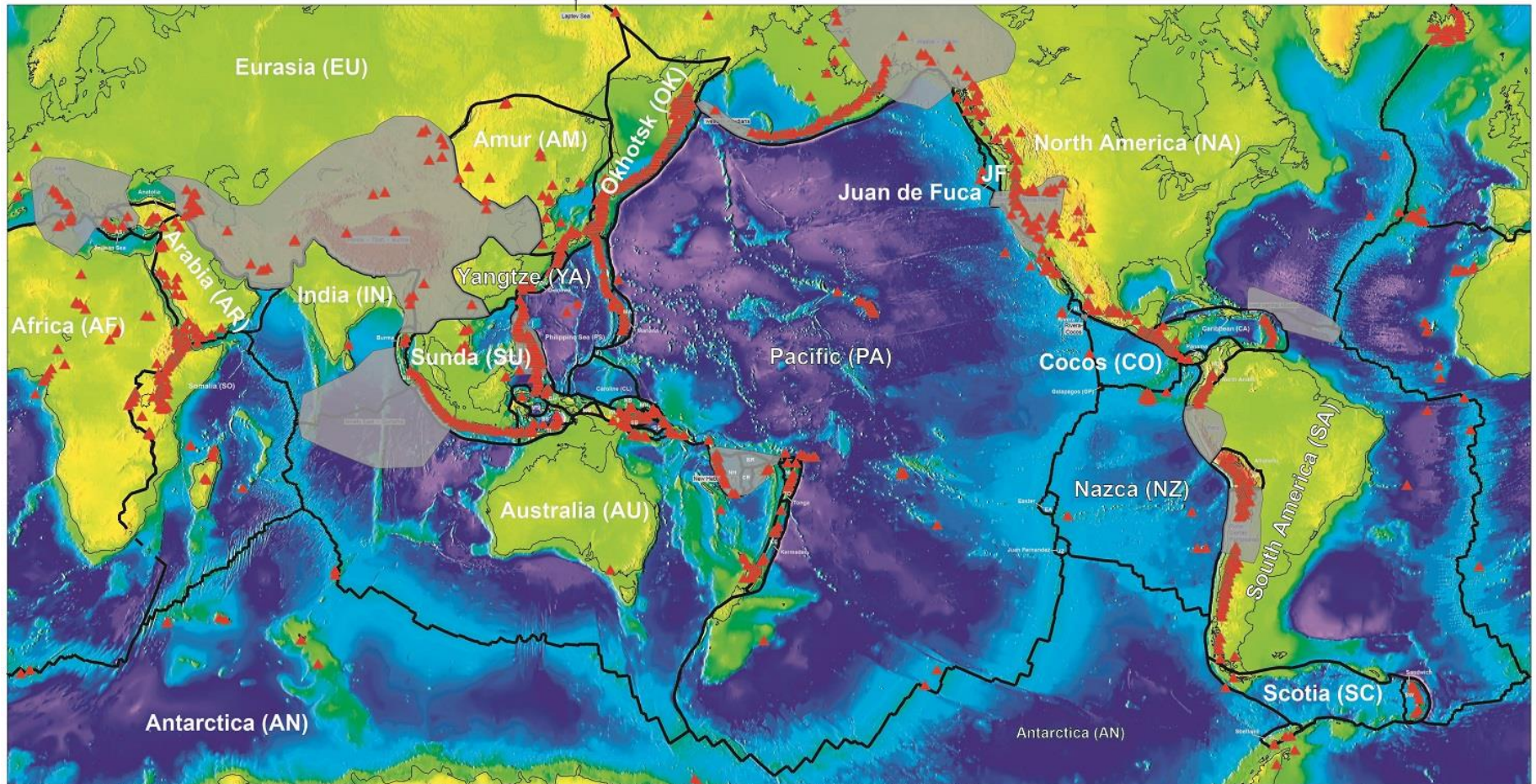
Furthermore, a good knowledge on the previous regional tectonic and geodynamic settings will also help to understand the magmatism process.

1.1.1.1 Magmatism developed at an active plate margin setting

Magmatism yielded at an active plate margin mainly divided into two settings, one is the plate subduction related and another is plate rifting related. The magmatism under the subduction setting, e.g., island arc magmatism, may be produced by the partial melting of the thickened lower crust during the collapse period, which usually developed at an continental-continental subduction setting (e.g. Himalaya magma belt; Inger and Harris, 1993), or the melting of the lower crust assisted by the thermal and fluid addition from the enriched mantle wedge, which is modified by the material contribution from the footwall side of the subduction (e.g. Tatsumi et al., 1986). Therefore, the source of the felsic magma is derived from the lower crust with small magma addition from mantle due to the limitation in magma mixing, but mafic rocks, which is derived from mantle, are usually observed (Sparks and Marshall 1986; Defant and Drummond, 1990). In the plate rifting setting, the mafic and felsic usually co-exist, and are characterised by the bimodal feature. The emplacements of magma under a plate margin setting usually are along the plate margin, and the long axis of a single pluton is of the parallel with the plate margin (e.g. Aspden et al., 1987).

1.1.1.2 Magmatism under an intraplate setting

The mechanism of magmatism developed at an intraplate setting is more complicated than that in the plate margin one (Wilson, 2007). This magmatism may be driven by the mantle convection or lithosphere extension, the magma derived from the mantle will directly intrude into the crust to form intrusive rocks or directly to the surface to form the extrusive rocks. For example, the Hawaiian Volcanic Complex (e.g. Romer et al., 2001) the oceanic island basalt (e.g. Hawaii hot spot; Richards et al., 1989) and flood basalt in intracontinental (e.g. Emeishan flood basalt; Xu et al., 2004). Magma emplacement rate of this extrusive magma is usually faster than that of the intrusive one, and the distribution of igneous bodies mainly depends on the location of the magma supply channel, the rheology and the rigidity of crust.



Bird, P., An updated digital model of plate boundaries, *Geochemistry Geophysics Geosystems (G3)*, 4(3), 1027, doi:10.1029/2001GC000252, 2003.

Figure 1-2. Plate tectonic and distribution of the volcanism (modified from Bird, 2003).

1.1.2 Overview of the magma emplacement mechanisms

1.1.2.1 Introduction of the emplacement mechanism

Magma emplacement is one of stages of the magma evolution system, including the genesis, segregation, ascent, emplacement and/or eruption (Fig. 1-1), and is essential for the understanding of the continental crust evolution (Pitcher, 1979; Barley et al., 1997; Petford et al., 2000; Annen and Sparks, 2002; Barboni et al., 2015; Annen et al., 2015 and references therein). According to the different settings of final magma emplacement, the magmatic rocks can be divided into two basic types: intrusive and extrusive (Taylor and McLennan, 1995). The emplacement process of these intrusive bodies, especially in those regions with large volume of magma emplaced at a shallow crustal level, will change the thermal state of the country rocks and yield the magma-related mineral deposit (Hedenquist and Lowenstern, 1994; Thompson et al., 1999). Therefore, the study of the magma emplacement of the intrusive rocks is essential.

During the emplacement, a variety of features of the process have been recorded in the pluton and its country rocks, which reflect the interaction between the hot magma and its country rocks as well as the creation of the space for magma emplacement. Previous studies found that the features of the intrusive bodies are not only controlled by the composition, temperature and pressure of the magma itself, but also strongly affected by the rheological conditions of the crust, synmagmatic regional tectonic and geodynamic setting (Castro, 1987; Hutton, 1988; Moyén et al., 2003; de Saint-Blanquat et al., 2006; Glazner and Bartley, 2006; Caricchi, et al., 2007; Wei et al., 2014). Consequently, the deciphering of the magma emplacement process, i.e. the rate of magma ascent (Mourtada-Bonnefoi and Laporte, 2004; Humphreys et al., 2008; Rutherford, 2008), the style of magma channel (Clemens and Mawer, 1992; Paterson, 2009), the depth of emplacement (Moyén et al., 2003; Menand, 2011 and references therein), the deformation and thermal conditions of the granite and its country rocks (Paterson et al., 1989; de Saint-Blanquat et al., 2001, 2006; Žák et al., 2007; Byerly et al., 2017) and the geometry of the pluton (Cruden, 1998; O'Driscoll et al., 2006; Stevenson et al., 2007; Mathieu et al., 2008; Cruden et al., 2017), can quantify these factors and give hints of further studies on both deep and shallow process of the crust evolution.

In this part, we compile the general characteristics of magma emplacement mechanisms and the relative possible interpretations (Fig. 1-3).

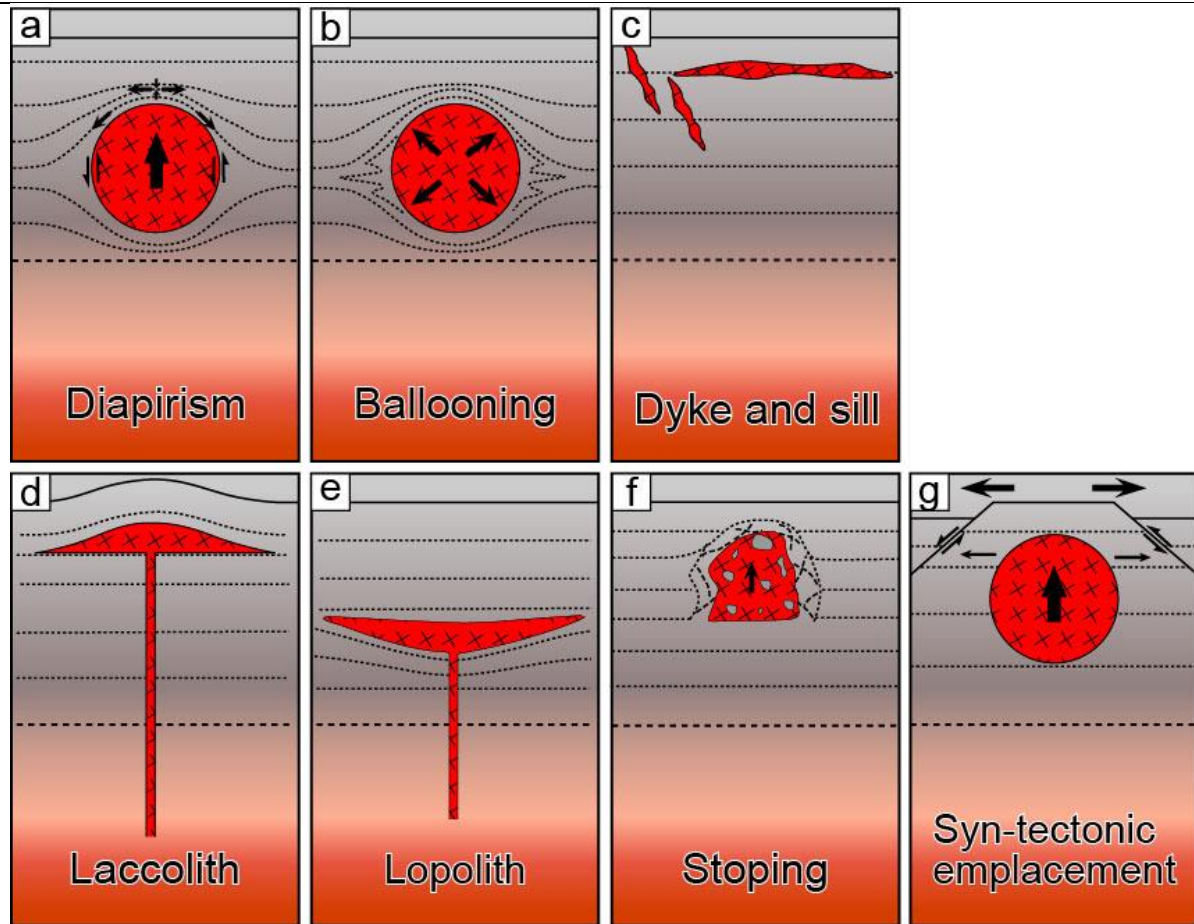


Figure 1-3. Overview of the current popular magma emplacement mechanisms (according to Goodson, 2014).

The magma emplacement has long been studied, and was classified into two basic types, i.e. forceful and permissive, according to the rate contrast enter magma uprise and tectonic “cavity” opening, respectively (Hutton, 1988; Pitcher, 1979). However, the rate of magma emplacement is higher by several orders of magnitude than the tectonic rate (Ragan et al., 2009), thus, this classification was largely questioned and against by recent studies. Therefore, the incremental emplacement of dikes or sills, which describe a gradual accumulation of magmatic batches process, is proposed and becomes the popular way to explain the mama emplacement and solve the space problem in the shallow crust level (Annen, 2015), especially for large scaled pluton.

1.1.2.2 Diapirism and ballooning

Diapirism (Fig. 1-3a and -3b) was redefined by Paterson and Vernon, (1995), which considered as the movement of the magma with or without pierce through the country rocks. While, the ballooning (Fig. 1-3b) is the in situ radial inflation of the magma chamber with successively displaced magma and bulk shortening of the country rock is needed to produce the space for magma emplacement (Bateman, 1984).

In the diapirism and ballooning models, the buoyancy of magma is the major force that drives

the transport and displacement of the magma (Roberts, 1970). Accordingly, the magma will emplace at the place where the magma buoyancy alone is not enough to break the overlain stiff crust (Vigneresse, 1995). Gradually accumulated magma with thermal energy partitioning into the country rocks will heat the country rock and attenuate the rigidity of the country rock to facilitate the ductile deformation of the country rock (Burchardt et al., 2010 and references therein). According to Bateman, (1984), the internal force of magma chamber should be similar to or higher than the lithostatic pressure of the country rock to maintain the diapir and ballooning form. The increasing of the internal force of magma chamber may be due to the additional magma input or increasing of the crystallisation of the magma.

The features of these mechanisms are usually characterised by (1) spherical or ellipsoid shape, when the tectonic absent; (2) zonation of the pluton composition; (3) gradually outward increasing of the internal ductile deformation of the granite; (4) high-temperature thermal aureole, due to the in-situ cooling (ca. 650°C) and the dissipating of the pluton accommodated by the country rock; (5) deformed thermal aureole with steep lineation and deflected foliation parallel with the pluton margin, due to ductile shortening or sagging of the country rocks (Cruden, 1988; Paterson and Vernon, 1995).

1.1.2.3 Dykes and sills

More and more studies reveal that the intrusive bodies emplaced at the shallow crust have a tabular shape and layering of the composition, which is different from the diapirism or ballooning one. Accordingly, the dyke and sill emplacement model is proposed to explain the construction of tabular plutons (Burchardt, 2008; Gudmundsson, 1990, 2011).

Dyke (Fig. 1-3c) concerns the magma transport along the fractures produced by the elastic cracking of country rocks due to the tensional stresses from some specific processes, or uprise along pre-existed fractures (Weinberg, 1999). Sill (Fig. 1-3c) describes sheet-like bodies that conformably intrude into the layers of the country rocks, with aspect ratio higher than ten (Corry, 1988), which is deflected from the vertical to sub-vertical transported dykes with over- or under-accretion (Burchardt, 2008 and references therein).

The viscosity of the magma and aspect ratio of the dyke control the development and propagation of the dyke in the crust. During the ascent of the dyke with very limited deformation is partitioning into the country rock (Rubin, 1993). The formation of the sill is deflected from the vertical or sub-vertical transported dyke and there are several possibilities to explain the deflection mechanism of the dyke (Gudmundsson, 2011 and references therein). Firstly, the rotation of the maximum principal compressive stress from vertical to horizontal, where the density of the magma is equal to the country rocks (Roberts, 1970). Secondly, the lithology contrast boundary, where stress barriers present and cause the deviations of local stress field (de Saint-Blanquat et al., 2001,

2006; Menand, 2008; Gudmundsson, 2006). Thirdly, previously existed discontinuity interface, for example, the unconformities (Sylvester et al., 1978; Kavanagh et al., 2006; Mathieu et al., 2008), or the interface of transition between contraction and extension in the crust (Byerly et al., 2017).

In the dykes and sills model, the distinctive feature is the geometry of the pluton, which presents a large aspect ratio and concordant contact with the country rock. Sharp contact with narrow deformation and thermal aureole is developed on the country rocks, due to the high velocity of magma transport in the dyke. Composition layering can be observed in macroscopic scale, or dyke parallel fabric and physical property difference (Knight and Walker, 1988; Herrero-Bervera et al., 2001; Morgan et al., 2017). Furthermore, the orientation of the long axis of the pluton usually parallel to the synmagmatic or inherited tectonics.

1.1.2.4 Laccolith and lopolith

As reviewed by Corry (1988), Laccolith (Fig. 1-3d) is resulted in magma intruding along the bedding plane with a convex top, flat bottom and diameter to thickness ratio less than ten. Alternatively, the lopolith (Fig. 1-3e) describe a pluton with an inward dip floor and roof.

The laccolith is formed by magma intruding along the strata plane with roof lifting to accommodate the magma intruding with internal force from gradually accumulated magma in the chamber. Usually, the laccolith is emplaced at shallow crust level, where the magma internal force can balance the lithostatic pressure from the country rocks and bend it (Morgan and McGovern, 2005; de Saint-Blanquat et al., 2006). Therefore, the laccolith-shaped pluton is usually characterised by doming and ring-fractures developed in the roof and wall rocks. The foliation developed in the margin of the pluton is parallel with the contact with outward dipping of the country rocks and ductilely deformed marginal part of the pluton. Moreover, the degree of deformation is decrease from external to internal part of the pluton, (Aranguren et al., 2003; Stevenson, 2007; Currier et al., 2015).

The lopolith is formed by sagging of the country rocks through ductile deformation (Corry, 1988 and reference therein). Lopolith-shaped pluton is not usually observed, as it is usually develop in a deeper crust level (Mathieu et al., 2008) and produces the space by ductile deformation of the floor rocks driven by the gravitation potential energy of the magma (Corry, 1988 and references therein). Accordingly, a lopolith-shaped pluton is characterised by a thick central region and inward sloping side-walls, gravity controlled magmatic layering in the pluton (Duchesne, 1978) and the composition is usually mafic one with high density to drive the foundering of the floor of the pluton (Vanko and Bishop, 1982; O'Driscoll et al., 2006; Roman et al., 2016).

1.1.2.5 Stopping

Stopping (Fig. 1-3f) is responsible for magma emplacement through the thermal cracking, diking,

tectonic stress and focuses porous flow to break the country rocks and involves it into the pluton to accommodate the successively magma arrival and intrude at different crust level (Daly, 1903; Paterson, 2008).

Glazner (2006) has reviewed the stopping mechanism and detailed discussion of the evidences to support the stopping hypothesis proposed by Daly (1903) and its limitations of this mechanism have been given in Glazner (2007). However, the stopping is not totally excluded, but combined with other mechanisms. The features that previous studies presented are as follow: (1) irregular shape but discordant contact; (2) xenoliths from the country rock in the pluton margin; (3) chemical contamination by the country rocks; (4) brittle deformation instead of ductile deformation of the country rocks (Glazner et al., 2006 and references therein; Huber et al., 2011).

1.1.2.6 Syntectonic magma emplacement

Syntectonic magma emplacement (Fig. 1-3g) means that the magma emplacement process is assisted or dominated by the regional tectonics when the magma is involved in the tectonic system (Hutton, 1988).

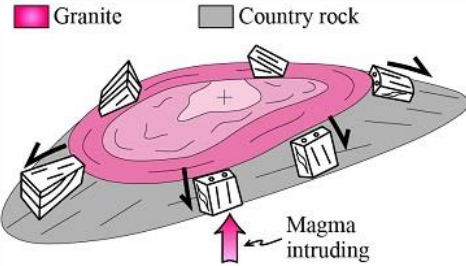
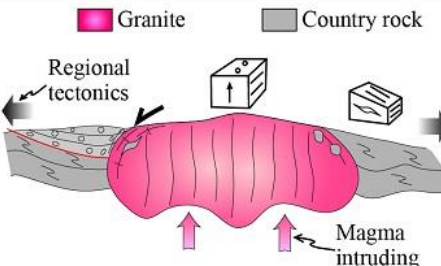
The role of tectonics in magma emplacement has long been studied and considered as the permissive emplacement, when the magma emplacement is dominated by regional tectonics (Pitcher, 1979). However, this model is challenged by two following points: (1) the tectonic deformation rate is usually lower than the magma supply rate and (2) no cavity (space) is existed in the crust before the magma emplacement (Hutton, 1988). However, the construction of a large scaled plutons is difficult to explain by the forceful model alone. Therefore, the deformation of the country rocks, including rotation, translation and strain, by the regional tectonics is still necessary for large pluton construction (Hutton, 1988; Tikoff et al., 1999).

More and more recent studies confirm the significant role of the tectonics on the magma emplacement and several features of this kind of mechanism can be listed here. (1) the geometry or spatial distribution of the plutons is often parallel with the regional tectonics; (2) the pluton is often in the tectonic (faulting) contact with the country rocks (Wei et al., 2014), and the contact zone between the pluton and country rocks is well deformed, even mylonised, accommodated to the regional tectonics (Faure and Pons, 1991); (3) the deformation intensity decreases from tectonic contact to the interior of the pluton (Paterson et al., 1989); (4) the petro-fabric of the pluton, especially for fabrics developed in the margin of the pluton, is consistent with regional structures (Allibon et al., 2011; de Saint Blanquat et al., 2011; Wei et al., 2014).

In summary, we consider that the contribution of the tectonics is pivotal, which not only affect the emplacement, but also the entire magma evolution system. We also recognize that the final location of emplacement of the magma is determined by both the magma itself and regional tectonics. Therefore, we briefly classified the emplacement mechanisms into two major types, i.e.

forceful and permissive (syntectonic), and features of different kinds of emplacement mechanisms are listed in Table 1-1. However, pre-magmatism tectonics, which are usually overprinted or modified by later tectonics, are undervalued, especially for the regions that have experienced several phases of deformation. Consequently, our studies on the emplacement of Jurassic granites in the South China Block need detailed considerations on the pluton construction, syn-magmatic and pre-magmatic tectonics.

Table 1-1. A conclusive classification of different magma emplacement mechanisms and its associated features

| <i>Mechanism</i> | | <i>Forceful</i> | <i>Permissive (Passive or syn-tectonic)</i> |
|--|------------------|--|---|
| <i>Features</i> | | | |
| <i>Sketch of the pluton, country rock and characteristics of emplacement</i> | |  |  |
| <i>Mode of pluton building</i> | | diapirism, ballooning | dyke accretion, cauldron subsidence |
| <i>Deformation and fabric pattern</i> | <i>Wall rock</i> | ductile deformation around the pluton and its aureole | ductile deformation by tectonics, brittle fracturing |
| | <i>Pluton</i> | concordant planar and linear fabrics between the pluton and wall rocks along the contact | preferred mineral orientation corresponding to the regional tectonic regime |
| <i>Dynamics of pluton emplacement</i> | | internal force (magma bouyancy) | external force (regional tectonics) |
| <i>Part of references</i> | | Schuling, 1962; Faure and Cottreau, 1988; Morgan et al., 2013. | Hutton, 1990; Stevenson, 2009; Nédélec and Bouchez, 2015; |

1.2 Overview of the study

1.2.1 Research background

1.2.1.1 Mesozoic magmatism of the South China Block

The Mesozoic magmatism in the South China Block (SCB in Fig. 1-4a) seems presenting a unique case in the world, not just by its vast distribution, extending about 1500 km along the NE-SW strike and 800 km wide in the southeastern part of the SCB, but also by its long duration of ca. 150 Myrs (Figs. 1-4b and 1-4c). Meanwhile, the Jurassic large area and variety of mineralization in the South China Block had highly attracted the attention of geoscientists since the last century (Hua et al., 2005; Hu and Zhou, 2012; Mao et al., 2013). From the map-view distribution of Mesozoic granitic plutons in the SCB (Fig. 1-4b) and the review of previous achievements, several features can be recognized:

(1) Mesozoic granitic plutons are widely distributed without any apparent alignment. Individual plutons do not any particular elongated shape, and some of them developed in the inland area show a rather sub-rounded shape, for example, the Qitianling, Huashan and Guposhan plutons located at the Nanling area (Fig. 1-4b; Shu et al., 2011);

(2) The majority of Triassic granites are of S-type, Jurassic granites show metaluminous to weak peraluminous feature, and Cretaceous granites are accommodated with large volume of volcanic rock and mantle input (Zhou et al., 2006);

(3) So far, reliable Triassic volcanic rocks recorded in the Cathaysia Block, i.e. the actual southeastern part of the SCB, are absent, and Jurassic volcanic rocks (ca. 175 Ma) can be only locally found in the Nanling area (Fig. 1-4b; Zhou et al., 2006);

(4) The Mesozoic granites in the SCB with the ratios of 15%, 45% and 40% for Triassic, Jurassic and Cretaceous granites, respectively, are mainly exposed in the SE part of SCB (Zhou et al., 2006). With the improving of geochronological dating technique, more and more Jurassic plutons are being reported in the coastal area of the SCB (Liu et al., 2012; Zhang et al., 2015);

(5) Substantial and variety of mineralization have been also founded in Jurassic plutons (Mao et al., 2013).

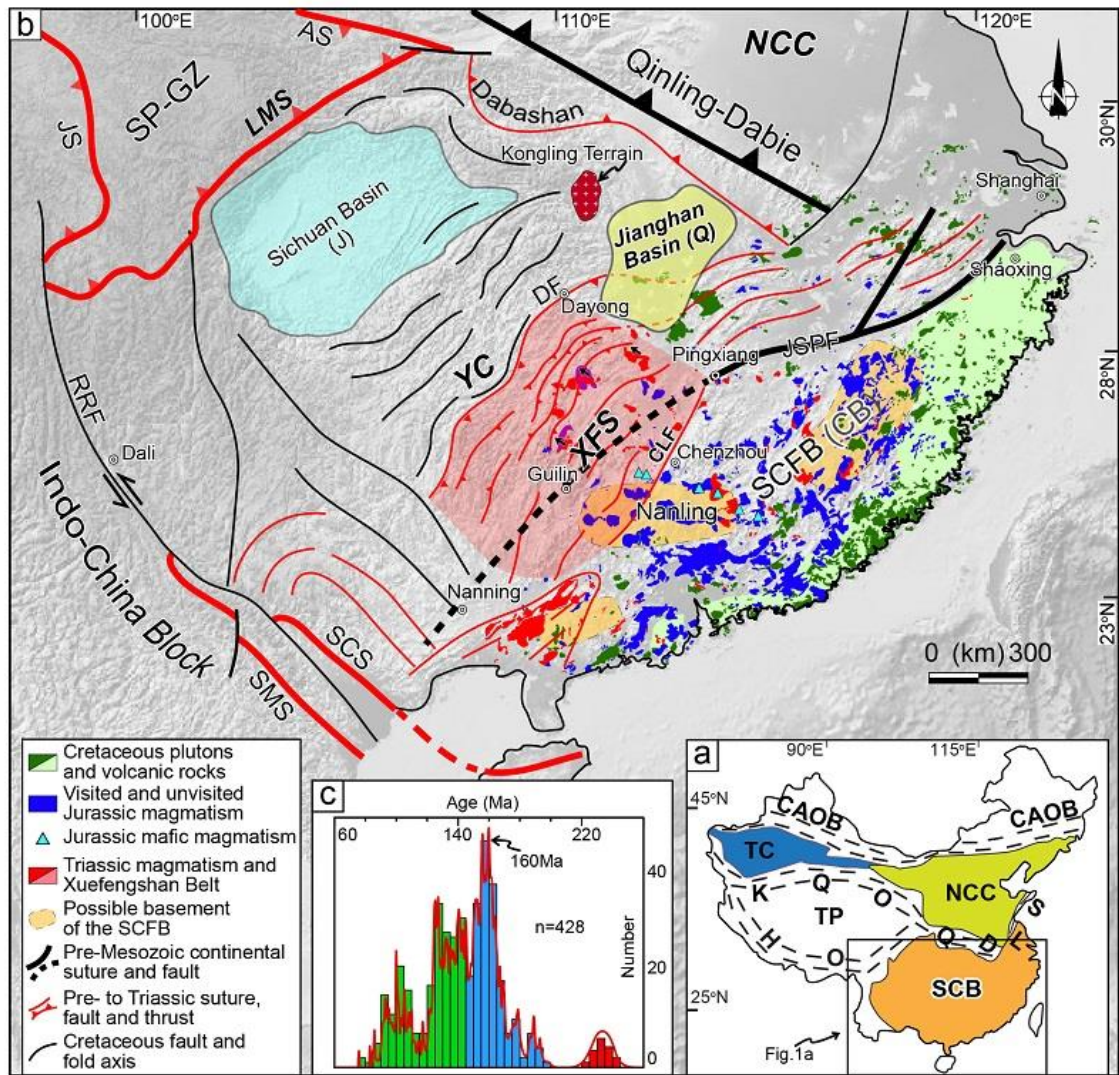


Figure 1-4. (a) Sketch of major continental blocks in China. Abbreviations are CAOB: Central Asia Orogenic Belt, HO: Himalaya Orogen, KQO: Kunlun-Qiangtang Orogen, NCC: North China Craton, QD: Qinling-Dabie Orogen, SL: Sulu fault, SCB: South China Block TC: Tarim Craton, TP: Tibet Plateau. (b) Tectonic framework of the South China Block and its surrounding areas. Abbreviations are AS=Animaqin Suture, CLF=Chenzhou-Linwu Fault, DF=Dayong Fault, ICB=Indochina Block, JS=Jinshajiang Suture, JSPF=Jiangshan-Shaoxing-Pingxiang fault, NCC=North China Craton, RRF=Red River Fault, SCB=South China Block, SCFB=South China Fold Belt, SCS=Song Chai Suture, SMS=Song Ma Suture, SP-GZ=Songpan-Ganzi Block, XFS=Xuefengshan belt and YC=Yangtze Craton.; the red solid and dash lines represent the Triassic collision and intracontinental deformation; the black thick solid line indicate the pre-Triassic tectonic events and the thin black solid line means the Cretaceous tectonic events. (c) Age distribution of the Mesozoic magmatism, the red, blue, and green colors stand for the Triassic, Jurassic, and Cretaceous magmatism, respectively (According to Zhou et al., 2006; Faure et al., 2016).

1.2.1.2 Previous opinions on the tectonic and geodynamic settings of the Mesozoic magmatism in South China

Recently, the studies on the regional structures, deformation and magmatism in the SCB reveal the crustal shortening and extension tectonic settings for the Late Triassic and Early Cretaceous, respectively (e.g. Chu et al., 2012a and 2012b; Wei et al., 2014). However, the Jurassic tectonic regime, which is pivotal for understanding the Mesozoic tectonic evolution of the SCB and its amplitude mineralization, is still in dispute. Several geodynamic models have been proposed to explain the formation of the Mesozoic magmatism and its related tectonic setting, which are essentially based on the detailed petrological, geochronological and geochemical studies (e.g. Hsü et al., 1990; Xie et al., 1996; Zhou and Li, 2000; Li and Li, 2007; Dong et al., 2008; Jiang et al., 2009; Chen et al., 2008). These models can be classified into three groups, i.e. the mantle plume related (Zhang et al., 2013; Fig. 1-5), the Paleo-Pacific slab subduction related (Zhou and Li, 2000; Li and Li, 2007; Fig. 1-6) and the intracontinental subduction or orogeny related models (Dong et al., 2008; Chen et al., 2008; Fig. 1-7). However, some geological and chronological features still cannot be explained by these models yet.

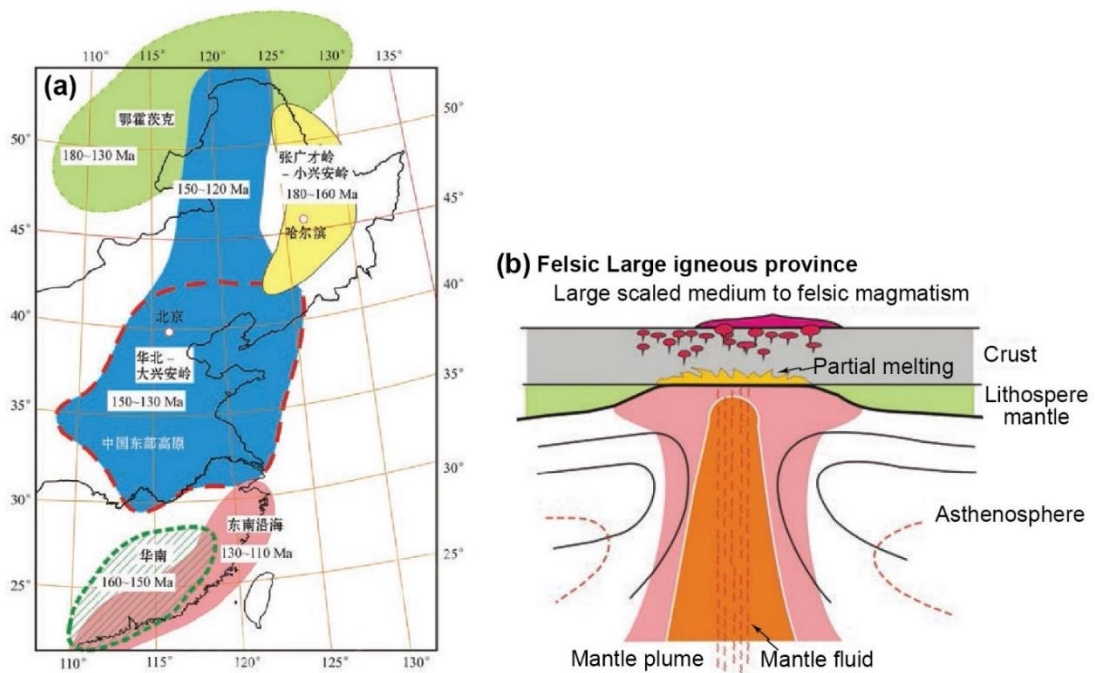


Figure 1-5. (a) Distribution of the large magmatic provinces in the East Asian. (b) Schematic carton of the formation of the late Jurassic (160-150 Ma) magmatism in the South China Block (modified from Zhang et al., 2013).

The super mantle plume model was proposed to explain the formation of the widespread Mesozoic magmatism (Fig. 1-5), suggesting that the asthenosphere mantle materials arrived at the lower continental crust to trigger the partial melting of the lower continental crust and yield the dominantly medium to felsic magmatic rocks during the peak of Mesozoic magmatism (ca. 160-150

Ma). Moreover, mantle derived fluid also contributed to the widely distributed mineralizations, for instance, Au, Cu, W, Sn, Mo, Bi and U (Zhang et al., 2013). Nevertheless, the Triassic and Jurassic volcanisms and mafic magmatic rocks are rarely found in the SCB (He et al., 2010), and the mantle plume was considered as a short duration event (Campbell and Griffiths 1990), while, the Mesozoic magmatism is lasted about 150Ma. Moreover, the topographical responses of the mantle plume, for instance, doming and circular rifting of the country rocks are not observed in the SCB.

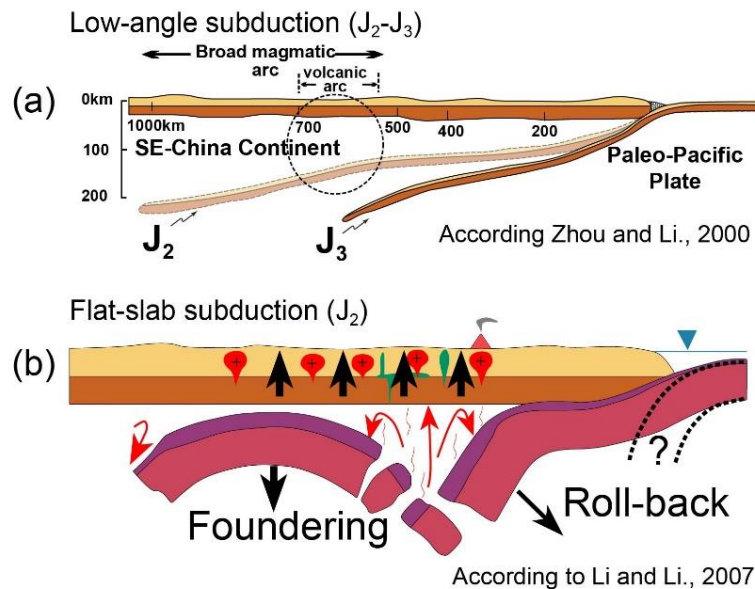


Figure 1-6. Paleo-Pacific slab subduction geodynamic models to explain the Mesozoic magmatism in the South China Block (according to Zhou and Li, 2000; Li and Li, 2007).

The Paleo-Pacific slab subduction models (Fig. 1-6), including the changing of subduction angle of the slab (Zhou and Li, 2000), flat slab subduction (Li and Li, 2007), retreat of the subducted slab (Jiang et al., 2009) and the oblique subduction (Wang et al., 2011), were proposed, which becomes the most popular model, to interpret the development of the Mesozoic magmatism in the SCB. These models are aimed at to explain the gradually temporal and spatial distribution of granites of the late Mesozoic magmatism from the inland (~180 Ma) to costal (~125 Ma) area with the generally regional NE-SW trending fold-fault system, which is parallel with the continental margin, and its associated mineralizations in the southeastern part of the South China Block. However, the slab subduction models are challenged by several recent results, for example, numerous recent geochronological studies show that Jurassic plutons are widely distributed in the SE costal area with a planar distribution (Liu et al., 2012; Cui et al., 2013; Zhang et al., 2015); There is no reliable ophiolite to prove the existence of the Paleo-Pacific oceanic slab subduction (Lu et al., 2014), and the current wide distribution (>800 km) cannot be explained by the subduction model. No consistent Jurassic structures and tectonic records are reported inside of the SCB. Moreover, the development of different type of the ore deposits may also related to different country rock association and basements (Huang et al., 2017).

In summary, it seems that no exiting model can satisfactorily explain the features of the Mesozoic geological phenomena, consequently, the tectonic setting and geodynamics for the Mesozoic magmatism in the SCB are still open questions.

1.2.2 Research purpose and contents

As mentioned above, the magma emplacement mechanism is a fundamental question and still hotly debated due to its significance for the understanding of the entire magma system and its associated mineralizations, and the Jurassic tectonic and geodynamic settings remain poorly understood. The study of magma emplacement process can help to restore the synmagmatic tectonic regime (e.g. Hutton, 1988; de Saint-Blanquat et al., 1997 and 2001), especially for those zones intruded by several phases of magma and overprinted by multiphases of tectonics.

Hence, the widespread Jurassic magmatic plutons in the SCB can be targeted as an ideal nature lab to study the magma emplacement mechanism and its implications for the tectonic and geodynamic settings. Four questions have been summarized and will be answered by our study:

- (1) What are the emplacement mechanisms of the Jurassic plutons in South China?
- (2) What is the tectonic regime for the Jurassic magmatism: compression, extension, transpression or atectonic?
- (3) Whether there is a link among tectonics - magmatism - mineralization?
- (4) What is the geodynamic context for this period (subduction of the plate, plate rollback or thinning of lithosphere mantle, etc.)?

1.2.3 Research design and methodology

As mentioned above, the SCB is consisted of several micro blocks, characterized by distinct features concerning its magma association, mineralization and basement composition. Accordingly, we divided the study area into three major units, i.e. the Nanling area, the Wuyishan area and the SE coastal zone, to carry out our research (Fig. 1-8). Detailed research design for this study is listed in the following:

(1) To get an overview of the Jurassic plutons in the SCB, detailed field investigations have been done on 41 plutons and their country rocks, to see the similarities and differences among plutons developed in different geological units;

(2) Two representative plutons, i.e. the Qitianling and Shibeit plutons, were chosen for the detailed magma emplacement mechanism study with multidisciplinary methods. The field and thin section observations on the country rocks and plutons were used to evaluate the relationship between the regional tectonics and the pluton emplacement. The magnetic fabric study of the pluton was applied to restore the process of pluton building and its interaction between the magma and its wall rocks. The geometry of plutons was modelled with the gravity anomaly and also will throw

light on the magma supply channel. Consequently, a realistic emplacement model will be proposed based on our and previous data;

(3) The southeastern part of the SCB, i.e. the Cathaysia Block, is long been considered as a fold belt zone by some researchers, namely the South China Fold Belt (e.g. Huang, 1945), but this opinion didn't attract enough attention within the geoscience community, though numerous regional geological and geographic phenomena challenge to consider this area as a rigid body. Therefore, we have carried out the paleomagnetic studies on these two plutons of 600 km apart and to constraint the rigidity of the Cathaysia Block;

(4) Through the compilation of previous geochronological, geochemical, geophysical and structure data with our newly obtained results, new understanding on the Jurassic magmatism in South China will be discussed in terms of the magma genesis, emplacement mechanism, tectonic and geodynamic settings.

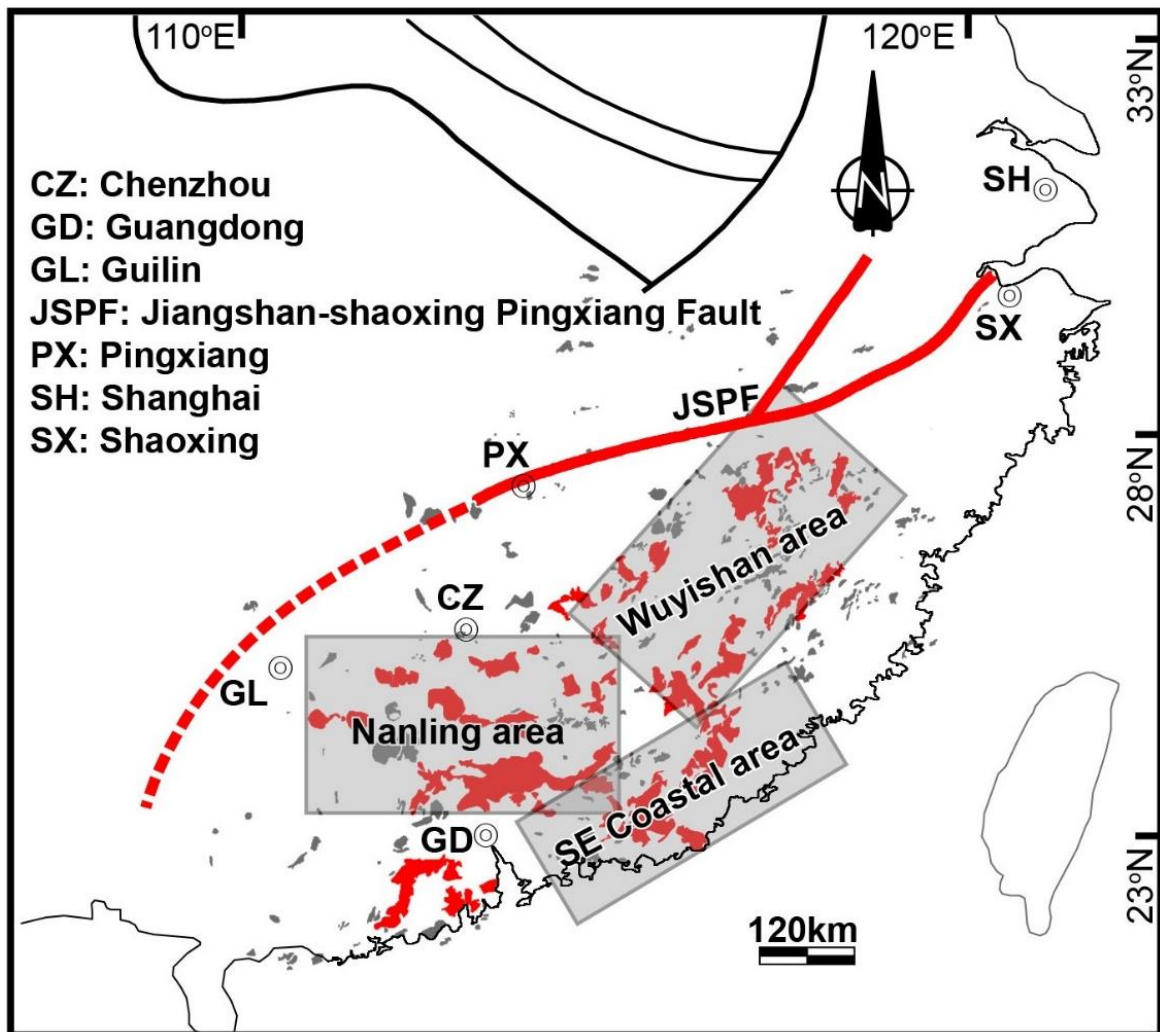


Figure 1-8. The distribution of the Jurassic plutons and major tectonic units in the Cathaysia Block.

The red one the represents the plutons we have investigated, and the grey one are not visited yet (According to Zhou et al., 2006; Li et al., 2009).

1.2.4 Workload of the study

This thesis is under constructed by the professors from the Nanjing and Orléans universities. Detailed workloads are listed in Table 1-2.

1.2.5 Major findings and innovations

The major findings of this study can be concluded below:

(1). In the microscopic scale, the observations on thin section of granites and wall rocks from 41 plutons and their country rocks show the typical magmatic texture with euhedral minerals without elongation nor preferred mineral orientation. Moreover, the country rocks are characterised by typical sedimentary texture, indicating weak interaction between the granite and country rocks during magma emplacement;

(2). The detailed magnetic fabric investigation on the Qitianling and Shibeil plutons shows that granites have low degree of anisotropy and reveals the well-developed and consistent magnetic foliations but dispersed lineations. The foliation is usually parallel to the structure of country rocks (e.g. unconformity, schistosity or folding axis). Our studies suggest that the country rocks, instead of the regional tectonics, control the development of magnetic fabrics in these plutons. In other words, the pre-magmatic structures control the petrofabric pattern of the plutons, instead of regional tectonics or lithospheric magmatic convection;

(3) In the outcrop scale, the progressive facies change has been often observed, however, few cold intrusive boundaries between two successive intrusions have been found, implying that the magmatic pulses or batches seem continuously intruding into the (middle) crust, i.e. two successive pulses are close in time;

(4). In the pluton scale, from our field observations on the forty-one Jurassic plutons covering almost all principal magmatic zones, the most remarkable phenomenon is that the contacts between plutons and their country rocks are sharp without ductile deformation on both sides, where only hornfels facies and narrow thermal aureoles were observed on the country rock side. These features are different from the features observed on plutons emplaced under the well-known forceful and syntectonic mechanisms. Furthermore, the fact that no emplacement related deformation has been observed in a such large zone implies that the Jurassic is a tectonically calm period with respect to the Triassic and Cretaceous, the deformation is less intensive during this period, at least within the Cathaysia Block;

(5) In the regional view, Jurassic granitic plutons are widespread in the southeastern part of the South China Block, i.e. the ancient Cathaysia Block, from the inland area to the coastal region without any regular temporal – spatial distribution. This feature is incompatible with the actually popular Pacific-ocean subduction model;

(6) In the plate scale, our paleomagnetic studies carried out on the contemporaneous Qitianling

and Shibeï plutons revealed a significant different relative movement between these two 600km-apart plutons since the emplacement of plutons, implying that the Cathaysia Block has experienced an internal deformation, therefore, this block cannot be considered as a rigid one.

Table 1-2. The list of workload of this study

| Content | Unit | No. | Notes |
|---------------------------------|----------|-------|---|
| Field observation | zone | 3 | Nanling, Wuyi and Fujian and Guangdong coastal areas |
| | day | 80 | On 41 Jurassic plutons and its country rocks located at Huanan, Guangxi, Guangdong, Jiangxi and Fujian provinces, with total driving distance more than 10,000 km |
| | point | 502 | On the structure, petrology and texture of plutons and its country rocks |
| Thin section observation | sample | 55 | Oriented and non-oriented |
| Photos of geological bodies | piece | >1000 | Including granite, enclave, contact, country rocks, field panorama etc. |
| AMS measurement | specimen | 816 | 341 specimens for the Qitianling pluton, 168 specimens for the Dadongshan pluton, 245 specimens for the Shibeip pluton and 62 specimens for the Huangcun pluton |
| Magnetic mineralogical analysis | sample | 55 | Thermo-magnetic (18), IRM (20) and hysteresis loop curve (17) measurements |
| Paleomagnetic measurement | specimen | 343 | 221 specimens for the Qitianling pluton and 122 specimens for the Shibeip pluton |
| Density measurement | sample | 53 | Granite for the Qitianling pluton |
| Hornblende geobarometer | sample | 3 | 3 thin sections from the Qitianling pluton for geochemical analysis, with 126 spots on the hornblende, 31 points on the biotite and 27 points on the plagioclase |
| Gravity modeling | profiles | 12 | 7 profiles for the Qitianling pluton and 5 for the Shibeip pluton |

By synthesizing our new results from field and laboratory, the previous achievement, including essentially petrology, geochemistry and geochronology, as well as the knowledge on the tectonic evolution of the South China Block, we can summarize the new scenario of the Jurassic magmatism in South China as following. The ancient Cathaysia Block, i.e. the actual southeastern part of the South China Block and the zone where the Mesozoic Magmatism took place, was composed of several sub-blocks and has experienced several important tectonic events since its agglomeration with the Yangtze craton at the Neoproterozoic. Consequently, it has been well deformed, fractured and presents a high heterogeneity in geology and structure. Therefore, it cannot be considered as a rigid block evidenced by our paleomagnetic studies, this gives the reason to Huang (1945) to call it as the South China Fold Belt. Due to its lower rigidity with respect to the Yangtze craton, this belt has absorbed the deformation and been probably entirely thickened by the Triassic tectonics (multidirectional subduction-collision of the South China Block under its surrounding ones and its intracontinental deformation).

The crustal thickening increases the pressure and temperature in the lower crust as well as the contacting surface with the mantle. With the increasing mantle thermal contribution, after the Triassic compressive tectonics, the depression of the thickened crust can produce partial melting in the low crust. With lower melting temperature of the water-rich lower crust, the melt can be produced in important volume in this belt. The melt served probably the well-developed pre-magmatism fractures and structures as its upwelling channels that may explain why the pattern of the distribution of the Jurassic plutons: widespread without alignment neither the apparent control of major fault. Moreover, each pulse or batch of upwelling melt can be in relatively small volume as it does not need an important buoyancy to make its channel. In other words, the partial melting and its upwelling can take place in a small temporal shift, and one pulse or batch may follow another closely in time, that may explain why cold intrusion boundaries have been rarely observed within plutons. As no important Jurassic deformation has been observed in this belt, the Jurassic may be considered as a tectonically calm period. In this case, the procedure of depression - partial melting of the lower crust and - upwelling of melt may take long time. This may be the case for the Jurassic magmatism in South China, which took about 40 Myrs. If we summarize the mechanism of the Jurassic magmatism in few key words, they may be: crustal thickening by the Triassic tectonics, partial melting of the water-rich lower crust, upwelling by buoyancy, intrusion in pre-magmatism inherited structure.

Chapter 2. Regional geological setting

2.1. The components and basements of the South China Block

The South China Block, Tarim Craton and North China Craton are considered as three major and stable continental blocks since the Neoproterozoic (e.g. Huang, 1977; Ma and Wu, 1981). However, the South China Block, differing from Tarim and North China Craton, is a block formed by the collision of the Yangtze, in its northwestern part, and Cathaysia block, in its southeastern part, at ca. 850Ma along the NE-SW striking Jiangshan-Shaoxing suture. The Jiangnan orogen formed by the continental collision between the Yangtze Craton and Cathaysia Block (Jiangshan-Shaoxing fault in Fig. 2-1, Li et al., 1997, 2003a; Li et al., 2008; Zheng et al., 2007), according to the lithological association of basements, different ages for the low grade metamorphism, Neoproterozoic arc related magmatism and ophiolitic rocks along the Jiangshan-Shaoxing Suture zone, as well as geophysical data and topography (Fig. 2-1).

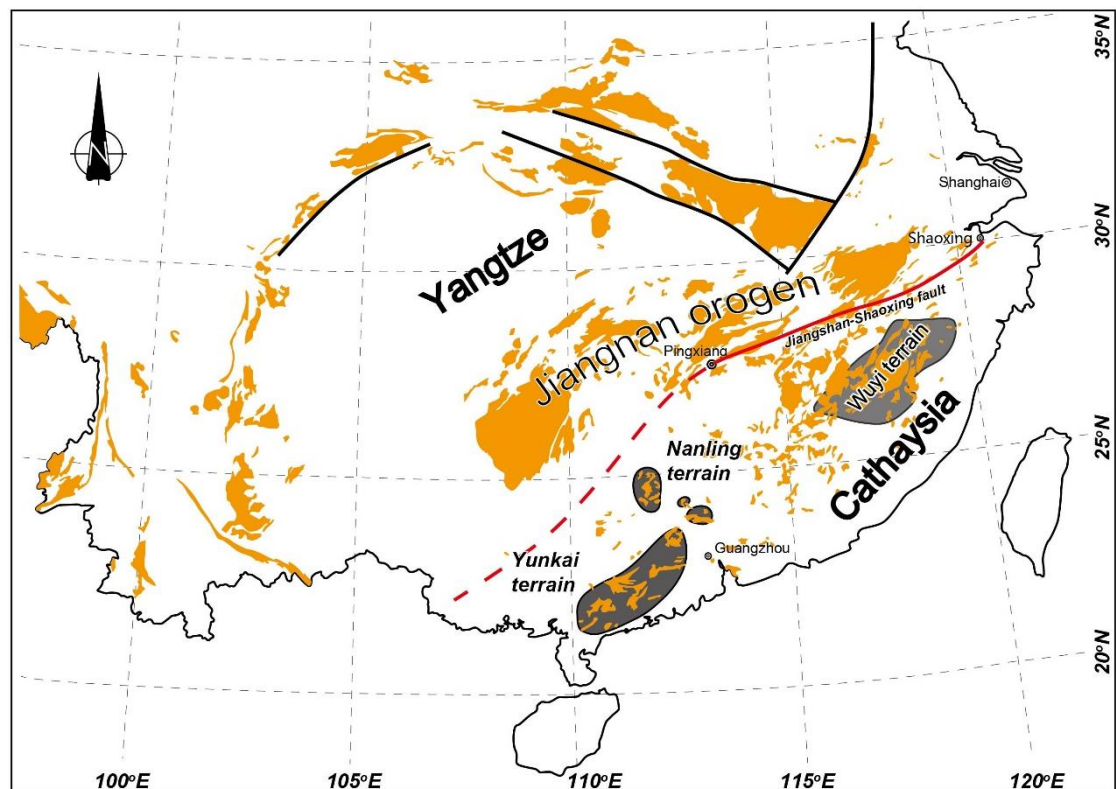


Figure 2-1. Distribution of Precambrian outcrops in the South China Block and the possible basement for Cathaysia Block (according to Dong et al., 1986; Yu et al., 2009).

The Yangtze Craton is accepted as a rigid craton with an Archean TGG association exposed as the Kongling complex located in the northern part, with LA-ICP-MS zircon U-Pb ages from the granitoids gneisses at 3.3Ga and detrital zircon ages between 2.87-3.28Ga from metapelites (Qiu et al., 2000; Gao et al., 2011). The Kongling complex and Paleoproterozoic strata, mainly exposed in

the northern part of the Yangtze Craton, are intruded by Paleoproterozoic Quanjitan granite (ca. 1.85Ga). The Neoproterozoic low-grade green schist facies Banxi Group unconformably overlies upon the pre-Neoproterozoic series. The Neoproterozoic to Sinian rift series are widely exposed in the south of the Yangtze Craton (Zhao et al., 2012 and references therein). Even few Paleoproterozoic outcrops can be found in the southern part of the Yangtze Craton, the studies of the Bouguer gravity anomaly and seismic velocity data show a similar crustal density for all the Yangtze Craton (Deng et al., 2014), indicating that the northern and southern parts of the Yangtze Craton represent a single block with a common Archean basement.

The Cathaysia Block is apparently different from the Yangtze Craton in term of the basement. It is considered as an accreted block roughly divided into three terranes, i.e. Wuyishan, Nanling and Yunkaidashan terrane, exposed as discrete high-grade metamorphic complex with Paleoproterozoic ages (Fig. 2-1; Yu et al., 2009, 2010, 2012). The Badu complex, considered as the oldest outcrop in the Cathaysia Block and located at the north of the Wuyishan terrane, consists of Paleoproterozoic rocks intruded by S-type granites, e.g. the Xiaji granite ($1888 \pm 7\text{Ma}$), the Lizhuang granite ($1875 \pm 9\text{Ma}$). Moreover, some inherited zircons from the metasediments have zircon crystallization age at 2.5Ga and metamorphic age at ca. 1.9Ga (Yu et al., 2012). Combining all these geochronological data, the Badu complex is suggested to be formed at ca. 2.5 Ga. The Nanling and Yunkai terranes were mainly composed of metasedimentary rocks and intruded by Paleozoic granites, which are considered as the metamorphic basement of the South China Block. However, recent geochronological data indicate that the formation of these two terranes was during the late Neoproterozoic to early Cambrian (ca. 850Ma to 520Ma), it seems that no reliable age data support a pre-Neoproterozoic basement, but, the age spectra of detrital zircon from these three terranes show Mesoproterozoic to Archean peaks (1.1Ga, 1.4Ga, 1.9Ga and 2.5Ga) and thermal overprint at the early Paleozoic (0.45Ga) (Xu et al., 2005; Yu et al., 2007, 2009; Zhou et al., 2015). All those evidences indicate that the Cathaysia Block may resulted in the agglomeration of several blocks, even no persuade evidences have been given, and had experienced multiphases of tectono-magmatic events.

2.2. Tectonic framework and evolution of the South China Block.

From the map of tectonic framework of SCB (Fig. 2-2), we can observe that the South China Block is strongly deformed and yield the generally NE-SW extended fold-fault system, called the Huanan fold belt (Li and McCulloch, 1996), the South China Orogenic belt (Ren et al., 1999) or the South China Fold Belt (Hong et al., 1998; Li and Li., 2007), and it had suffered polyphased tectono-magmatic events since the Neoproterozoic time. Therefore, to study the Mesozoic magmatism in the South China Block, it is necessary to have a pertinent view of this belt and its influence on the Jurassic magmatism.

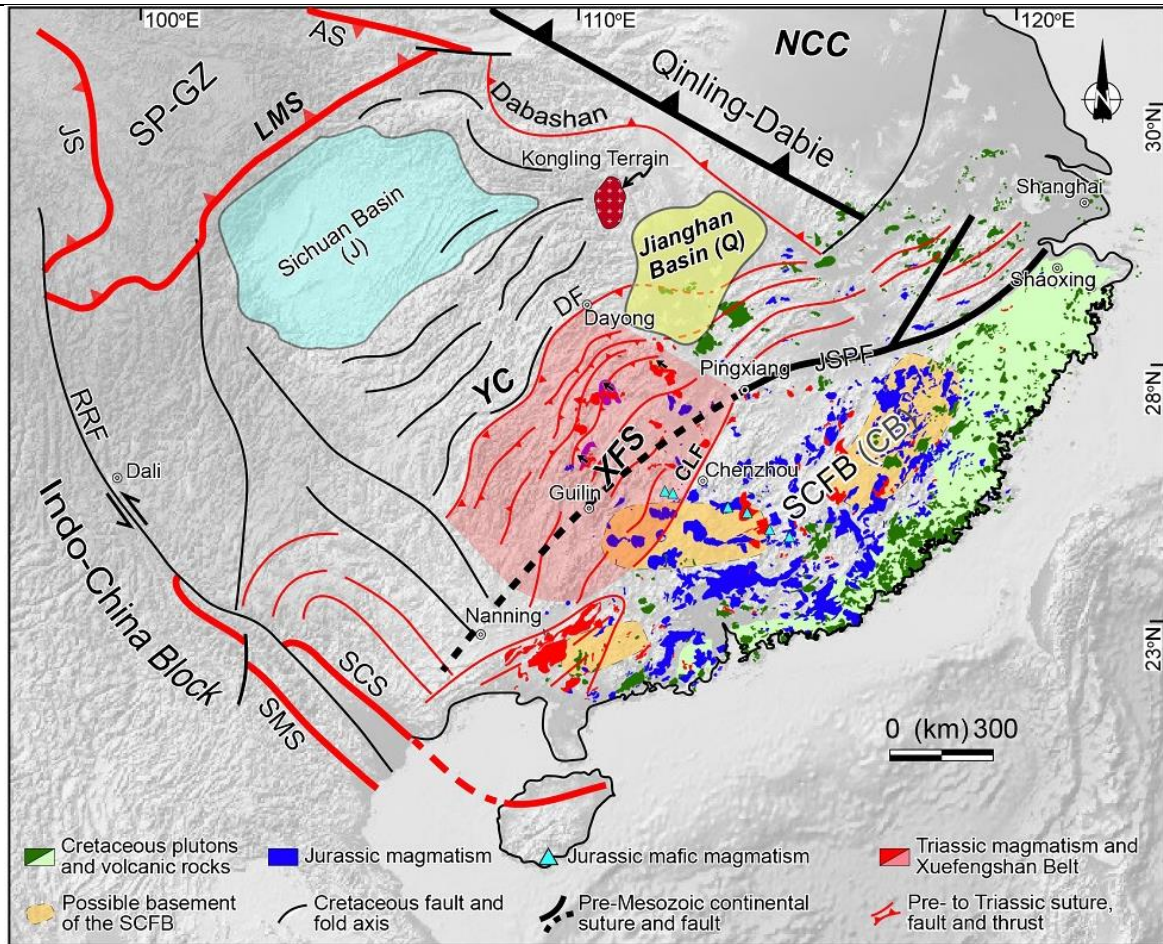


Figure 2-2. Tectonic framework of the South China Block and distribution of the Mesozoic magmatism (According to Zhou et al., 2006; He et al., 2010; Faure et al., 2016).

2.2.1 Pre-Triassic tectonic evolution of the South China Block

The collision between Yangtze and Cathaysia at the Neoproterozoic time along the Jiangshan-Shaoxing Suture has long been studied and the final closure time is considered at ca. 825Ma along the NE-SW striking Jiangshan-Shaoxing suture (Guo et al., 1989, 2001; Ren et al., 1989; Li and Li 2007; Shu et al., 2012), forming the so-called the Jiangnan orogen. Subsequently, the rifting of the continental crust inside the South China Block occurred along or cross-cut the suture zone, evidenced by the Neoproterozoic rifting related sediments from 820Ma to 690Ma (Fig. 2-1; Wang et al., 2003a). During the early Paleozoic time, the Sinian to Ordovician strata are strongly deformed by S-verging folds. Some parts underwent an amphibolite facies metamorphism followed by crustal melting giving rise to migmatites and S-type granites (Faure et al., 2009, Charvet et al., 2010). The Silurian strata are missing in the Cathaysia Block. In the Nanling area, the Paleozoic fold axis strike nearly E-W trending. Furthermore, the early Paleozoic (440-425Ma) magmatism (Zhou et al., 2006; Huang et al., 2013; Wang et al., 2013b) and migmatization (Liu et al., 2010; Wang et al., 2013a) were also reported in the Cathaysia Block. The significance of the rift closure, and these intracontinental tectonics remains unclear.

2.2.2 The Qinling-Dabie orogen

The collision of the North China Craton with the South China Block at the Paleozoic time took place along the Qinling-Dabie suture (Fig. 2-1 in chapter 3; Mattauer et al. 1985; Faure et al.; 1999; Hacker et al., 2004). After a Carboniferous-Permian rifting in the south foreland of the Qinling orogen, and the closure of this basin driven the subduction of the South China Block under the North China Block, exhumed UHP minerals, such as coesite, between 240-230Ma dated by the SHRIMP U-Pb on coesite-bearing domains of metamorphic zircon (Xu et al., 2006).

2.2.3 The Longmenshan thrust belt

The subduction of the South China Block under the Songpan-Ganzhi block occurred along the Longmenshan thrust belt, located at the NW margin of the South China Block (Burchfiel et al., 1995). Meanwhile, the opposite-subduction along the Animaqin and Jinshajiang sutures in the north and south (Fig. 2-2), respectively, produces the syn-tectonic magmatism in the Songpan-Ganzhi area (Roger et al., 2008, 2010; Yan et al., 2011). Due to the huge thickness of flysch cover, the nature of the basement of the Songpan-Ganzhi block is still ambiguous. However, the southeastward thrust of the Songpan-Ganzhi sediments during the middle to late Triassic time is supported by the $^{40}\text{Ar}/^{39}\text{Ar}$ dating at $237 \pm 0.9\text{Ma}$ (Yan et al., 2011) and the early Jurassic strata unconformably overlain on late Triassic strata with the youngest concordia detrital zircon age at 203Ma (Luo et al., 2014), indicating that the Longmenshan thrust belt was activated during 237 to 200Ma.

2.2.4 The Indochina - South China Block collision

The closure of the eastern branch of the Paleo-Tethyan Ocean resulted from the southward subduction of the South China Block below the Indochina Block the Jinshajiang-Songma-Songchai suture (Liu et al, 2012; Faure et al., 2014, 2016; Lepvrier et al., 2004 and references therein), which has been reworked by the Red River sinistral fault at the Cenozoic (Leloup et al., 1995). The final collision age, defined by the Norian unconformity contact, $^{40}\text{Ar}/^{39}\text{Ar}$, monazite U-Th-Pb and zircon U-Pb dating on the post-orogenic granite, is supposed between 245 to 220Ma (Faure et al., 2016 and references therein). The subduction of the South China Block under the Indochina Block may relate to the bended and nearly E-W trending fold (Fig. 2-2) and the S-type Darongshan granite ($230 \pm 4\text{Ma}$; Deng et al., 2004).

2.2.5 Triassic intracontinental deformation

The Triassic intracontinental deformation was identified in the Xuefengshan area at the northwestern margin of the Cathaysia Block (Fig. 2-2), characterized by a series of NE-SW

extending fold-thrust and back thrust (Chu et al., 2012a, 2012b). The U-(Th)-Pb dating of monazite from the metamorphic rocks of the lower part of the decollement at 243-226Ma and U-Pb dating of the zircon from the granite, which intruded in the Xuefengshan thrust belt at 225-215Ma. The Triassic deformation is mainly concentrated on the Cathaysia Block and circum-SCB. The Triassic and Jurassic strata of the Yangtze block were involved in the NE-SW trending fold, which is considered as Cretaceous related events, the Dayong fault is the boundary separating the Triassic event in the southeastern part and Cretaceous one in the northwestern part (Fig. 2-2; Yan et al., 2003).

To sum up, during the Triassic time, the South China Block collided with its surrounding blocks. The visible deformation occurred along the tectonic boundary, such as Qinling-Dabie, Longmenshan, Jinshajiang, Ailaoshan, Song Ma, SongChay and within the Cathaysia block. Part of the deformation is accommodated by thick sedimentary deposition in Songpan-Ganzi and the NE part of the Yangtze block and the Nanpanjiang basin in the SW part.

2.2.6 Mesozoic magmatism in the South China Block

The Mesozoic magmatism is widely distributed in South China with a surface of ca. 135,000 km². The relative surface proportion among the Triassic, Jurassic and Cretaceous granites are about of 40%, 46% and 14%, relatively (Fig. 2-2). The granites are usually classified according to the typical mineral association, for example, the amphibole bearing granite for I type, the cordierite-tourmaline-primary muscovite bearing granite for S type, and some chemical index (A/CNK) values.

Previous petrological and whole rock geochemical studies show that the majority of Triassic granites are peraluminous with A/CNK > 1.1 and typical S-type minerals, such as cordierite and garnet in the Darongshan granite (233±5Ma, Deng et al., 2004, 2005), euhedral muscovite in the Yangmingshan two-mica granite (218±10Ma, Chen et al., 2006), tourmaline and garnet in the Maofeng fine grained two-mica granite (219.6 ±0.9Ma, Ling et al., 2005), and these granites are thought to be developed in the inland area of the South China Block. However, recent studies find more and more Triassic granites also developed in the coastal area, e.g. the Qiuwang syenogranite 225 ± 2Ma and the Dashuang syenite 224.3 ± 2.9Ma (Zhu et al., 2013, 2016). Moreover, the zircon εHf (t) values of Triassic granites (230-210Ma) range from -2.8 to -8.7 (mean value at -5.4), confirming that the Triassic granite may be derived from the partial melting of the Cathaysia basement (Shu et al., 2015), nevertheless, the mechanism for the partial melting is still unclear.

The planar distribution of Jurassic granites (Fig. 1-8; Li et al., 2009), with the highest volume among the Mesozoic granites and the peak age at ca.160 Ma, mainly consist of metaluminous to weak peraluminous granite associated with little volcanic and mafic rocks. No large scaled contemporary basins can be found in SCB.

The Cretaceous magmatism differs from Triassic and Jurassic ones, and is characterized by the

presence of adakitic rocks, being the typical subduction related rock, and the widely distributed volcanism and plutonism in the coastal area (Xu et al., 2002; Wang et al., 2006). The geochemical investigations show typical island arc features, i.e. enrichment of LREE and LILE, lack of Nb and Ta (Li et al., 2000; Guo et al., 2012). Furthermore, the Cretaceous magmatism is accommodated with large scaled half-graben basins developed in South China Block (Li et al., 2014). Based on those observations, the Cretaceous magmatism is considered to be developed under a back-arc extensional regime (Li et al., 2000).

Chapter 3. Incremental emplacement of the late Jurassic mid-crustal, lopolith-like Qitianling pluton, South China, revealed by AMS and Bouguer gravity data

3.1 Introduction

Magmatic rocks form a large proportion of the continental crust. Constraining the production, segregation, ascent and emplacement or eruption of magmas is thus of fundamental importance for a comprehensive understanding of the evolution of the continental crust. Characterizing the emplacement of intrusions and intrusion-country-rock relations may provide key constraints on geodynamic or tectonic setting, brittle to ductile crustal behaviour, and volumes and rates of magma transfer within the crust or between mantle and crust (e.g., Byerly et al., 2016; de Saint-Blanquat et al., 2011; Paterson, 2009). On the basis of previous studies of the geometry, petrology and duration of the construction of intrusions, combined with researches on the fabrics and physical properties of intrusive bodies and country rocks, and spatially and/or temporally related regional tectonics, several end-member models for crustal magma ascent and emplacement have been proposed: (1) ascent and emplacement by dyking [e.g., Gudmundsson, 2011; Hutton, 1992; Ni et al., 2016; Scaillet et al., 1996], (2) magma ascent and emplacement in diapirs (e.g., Bateman, 1984; He et al., 2009; Petro et al., 2013), and (3) ascent through dyking or in diapirs yet emplacement in tabular, i.e. laccoliths, sills or lopoliths (e.g., Morgan et al., 1998; O'Driscoll et al., 2006; Scaillet et al., 1995; Schofield et al., 2012; Stevenson et al., 2007). Magma ascent and transport may take place syn-tectonically (e.g., Allibon et al., 2011; de Saint Blanquat and Tikoff, 1997; Wei et al., 2016) or during periods of tectonic quiescence (e.g., de Saint-Blanquat et al., 2006). Most studies have been carried out on plutons which were emplaced into the upper continental crust (i.e. at depths of <10 km) (e.g., Cruden, 1998; Petford et al., 2000 and references therein), while emplacement of plutons in mid- and deep- crustal level has been investigated in fewer studies (Clemens et al., 2017; de Saint-Blanquat et al., 2001; Dumond et al., 2005).

The South China Block (SCB), which hosts the Qitianling pluton that we have studied, comprises abundant Mesozoic granitic plutons that crop out over >127,000 km² (Zhou et al., 2006). Jurassic plutons make up ~30-40 % of the exposure of the Mesozoic granites (Fig. 3-1b). Numerous geochronological and geochemical studies have been carried out on the Jurassic plutons (Chen and Jahn, 1998; Zhou et al., 2006 and references therein), but no quantitative data are available to constrain their internal fabric and granite-country-rock intrusive relations (Zhu et al., 2009). The Qitianling pluton, which formed at ~146-163 Ma (SHRIMP and LA-ICP-MS zircon U-Pb ages by Zhu et al., (2009)) in the southeastern part of the SCB, is a well-known example of a mid-crustal intrusion, which crystallized at $\geq 3.6 \pm 0.9$ kbar and thus a depth of $\geq 9-14$ km (Zhao et al.,

2005).

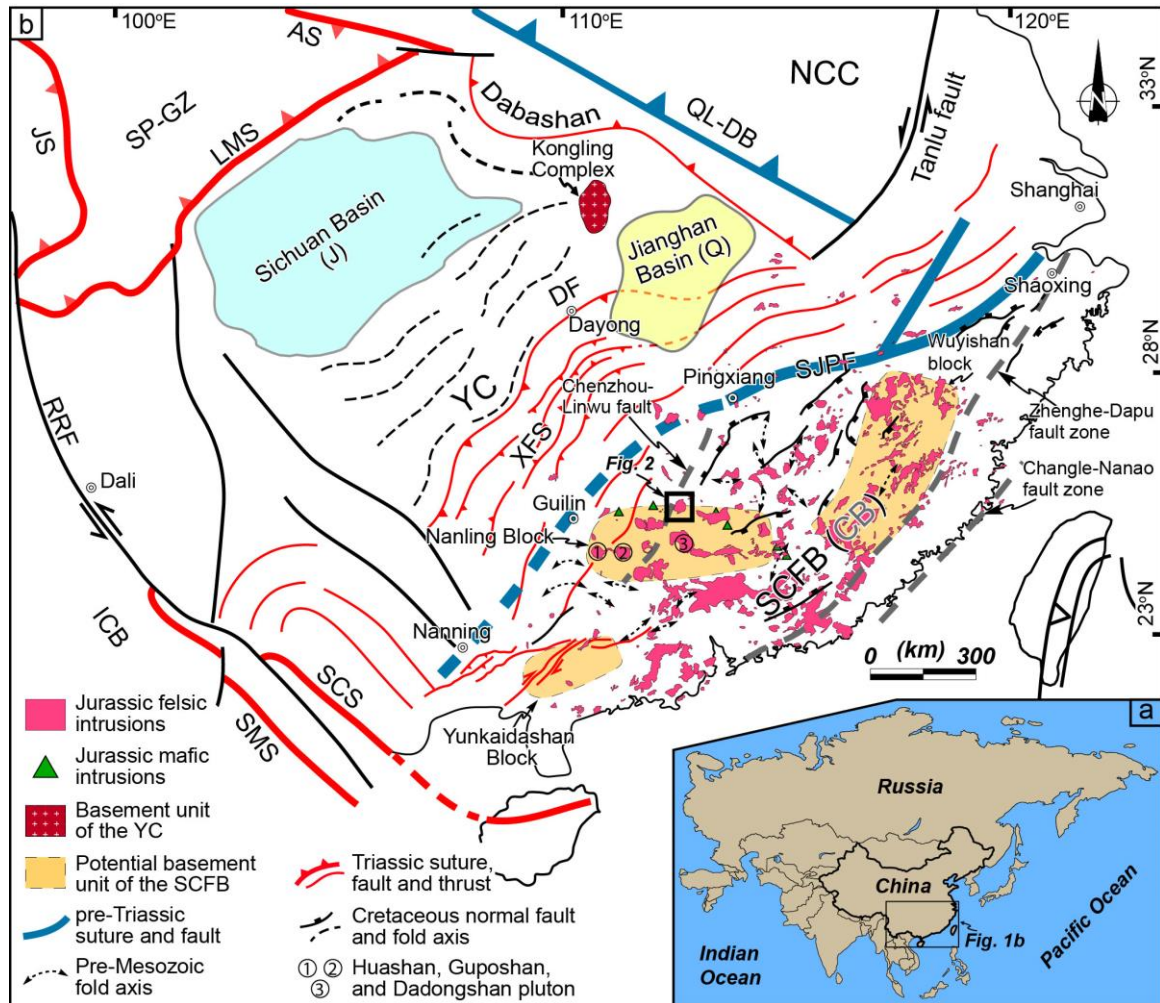


Figure 3-1. (a) Map of the Asian continent; (b) Tectonic framework of the South China Block and exposure of Jurassic felsic and mafic intrusions. The inset in (b) indicates the location of the Qitianling pluton. Abbreviations are: NCC: North China Craton, SP-GZ: Songpan-Ganzi Block, ICB: Indo-China Block, YC: Yangtze Craton, CB: Cathaysia Block, SCFB: South China Fold Belt, QL-DB: Qinling-DabieOrogen, LMS: Longmenshan Suture, JS: Jinshajiang Suture, SJPF: Shaoxing-Jiangshan-Pingxiang Fault, AS: Animaqin Suture, RRF: Red River Fault, SCS: Songchai Suture, SMS: Songma Suture, XFS: Xuefengshan Belt, DF: Dayong Fault. The Sichuan Basin is covered by thick Jurassic (J) sediments. The Jiangnan Basin is a Quaternary (Q) sedimentary basin.

In order to put constraints on the emplacement mechanism of mid-crustal intrusions and to provide insights into the crustal evolution of the SCB, the Qitianling intrusion was targeted because (1) its internal magmatic textures and sharp granite-country-rock contact are representative for most of the Jurassic granites in SE China (Zhou et al., 2006), (2) its geochemical variation and intrusion ages are well documented, (3) its emplacement depth is constrained, (4) Bouguer gravity anomaly data are available for restoring the 3D geometry of the pluton, and (5) it has larger and mostly unaltered outcrops (in quarries) compared to other Jurassic intrusions of the SCB. In this paper, we

present detailed field and microscopic observations, Anisotropy of Magnetic Susceptibility (AMS) measurements and gravity modelling to comprehensively characterize the emplacement mechanism and the evolution of the Qitianling pluton.

3.2 Geological setting

2.1 The South China Block

The South China Block (SCB) is a composite continental plate that was formed by the amalgamation of the Yangtze Craton in its northwestern part and the Cathaysia Block in its southeastern part along the NE-SW-striking Shaoxing-Jiangshan-Pingxiang Fault (SJPF in Fig. 3-1b) at ~850 Ma (e.g., Li et al., 2008; Faure et al., 2016). According to previous studies, the nature and basement compositions of the Yangtze Craton and the Cathaysia Block are significantly different (Fig. 3-1) (Chen and Jahn, 1998; Fletcher et al., 2004). The Yangtze Craton is a rigid and stable craton consisting of Precambrian basement including Archean TTGs (~3.3Ga Kongling Complex in Fig. 3-1b) (Gao et al., 2011). Geophysical data have revealed a homogeneous and ~45 km thick crust (Deng et al., 2014). The Cathaysia Block also comprises Precambrian basement, but it consists of at least three micro-blocks, namely, the Wuyishan, Nanling and Yunkaidashan sub-units comprising Paleo- to Mesoproterozoic (~1.1-2.5 Ga) metasedimentary and intrusive rocks (Wan et al., 2007; Yu et al., 2009, 2010). Geophysical investigations have also revealed heterogeneous density layers, indicating a complex crustal structure (Deng et al., 2014; Fletcher et al., 2004).

The SCB as a whole has experienced pervasive and polyphase tectono-magmatic events after its agglomeration at ~850 Ma: (1) Neoproterozoic rifting (Nanhua rifting) (Shu et al., 2011a; Wang and Li, 2003; Zheng et al., 2008), (2) an Early Paleozoic intracontinental orogeny (Charvet et al., 2010; Faure et al., 2009; Wang et al., 2010; Zhang et al., 2013), (3) Middle Triassic continental collision with the Indochina block to the south/southwest and with the North China block to the north (Faure et al., 2008, 2014; Gilder et al., 1999; Lin et al., 2005), and (4) Mid-Triassic intracontinental deformation along the NNE-SSW-striking Xuefengshan belt in the central part of the SCB (Fig. 3-1b) (Chu et al., 2012; Wang et al., 2007; Yan et al., 2011). Intense regional deformation has thus reworked not only the borders of the SCB in the northern (Qinling-Dabie-DabaShan), western (Longmenshan) and southwestern (Yunkaidashan-Ailaoshan) parts, but also the central part of the SCB (red solid lines in Fig. 3-1b). The southeastern central part of the SCB, the highly deformed ancient Cathaysia Block, was most extensively involved in regional deformation events possibly due to its low basement rigidity, and this region has thus been referred to as the South China Fold Belt (SCFB in Fig. 3-1) (Huang, 1945).

Jurassic strata, however, which mostly consist of sandstone in the study area, show only large-scale open folds, showing on evidence for penetrative deformation (i.e. high-temperature

foliations or lineations) (Shu et al., 2009) following the Triassic. Evidence for ductile or syn-emplacement deformation is equally devoid in Jurassic plutons in the SCB, including the Qitianling pluton and the spatially associated Huashan-Guposhan and Dadongshan plutons (Fig. 3-1b) (Feng et al., 2012; Shu et al., 2011b). The Jurassic plutons in SE China moreover show a random distribution (Fig. 3-1), i.e. they are in no way spatially grouped (e.g., in linear intrusive belts).

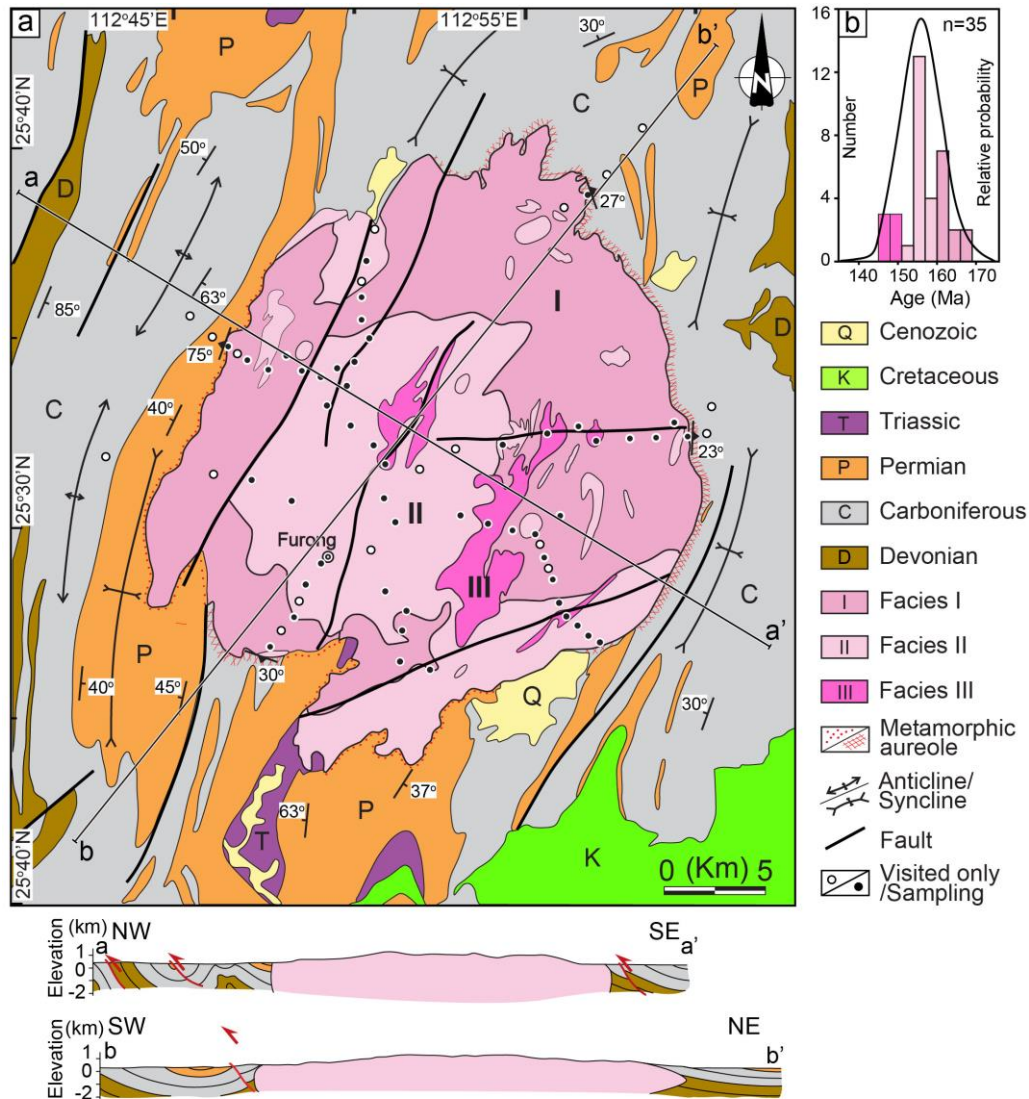


Figure 3-2. (a) Geological map of the Qitianling pluton and its country rocks with two geological profiles, i.e. aa' and bb' (modified after Zhu et al., 2009); (b) zircon U-Pb ages of the Qitianling pluton compiled from Zhu et al. (2009). Filled black and grey circles mark outcrops that were sampled and observed only, respectively.

2.2 The Qitianling pluton

The granitic Qitianling pluton has a sub-circular surface exposure with an area of ca. 530 km² (Figs. 3-1 and 3-2a). Zircon U-Pb ages of the granites range from ca. 146 Ma to 163 Ma (Fig. 3-2b) (Zhu et al., 2009). The pluton has intruded Carboniferous, Permian and Triassic strata comprising

limestone, mudstone and sandstone (Fig. 3-2a). Triassic and pre-Triassic strata are folded with NE-SW-striking fold axes (BGMHRN, 1988), forming part of the Xuefengshan fold-and-thrust belt. Mesozoic sediments are rare in the study area (Fig. 3-2a). The Qitianling pluton comprises three main granitic facies: (1) facies I, which consists of amphibole- and biotite-bearing, coarse- to medium-grained granite with locally abundant mafic enclaves and K-feldspar megacrysts (Figs. 3-2a, 3-4a and 3-4d); (2) facies II, which is composed of medium- to fine-grained, biotite±amphibole-bearing granite, and rare centimeter-sized mafic enclaves (Figs. 3-2a and 3-4b); and (3) facies III, which is a medium- to fine-grained biotite granite that lacks mafic enclaves (Figs. 3-2a and 3-4c). The three facies are metaluminous to weakly peraluminous with A/CNK values ranging between 0.91 and 1.1, and SiO₂ contents ranging between ~65% and 76% (Bai et al., 2005; Deng et al., 2005; Zhao et al., 2005). The composition of calcic amphibole in the facies I granites indicates a crystallization pressure of $\sim 3.6 \pm 0.9$ kbar (Zhao et al., 2005) calculated using Al-in-hornblende barometry.

3.3 Field observations and sampling

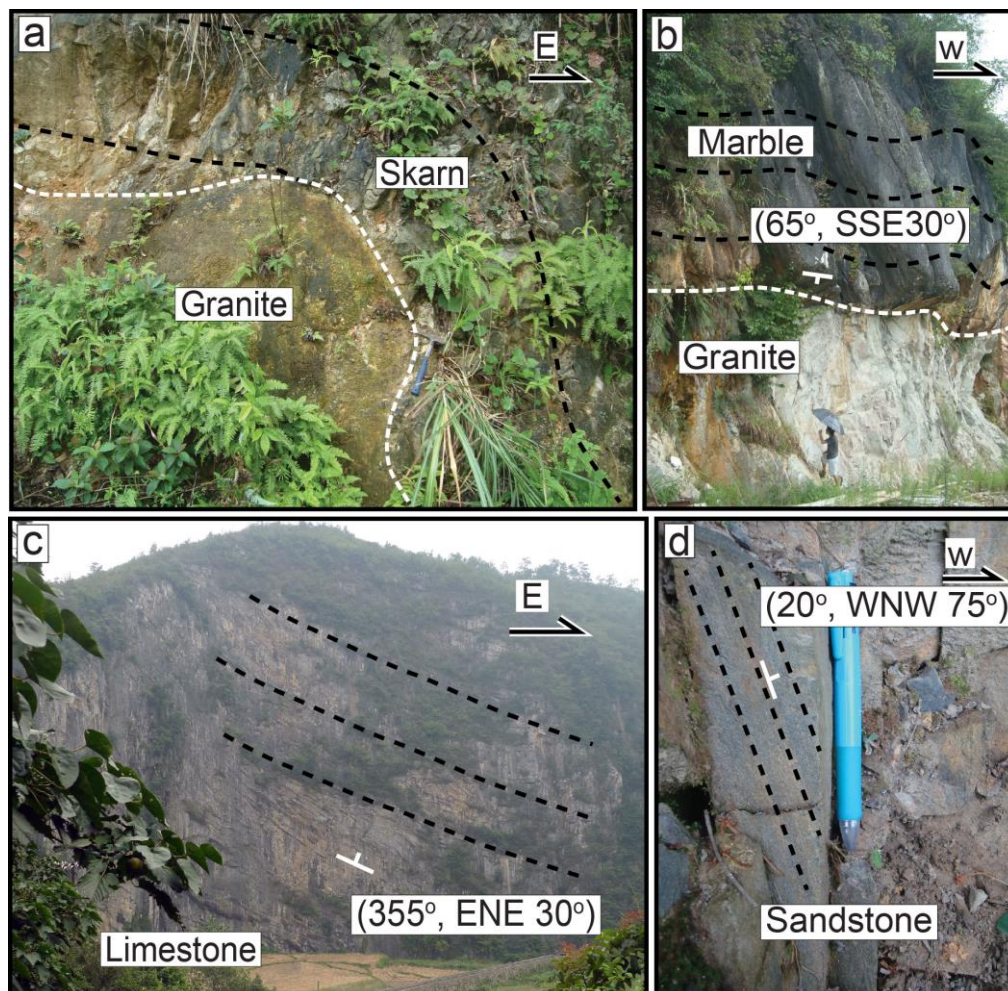


Figure 3-3. (a), (b), (c) and (d) The field photographs of the northern, southern, eastern and western contact zones between the pluton and its wall rocks, respectively. The black dashed lines highlight bedding in the country rocks, while the dashed white lines mark the contact between granites and

country rocks.

Our field investigations were conducted in seventy-two outcrops in the Qitianling pluton and its country rocks as well (Fig. 3-2). Previous mapping (BGMRHN, 1988; Zhu et al., 2009) and our observations show that the facies II granite forms the topographically most elevated parts (ca. 1356 m) of the intrusion, while facies I (ca. 340-980 m) and facies III granites (ca. 550 to 1130 m) occur at variable elevations (Fig. 3-2a and Table S1).

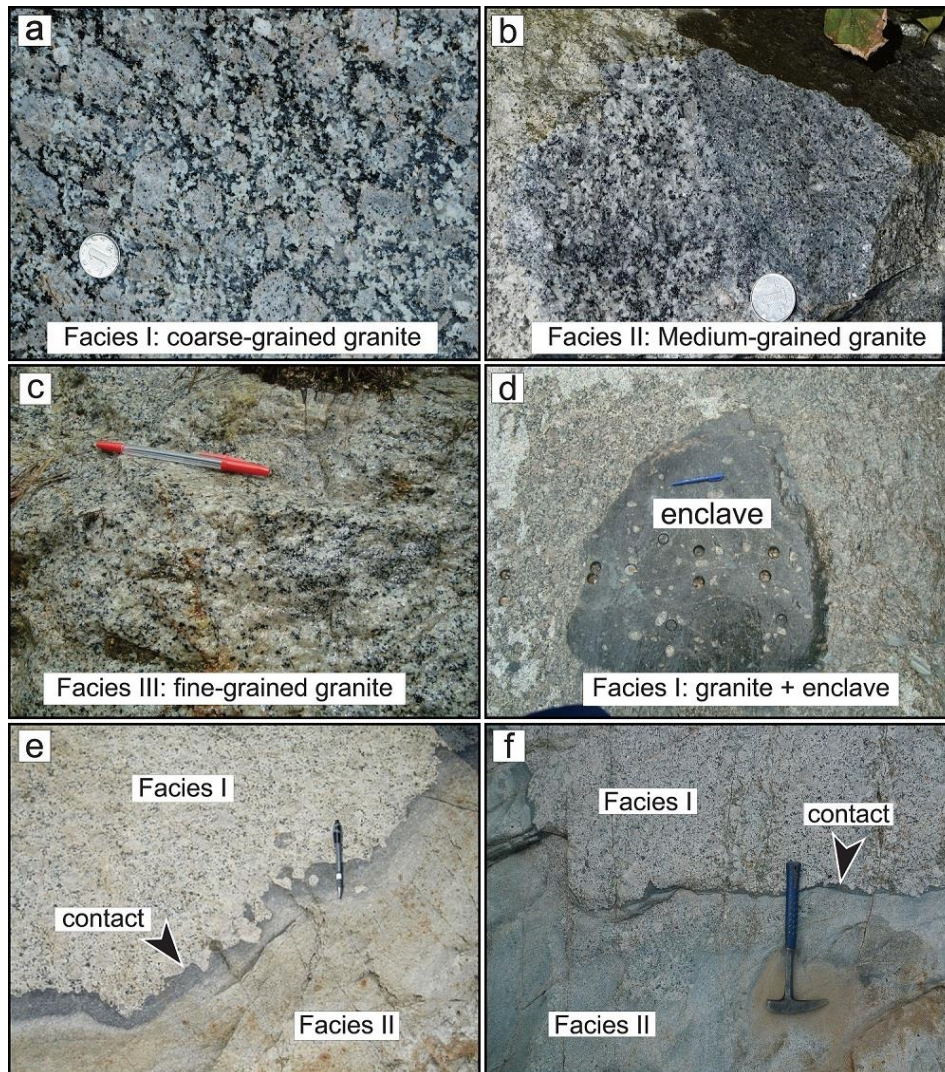


Figure 3-4. (a-c) characteristic exposures of facies I, facies II, and facies III granite; (d) a mafic enclave in the facies I granite; (e) and (f) a typical contact between the facies I and II granites.

The contact between the granites and the country rocks is irregular at the kilometer-scale with short granite lobes extending in NNE-SSW direction (Fig. 3-2). Country-rock xenoliths have not been observed in the field. The northern, southern and eastern margins of the pluton have gently outward dipping ($\sim 20-30^\circ$; Figs. 3-2, 3-3a, 3-3b and 3-3c) contacts with the country rocks. In contrast, the exposed granite-country-rock contact at the western margin is sub-vertical (Fig. 3-3d). Hornfels textures can be recognized within 5 to 10 metres wide zones in the Permian country rocks

(sandstones), and in 200 meter wide skarn zones along the northeastern contact. The bedding of the country rocks is tilted outward in the southwest and inward in the northwestern parts of the pluton which may be an inherited Triassic deformation feature or a feature developed during pluton emplacement (Fig. 3-3d). Locally, the country-rock bedding is irregular and bent close to the contact with the granite (Figs. 3-3a and 3-3b). However, both the skarn and hornfels contact zones lack foliations or lineations.

Contacts between the facies I and facies II granites are irregular wavy and gradational over ~10 cm, and they are characterized by a moderately steep dip (~30-60 °) toward to the pluton margin (Figs. 3-4e and 3-4f). The facies II granites are fine-grained and biotite-rich within ~5 cm of the contact, while the facies I granites show no obvious textural or mineralogical zonation toward to the contact (Fig. 3-4e). Contacts of the facies III with the facies I and facies II are not observed. All three granite facies lack obvious magmatic foliations and lineations. K-feldspar megacrystals and coarse-grained minerals including amphibole, plagioclase and biotite, show no preferred orientation in the center of the pluton or close to its margins (Figs. 3-4a, 3-4b and 3-4c). Mafic, hornblende- or biotite-rich schlieren have not been observed, while some mafic micro-granitoid enclaves locally occur in the facies I granites. The micro-granitoid-enclaves are generally ~5 to 50 cm in maximum dimension, with aspect ratios of 0.4 to 0.8, and mostly 0.7 ± 0.1 (Figure S1). They are only weakly elongated, showing no preferred orientation, and they are also irregularly distributed in the pluton.

AMS measurements were carried out, because they provide quantitative structural data that may not be gained in classical field studies, often providing key insights for constraining magma emplacement process (e.g., Morgan et al., 2017). AMS sampling was carried out at fifty-three sites, located along six roads that cover the three lithological facies from different parts of the pluton and also the country rocks (Fig. 3-2). The outcrops chosen for AMS analyses all have large exposure (several tens of square metres), which allowed us to collect at least 6 drill cores at each site. The distance between the sampling sites was ~2 km (Fig. 3-2).

3.4 Methodology and results

4. 1. Microscopic observations

Five oriented and twenty non-oriented thin sections of facies I, II and III granites, and metasandstone country rocks were used for mineralogical and qualitative textural characterization. Skarn country rocks were not further analyzed as they are severely altered (Fig. 3-3a). The facies I, II and III granites have typical magmatic fabrics, i.e. their main mineral components have euhedral-subhedral habitus, planar grain boundaries and they also lack high-temperature, intracrystalline deformation features (Figs. 3-5a, 3-5b and 3-5c). Consistent with these observations, none of the minerals shows a preferred orientation on the macro- or the micro-scale, thus lacking a

record of obvious foliations or lineations. Plagioclase and K-feldspar are prismatic to subhedral-interstitial, lacking subgrains or deformation twins, while they show well developed polysynthetic and Carlsbad twinning (Fig. 3-5b). Quartz is subhedral-interstitial, showing evidence for weak high-temperature deformation, such as undulose extinction and chessboard patterns. Sutured grain boundaries or subgrains are not developed. Biotite is characterized by subhedral-euhedral shape and straight cleavage planes with no evidence for bending or kinking (Figs. 3-5a, 3-5b and 3-5c). Magnetite and ilmenite are important accessory minerals (Figs. 3-5d and 3-5e). They are commonly intergrown with biotite with their long axis parallel to the biotite cleavage (Fig. 3-5d), or they occur as subhedral interstitial crystals (Fig. 3-5e).

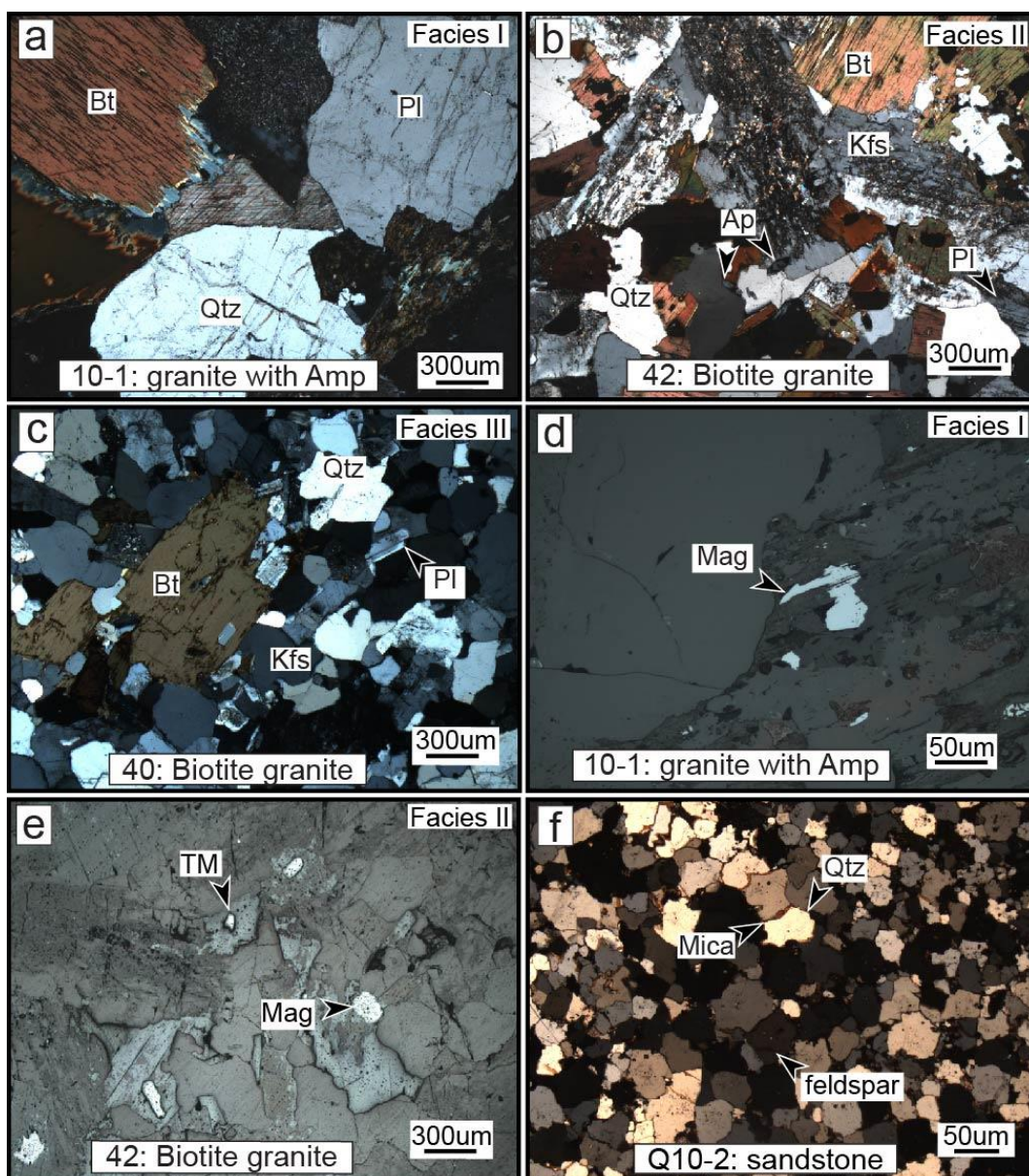


Figure 3-5. Microphotographs in crossed polarized light of (a-c) the facies I, II and III Qitianling granites; (d-e) microphotographs in reflected light of magnetite in facies I and facies II granites; and (f) microphotograph in crossed polarized light of a Permian metasandstone from within the thermal aureole of the Qitianling pluton. Abbreviations are: Ap: Apatite, Bt: Biotite, Kfs: K-feldspar, Mag: Magnetite; Pl: Plagioclase, Qtz: Quartz, TM: Titanomagnetite.

Metasandstone hornfels from the contact zones is characterized by an assemblage of fine-grained, equant quartz, feldspar and biotite grains (Fig. 3-5f). Andalusite or sillimanite have not been observed. Quartz shows rare sutured grain boundaries, but no undulose extinction or other high-temperature deformation features, indicating that high-temperature annealing took place after weak deformation. Biotite is subhedral to euhedral, free of bending or kinking. The microscopic observations thus reinforce our field observations, highlighting that the Qitianling pluton and its country rocks are devoid of significant intrusion-related brittle or ductile deformation.

4. 2. Magnetic mineralogical analysis

To characterize the carriers of the magnetic susceptibility of our samples for AMS analysis, i.e. diamagnetic, paramagnetic and ferromagnetic minerals, we have performed (1) a thermomagnetic characterization using a KLY3 kappabridge coupled with a CS3 furnace, (2) an isothermal remanence magnetization measurement with an IM30 pulsed magnetizer and a JR5 spinner magnetometer at the Institut des Sciences de la Terre d'Orléans (ISTO), and (3) magnetic hysteresis loop characterization using a vibrating magnetometer at the Laboratoire de Paleomagnétisme of the Institut de Physique du Globe de Paris (IPGP).

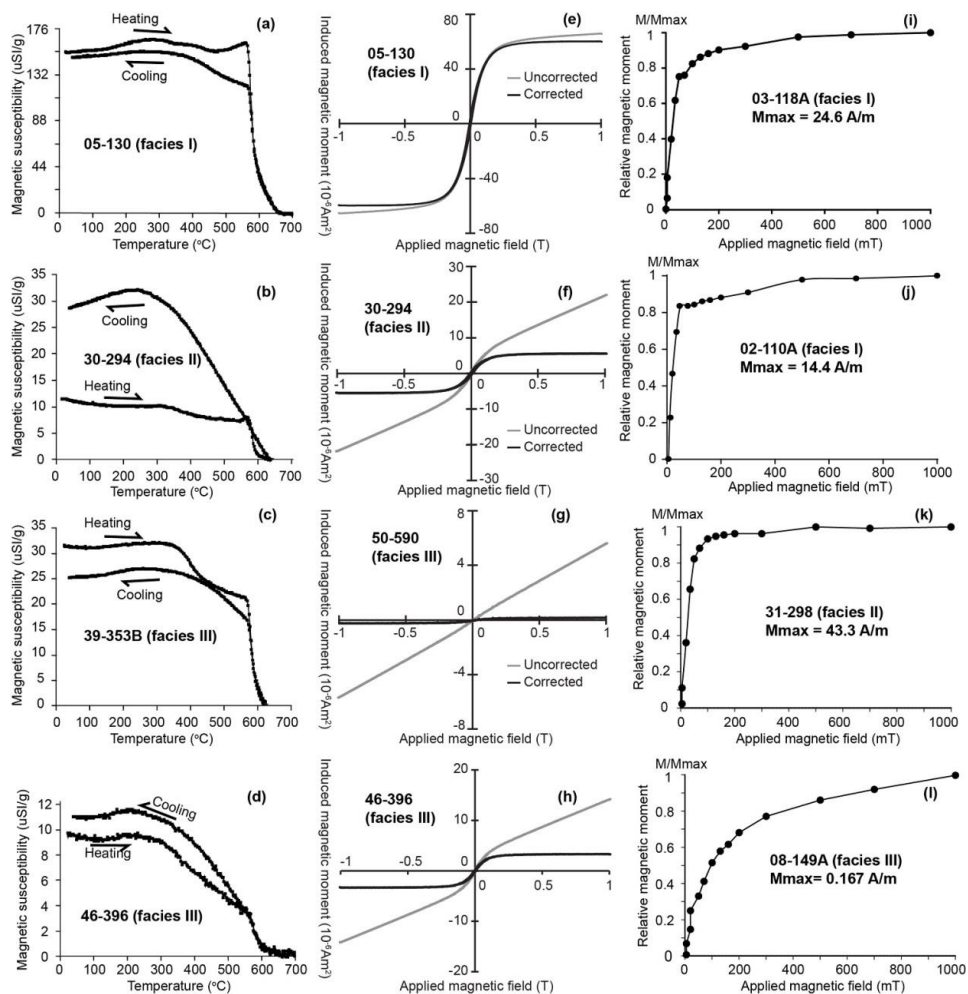


Figure 3-6. Magnetic mineralogical analyses of the three facies of the Qitianling pluton.

A total of ten fresh samples from the three granite facies were chosen for magnetic mineralogical analysis. Figure 3-6 shows representative results. The thermomagnetic measurements on all granites facies show a rapid drop of the magnetic susceptibility at 580°C (Figs. 3-6a, 3-6b, 3-6c and 3-6d) indicating the presence of magnetite. The facies II and facies III samples show an obvious continuous increase in susceptibility upon cooling (owing to oxidation reactions; Figs. 3-6b and 3-6d), and the gradually decrease of the magnetic susceptibility between 210 °C to 580 °C (Fig. 3-6d), indicating the presence of titano-magnetite in the granite. The hysteresis curve of the facies I granites (Fig. 3-6e) shows a dominance of ferromagnetic susceptibility (magnetite), and those of the facies II and III granites (Figs. 3-6f, 3-6g and 3-6h) highlight that the varying content of ferromagnetic minerals and the magnetic susceptibility predominantly relates to the presence of paramagnetic minerals (e.g., hornblende, biotite and feldspar) and that magnetite is a comparatively subordinate carrier. Sudden saturation of the isothermal magnetic remanence at ~50 mT is characteristic for the facies I and II granite samples (Figs. 3-6i, 3-6j and 3-6k), indicating the preservation of ferromagnetic minerals. The facies III samples, which have the lowest magnetic remanence intensity among all samples, show gradual saturation (Fig. 3-6l), suggesting that the paramagnetic minerals are probably the major magnetic carriers. Figure 3-7 plots all the hysteresis loop measurements, and reveals that the majority of magnetite of the analyzed samples is in the pseudo-single-domain zone (Day et al., 1977; Dunlop, 2002). This implies that the principal axis of the magnetic susceptibility ellipsoid concurs with the major morphological axis of minerals, thus recording magmatic or tectonic foliations and/or lineations (e.g., Borradaile and Mothersill, 1984).

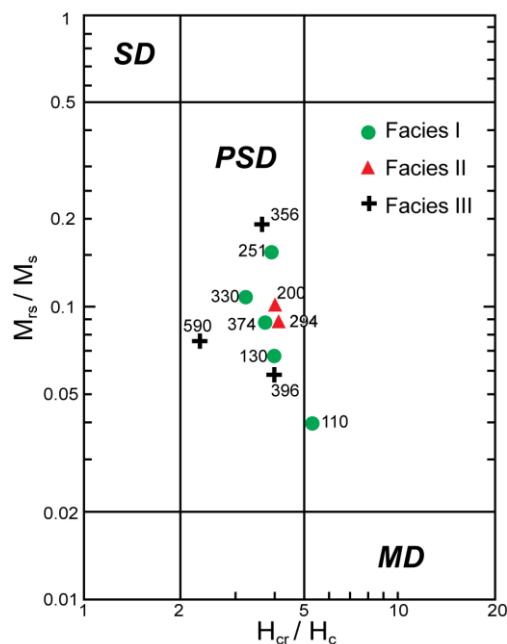


Figure 3-7. Day-plot of hysteresis parameters for the Qitianling pluton. M_{rs} : the saturation intensity of magnetic remanence, M_s : the saturation intensity of induced magnetization, H_{cr} : the coercivity of magnetic remanence, H_r : coercivity of the measured sample. SD: Single-Domain, PSD:

Pseudo-Single-Domain, MD: Multidomain.

4. 3. AMS parameters

The AMS measurements were carried out with a KLY3 Kapprabridge at the Institut des Sciences de la Terre d'Orléans. The intensity of the bulk magnetic susceptibility of the three granite facies decreases from facies I to III with mean intensities of 35.06×10^{-4} SI, 27.25×10^{-4} SI, and 2.94×10^{-4} SI, respectively (Fig. 3-8a). All measured samples have a relatively low anisotropy degree except for site 30 (PJ<1.12; Fig. 3-8b). The bulk magnetic susceptibility (Km) and the degree of anisotropy (PJ) are not correlated (Fig. 3-8b). The shape parameter (T) mainly ranges between -0.64 and 0.88 (Fig. 3-8c), showing a dominant oblate shape (ca. 80%) for the magnetic fabrics.

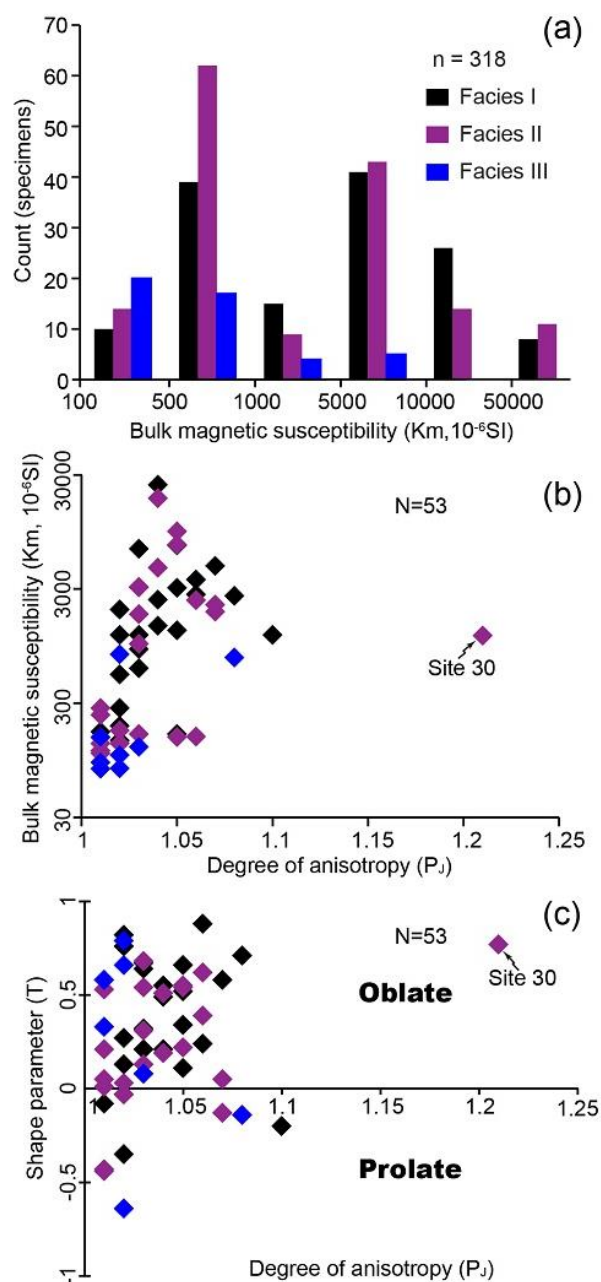


Figure 3-8. (a) Distribution of bulk magnetic susceptibility of the three granite facies in the Qitianling pluton; (b) and (c) parameters of anisotropy of the magnetic susceptibility.

4. 4. AMS results

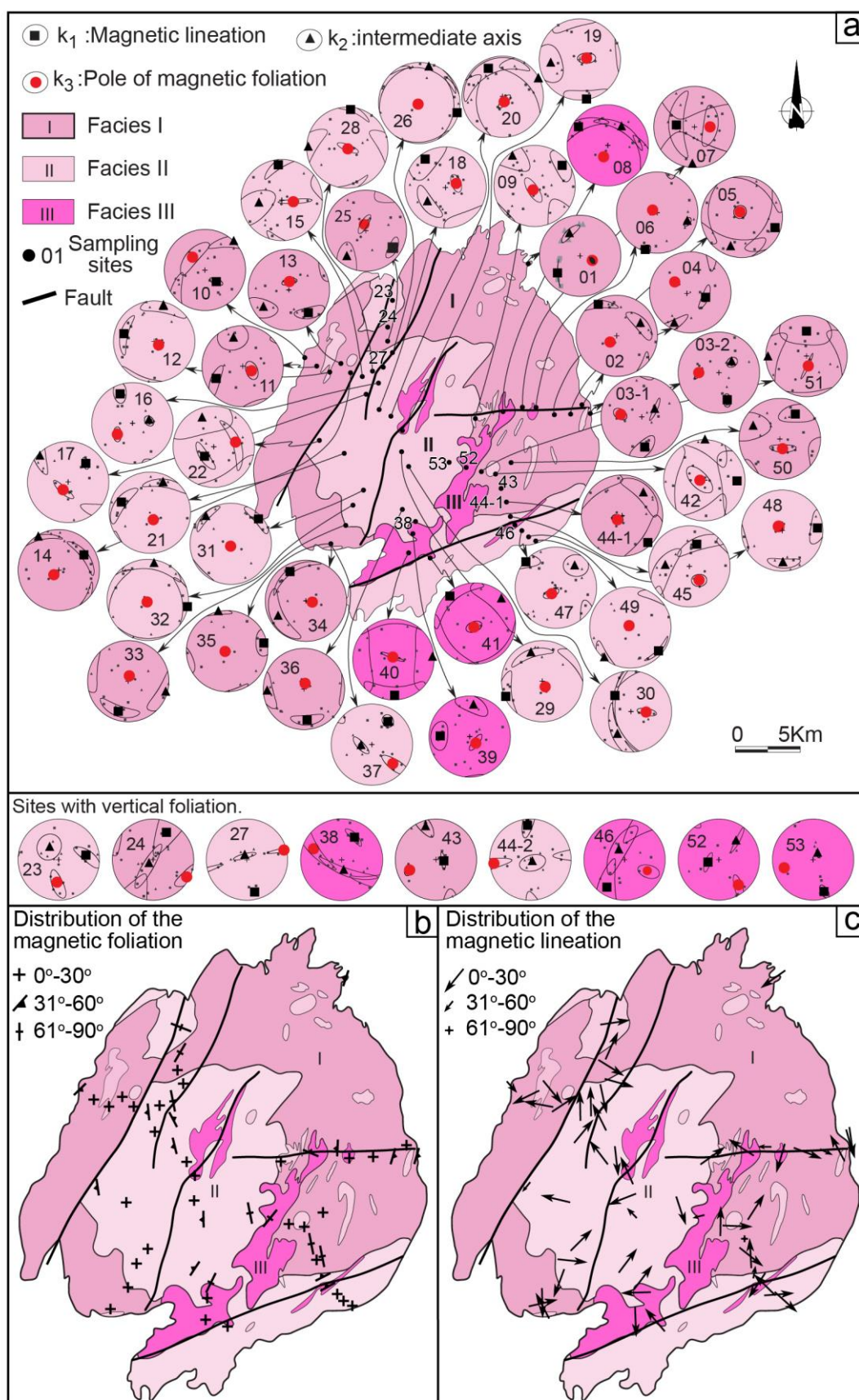


Figure 3-9. (a) AMS results for each sampling site in the Qitianling pluton, (b) and (c) distribution of the average magnetic foliations (K3) and lineations (K1) for each site. Averages were determined for 5-10 measurements per site. Small inset numbers are site numbers referred to in the text.

Figure 3-9 shows the AMS results for all 318 specimen from 53 sites of the Qitianling pluton. Detailed data are provided in the supporting information Table S1. At the site scale, the poles of the magnetic foliation (k3) are highly grouped. The majority of the granite specimen from 30 sites show horizontal to sub-horizontal foliations (Fig. 3-9a) with dip angles of $\sim 9^\circ$ to 23° (Table S1). These foliations characterize most of the exposure of the pluton including outcrops of the central part as well as outcrops close to pluton margins (Fig. 3-9b). Sites located at the eastern, northeastern and southwestern margins of the pluton, however, show outward dipping magnetic foliations.

Specimen from nine sites have steep to moderately steep magnetic foliations (dip angles $> 60^\circ$). Four of these sites (23, 24, 27 and 46) are close to map-scale fault planes, two sites (38 and 52) are located at the contact between facies II and facies III granites, while two other sites (43 and 53) are $> 3\text{km}$ away from apparent fault planes but close to facies contacts, and one additional site (44-2) is characterized by sub-vertical magnetic foliations. In addition, these foliations have variable orientations with a high standard deviation of 37° (Table S1). The remaining thirteen sites have moderately steep foliations with dip angles between 31° and 60° and mostly $< 45^\circ$ with irregular dip directions. These sites are located (1) near granite-country rock contacts (sites 01, 03, 04 and 10), (2) near facies contacts (sites 08 and 45), or (3) in fault areas (sites 07, 15, 16, 18, 22), otherwise (4) in the central parts of the facies II granites (sites 30 and 37). The magnetic lineations (k1) are highly variable. Within single outcrops, lineations measured in different specimen vary significantly, consequently, the site mean declination (k1) values have standard deviations of $\sim 7^\circ$ to $\sim 75^\circ$ ($n=5\sim 10$; black squares in Fig. 3-9a; Table S1). Gently plunging lineations ($0\text{--}30^\circ$) are predominant, but steeply plunging ones ($>30^\circ\text{--}90^\circ$) do occur (Fig. 3-9c). Some, but not all of the outcrops with moderate ($30^\circ\text{--}60^\circ$) to steep ($60^\circ\text{--}90^\circ$) foliations, show steep lineations. Occasionally, neighbouring outcrops show sub-parallel average lineation orientations, but this pattern is highly variable, where lineation orientations from adjacent outcrops may also vary significantly (by $>45^\circ$). The locally present microgranitoid enclaves show magnetic foliations and lineations sub-parallel to these of their host granites (e.g., 03-1 and 03-2 in Fig. 3-9a).

4.5. Gravity modelling

Gravity modelling has been successfully applied to explore subsurface structures on the basis of gravity anomalies that reflect the density contrasts between crustal lithologies (e.g., Vigneresse, 1990; Martelet et al., 2013). We have applied this method to characterize the shape of the unexposed part of the Qitianling pluton. The primary data that we have used include: (1) Bouguer gravity anomaly data, (2) density values of major rock types, and (3) a digital elevation model of the Qitianling pluton and its surrounding area. The Bouguer gravity anomaly data are from the Chinese Bouguer gravity anomaly database, which are acquired, treated and provided by the geological survey center of China, i.e., (1) a 1:200,000 original Bouguer gravity anomaly map of

the Qitianling pluton, and (2) a 1:2,500,000 Bouguer gravity anomaly map of the Hunan province covering the Qitianling pluton and its country rocks. Density values of the facies I to III granite samples were measured at the Nanjing University using a Matsuhaku Electronic Densimeter GH-300. One granite sample from each sampling site was measured twice at a density precision of 0.001g/cm^3 . Fifty-three samples were measured, which show a closely comparable density (i.e. $2.62\pm 0.01\text{ g/cm}^3$; Table S2). Their mean density value of 2.62 g/cm^3 was therefore used for modelling the gravity anomaly of the pluton. The densities and thicknesses of the country rock previously measured by the Chinese Geological Bureau of Hunan Province (BGMRHN, 1988), were also used in this study (Table S3). The results show that the Silurian and the Ordovician strata with similar lithologies (flysch-like metasediments, metashales, and metacarbonates) have densities comparable to those of the Devonian strata (carbonates and terrigenous sediments). Due to the limited thickness of the Silurian and Ordovician strata in the study area (BGMRHN, 1988), an identical density value of 2.68 g/cm^3 was adopted for all the above-mentioned country rocks of the Qitianling pluton (Fig. 3-10 and Table S3). For the same reasons, density values of 2.54 g/cm^3 and 2.70 g/cm^3 were used for the Jurassic-Cretaceous strata, and for the Cambrian to Neoproterozoic strata, respectively (Table S3). The Digital Elevation Model for the Qitianling area, with a resolution of 90 m at the equator, has been downloaded from <http://srtm.csi.cgiar.org/>.

The original Bouguer gravity dataset consists of regional and long wavelength signals that include depth and surface signatures. To infer the subsurface shape of the pluton, regional long wavelength signals of the Bouguer anomaly corresponding to the deepest density contrasts were removed. The 1:2,500,000 regional Bouguer gravity anomaly map of Hunan province was used to calculate the long wavelength gravity anomaly trend using a low-pass Butterworth filter with cutoff wavelengths of 50 km, 70 km, 100 km and 150 km. Therein, the 100 km wavelength cutoff was chosen as the best regional trend as the residual Bouguer anomaly (original Bouguer anomaly minus regional trend) best matches gravity anomalies and surface geological features.

In the residual Bouguer gravity anomaly map (Fig. 3-10), the Qitianling pluton shows a negative anomaly with an anomaly center in its southwestern part (Fig. 3-10). The country rocks show variably positive anomalies. Seven independent cross-sections with twelve intersections were designed for gravity modelling (solid white lines in Fig. 3-10), including four NW-SE striking profiles, which are oriented perpendicular to the strike of the regional Triassic fold-thrust belt. The other three profiles were modelled in NE-SW direction, i.e. parallel to the regional tectonic axes. Subsequently, numerous repeated attempts were made to match all the profiles to have similar depth at the intersection. Altogether, the seven profiles show that the pluton has (1) a flat-top which is suggested by the low-angle ($<20^\circ$) intrusive contact, in particular along the NE-SW-striking profiles (EE', FF' and GG' in Fig. 3-10); (2) a maximal thickness of ~ 5 km in the southeastern part and a thickness that progressively decreases northeastwards to a minimum of ~ 1 km; (3) a roughly

symmetric geometry in NW-SE direction (profiles AA', BB', CC', DD' in Fig. 3-10); (4) a flat bottom without a significant relief, except for profile EE' which is likely affected by gravity signals from the country rocks; and thus (5) an overall tabular (laccolith, sill or lopolith) shape.

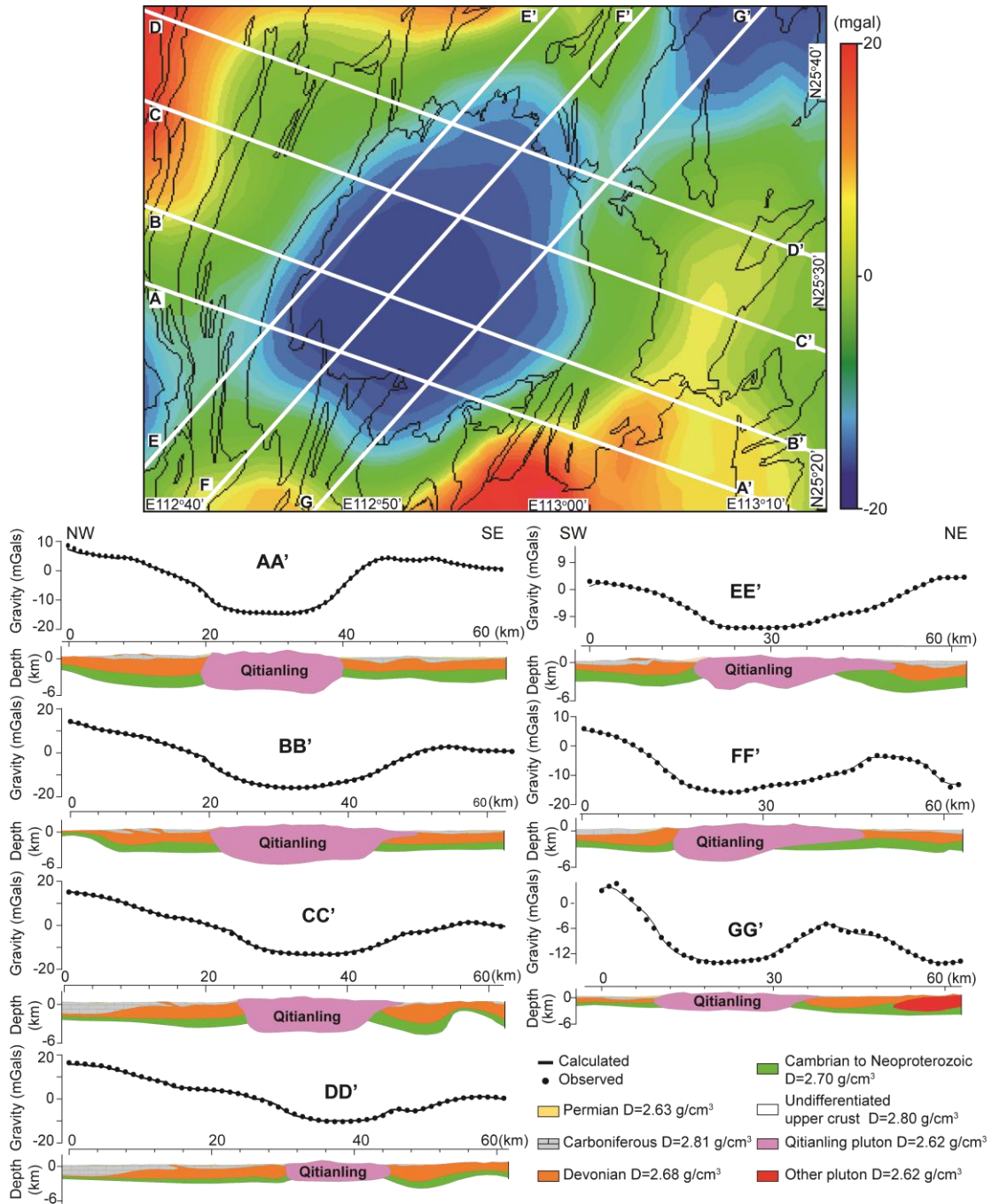


Figure 3-10. Residual Bouguer gravity anomaly map for the Qitianling area and interpreted profiles of Bouguer gravity anomalies. The thin black lines in the map outline surface geological boundaries (see Fig. 3-2 for comparison); the heavy white lines mark the location of the gravity modelling profiles. Profiles AA', BB', CC' and DD' extend in NW-SE direction, perpendicular to the Triassic fold axis developed in the wall rocks. Profiles EE', FF', and GG' extend in NE-SW direction, parallel to the Triassic fold axis of the wall rocks. The black dots and lines of the profiles are plots of measured residual Bouguer gravity anomaly values and calculated gravity anomalies, respectively.

3.5 Discussion

5.1. Origin of the magnetic fabrics

In the Qitianling pluton, 96% of the characterized sites have a degree of anisotropy (PJ) lower than 1.08 (Fig. 3-8b). Approximately 80% of the measured magnetic fabric ellipsoids plot in the oblate field (Fig. 3-8c). Microscopic observations indicate that magnetite is predominantly sub-equant (Fig. 3-5e), but some magnetite grains that occur subparallel to the biotite cleavage planes show an oblate shape (Fig. 3-5d), accounting for the oblate magnetic fabrics. The prolate magnetic fabrics, with obvious negative T values range from -0.13 to -0.64 (Fig. 3-9, Site 9, 10, 22, 27, 38, 39 and 47), which may record magma flow at some sites close to the boundaries of the different granite facies or granite and country rock contacts. Evidence for deformation-driven (1) synmagmatic crystal re-orientation or (2) sub-solidus recrystallization is lacking. Considering field and thin section observations, we consider the magnetic fabrics of the Qitianling pluton as primary magmatic ones (e.g., Borradaile and Henry, 1997; Tarling and Hrouda, 1993). Thus we suggest that those fabrics developed during cooling and crystallization of the magma without contribution from syn- or post-magmatic tectonics. This inference is in agreement with studies from other plutons (de Saint-Blanquat et al. 2001; Byerly et al., 2016).

5.2. Emplacement into ductile crust

Amphibole geobarometry estimates suggest that the Qitianling pluton was emplaced at $\sim 3.6 \pm 0.9$ kbar (Zhao et al., 2005). The aluminium content of magmatic hornblende is sensitive to the pressure change (Hammarstrom and Zen, 1986; Hollister et al., 1987), and the Al-in-hornblende barometer requires that the hornblende grains are intergranular and their compositions are collected from the edge of the grains indicating that the magma was close to the solidus (Hollister et al., 1987), we propose that the geobarometry result is equal to the emplacement pressure. Assuming a lithostatic pressure gradient of 3 km/kbar (van der Pluijm and Marshak, 2004), the current exposure of the Qitianling pluton should thus have been originally emplaced at mid-crustal depths of 9 to 14 km.

Accurate constraints on the temperatures of the country rocks during the emplacement of the Qitianling pluton are unfortunately lacking. If we assume a normal geothermal gradient of 30 °C/km (van der Pluijm and Marshak, 2004), then the temperatures of the country-rocks prior to emplacement and away from thermally affected pluton-country-rock zones can be estimated to have been ~ 270 – 420 °C, and ~ 420 – 570 °C at depths of ~ 9 – 14 km, and ~ 14 – 19 km, respectively, corresponding to the reconstructed paleo depths of the top and the bottom of the pluton (Fig. 3-10). Considering the widespread occurrence of Jurassic intrusions in southeast China and the study area,

a higher geothermal gradient (>30 °C/km) seems possible, and could have certainly prevailed in the thermally affected pluton-country-rock contact zone. At the inferred or higher temperatures, ductile deformation of the quartz-rich country rocks would have been possible, even at high or moderately strain rates (i.e. at 10^{-9} sec $^{-1}$ and below strain rates of 10^{-12}) (e.g., Kruhl et al., 2007).

At the exposure level, the Qitianling pluton appear to have significantly heated its country-rocks, as there is no evidence for partial melting, even at the immediate contact, and the thermal aureole is very narrow, generally about 20 m to locally 200 m wide. Evidence for significant ductile deformation in the form of foliation or lineation in this zone is also absent. The coarsely sutured grain boundaries of quartz in the country rocks along the contact zone indicate that thermal annealing at >350 - 400 °C followed weak ductile deformation (e.g., Passchier and Trouw, 1998). The lack of evidence, i.e. preferred mineral orientation, for any significant syn-magmatic ductile deformation in the country-rocks of the pluton, the gently outward dipping contact of the wall rocks, the irregular geometry of the pluton and the lack of regional syn-magmatic deformation further highlight that (1) the displacement of the country rocks producing the space for the Qitianling pluton must have been predominantly vertical, i.e. affected the roof zone or the floor of the intrusion; and (2) no significant regional deformation took place during the construction of the Qitianling pluton in the late Jurassic, this is also in agreement with the regional tectonic observations of Shu et al. (2011a).

As highlighted above, the study area underwent long and multi-stage tectonism from the Neoproterozoic to the Triassic, while regional-scale evidence for significant and consistent deformation is lacking. Especially the Phanerozoic intracontinental deformation events, however, resulted in a highly and deeply fractured crust (Wang et al., 2013 and references therein). The abundant and large-scale pre-Jurassic fractures may have served as channels that facilitated magma ascent. Emplacement may have commenced by dyking, while later magma pulses deflected into sill- to lopolith-like sheet when the magma meet the “traps” in the highly fractured crust as mentioned in (Gudmundsson, 2011). Large-scale, sub-vertical fractures may have also allowed for efficient fluid percolation and thus for efficient heat removal from the intrusions, so that contact metamorphism and thermal aureoles remained limited. We suggest in summary that the Qitianling pluton was emplaced into a highly fractured middle crust, and that none of its country rocks have experienced significant ductile deformation during magma emplacement.

5.3. Sill- to lopolith-like emplacement

The Qitianling pluton has a sub-circular surface exposure, but the Bouguer gravity anomaly data (Fig. 3-10) indicate that the pluton shows a slight subsurface elongation in NE-SW direction with a length (~ 30 km)/width (~ 23 km) ratio of $\sim 1.3:1.0$. The Bouguer gravity anomaly data further reveal that the pluton extends to a depth of ~ 6 km with a flat bottom and shallow to moderately

steep-dipping sidewalls. Roof pendants are not exposed inside of the pluton and we therefore have no direct control on the top shape of the pluton. However, the mostly sub-horizontal, yet gently outward-dipping magnetic foliations (dip angles $< 30^\circ$ at sites 01, 02, 03, 10, 11, 36, 48 and 49; Fig. 3-9a) suggest that the current topographic surface is close to the roof of the pluton. Thus, the overall geometry and the magnetic foliations indicate a tabular shape for the Qitianling pluton (Fig. 3-10).

The sub-horizontal foliations may have developed by sub-vertical magma flow against a roof at the head of a diapir (Kratinová et al., 2006), but emplacement of the Qitianling pluton as a diapir is unlikely considering (i) its overall oblate geometry, (ii) its horizontal to sub-horizontal magnetic foliations developed over an elevation range of ~ 800 m (Fig. 3-9 and Table S1), and (iii) the lack of significant ductile deformation in the country rocks. The sub-horizontal magnetic foliation could have therefore developed by (1) magma flow sub-parallel to a roof (e.g., Horsman et al., 2009; McNulty et al., 2000), (2) flattening of magma mush against a roof driven by under-accreted magma pulses (McNulty et al., 2000), or (3) vertical gravitational potential energy resulting in partial sagging of overlying rocks or magma mush (Bain et al., 2013)

Emplacement of magmas as sill- or lopolith-like intrusions, is typical for mid- to deep-crustal levels, commonly along fractures, faults and/or lithological boundaries in combination with variable degrees of ductile deformation of country rocks or preferential floor sinking (Cruden, 1998; Horsman et al., 2005; Mathieu et al., 2008). Such a mode of emplacement is consistent with the estimated emplacement pressure of $\sim 3.6 \pm 0.9$ kbar and paleo-depths of ~ 9 -14 km, and the roughly tabular geometry of the Qitianling pluton. The slight subsurface elongation of the Qitianling pluton in NE-SW direction could imply syn-magmatic country-rock displacement, but none of the wall rocks show significant deformation or in fact any variation in deformation intensity in different sections (Fig. 3-2). Additionally, any regular or preferred orientation of magnetic lineations cannot be recognized (Fig. 3-9c). Therefore, syn-magmatic deformation or regional tectonic stress is unlikely to have produced the NE-SW elongation of the pluton. Pre-existing structures, i.e. generally NE-SW-striking lithological boundaries and regional pre-Jurassic fold and/or fault planes, produced by polyphase tectonic events since the Neoproterozoic (Shu et al., 2012; Wang et al., 2013), could have controlled and indeed facilitated emplacement in NE-SW direction.

5.4. Incremental magma emplacement

In all 72 visited outcrops, only one direct internal contact between the facies I and II granites was observed, despite concentrated efforts near mapped facies boundaries, while similar contacts have also been described by Zhu et al. (2009) from other locations. The scarcity of the outcrop-scale contacts may indicate that they were likely obliterated by re-melting or re-crystallization during subsequent injections of magma, and/or that most injected magma sheets were significantly larger than the outcrop scale (i.e. >10 m in vertical and >100 m in horizontal dimension), which would

have reduced the likelihood that contacts are exposed (e.g., Coleman et al., 2004; John and Blundy, 1993). In the following, we propose two possible conceptual models (Fig. 3-11) to explain the key observations and results from our and previous studies, including: (a) undeformed country rocks with narrow thermal aureoles characterized by hornfels metasandstone (~ 10 m wide) or skarn (~ 200 m wide) along the contacts of the pluton; (b) distribution of three granitic facies (I, II and III) with continuous whole-rock compositional and mineralogical variation; (c) the irregular wavy contact between facies I and facies II with fine-grained, biotite-enriched zones in the facies II granite; (d) the commonly sub-horizontal and only locally steep to moderately steep magnetic foliations in all three granitic facies; (e) predominantly sub-horizontal yet variably oriented magnetic lineations; (f) the scarcity of exposed dykes; (g) the significant zircon U-Pb age range of the exposed granites; and (h) a sub-circular sill- or lopolith-like 3D pluton shape. We consider incremental emplacement as the likely process, which is favoured by the vast majority of current pluton emplacement models based on field, geochemical, and geochronological data and numerical modeling data (e.g., Annen et al., 2015; Coleman et al., 2004; Deniel et al., 1987; Scaillet and Searle, 2006). The large spread in crystallization ages determined for the exposed Qitianling granites (i.e. ~148-163 Ma) are consistent with incremental emplacement, but we critically discuss the record of the available age data and the need for further detailed investigation.

5.4.1. Model 1-Large-sheet emplacement, in situ fractionation

Large individual sheets emplaced in tabular intrusions are recognized to have radii of up to ~25-50 km (Annen et al., 2015; Caricchi et al., 2014). The exposed section of the Qitianling pluton may thus represent large, sub-circular magma sheets constructed by continuous magma pulses, with a radius of ~20 km (Figs. 3-2a and 3-11b). In situ fractionation can account for the continuous whole-rock compositional and mineralogical variations (Bai et al., 2005; Deng et al., 2005; Xie et al., 2010) and the overall sub-circular map-scale facies distribution (Fig. 3-2). The zoning from the facies I (hornblende-biotite) granites exposed along the margins of the pluton over the facies II (biotite-hornblende) granites to the facies III (biotite) granites occurring in the center of the pluton, could record inward cooling and crystallization.

A majority of the magnetic foliations and lineations is sub-horizontal, and may indicate sub-horizontal magma flow within the sheet, or alternatively suggest magmatic flattening against sub-horizontal roof and floor zones. The generally sub-horizontal magnetic foliations also suggest that magma emplacement and crystallization most likely took place during a period of tectonic quiescence. The variation of magnetic lineation orientation in a small scale, i.e. often between outcrops, may reflect uncertainties of the measurements rather than true differences or fabric relaxation subsequent to magma flow. Some of the steep to moderately steep magnetic foliations (and some lineations) occur close to map-scale fault zones in relatively altered granites, and we

therefore consider that these magnetic foliations (lineations) have been overprinted by re-crystallization during late-stage hydrothermal alteration, as strong chloritization of biotite and amphibole are evident in hand specimen and in thin section. Other steep to moderately steep magnetic foliations may indicate the existence of undetected/unmapped fault zones, or local zones in which magma flowed sub-vertically, e.g., along surfaces where magma locally slumped or upwelled. The exposed contacts between facies I and facies II with moderately steep dip angles may equally represent such local vertical magma flow (slumping or upwelling) of a comparatively crystal-poor, more evolved magma (II) against a relatively rigid, more mafic magma mush (facies I). The concentration of biotite in the facies II granites along the contact may record flow-zoning (e.g., as in biotite-rich schlieren).

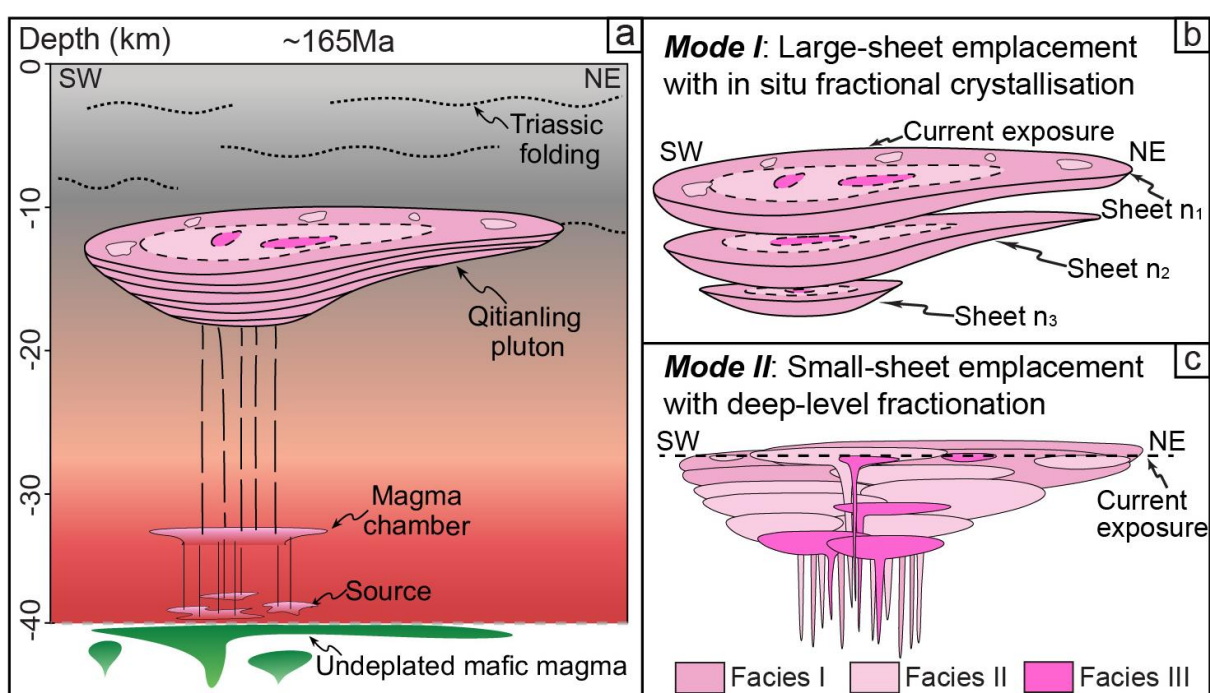


Figure 3-11. (a) Schematic sketch summarizing the original intrusion setting, (b) Downward accretion of multiple sill-like or lopolith-like magma injections in multiple large-diameter sheets that fractionated in situ to form the facies I, II, and III granites, and repeated for several times to construct the Qitianling pluton, (c) Multiple large- to small-diameter sheets, where the intrusion of facies I magma was followed by the intrusion of facies II and then facies III magma.

The large zircon U-Pb age range (163-146 Ma) of the Qitianling pluton (Zhu et al., 2009) cannot be explained by in situ crystallization of one magma sheet, as thermal modelling results suggest that the crystallization of incrementally emplaced granitic sheets with thicknesses of hundreds of metres may take place within several hundreds of thousand years (Annen et al., 2006, 2015; Blundy and Annen, 2016). However, some of the range in the crystallization ages may relate to analytical errors (i.e. ages determined by LA-ICPMS method; Table 1 of Zhu et al. (2009)), while age data determined by high precision SHRIMP and CA-ID-TIMS are limited (Table S4). The majority of samples (mainly facies II granites) define an age peak at ~155 Ma (Li et al., 2005; Zhu

et al., 2009). The facies I granites appear slightly older (~160-163 Ma) (Fu et al., 2004; Zhu et al., 2003, 2005, 2009), but several (although not all) samples overlap within error with the ages of the facies II granites. Facies III granites appear significantly younger (146-149 Ma) (Li et al., 2006; Zhu et al., 2009), but they may have partly re-set ages, as they are discordant and as they were acquired on high-U zircon (e.g., Figure 3-2 and Table 1 in Li et al. (2006) and Zhu et al. (2009), respectively).

5.4.2. Model 2- Small-sheet emplacement, deep-level fractionation

The study of Zhu et al. (2009) suggested that the three granite facies of the Qitianling pluton represent magma pulses of variable age, i.e. that the facies I to III granites were emplaced at ~160-163 Ma, ~153-157 Ma, and ~146-149 Ma, respectively. Despite the uncertainty of the age of the facies III granites, as highlighted above, the more precise SHRIMP age data nevertheless indicate that the ages of the facies I and facies II granites differ with an age gap of up to ~4 myrs (Figure S2 and Table S4) (three ages of the facies I and II granites do not overlap within error). This ~4 myrs age gap is far too long for the in situ crystallization of one single magma sheet (Annen et al., 2006, 2015; Blundy and Annen, 2016; Coleman et al., 2004; Matzel et al., 2006; Schoene et al., 2015), but it is in agreement with the exposure of multiple small-scale magma sheets that were emplaced over a few million years. The wavy contacts between the facies I and facies II granites and their gradation over a few centimeters (our data; Zhu et al. (2009)), and the fine-grained, biotite-rich margin of the facies II granite (Fig. 3-3e), may represent a magmatic (quench) contact between a highly crystalline magma mush that crystallized to form the facies I granite and a hotter and relatively crystal-poor magma that crystallized to form the facies II granite. Emplacement of new magma batches into partially crystallized magma mush would have accommodated most of strain and temperature increase, preventing significant strain partitioning into country rocks and resulting in a narrow thermal aureole with weak to no deformation.

Previous studies indicate that individual magma sheets may also have small radii of $\leq 1-5$ km (Annen et al., 2015; Caricchi et al., 2014). For the Qitianling pluton with its radius of ~ 20-15 km at surface and at depth, and its sub-circular zoning from facies I to facies III granites, we envision that each facies is made up of some larger and multiple smaller individual sheets, where the facies II and facies III injections were preferentially injected into the more central and sub-solid part of the system. The irregular and ~NNE-SSW oriented facies boundaries (Fig. 3-4e) in the SE part of the pluton are accounted for in this model. The continuous compositional and mineralogical variation from the facies I to the facies III granites would have to record fractionation of the granitic magmas at deeper crustal level or be source-inherited compositional variation.

The predominantly sub-horizontal magnetic foliations and lineations may record sub-horizontal magma flow within sheets and/or magmatic flattening against sub-horizontal roof and floor zones.

The variable magnetic lineation directions could have developed by magma flow in different sheets (Fig. 3-8). The steep magnetic foliations and lineations in fault zones may record localized re-crystallization as a result of sub-vertical fluid flow, but the fault zones may also coincide with former sub-vertical magma transfer zones. The steep and moderately steep (~30 to 60 °) magnetic foliations close to the facies I and II boundaries and within the different granite facies may delineate sidewalls (or near-sidewall zones) of small-scale, sill- or lopolith-like injections. Several elongated, small-scale exposures of facies II and III granites (Fig. 3-2) may also represent vertical magma transfer zone. The scarcity of dykes is consistent with possible downward-accretion.

5.5. Magma feeder zone(s)

Previous work has revealed that the Qitianling pluton shows a sub-circular geometry in Bouguer gravity and aeromagnetic anomalies (Guo et al., 2006). This argues against magma supply through one main feeder zone, e.g., one laterally extensive dyke. Instead, we envision that the magma was supplied through a number of pipe-shaped conduits comparable in dimension to the elongated facies II granite exposures in the facies I granite or comparable to magma channels described for the lower crust (Bouilhol et al., 2015; Paterson, 2009). To account for the sub-circular Bouguer gravity and aeromagnetic anomalies, these pipe-shaped magma feeders must be either small (i.e. unresolved by the geophysical data) and/or abundant, occurring below all parts of the pluton. If the proposed small-scale sheets with radii of <2-5 km exist (model 2), vertical magma feeder zones must be abundant.

3.6. Conclusions

We have used a combination of multidisciplinary methods, including field and microscopic observations, AMS fabric characterization, and Bouguer gravity modelling, to decipher the emplacement processes for the Jurassic Qitianling granitic pluton, South China. The results indicate that the Qitianling pluton forms a ~25 km wide and ~6 km thick lopolith-like intrusion that was incrementally emplaced by multiple magma sheets during a period of tectonic quiescence, i.e., that emplacement was largely driven by internal magma forces, while pre-existing (pre-Jurassic), passive crustal-scale faults are inferred to have facilitated magma ascent and heat transfer from the cooling pluton. We consider that the pluton either formed by accumulation of large magma sheets (> 20km in diameter) that fractionated in situ or that it formed by emplacement of multiple small magma sheets that represent magma fractionated at deeper crustal level or compositionally variable source-derived melts.

To unequivocally distinguish between these modes of pluton construction, additional high-precision dating is urgently needed. We highlight that AMS fabric characterization can be

particularly useful in mapping out suspected magma sheets with cryptic contacts and weak internal fabrics in granite plutons and for identifying crucial targets for high-precision age dating. The outcrop spacing and the overall exposure of the Qitianling pluton were insufficient to map out individual magma sheets where they may be present (e.g., following zones with moderately steep foliations), but high-precision age dating will target these zones (outcrops on both sides of steep to moderately steep foliations) to unequivocally constrain and further characterize age variation of the exposed facies I to facies III granites.

We highlight that the Jurassic was a period of relative ‘tectonic quiescence’ in the South China Block (SCB), where regional deformation mostly formed large, open-scale fold belts. If and how the volumetrically significant granite magmatism has affected, and perhaps even controlled, regional deformation (e.g., de Saint-Blanquat et al., 2011; Merle and Vendeville, 1995) is a target of current field investigations and numerical modelling.

Chapter 4. The emplacement mechanism of the late Jurassic Shibeï pluton in the Wuyishan area, South China Block

4.1 Introduction of the research

Magma emplacement mechanism has been long studied and several models have been proposed to solve the “space problem”, which are mainly classified into “forceful and permissive” models (e.g. Daly, 1903; Pitcher, 1979; Hutton, 1988). However, several parameters of the permissive model have been challenged by many later studies (e.g. Clemens and Mawer, 1992; Cruden, 1998), hence, the role of tectonics in the magma emplacement was less considered. Recently, the rheological behavior of the crust, brittle or ductile, has been widely studied, the deformation and thermal state of the country rocks related to the magma emplacement have attracted more and more attention. Consequently, numerous multidisciplinary studies have been carried out to acquire more pertinent understanding on the emplacement process of plutons (e.g. Collins and Sawyer, 1996; Paterson and Fowler, 1993; Moyen et al., 2003; He et al., 2010; Menand, 2011 and references therein). The peraluminous granite, usually considered as the product of the melting of continental crust coeval with regional tectonics continental collision, strike-slip or normal faulting (Barbarin, 1996) can be a suitable target to assess the contributions of magma, tectonics and crustal condition to the emplacement process.

The South China Block is characterised by a widespread Mesozoic magmatism (Fig. 4-1), though numerous petrological, geochemical, and geochronological studies, have been carried out, its tectonic and geodynamic settings are still in dispute (Zhou and Sun, 2000, Ren et al., 2002; Wang et al., 2005; Li and Li, 2007, Shu et al., 2009; Michel et al., 2016). The study of the fabrics in magmatic rocks, which results of the interplay between magma dynamics and regional tectonics is an efficient way to understand the synmagmatic tectonic setting. The Jurassic magmatism in the South China Block (Fig. 4-1b) mainly consists of metaluminous and subordinated peraluminous granitic bodies (Zhou et al., 2006). The peraluminous Shibeï pluton, which presents an ASI value higher than 1.1 and is considered as a crustal derived one (Wang et al., 2016), was chosen for further study.

To recognize the magma emplacement process of the Shibeï pluton, detailed macroscopic (field) and microscopic (thin section) observations have been carried out within the pluton and on the contact between the pluton and its country rocks, where their intensive interaction are often recorded. To constrain the petro-fabrics of granites, the samples for Anisotropy of Magnetic Susceptibility (AMS) measurements were collected with a good covering of the pluton (Fig. 4-2). Gravity modelling is also envisaged to reveal the 3-D view of the pluton, which may provide information of the magma emplacement context.

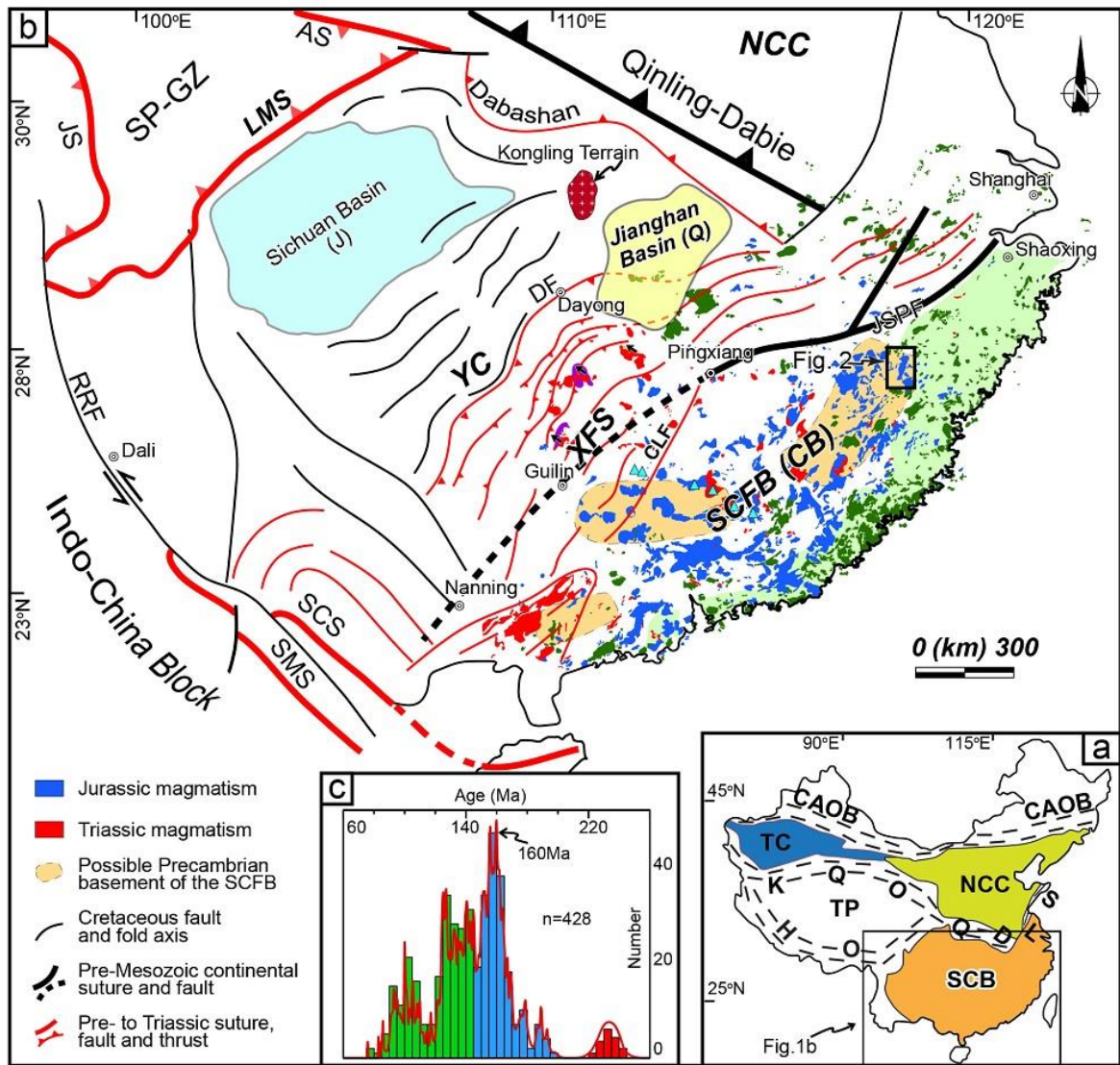


Figure 4-1. (a) Sketch of the main geological units in China. (b) Tectonic framework of the South China Block with inserted thermal events records. (c) Age range of the Mesozoic magmatism in the SCB

4.2 Geological setting of the Shibeï pluton and its surrounding area

Our study zone is located the northeastern part of the ancient Cathaysia Block, which is collided with the Yangtze Craton in the Neoproterozoic (ca. 850 Ma; Wang et al., 2007; Li et al., 2009 and references therein) along the Jiangshan-Shaoxing-Pingxiang Fault to form the South China Block (SCB), and remarked by the widespread Mesozoic magmatism (Fig. 4-1b). According to previous studies, the Cathaysia Block is considered as an amalgamated one since the Neoproterozoic time by four lithotectonic units, e.g. Badu, Mayuan, Wuyi, Yunkai, their boundaries were identified within the Cathaysia Block (e.g. Zhao et al., 1999; Yu et al., 2010). Recent studies show that the affinity between Badu and Mayuan units with similar Hafnium and Neodymium isotope and geochronological spectra of the detrital zircon from the metasedimentary rock in these two units.

The Shibeï pluton is located at the northeastern part of the Wuyishan area, where the Proterozoic metamorphic rocks of the Mayuan group are well developed, Paleozoic and early

Mesozoic strata are rare, and locally observed, Late Jurassic to early Cretaceous terrigenous volcanoclastic rocks are widely distributed and unconformably overlain on the Pre-Mesozoic strata (Fig. 4-2b; BGMRFJ, 1985).

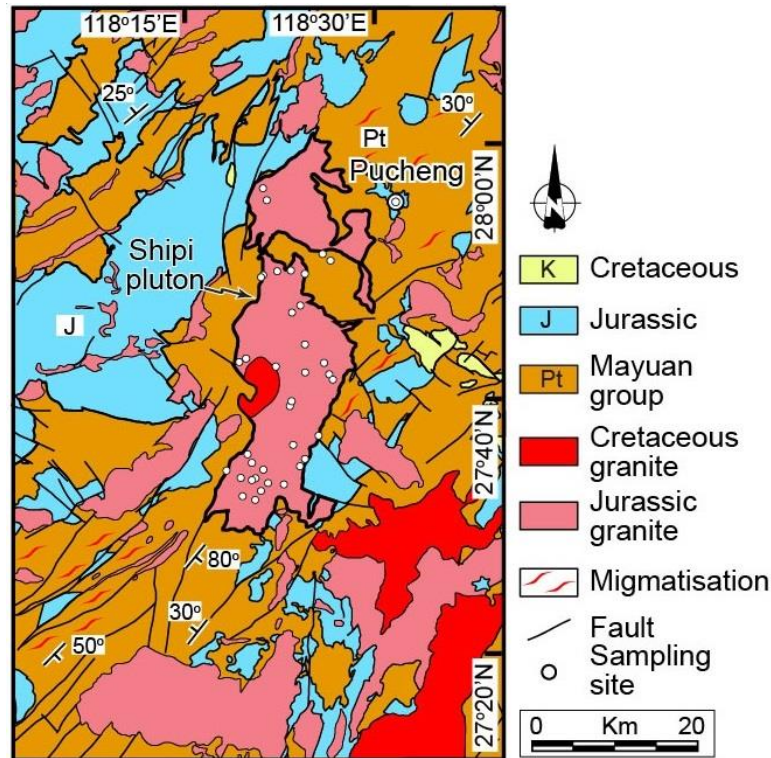


Figure 4-2. Geological map of the Shibeï pluton and its surrounding area with AMS sampling sites (According to BGMRFJ, 1985).

The Shibeï pluton is an intrusive complex (Wang et al., 2016), which is mainly constructed by late Jurassic (~155 Ma) and early Cretaceous intrusions (~110 Ma, Fig. 4-2). The pluton presents a surface of ca. 570 km² and topographic relief less than 1000 meters. The exposure of the Shibeï pluton shows an N-S elongated geometry with a length-width ratio about 6: 1.

The Shibeï pluton is intruded in the Paleoproterozoic Mayuan group, which consists of paragneiss, pelitic schist, marble, calcsilicate, quartzite, migmatite and amphibolite and is widely exposed in our study area (Fig. 4-2; Zhao et al., 1999; Liu et al., 2010). The Mayuan group is intensively deformed by at least three phases of deformation (Zhao et al., 1999), but the current NE-SW striking anticline-syncline system is produced by the last stage deformation of the Triassic dextral transpression (~245 Ma, Fig. 4-1; Xiang et al., 2008; Xu et al., 2011, 2012; Li et al., 2017) and probably reshaped by Cretaceous tectonic sequences, characterized by extension tectonics due to the Pacific oceanic plate subduction under the SCB (Fig. 4-2; Ma et al., 2002; Li et al., 2014). Furthermore, the strong and widespread early Paleozoic migmatization (~450 Ma; Liu et al., 2010) is also recorded in the Mayuan Complex.

Previous geochemical studies show that the Jurassic Shibeï pluton has SiO₂ content of ~ 75.7 %, alumina saturation index (ASI) between 1.0 to 1.1, and negative ϵ_{Hf} (-15.7) and ϵ_{Nd} (-14.5) values, indicating that this granite is derived from partial melting of continental crust and considered as a

highly evolved magmatic body.

4.3 Field observations and sampling

The Jurassic Shibeï pluton mainly consists of medium to coarse grained monzogranite, biotite granite and some fine grained granite, with feldspar crystals scale ranging from 1-5 cm in size (Fig. 4-3a). The evidences for schlieren of the lithology zonation of the pluton is not observed. Randomly oriented mafic enclaves are locally found in the Shibeï pluton with size ranging from 5 to 20 centimeters and length-width ratio between 1 and 1.3.

The metamorphic country rocks were intensively deformed by multiphases of pre-Jurassic tectonics. The contact between the pluton and its wall rock is sharp and vertical, and concordant with the foliation of the wall rock. Bulging of the wall rock is also observed, implying the deflation of the wall rock during emplacement of the magma. Preferred mineral orientation in the pluton margin is rare, and no thermal aureole is observed in the wall rock, but the contamination of mafic materials from the wall rock into the granite can be observed. Post-solidus relative movement along the contact was not observed during our field work.

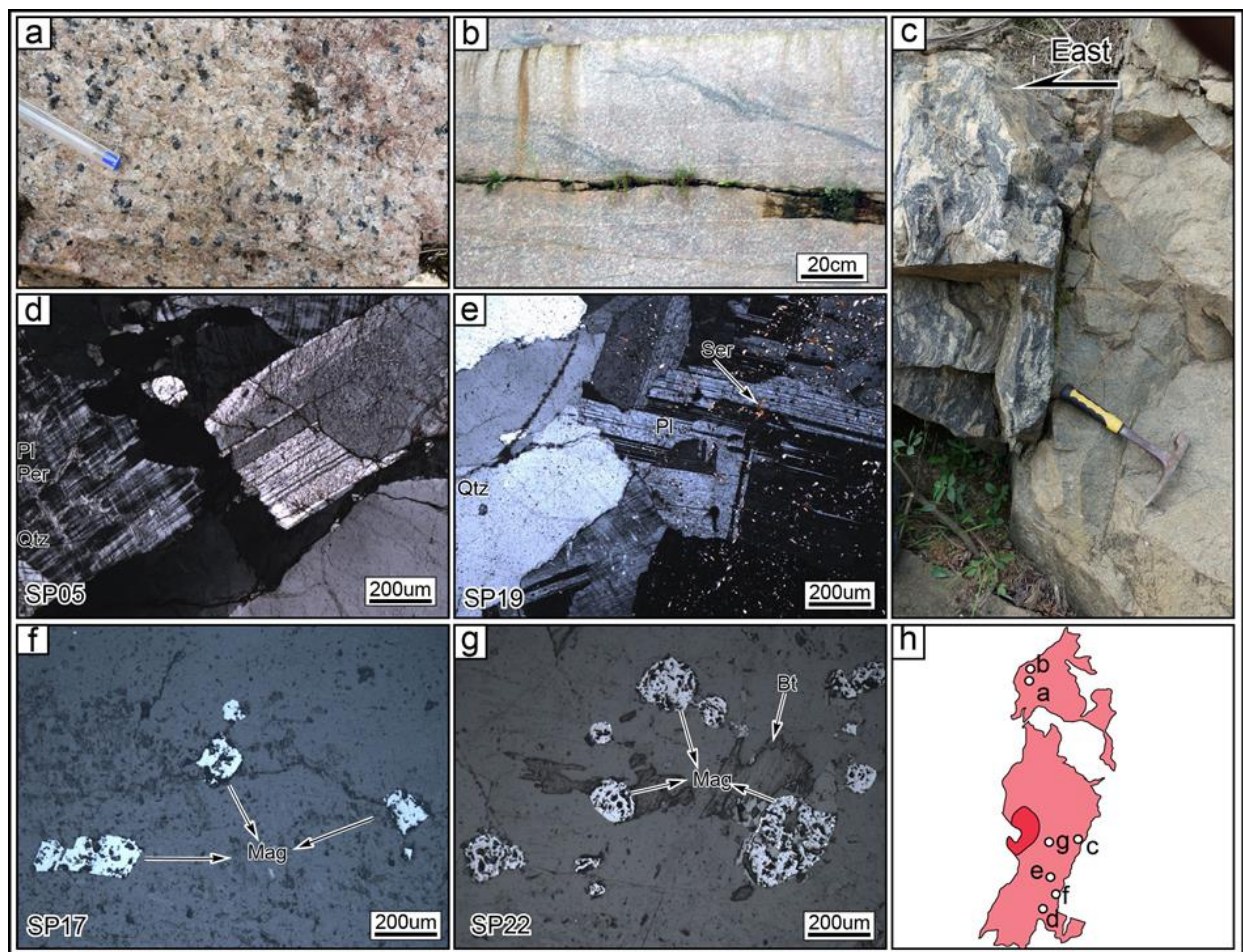


Figure 4-3. (a), (b) and (c) concern the field observations of the Shibeï pluton. (d), (e), (f) and (g) are the thin section images of the granite. Abbreviations of the minerals in the images are as following: Mag: magnetite, Per: perthite, Pl: plagioclase, Qtz: quartz. The location of the observation is presented on the sketch map of the Shibeï pluton (h).

Locally, a Cretaceous intrusion has also been identified. It is mainly composed of medium to coarse grained quartz, alkaline feldspar, and amphibole granites, with feldspar grain size varies between 2 to 5 centimeters.

A total of 37 sites, spreading from the external to internal parts of the pluton, were chosen for AMS sampling based on our field observation. At least 6 cores are collected from each sites with an interval of 3 to 4 meters between two cores, and about 1.5 km between two sites.

4.4 Petrofabrics of the Shibeï pluton

4.4.1 Petrographic features of the granite

Ten thin sections of the Jurassic granite of the Shibeï pluton have been microscopically investigated, and show that this granite is mainly composed of quartz, plagioclase, perthite, K-feldspar, biotite, sericite and associated zircon, magnetite and pyrite (Figs. 3d, 3e, 3f and 3g). Granite from the external part of the pluton, (e.g. Sample SP05), presents a typical magmatic texture, i.e. euhedral crystals with well-preserved twinning of the feldspar and straight grain boundary, only undulose extinction in quartz grains is observed (Fig. 4-3d). Sample SP19, located in the center of the pluton (Fig. 4-3e and 4-3h), displays a similar texture as Sample SP05, but with the bulging of the Qtz, indicating that the granite has experienced a sub-solidus deformation, probably due to the interaction between different magma batches or caused by the roofing of the pluton. Moreover, magnetite is widely developed in our samples, which show irregular shape and are developed either inside of the feldspar and biotite, or as interstitial crystals (Figs. 3f and 3g).

4.4.2 AMS of the Shibeï pluton

Our AMS measurements are performed in the laboratoire de Magnétisme des Roches d'Orléans at the Institut des Sciences de la Terre d'Orléans with the KLY-3 kapabridge. Three approaches, thermomagnetic mineral analysis by the KLY3 kappabridge coupled with a CS3 furnace, isothermal remanence magnetization (IRM) measurement with an IM30 pulsed magnetizer and a JR5 spinner magnetometer in the ISTO, and magnetic hysteresis loop characterization using a vibrating magnetometer at the Laboratoire de Paleomagnétisme of the Institut de Physique du Globe de Paris (IPGP), were applied to identify the magnetic susceptibility carriers in the granite to get a proper interpretation of our magnetic fabric data, due to the different contribution of magnetic minerals to the magnetic fabric of one specimen (Rochette et al., 1992).

4.4.2.1 Magnetic mineral analysis

The representative magnetic mineralogical analysis results are presented in Figure 4. The thermal magnetic measurements (Fig. 4-4a, 4-4b and 4-4c) show a gradually drop at 350-400°C and

rapid one at 580°C for all three granite samples, indicating the existence of magnetite and probably maghemite in the Shibeï granite. The progressive decrease of the magnetic susceptibility until arrived to about 680°C indicates the existence of hematite which may be part of magnetic minerals in the granite, or newly formed from the mineral transformation of maghemite and magnetite during the heating as the cooling curves show relatively weak susceptibility (Dunlop and Özdemir, 1997). The hysteresis curves present similar narrow, S-shaped and multidomain-like hysteresis loops (Fig. 4-4d, 4-4e and 4-4f; Suk et al., 1996), with little difference between uncorrected and corrected curves, indicating that the magnetic property of the granite is dominated by ferromagnetic minerals with little contribution from paramagnetic minerals. The rapid saturation of the magnetic remanence at applied magnetic field lower than 400 mT (Fig. 4-4g), also indicate the bearing of ferromagnetic minerals in the granite. According to McCabe and Channell (1994), the size of magnetite in our samples is ranged in the mixture of multidomain and pseudo-single domain.

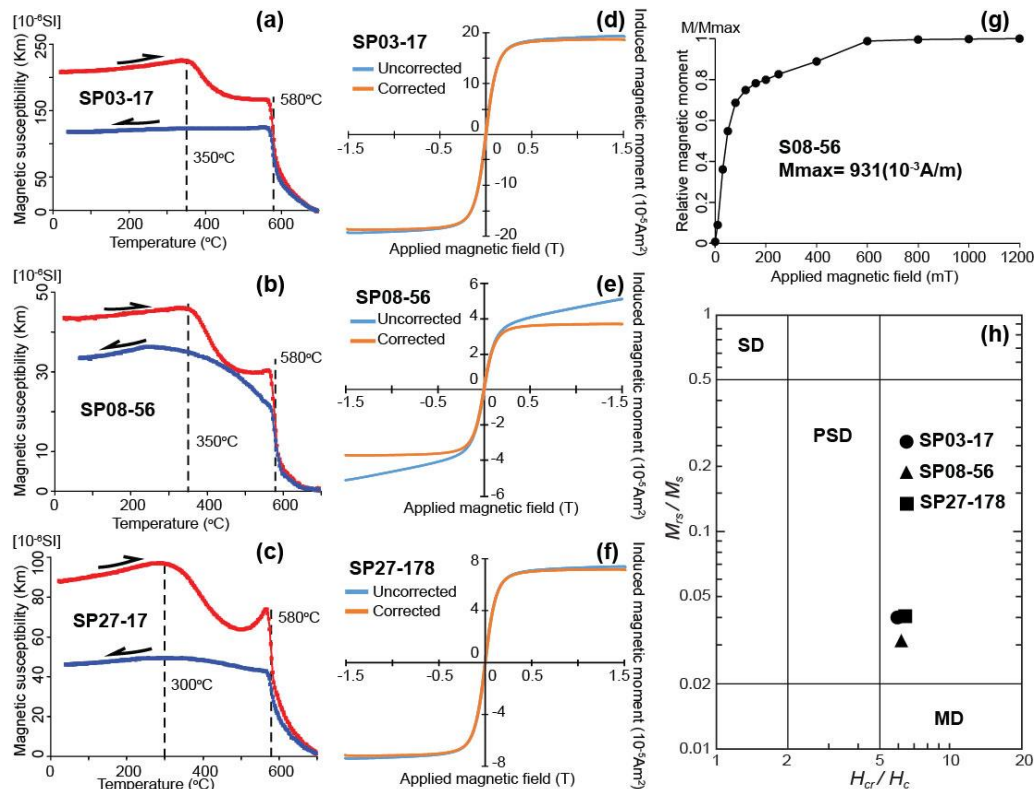


Figure 4-4. Magnetic minerals analysis of the samples from the Shibeï pluton.

Altogether, the magnetic susceptibility carriers in the granite of the Shibeï pluton principally are of magnetite in multi- and pseudo-single domain, with probably weak contribution of maghemite and possible hematite. The magnetic fabrics provide by this type of minerals are comparable to the petrographic ones (Rochette, 1992, Borradaile and Henry, 1997). Therefore, the AMS study will be an efficient way to determine the average orientation of the magnetic minerals in the granite as well as information on the pluton emplacement (Martín-Hernández et al., 2004).

Total of 230 specimens from 37 sites were collected for AMS measurement, the bulk magnetic susceptibility (Km) of the specimens are range from 9×10^{-6} to 43×10^{-3} SI (Fig. 4-5a) and about

70% of specimens have K_m value higher than 1×10^{-3} SI, due to the existence of ferromagnetic minerals in the sample (Hroudá, 1990). About 30% of the specimens showing relatively low bulk magnetic susceptibility indicate that these specimens are paramagnetic mineral bearing. The site-mean value of degree of anisotropy (P_J) ranges from 1.01 to 1.28, and 65% of sites have P_J value lower than 1.10 (Fig. 4-5b). Furthermore, the P_J value is increasing with the increase of the K_m value (Fig. 4-5b), suggesting that the high P_J values may be due to the high concentration of magnetite (Rochette et al., 1992). The site-mean shape parameter (T) values range between -0.11 and 0.69, except for Site 16 with a T value of -0.6, with the oblate shape for the majority of specimens (Fig. 4-5c).

4.4.2.2 Magnetic fabric parameters

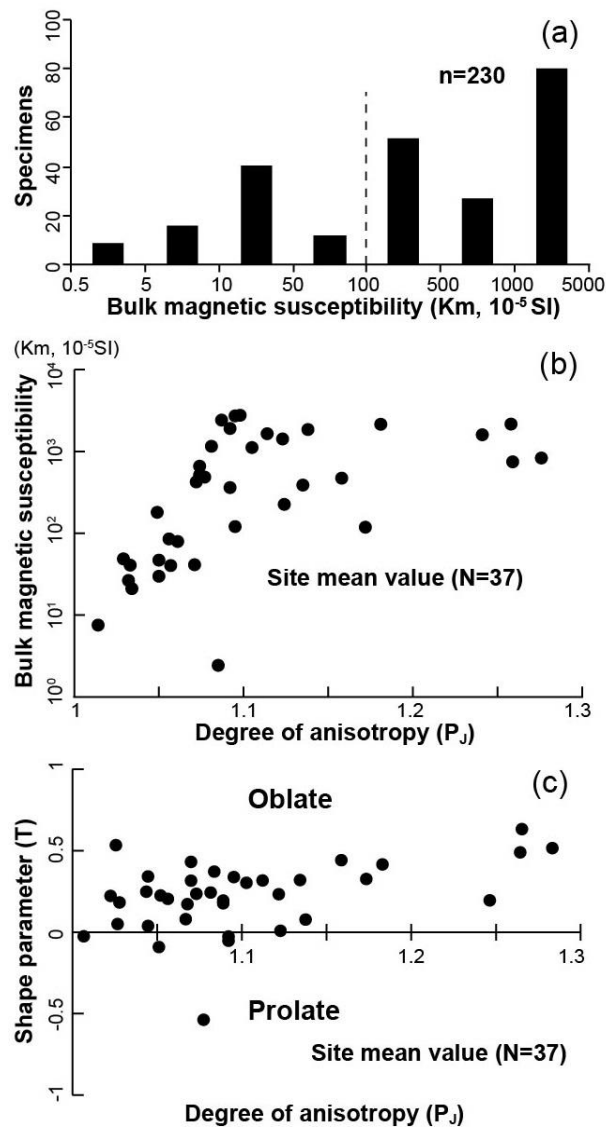


Figure 4-5. Magnetic parameters of the granitic specimens from the Shibeï pluton

4.4.2.3 AMS results of the Shibeï pluton

Our samples from the Shibeï pluton can be classified into two groups according to its spatial distribution, i.e. external and internal group. The internal group consists of 20 sites (Fig. 4-6), and the external group is composed of 17 sites (Fig. 4-7).

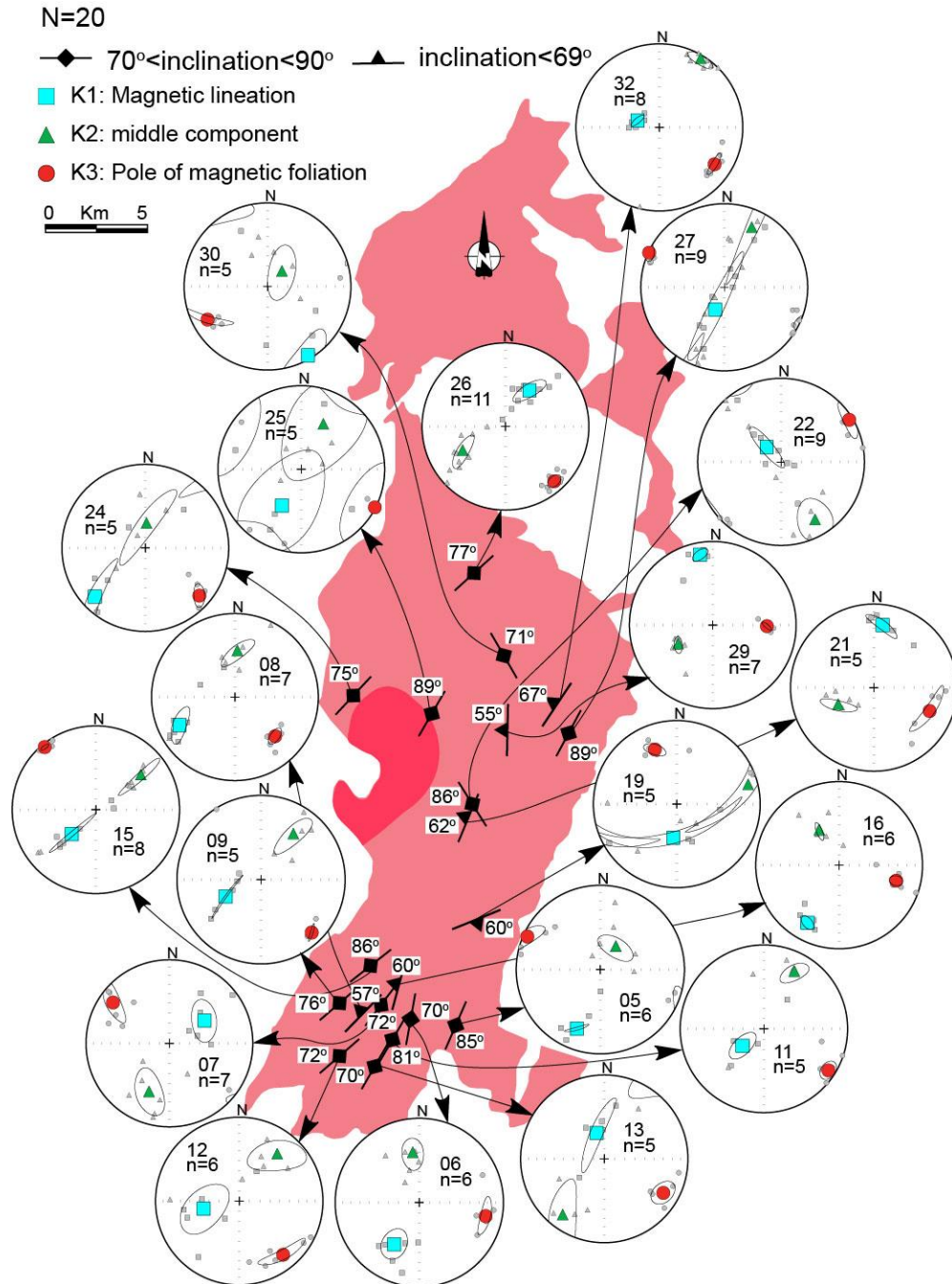


Figure 4-6. Magnetic fabrics of the internal group of sampling sites

The internal group provides a relatively good consistence of their magnetic fabrics. All of the twenty sites present vertical to sub-vertical dip ranging from 55° to 89° with a mean value of 73° . Eighteen out of 20 sites show a NE-SW strike of the foliation, and the remaining two sites (Site 22 and 30) present a NW-SE one (Fig. 4-6). The magnetic lineation is relatively dispersed, and varies from horizontal to vertical (stereographic projection of site-mean AMS measurement in Fig. 4-6).

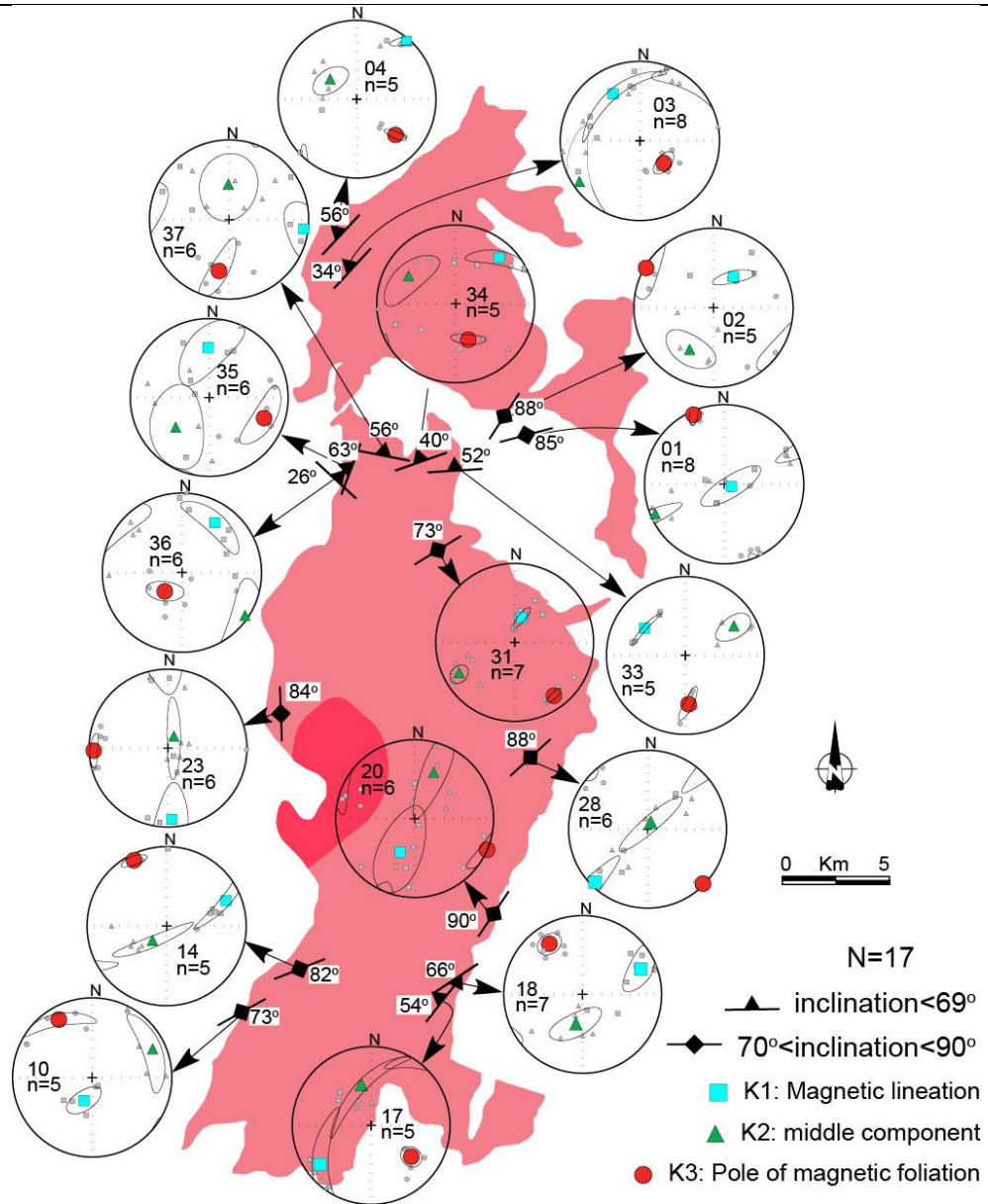


Figure 4-7. Magnetic fabric of the external group of sampling sites

The magnetic fabrics from external group can be divided into two sub-groups. Sites 3, 10, 14, 17, 18, 20, 28 and 31 from the southern and eastern parts of the pluton present, as those from the internal group, a NE-SW striking and vertical to sub-vertical magnetic foliation with dip angle ranging from 54° to 90° . Concerning the lineation, similar to those of the internal group, they are scattered and vary from horizontal to vertical (Fig.7 and Fig. 4-10). However, the magnetic fabrics from Sites 1, 2, 4, 23, 33, 34, 35, 36 and 37 located at the northern and northwestern sides of the pluton are characterized by gentle outward dipping magnetic foliations, with dip angle ranging from 26° to 63° , which are consistent with the foliation of the country rocks (Fig. 4-2b). The strikes of foliation are globally parallel to the contact between the granite and the country rocks (Fig. 4-7). No tendency can be defined for the lineation, showing a highly dispersed distribution (Fig. 4-7 and Fig. 4-10).

4.5 Gravity modelling

The regional gravity anomaly reflects the regional density architecture of the underlying strata, therefore, the proper interpretation of the gravity anomaly data can help to reveal the extension of the geological units at depth. Especially for an intrusive body, which usually has a large density contrast with respect to its country rocks. Therefore, we applied the gravity modelling method to shape the Shibeï pluton intruded in the Paleoproterozoic Mayuan group, which is mainly composed of high grade metamorphic rocks with higher density than the Shibeï granite.

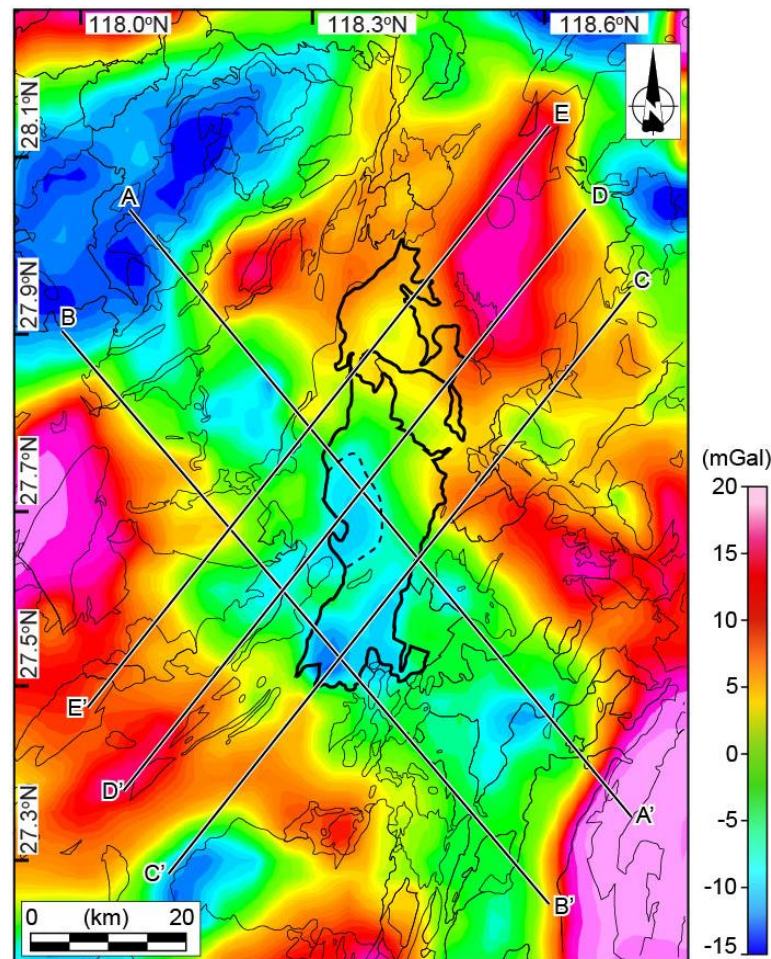


Figure 4-8. The residual Bouguer gravity anomaly of the Shibeï pluton and its surrounding areas.

The 1:200,000 original Bouguer gravity anomaly map for the Shibeï pluton area is from the Chinese Bouguer gravity anomaly database. The regional gravity data for Fujian province, covering the Shibeï pluton and its country rocks, are download from <http://bgi.omp.obs-mip.fr/>. The Digital Elevation Model for the study area, with a resolution of 90 m at the equator, is downloaded from <http://srtm.csi.cgiar.org/>. Due to the limited outcrops of the Paleoproterozoic Mayuan group, we applied the density value of 2.69 g/cm^3 to the rocks at uppermost part of the Mayuan group, referring to its lithological association by the geological survey of the Fujian province (BGMRFJ, 1985). The density values for deep country rocks and strata are originated from the density study of the crustal structure of the South China Block by Deng et al. (2014). The density value of 2.62

g/cm^3 is applied to the Jurassic granite, which presents an average value for the biotite granite developed in South China.

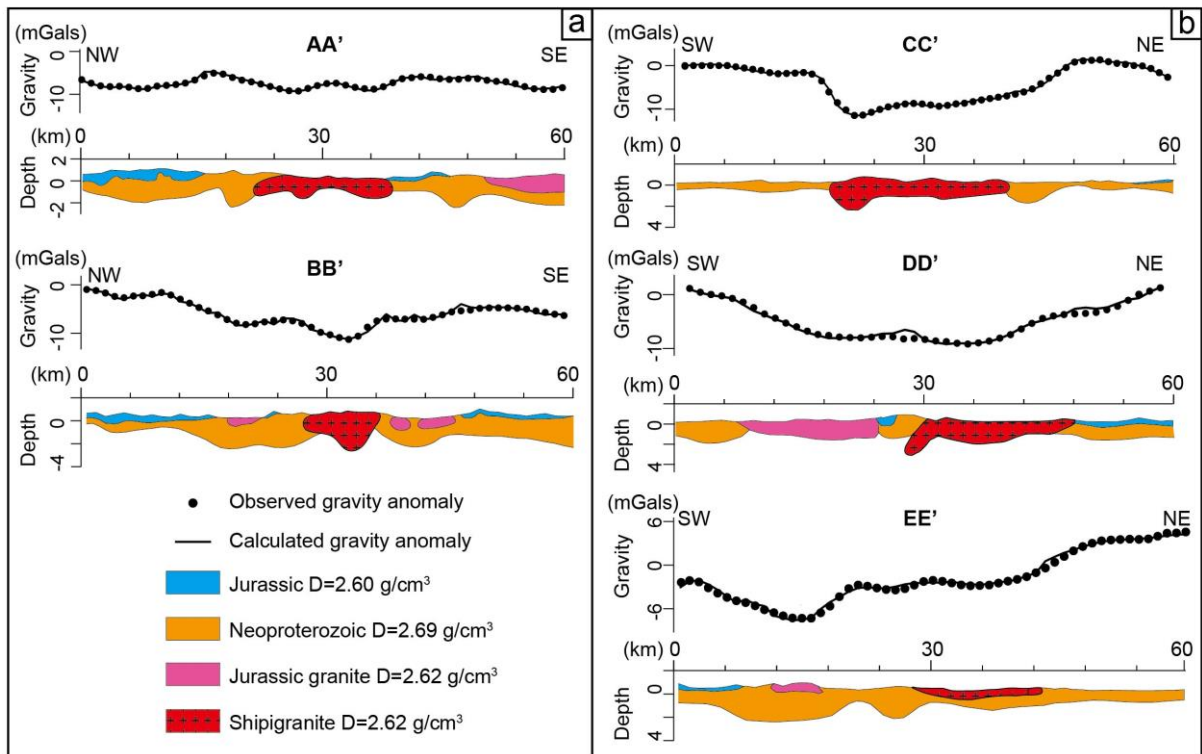


Figure 4-9. Interpreted profiles of the Bouguer gravity anomaly of the Shibeig pluton and its surrounding areas.

The original Bouguer gravity data include the regional and long wavelength signals of surface and depth materials, respectively. Therefore, the long wavelength signals need to be removed, to get a more suitable gravity anomaly information produced by the surface geological body. The regional Bouguer gravity anomaly data of Fujian province was used to deduce the long wavelength gravity anomaly trend of this region. Several low-pass Butterworth filters are applied to remove the long wavelength signal with cutoff wavelengths of 50 km, 70 km, 100 km and 150 km. After removing the regional long wavelength signals from the Shibeig gravity anomaly data, we get the residual gravity anomaly data. Through the comparison between different residual gravity anomaly data, we choose the residual gravity anomaly data with the cutoff of wavelength of 75 km, by which the anomaly matches better with surface geological features.

In the residual Bouguer gravity anomaly map (Fig. 4-8), the Shibeig pluton shows two negative anomaly centers. The higher negative one is located in its southern part corresponding to the Jurassic granite. The less negative center is located at the western margin of the pluton (Fig. 4-8), which may correspond to the Cretaceous granite (BGMRFJ, 1985; Wang et al., 2015). According to the regional tectonic features and our gravity data, five profiles of gravity modeling are made: two of them perpendicular to the regional geological structure (AA' and BB' in Fig. 4-8 and Fig. 4-9a), and three parallel with the regional structures (CC', DD' and EE' in Fig. 4-8 and Fig. 4-9b).

Figure 4-9 presents our gravity modeling profiles. According to the gravity data and our interpreted profiles, we can find that (1) in the regional scale, a NW-SE orientated negative gravity anomaly belt is observed in the Mayuan group cross the Shibeï pluton, suggesting that the Paleoproterozoic basement is probably heterogeneous; (2) the average thickness of the pluton is about 1.5 km, with a northward decrease from the deepest part in the south up to 2.4 km (Fig. 4-9) to the shallowest part in the north at ca. 0.5-1 km (EE' profile in Fig. 4-9b); (3) an oblate shape of the Shibeï pluton is revealed, with a ratio among length, width and thickness of 32:8:1; (4) a relatively flat bottom in the NE-SW direction seems obvious (profiles CC', DD' and EE' in Fig. 4-9b).

4.6 The emplacement mechanism of the Shibeï pluton

4.6.1 The acquisition and the implication of the magnetic fabrics of the granite

4.6.1.1 The acquisition of the magnetic fabric

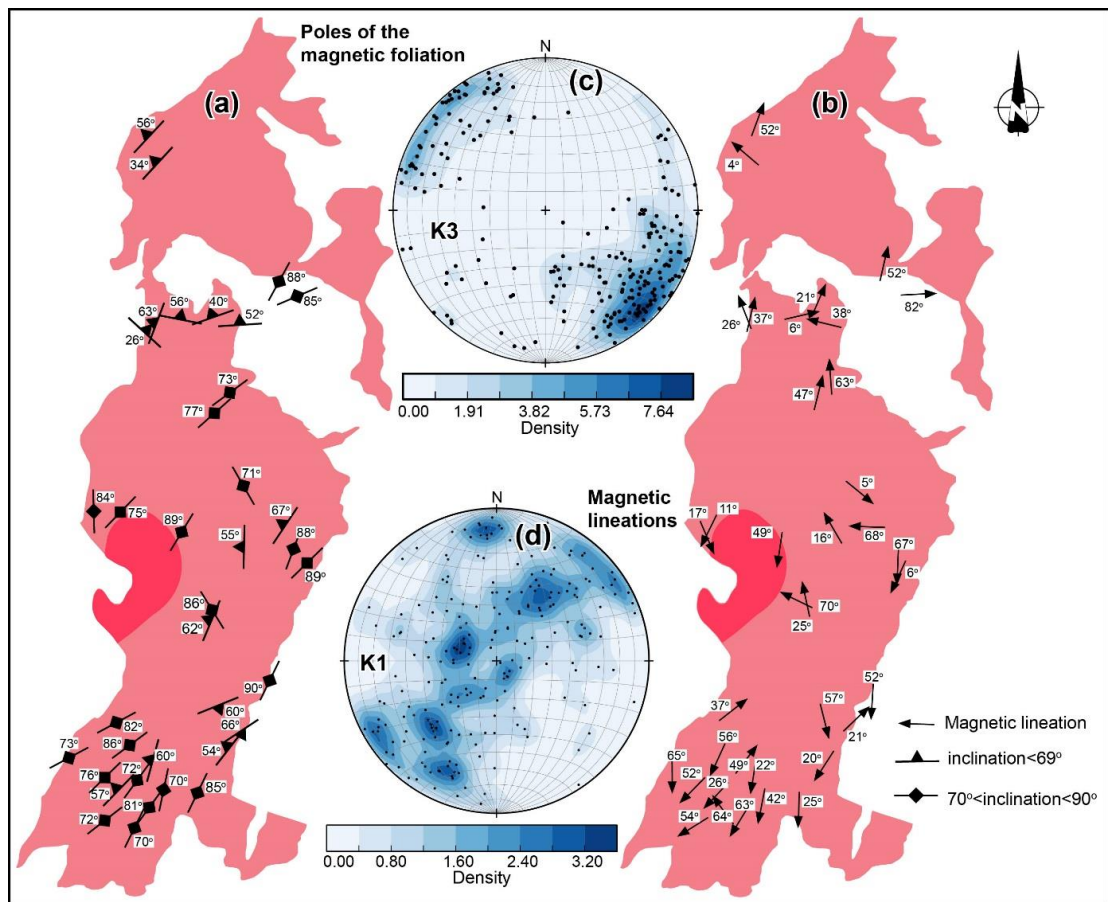


Figure 4-10. The summary of the magnetic fabrics. (a) and (b): map views of the poles of magnetic foliation and the magnetic lineation, respectively; (c) and (d), equal-area projections of the poles of magnetic foliation and lineation, as well as their corresponding of density diagram in specimen unit, respectively.

As mentioned above, our microscopic observations present a typical magmatic texture (Fig. 4-3c and 4-3d). The granites collected from the external of the pluton possess euhedral quartz grains and lack of high temperature deformation features, e.g. annealing/recrystallization of the quartz grain, and grain boundary migration are absent, implying the absence of synmagmatic mechanical deformation at the pluton edge during the emplacement of the magma. The shape preferred orientation of the quartz, feldspar and biotite grains are also absent, indicating that the granite did not experience a synmagmatic regional tectonic control nor a post-solidus deformation. Furthermore, the P_j values of most of paramagnetic mineral-bearing granite are lower than 1.10. Therefore, we propose that the magnetic fabric is a primary one, without overprint or reset by synmagmatic or post-solidus regional tectonic events, and it was acquired during the magma emplacement and crystallization.

4.6.1.2 The implication of the magnetic fabrics

The magnetic foliation of the Shibeï pluton is quite similar, and is characterized by a sub-vertical to vertical magnetic foliation with NE-SW striking (Fig. 4-10a), except sites 33, 34, 35, 36 and 37 in the margin of the pluton (Fig. 4-6). However, the difference in the inclination is significant between the sites from the southern and northern parts of the pluton.

The sites in the southern part of the pluton are dominantly characterized by sub-vertical to vertical magnetic foliation (Fig. 4-10a and 4-10c), which crosscut the foliations of the country rocks (with a range from 30° to 60°). The strike of the magnetic foliation is parallel with that of the country rocks, and the magnetic foliation is probably parallel to the fold axial plane, which may present a relatively weak surface. Therefore, it is natural to propose that the magma supply channel was controlled by the structure inherited from the country rocks, and the fabric of the Shibeï pluton was controlled by the magma mobility.

However, the majority of sites in the northern part of the main body of the Shibeï pluton have gentle outward dip foliation (Fig. 4-10), which is consistent with the dip angle of foliation of the country rock. Furthermore, the schlieren of the granite in Site 03, located at the northern margin of the pluton, has a similar geometry (310° , 25° NW) than the magnetic foliation of the granite, indicating that the emplacement of the magma in the northern part is controlled by the structure of the country rocks. This geometry of the foliation change may be probably explained by the structural change of the country rocks as the study area experienced multi-phases of deformation and the metamorphic country rocks show a rather complicated structure of deformation.

The magnetic lineation, which usually reflects the magma flow direction in the Shibeï pluton presents a dominantly NE-SW strike, subordinated with some sites in NNW direction (Figs. 10b and 10d). Furthermore, the plunge of lineation is highly variable, ranging from 4° to 82° . Nevertheless, 78% of magnetic lineations have a plunge lower than 60° , and 72% of these sites

lower than 45° , suggesting that the magma flow is globally lateral or sub-horizontal along the channel (Borradaile and Henry, 1997; see also Talbot et al, 2005, JGR 110). About 20% of sites, i.e. sites 1, 10, 11, 13, 22, 27, 31 and 32, of the Shibeï pluton, present the plunges higher than 60° , with only one site, i.e. Site 1, up to 82° . These steep plunge sites are also accommodated with sub-vertical to vertical magnetic foliation, with mean value of the dip angle of magnetic foliation at 76° . Those sites with steep plunge are mainly located at the southern of pluton and spread from the margin to the center of the pluton. Therefore, we propose that the plunge of the magnetic lineation may represent the direction of magma flow, moderately to highly inclined along the vertical plan in the southern part, and moderately inclined flow along the flat foliation in the northern part.

4.6.2 The construction of the Shibeï pluton

4.6.2.1 The geometry of the Shibeï pluton

As mentioned above, the roof of the pluton was observed at the center of the pluton (Fig. 4-3a), denoting that the current topography corresponds approximately to the roof of the pluton. Our gravity modelling suggests that the Shibeï pluton is a tabular-shaped pluton, with an average thickness of ca. 1.5-2 km. The thickest part of the pluton is located at the southwestern part of the pluton, and the pluton becomes thinner northeastwards, parallel with the strike of the magnetic foliation (Figs. 8 and 9). The similar thickness of the pluton in NE-SW direction, which is parallel to the strike of the magnetic foliation, is revealed by the gravity modelling (Fig. 4-9b). This seems supporting the lateral flow of the magma along the channel.

4.6.2.2 The magma supply channel and space for emplacement

Our AMS and gravity modelling data suggest that the construction of the Shibeï pluton is probably initiated along vertical to sub-vertical and NE-SW striking fractures in the country rocks. As mentioned above, the magnetic fabric is a primary one, which is formed during the emplacement of the magma. Therefore, the similar NE-SW striking magnetic lineation, rather than oriented in the direction of dike accretion, indicates the absence of synmagmatic emplacement regional tectonics to produce the space for magma emplacement. This opinion is reinforced by our field and thin section observations likewise. Moreover, the Triassic thermal tectonic events are widely reported in the SCB (Fig. 4-1b), but Jurassic geochronological data of the tectonic events are not recorded yet. Therefore, we propose that the magma supply channel and space for emplacement of the Shibeï pluton was related to inherited structures existed in the country rocks.

The Mayuan group is composed of highly deformed rocks (Zhao et al., 1999), with fold and fault axes parallel with the magnetic foliation of the granite. The Mayuan group is considered as the basement of the Cathaysia Block, but there is a negative gravity anomaly belt under the Mayuan

group and seems perpendicular to the magnetic foliation of the Shibeï pluton. This belt may represent the suture of gradually amalgamated different blocks, with or without reshaped by subsequently tectonics. Recent thermal geochronological studies suggest that the Mayuan group is strongly deformed and reshaped by the multiphases of tectonic events (Fig. 4-1 and references therein). For example, the Paleozoic (ca. 450-400 Ma) NNE trending sinistral oblique shear zone and early Triassic (ca. 245-230 Ma) NNE-SSW striking dextral shear zone are revealed inside of the Mayuan group (Li et al., 2017). Therefore, the inherited structures of the Mayuan group may have affect the emplacement of the Shibeï pluton.

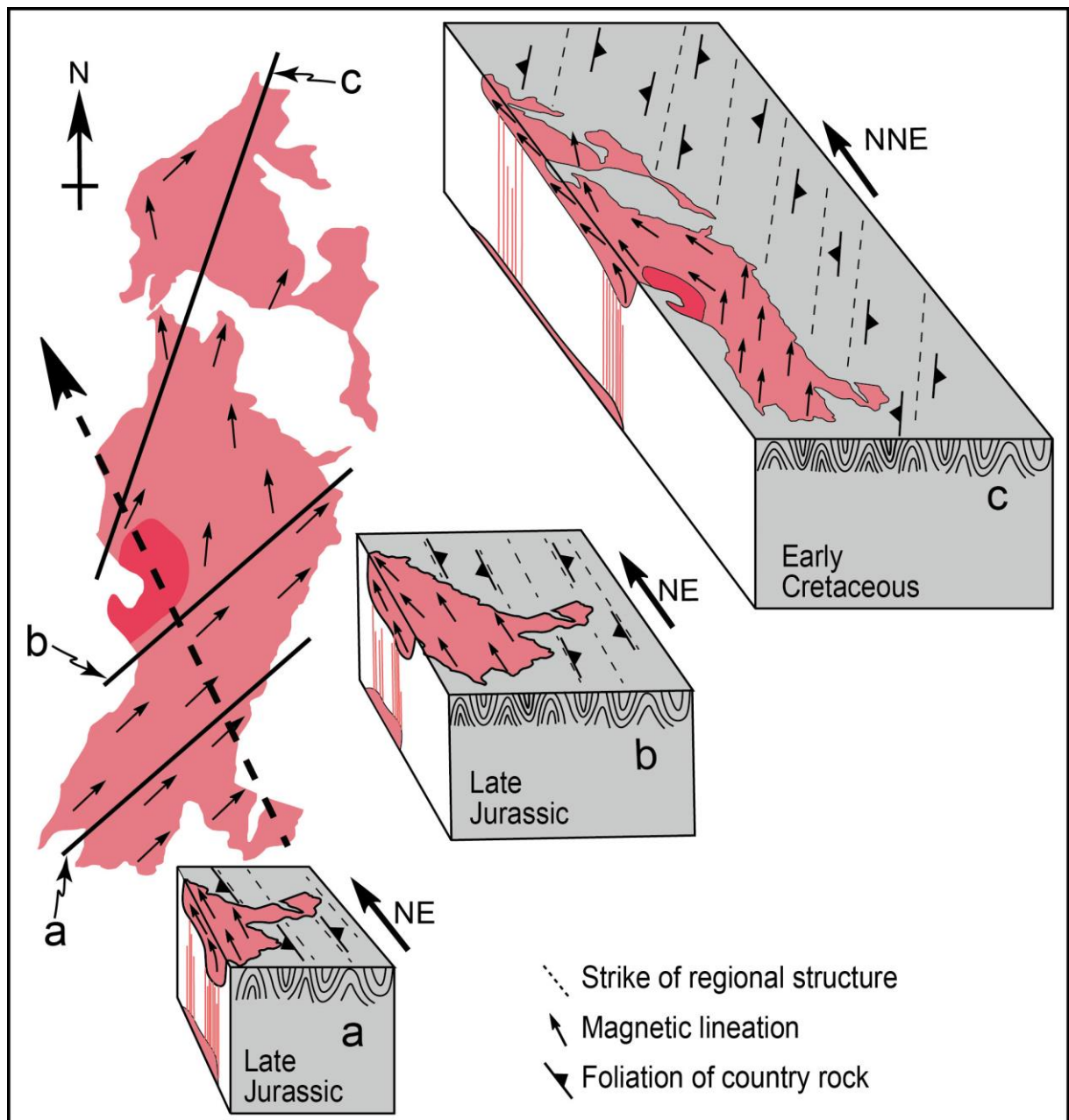


Figure 4-11. Lateral dike accretion model of the Shibeï pluton and different stages of dike accretion of emplacement process are briefly presented.

The negative Bouguer gravity anomaly belt that crosscuts the Mayuan group (Fig. 4-8) suggests a lower density material belt with respect to the current exposures of the Mayuan group underlain

the Mayuan group. The negative density belt extends in NW-SE direction and crosses the pluton, moreover, its strike is oblique to those of foliation of the country rocks and magnetic foliation of the pluton, but parallel with the dike accretion direction as we proposed in Figure 10a.

Altogether, we propose that the magma may emplace along those fractures or lithology contrast boundaries inside of the Mayuan group.

4.6.2.3 The mechanism of the magma emplacement

In light of our field and laboratory experiment results, we propose the following two-stage scenario to explain the emplacement process of the Shibeï pluton. The Shibeï pluton is constructed by a NW-ward lateral accretion of dikes from the southeastern part of the pluton extending in the NE-SW direction (thick dash line in Fig. 4-11).

During the Late Jurassic stage, the NE-SW orientated fractures or fold axes, produced by multiphases of pre-Jurassic tectonic events, developed in the Mayuan group are mechanically weak zones that can be used as channels for magma ascent. During this stage, the melts of the lower crust would uprise along these structures to form the sub-vertical NE-SW striking foliation. The magma flow parallel to the foliation strike would yield the dominantly sub-horizontal to moderately inclined magnetic lineation. Since the Paleoproterozoic cover is broken through by the first diking, the lateral dikes along its boundary are progressively accreted northwestwards from the southeast, as attested by the similar vertical to sub-vertical and NE-SW oriented magnetic foliation. The foliation geometry changes in the northern part of the pluton from the NE striking and vertical foliation to variable strike and moderate inclination, following the pluton shape or the foliation of the country rocks. In fact, the change of foliation geometry may be due to the structural change of the country rocks. The late Cretaceous stage concerns the final stage of the magma emplacement, recording the concordant magnetic foliation, the schlieren at the NW margin of the pluton, and the mainly N-S oriented magnetic lineation in the northern part of the pluton.

Therefore, we speculate that the partial melting of the lower crust intrudes along the fold structure, which presents a relatively weak zone, in the Mayuan group and laterally accreted to construct the pluton, in other words, the Shibeï pluton construction is controlled by the pre-Jurassic structures of the country rocks. The lateral inflation of the country rocks seems necessary to create the space for the emplacement of magma batches.

4.7 Conclusions

Though our multidisciplinary study, the emplacement of the Shibeï pluton is well constrained by the following acquisitions:

(1) No preferred minerals orientation can be identified by our field observations, and the thin sections investigations also present typical magmatic textures, without sub- and post-solidus

deformation, therefore the fabrics are primary ones.

(2) Consistent vertical magnetic foliation for the internal and external granite in the southern part of the pluton, which cross cut the bedding of the country rocks and parallel with the axial plane of the folds of the country rocks. The low dip-angle magnetic foliation is parallel with the bedding or fracture in the country rocks, with different randomly oriented magnetic lineations.

(3) Gravity modelling revealed that the Shibeï pluton have an oblate shape, with the thickest part up to 2.5 km located at the southern part of the pluton. The magma supply channel may correspond to ancient fractures in the country rocks reactivated during the magma intrusion.

In summary, we propose that the late Jurassic epoch may a quiet tectonic period and the emplacement of the Shibeï pluton is through dike accretion, each phases of diking is extending in the NE-SW direction and gradually accreted in the NW direction. As no synmagmatic control of the emplacement, magma are guided by the inherited structures developed in the country rocks.

Chapter 5. A rigidity test of the southeastern part of the South China Block (the ancient Cathaysia Block): insights from paleomagnetic studies on Jurassic plutons

5.1 Introduction of the research content

The paleomagnetism is an indispensable method to study plate kinematics. It has provided the first proof of continental drift (Wegener, 1912; Runcorn, 1973), with the discovery of oceanic magnetic anomalies belt (Raff and Mason, 1961), and largely contributed to the establishment of the plate tectonics theory. The application of paleomagnetism to plate tectonics is based on two hypotheses: (1) the geomagnetic field is a central axial dipole, and (2) the studied plate is a rigid body.

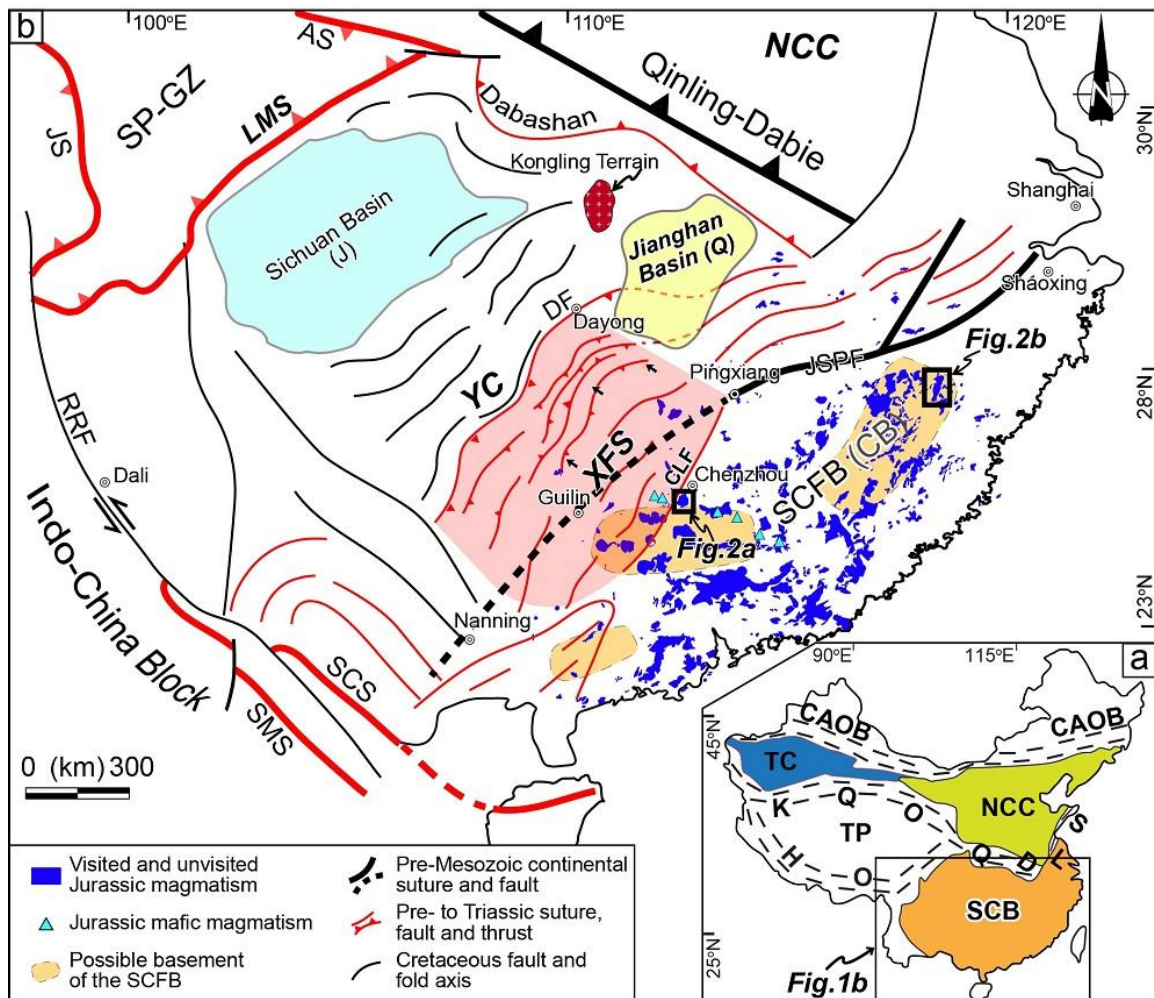


Figure 5-1. (a) Sketch of the major geological units in China. (b) Tectonic framework and distribution of the Jurassic magmatism in the South China Block with location of the two plutons studied in this chapter.

In this study, we are interested in the southeastern part of the South China Block (SCB in Fig. 5-1a), the ancient Cathaysia block (CB in Fig. 5-1b). In this zone, the internal deformation is visible

in numerous areas, especially characterized by the presence of reliefs, basins and granitic plutons. Analysing the magnetic remanence and calculating their corresponding paleomagnetic poles from different plutons will allow us recognize if these plutons experienced relative movements, and therefore if this zone underwent an internal deformation, as similar paleomagnetic poles should be acquired from the same Jurassic bodies, when the magnetic remanence are not reset by subsequent thermal events. In other words, whether if this zone is rigid or not. So, we apply the paleomagnetism here to test the rigidity of the SCB.

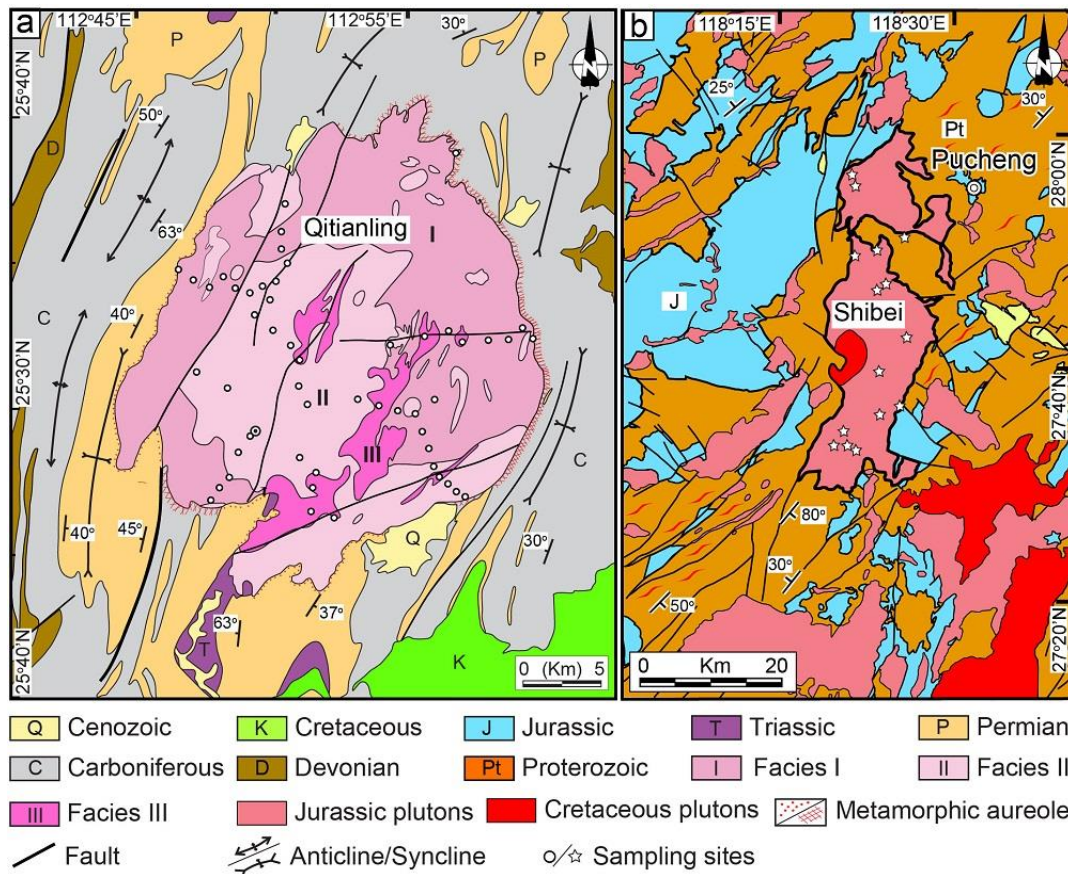


Figure 5-2. (a) and (b) Geological map for the Qitianling pluton and the Shibeai pluton.

Two granitic plutons have been targeted in this study: the Qitianling and Shibeai plutons (black rectangles in Fig. 5-1b and Fig. 5-2). The Qitianling pluton yields zircon U-Pb age peak at ca. 155 Ma (Zhu et al., 2009), and the Shibeai pluton is dated at 155.9 ± 1.7 Ma (Wang et al., 2016). Moreover, the distance between these two plutons is about 600 km (Fig. 5-1b), which is large enough to cover the error due to the calculation. Thereby, systematic sampling on the two plutons, magnetic remanence measurements and paleomagnetic poles calculation of the Qitianling and Shibeai pluton will be given. The comparison of the paleomagnetic poles of these two plutons will bring new insights on the SCB rigidity.

5.2 Regional geological context

The South China Block (SCB) is formed by the collision of the Yangtze and the Cathaysia

blocks (Figure 5-1b; e.g. Zhao and Cawood, 1999). The Yangtze and Cathaysia block were gradually agglomerated from ca.950-900 Ma (Metcalf, 2006) to ca.825 Ma (Li et al., 1997; Wang et al., 2007). After this assemblage, this composite block experienced several phases of tectonics and magmatism during the Neoproterozoic, Paleozoic and Mesozoic times. Furthermore, the most spectacular geological phenomenon is the widespread Jurassic magmatism (Fig. 5-1b), the exposure of which are dominantly concentrated in the southeastern part of the SCB.

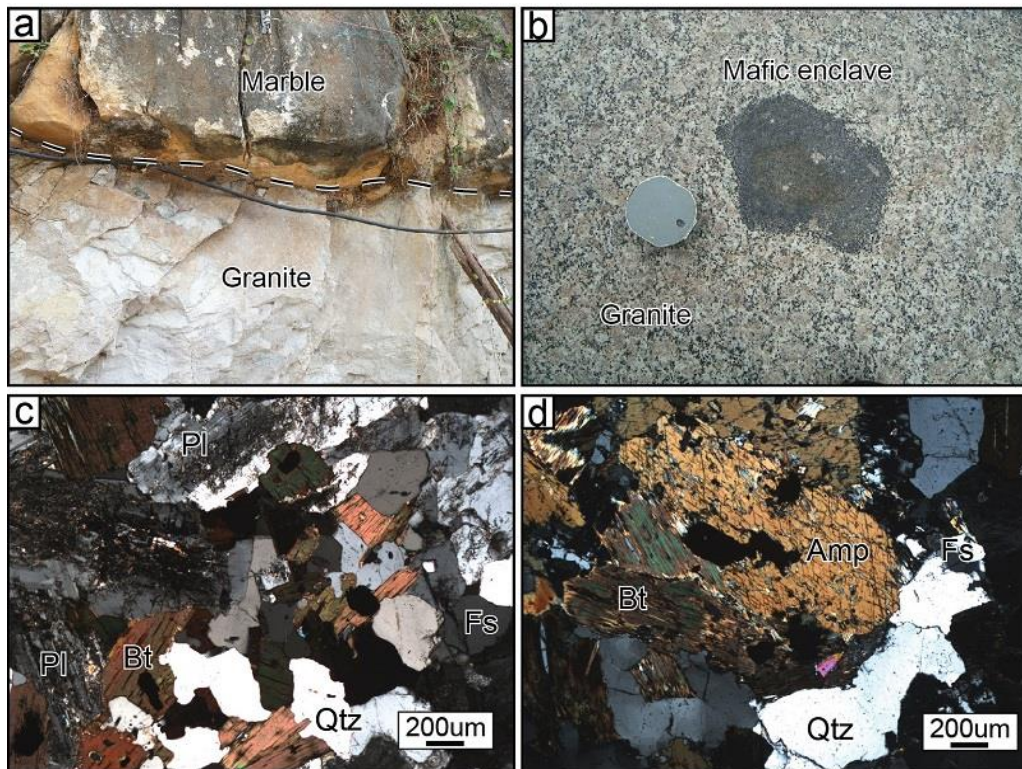


Figure 5-3. (a) Contact between the pluton and country rock. (b) Granite and the enclave in the pluton. (c) and (d) thin section observations of the granite of the Qitianling pluton. Abbreviations: Amp: Amphibole, Bt: Biotite, Fs: Feldspar, Qtz: Quartz.

Several hypotheses have been proposed to explain this distribution of these granitic plutons: (1) Gradual steepening of the low-angle of subduction of the Paleo Pacific plate (Zhou and Li, 2000); (2) Paleo Pacific oceanic flat-slab or plate subduction between 250 to 190 Ma, followed by a break-off of the subducted slab into the mantle between 190 to 150 Ma (Li and Li, 2007); (3) Retreat of the subducting plate (Jiang et al., 2009); (4) First a translation of magmatic arc from the coast to the interior, then a second translation of magmatism from interior to the coast (Jiang et al., 2015). However, these hypotheses are essentially based on geochemical and geochronological results.

5.2.1 The Qitianling pluton

The Qitianling pluton (ca. 155 Ma) is located at northwest side of the Cathaysia Block (Fig.

5-1b), which mainly emplaced into Carboniferous and Permian strata. Previous studies divided the granite into three facies, i.e. facies I: amphibole bearing granite with locally developed mafic enclaves, facies II: Biotite granite with locally exposed assimilated enclaves, facies III: fine grained biotite granite. The thin section investigations present typical magmatic textures with euhedral quartz (Qtz), plagioclase (Pl), K-feldspar (Kfs) and biotite (Bt) (Fig. 5-3). The sharp contact between granite and its country rocks and no relative movement between them can be observed. The entire pluton also lack of sub- to post-solidus deformation, which represented by preferred mineral orientation. Therefore, we suppose that the current pluton geometry is not changed by subsequent tectonic events.

5.2.2 The Shibeï pluton

The Shibeï pluton is located at the northeastern part of the ancient Cathaysia block (Fig. 5-1b and Fig. 5-2b). It is a composite pluton composed by Jurassic and Cretaceous intrusions. The Jurassic part is the target of this study (Fig. 5-2b). The pluton lithologically consists of I-type alkaline granite (Zhou et al 2006; Wang et al 2016). These granitic rocks are composed of K-feldspar, quartz, plagioclase, biotite with a weak proportion of monzogranite (Fig. 5-4a and 5-4b). U-Pb dating on nineteen zircon grains have provided an average age of 155.9 ± 1.7 Ma for this pluton (Wang et al 2016).

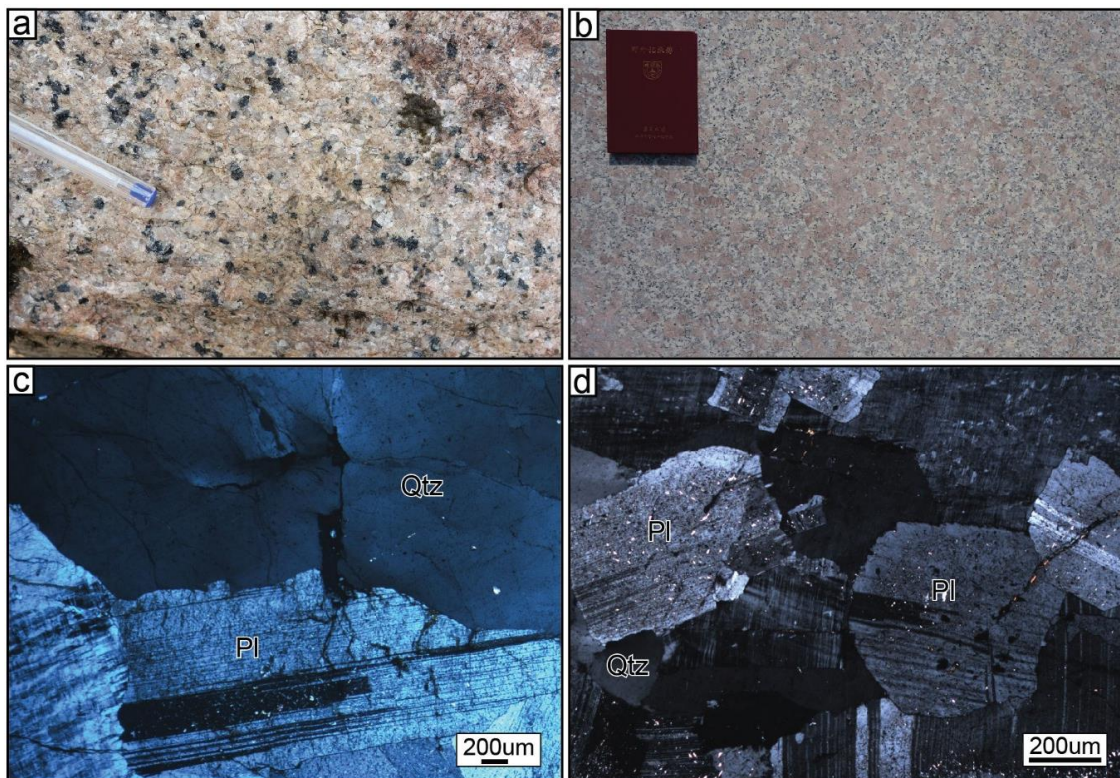


Figure 5-4. (a) and (b) petrography of the Shibeï pluton, (c) and (d) thin section observations of granite from the Shibeï pluton. Abbreviations in the pictures: Pl-Plagioclase, Qtz-Quartz.

The field macroscopic observations, and thin section microscopic investigations show that the granite have euhedral to sub-euhedral crystals of granites, and lack of mineral preferred orientation (Fig. 5-4). The measurements of Anisotropy of Magnetic Susceptibility (AMS) of granites present a weak anisotropy degree. Accordingly, we consider that the pluton did not suffered any significant deformation posterior to its cooling.

5.3 Sampling and laboratory analyses

5.3.1 Sampling and specimen preparation

Few paleomagnetic studies have been carried out in granitic plutons due to the impossibility to make the fold test and the difficulty to know if the pluton has been tilted since its cooling. Therefore, before the sampling, we have to make sure that the pluton did not experienced any post-solidus deformation, neither been tilted along a horizontal axis.

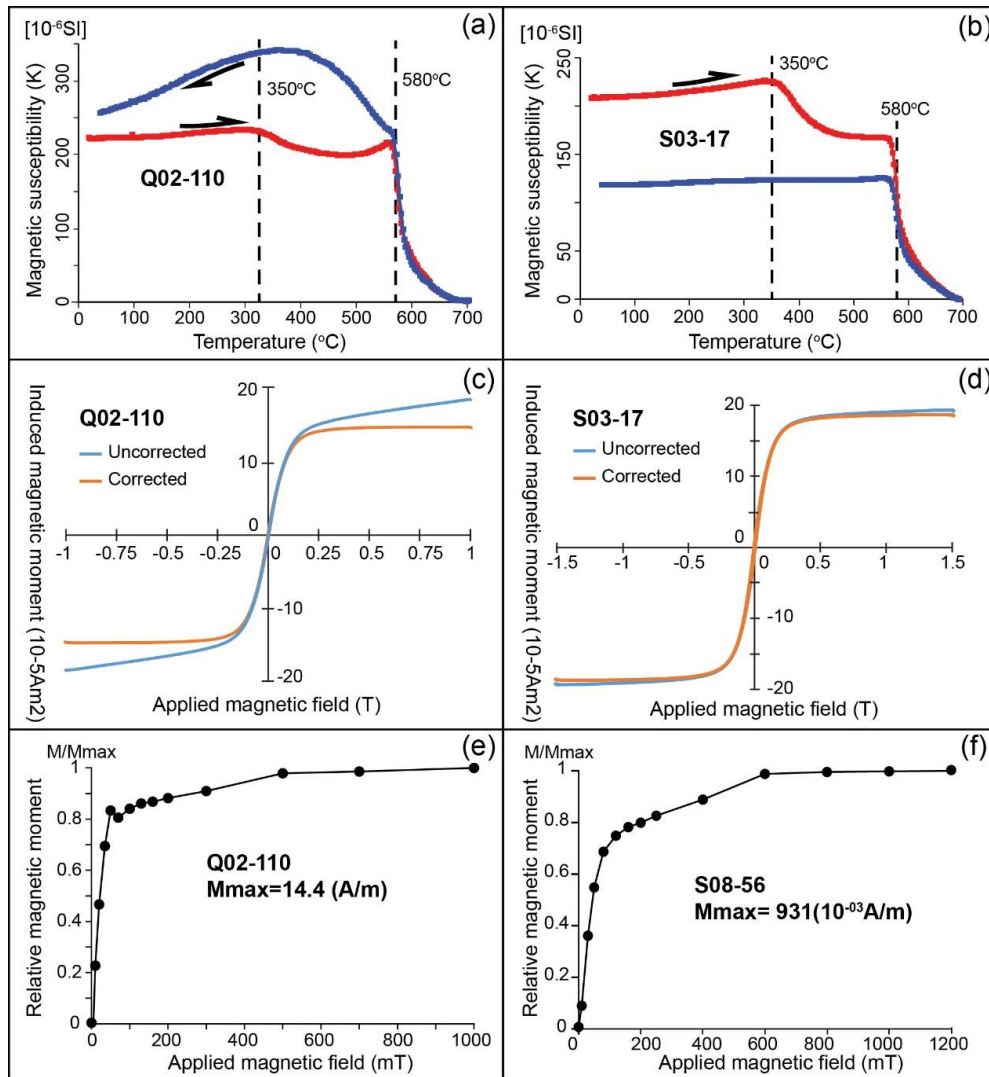


Figure 5-5. Representative magnetic mineral analyses results. (a) and (b) thermal magnetic mineral measurement. (c) and (d) hysteresis loops. (e) and (f) Isothermal Magnetic Remanence measurement.

A total of 53 sites and 37 sites have been collected with an interval of 2 km and homogeneous distribution from the Qitianling and Shibeï pluton, respectively (Fig. 5-2). Six to eight cores are taken in each site with a portable drill. The cores were oriented with magnetic and solar, when possible, compasses. The difference in these two azimuths of the Qitianling pluton is 7.5 ± 2.0 and the Shibeï pluton is $-9.4^\circ \pm 1.2^\circ$, and these averages are applied to those without solar measurement. The standard cylinder specimens of 2.5 cm in diameter and 2.2 cm in height are prepared for the laboratory measurements.

5.3.2 Magnetic mineralogical investigation

Before the magnetic remanence demagnetisation, several magnetic mineralogical investigations such as Isothermal Remnant Magnetization (IRM), magnetic hysteresis cycles and thermal magnetic experiments have been carried out in the purpose to recognize the magnetic remanence carriers.

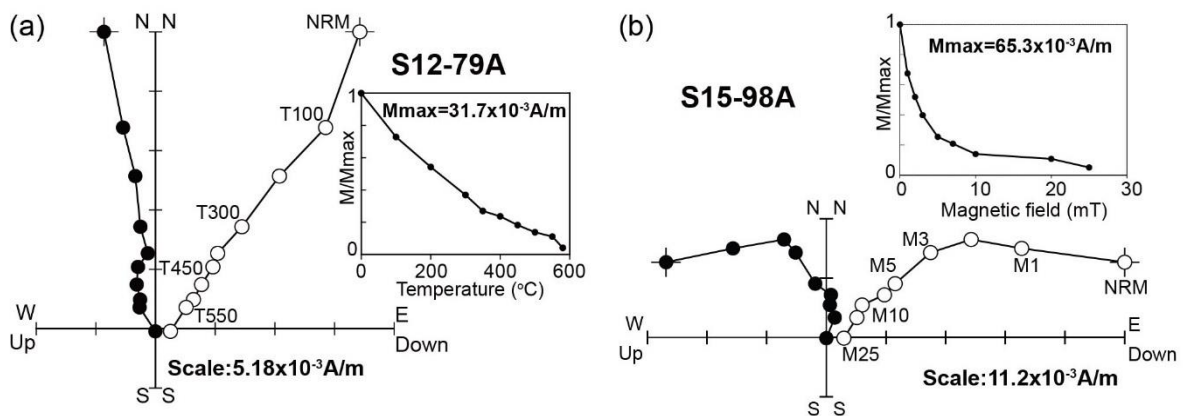


Figure 5-6. Orthogonal demagnetization diagrams (in situ coordinates) for the Jurassic Shibeï pluton.

The representative data of three different methods show rather similar magnetic behaviours (Figs. 5-5). The rapid drop of the magnetic susceptibility at 580 °C, and gradual drop at 350 °C indicate the existence of magnetite and titanomagnetite in the granite, respectively (Fig. 5-5a and 5-5b). The magnetic susceptibility has been reduced after the heating for sample S03-17 (the red line is higher than the blue one), indicating that the mineral transformation took place during the heating. Combining with above analyses, it seems that hematite and partial magnetite (with higher magnetic susceptibility) have been transformed to hematite (with lower magnetic susceptibility). Typical S-shaped and multidomain-like hysteresis curves for samples Q02-110 and S03-17 (Fig. 5-5c and 5-5d; Suk et al., 1996), with very approximate value of the induced magnetic moment between uncorrected and corrected curves, indicate that ferromagnetic minerals are the dominant magnetic carriers with little contribution from paramagnetic minerals. The rapid increase of IRM

before 100 mT and a less rapid until the saturation at about 600 mT for the samples Q02-110 and S08-56 (Fig. 5-5e and 5-5f), showing that the minerals are weakly coercive, likely magnetite and pyrrhotite or maghemite. Therefore, these kind of minerals can be demagnetized by either thermal or alternative magnetic field (AF) techniques or both.

5.3.3 Demagnetization of specimens and calculation of paleomagnetic direction

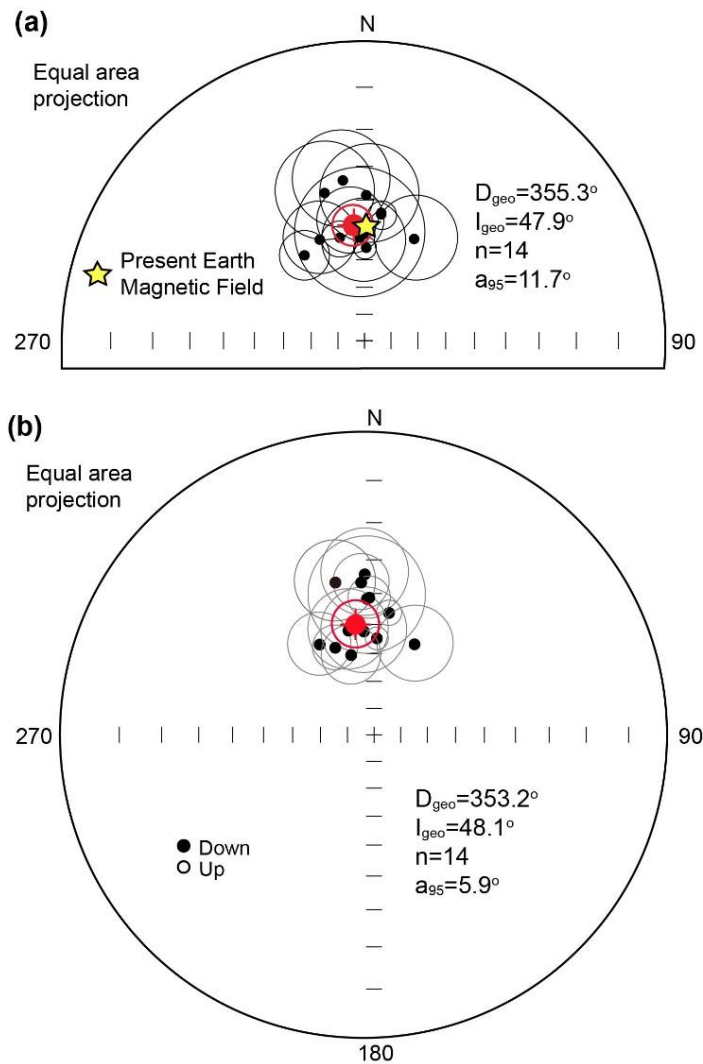


Figure 5-7. Equal-area projections of site-mean low (a) and high (b) temperature/field directions. Black dots and ellipses are the site-mean direction and α_{95} confidence, respectively.

The specimens have been progressively demagnetized by both thermal and AF techniques. About 12 to 15 steps have been applied for the demagnetization: thermally from room temperature to 580 °C, and from 0 to 100 mT by AF. Both progressive demagnetizations reveal two components, namely low temperature/field and high temperature/field components (Fig. 5-6). Detailed results of the paleomagnetic directions for the Qitianling pluton are listed in Pons et al, (2016). For the Shibei pluton, the low temperature/field components have been isolated from 0 to 200 °C or 0 to 10 mT

(Fig. 5-6a and 6b). The mean direction of the low temperature/field components have been calculated for the Shibeï pluton from 14 sites at $D = 355.3^\circ$, $I = 47.9^\circ$, $n = 14$ sites, $\alpha_{95} = 11.7^\circ$ (Fig. 5-7a). This direction envelops the Present Earth Magnetic Field, therefore, this component presents probably a recent remagnetization (Fig. 5-7a).

The high temperature/field components are isolated from about 250 to 580 °C and 15 mT to 100 mT (Fig. 5-7b). Table 5-1 presents the paleomagnetic directions calculated from these high temperature/field components with an age-mean direction at $D = 353.2^\circ$, $I = 48.1^\circ$, $n = 14$ out of 15 sites and $\alpha_{95} = 5.9^\circ$ (Fig. 5-7b). The direction of Site 32 is outside from others due to probably its position close to the country rocks, therefore, it is excluded from the final average.

According to the paleomagnetic direction and the geographic coordinates of each sampling site, their corresponding paleomagnetic poles have been calculated and listed in Table 5-1, with an age-mean pole at $\lambda = 83.9^\circ \text{N}$, $\phi = 46.6^\circ \text{E}$, $k = 46.7$, $n = 14$ sites, $A_{95} = 5.5^\circ$.

Table 5-1. The Paleomagnetic measurement on the Shibeï pluton.

| Granite from the Shibeï pluton (SE of South China: 118.5 E, 27.5 N) | | | | | | | | |
|---|-------|-----|--------|--------|--------|-------------------|-----------|------------|
| Site | n/N0 | R/N | Dg (°) | Ig (°) | k | α_{95} (°) | Pole lat. | Pole long. |
| Higher-temperature Component | | | | | | | | |
| S02 | 05/06 | 0/6 | 329 | 51.7 | 52.99 | 10.6 | 62.8 | 46.3 |
| S03 | 05/06 | 0/6 | 345.8 | 35.2 | 41.3 | 12 | 75.6 | 1 |
| S04 | 06/06 | 0/6 | 1.5 | 39.1 | 20.08 | 15.3 | 86.4 | -90.1 |
| S06 | 06/07 | 0/7 | 353.2 | 36 | 17.63 | 16.4 | 80.7 | -42 |
| S07 | 06/07 | 0/7 | 7 | 45.9 | 270.34 | 4.8 | 83 | -140.3 |
| S09 | 07/08 | 0/8 | 336 | 55.1 | 63.1 | 7.7 | 68.1 | 56.3 |
| S12 | 07/09 | 1/9 | 346.2 | 51 | 25.89 | 13.4 | 77.3 | 51.1 |
| S15 | 07/09 | 1/9 | 24.1 | 53.8 | 22.78 | 12.9 | 68.3 | -175.8 |
| S18 | 07/07 | 0/7 | 358 | 41.3 | 104.00 | 6.6 | 85.8 | -35.9 |
| S20 | 07/09 | 0/9 | 346.6 | 51.9 | 70.16 | 6.2 | 76.4 | 57.2 |
| S22 | 09/09 | 0/9 | 354.4 | 52.2 | 18.59 | 14.4 | 72.3 | -150.4 |
| S26 | 09/09 | 0/9 | 1.0 | 55.6 | 181.4 | 3.8 | 79.3 | 117.4 |
| S31 | 07/08 | 0/8 | 355.2 | 36.5 | 64.43 | 8.4 | 81.6 | -28.8 |
| S32 | 07/07 | 0/7 | 288.3 | 57.6 | 42.7 | 9.3 | 29.3 | 54.3 |
| S34 | 06/06 | 0/6 | 344 | 59.4 | 78.45 | 10.4 | 70.2 | 74.7 |
| Mean PCA | - | - | 353.4 | 48.2 | 46.7 | 5.9 | 83.9 | 46.6 |

Note: n: the number of specimens which are used for further calculation, N0: the total specimens for each site that used for paleomagnetism measurements

5.4 Discussion of the paleomagnetic results and its implications

5.4.1 The Shibeï pluton as the target of study

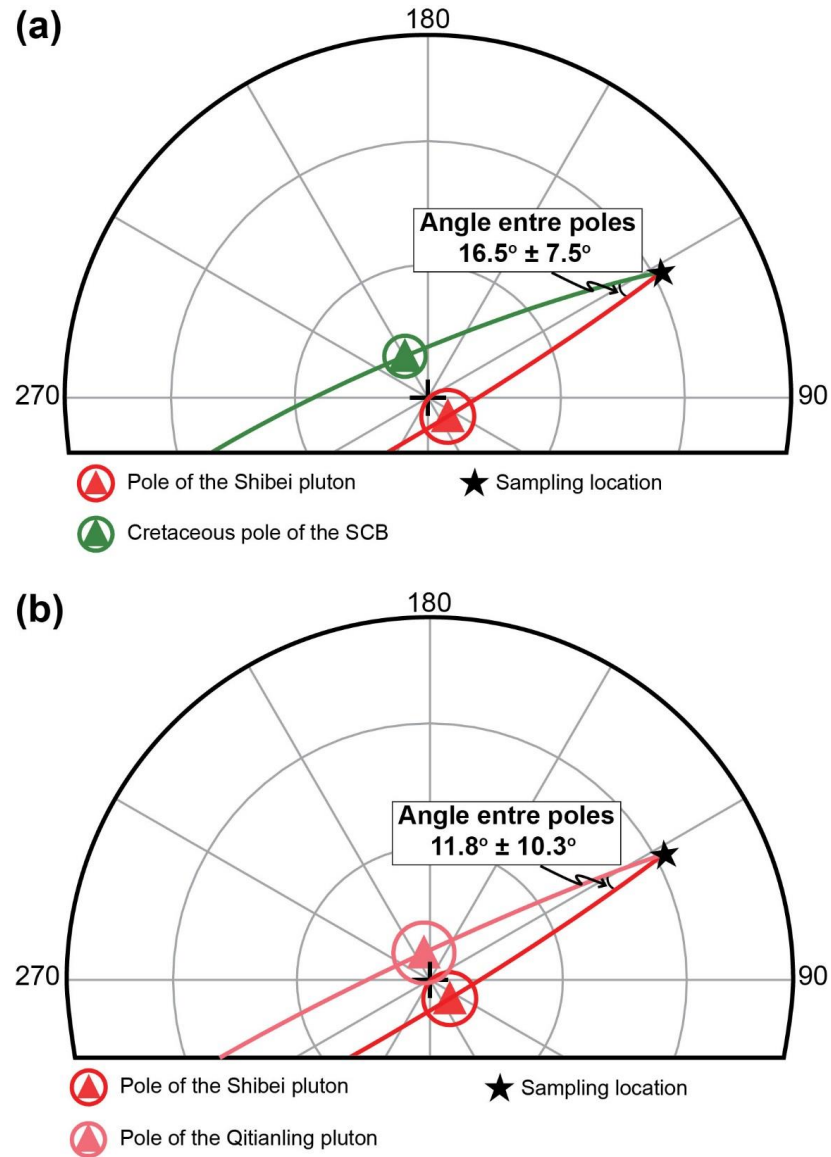


Figure 5-8. (a) Paleomagnetic poles comparison between the Shibeï pluton and the Cretaceous one. (b) Comparison of the paleomagnetic poles of the Shibeï and Qitianling pluton respectively.

In the purpose to test the rigidity of the South China Block, the Shibeï pluton is a good target to carry out this topic thanks to following two reasons: (1). The macroscopic (field) and microscopic (laboratory) observation show that the Shibeï pluton did not experienced any visible posterior deformation since its emplacement, therefore we can make a paleomagnetic study to evaluate its paleogeographic position at the granite intrusion time, i.e. 155.9 ± 1.7 Ma; (2). The contemporaneous Qitianling granitic pluton about 600 km in the west from the Shibeï pluton has been previously studied which provides the possibility to make a comparison and therefore to make this test.

5.4.2 Origin of the magnetic remanence

It is well known that the abundant Cretaceous magmatism was produced in South China, which may remagnetize the older rocks, including the Jurassic granite. So, the first worry that we can have on our data is whether if they have been remagnetized by the thermal event of the widespread Cretaceous magmatism in our study area (Zhou et al., 2006). Zhu et al. (1998) made a synthesis on the Cretaceous paleomagnetic results and give an average paleomagnetic pole of the SCB at 79.4 N and 209.0 E with A95 of 4.6° (Fig. 5-8a). The comparison of this paleomagnetic pole with that of the Shibeï pluton from this study provides a significant angular difference of $16.5 \pm 7.5^\circ$ between these two paleomagnetic poles (Fig. 5-8a), implying that the paleomagnetic results from the Jurassic Shibeï pluton cannot be considered as remagnetized by the Cretaceous magmatism. Moreover, it is still few with respect to the number of samples which present a normal polarity, several samples from some sites show a reversed magnetic polarity, this may suggest that the record duration of the geomagnetic field may last enough long to average the secular variation. Therefore, it is reasonable to propose a primary origin of magnetic remanence for the Jurassic Shibeï pluton.

5.4.3 Age of the magnetic remanence

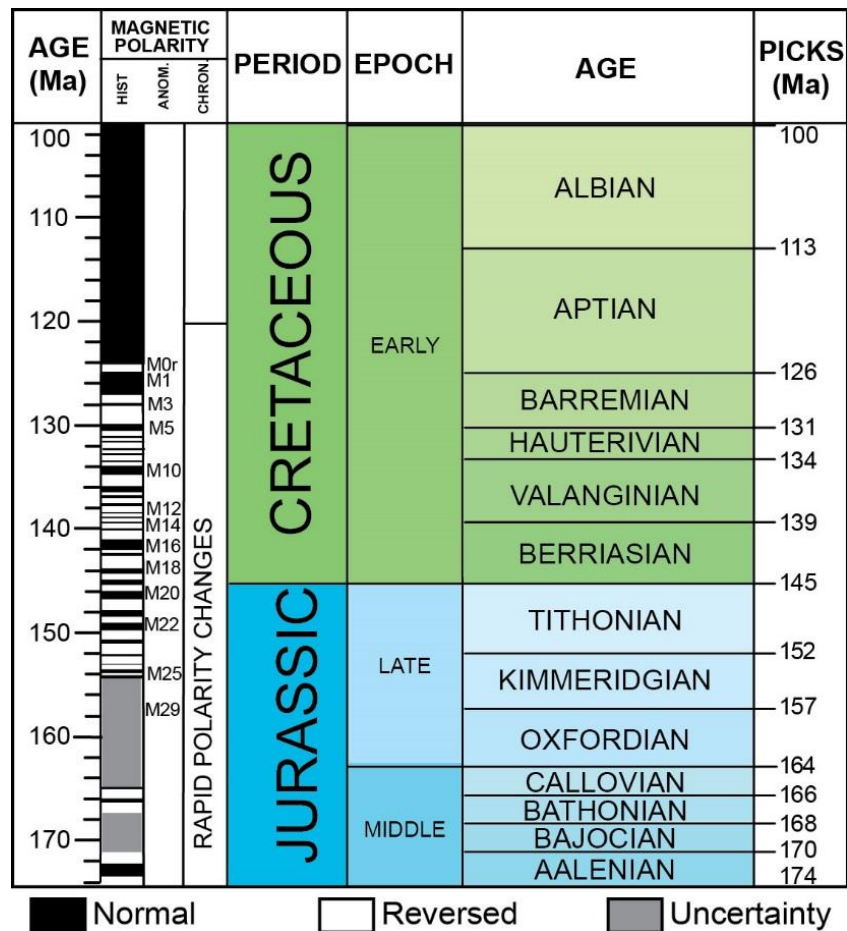


Figure 5-9. Geomagnetic polarity scale for the Cretaceous and Jurassic periods (according to International Commission on Stratigraphy, 2012).

As mentioned above, the majority of the demagnetized samples show the normal magnetic polarity, the weak proportion of samples with a reversed polarity may constrain the record time of the geomagnetic field by our samples during a period of the principal normal polarity. The U-Pb dating on zircons gives an ages of 155.9 ± 1.7 Ma (Wang et al 2016).

Assuming the thermal closure temperature of zircon at about ca. 900 °C (Lee et al., 1997) and taking the general cooling rate of granite plutons at 50 °C/Ma (Charles, 2013), the magnetic remanence isolated from 350 °C to 580 °C and carried by the magnetite from the Shibeï pluton may be recorded at about 149 to 150 Ma before. The world geomagnetic polarity scale (The Geologic Time Scale 2012: Boston, USA, Elsevier) for the Cretaceous and Jurassic period (Fig. 5-9) shows a higher polarity change rate for the all Jurassic period, nevertheless, the normal polarity is the principal one in the period between chrons M20 and M25 at about 150 Ma (Fig. 5-9). This seems compatible with the age of the magnetic remanence of the Shibeï granite estimated with the U-Pb dating and the cooling rate.

5.4.4 Comparison of paleomagnetic poles and rigidity test

Pons (2016) has carried out a paleomagnetic study on the Qitianling pluton and the results are similar to those from the Shibeï pluton: no Jurassic related deformation macro-and microscopically observed in both country rocks and pluton, the normal polarity for the majority of samples, the absence of the Cretaceous remagnetisation and the U-Pb age at about 155 Ma. The paleomagnetic pole from 3 facies of granites is calculated at 83.8 °N, 192.5 °E with A95 of 6.8 °.

Figure 5-8 (b) presents the two paleomagnetic poles from the contemporaneous Shibeï and Qitianling plutons. The angular difference of 11.8 ± 10.3 ° between them is statistically significant, implying that a significant relative movement has taken place between these two plutons since the Late Jurassic. If getting into details, this angular difference represents a relative rotation of 13.5 ± 10.3 ° and a relative motion in latitude of 0.2 ± 7.2 ° between these two plutons. In other words, the relative motion between these two plutons is essentially in rotation instead of in latitude. Accordingly, we can conclude that the South China Block cannot be considered as a rigid block at least at the block scale, therefore the special caution should be taken when we use paleomagnetic results from South China to study its kinematic evolution.

In geological sense, this paleomagnetic results are meaningful. As described in the Geological setting section, the study zone is located in the southeastern part of the South China Block that covers the major surface of the ancient Cathaysia block, moreover, the latter is also composed of several Proterozoic sub-blocks. After the formation of the SCB at about 850 Ma (Wang et al., 2007), several important tectonic events have been recorded, especially in the study zone (the Cathaysia block) and peripheral zones of the ancient Yangtze block, such as Neoproterozoic Nanhua rifting, Early Paleozoic intracontinental orogeny, Triassic multi-direction subductions of the SCB with

respect to its surrounding blocks and intracontinental deformation. The most remarkable geological and geographical features in the study zone are: (1) The topographic surface is in high relief without irregular range shapes; (2) The Jurassic plutons without major structural control are widespread; (3) the Cretaceous and Tertiary basins are numerous but in small size and with respect to those in the North China Block; these lines of evidence suggest that the study area does not represent a rigid body, and thus internal deformation should have occurred. This tends to the same sense to call the ancient Cathaysia Block as the South China Fold Belt (Huang, 1945).

5.5 Conclusions and perspectives

From this paleomagnetic study, the following conclusions can be drawn.

1. By the mineralogical investigation, thermal test and the presence of the two magnetic polarities, the primary magnetic remanence has been identified in the granites of the Shibeil pluton;
2. Assuming i) the blocking temperature of magnetite about 580-550 °C, ii) the closure temperature of zircon at about 900 °C, and iii) a cooling rate of 50 °C/Ma for the pluton, dated by U-Pb method on zircon at 156 Ma, the magnetic remanence is estimated at ca 150 Ma;
3. The comparison of the paleomagnetic pole from this study with the contemporaneous one obtained on the Qitianling pluton, located at 600 km presents a significant angular difference of $11.8 \pm 10.3^\circ$; implying that these blocks have experienced a different kinematic evolution since the pluton emplacement time, i.e. the Late Jurassic;
4. Synthesizing the geological and geographical phenomena with the paleomagnetic investigations, we can conclude that the southeastern part of the South China Block (the ancient Cathaysia block) experienced an internal deformation and behaved as a no rigid body. The term of 'the South China Fold Belt seems more convenient to the study zone. Therefore, particular caution should probably be taken when we apply the paleomagnetic method in this zone to study regional deformation. Of course, more paleomagnetic studies in a large area are needed to verify the last conclusion.

Chapter 6. Understanding of the Jurassic Large Granitic Province of SE China

6.1 Introduction of the research of Large Granitic Provinces

The Large Igneous Provinces (LIPs) involve enormous igneous bodies (Coffin and Eldholm, 1994). Its formation is one of the most important ways to create and make reworking of crust, therefore, the LIPs have been largely studied and classified into several types in terms of its lithology (mafic or silicic dominated LIPs; e.g. Bryan, 2007), tectonic context of emplacement (extrusive or intrusive LIPs; e.g. Sheth, 2007) and geodynamic setting (active plate margin or intraplate LIPs; e.g. Eldholm and Coffin, 2000).

According to Bryan, (2007), the variety of the LIPs is due to different tectonic and geodynamic settings. The LIPs yielded in an active plate margin are usually related to the plate subduction or crustal scale rifting, therefore, the long axis and the distribution of the magma bodies are usually parallel/perpendicular to the tectonic boundary, i.e. plate margin, for example, the Sierra Madre Occidental in the north of Mexican (e.g., Ferrari et al., 1999). The LIPs developed in an intraplate setting are usually driven by the asthenosphere mantle convection or extension/collapse of lithospheric mantle. Therefore, dominantly mafic magmatic rocks and the topography response, for example, radiating dyke swarm (Ernst, 1997) and regional uplifting or sagging (Peate and Bryan, 2008), will be observed.

The southeastern part of the South China Block (SCB in Fig. 1-4a) is characterized by a widespread Mesozoic plutonism (Fig. 1-4b) extending over 1500 km in length and 800 km in width with a total exposed surface area of ca. 135,000 km² (Fig. 1-4b, Zhou et al., 2006). The Jurassic plutons represent 47% (ca. 62,700 km² Zhou et al., 2006) of the Mesozoic ones. They can be considered as a Large Granitic Province (LGP) (Sheth et al. 2007). It presents several unique and remarkable features such as the widespread distribution (Fig. 1-4), predominant granitoid with a few mafic rocks, rare volcanites (Fig. 1-4a), long duration of about 40 Myrs (Fig. 1-4c; Zhou et al., 2006), and changing Mesozoic tectonic settings from Triassic shortening to Cretaceous extension. These features are different from those of the classic LIPs in the world mentioned above. However, the study of this Jurassic LGP in the SCB has attracted a little attention of the international geological community.

Previous studies mainly focus on the petrological, structural, geochemical and geochronological features of the individual plutons, and several models for the Mesozoic tectonic evolution of the SCB have been proposed (Fig. 1-4; Zhou et al., 2000; Li and Li., 2007; Jiang et al., 2009; Shu et al., 2009; Kiminami and Teruyoshi, 2013; Faure et al., 2016). The majority of these models consider that the Mesozoic magmatic and tectonic evolution were related to the long-duration of the Paleo-Pacific oceanic slab subduction under the SCB (Fig. 1-6). However, several basic geological

phenomena are incompatible with these geodynamic models, for instance, the lack of synmagmatic regional tectonic to control the genesis and emplacement process of the intensive Jurassic magmatism, the long-lasting Mesozoic magmatism of about ca. 140 Myrs (Fig. 1-4c) with different magma associations.

To enlighten the interaction between the Jurassic LGPs in South China and its related tectonic and/or geodynamic settings, we have characterized the granite-host-rock contacts and deformation for 41 Jurassic plutons (Fig. 1-4a) by field and thin section observations. We further in detail investigated the Qitianling pluton, a representative Jurassic pluton, via the Anisotropy of Magnetic Susceptibility (AMS) to reveal the petro- or/and tectonic fabrics through the study of the magnetic fabric and also the gravity modeling to constrain the pluton 3D shape. Based on these new data, we propose a new geodynamic model for the formation of the Jurassic LGP in the SCB.

6.2 Geological setting of the Mesozoic magmatism

The SCB (Fig. 1-4b) was formed by the amalgamation of the Yangtze Craton (YC in Fig. 1-4a) to the northwest with the Cathaysia Block (CB in Fig. 1-4a) to the southeast at ca. 850 Ma (e.g. Li et al., 2008). The NE-SW striking Jiangnan Orogenic Belt, formed during the Neoproterozoic collision, and the Jiangshan-Shaoxing-Pingxiang fault represent the ophiolitic suture zone (JSPF in Fig. 1-4a; e.g. Charvet et al., 1996, Li et al., 2001). The Yangtze craton is a rigid one with lithosphere and crustal thicknesses of ca. 170 km and 45 km, respectively (An and Shi, 2006; Deng et al., 2014). The Archean TGGs (3.3 Ga; Gao et al., 2011) exposed in the northern part of the Yangtze craton is considered as a basement component. In contrast, the lithosphere and crust thicknesses of the Cathaysia block are estimated at 100 km and 30 km, respectively (An and Shi, 2006). Variable Neodymium and Strontium isotope values of igneous, sedimentary and metamorphic rocks and strong lateral density variations of the Bouguer gravity anomaly data across the Cathaysia Block reveal that the basement of the Cathaysia Block is heterogeneous (Chen and Jahn, 1998; Deng et al., 2014). Moreover, the petrological, geochemical and geochronological data of the Paleoproterozoic strata, exposed in the Cathaysia Block and considered as the basement unit, show that the Cathaysia block is composed of three or more micro blocks with Paleoproterozoic basements (Guo et al., 1989; Fletcher et al., 2004; Yu et al., 2009).

Subsequently, the early Paleozoic (~450 Ma) intracontinental orogeny is characterized by an east-west striking fold-and-thrust belt, with south-directed faults resulting in a north-south shortening and associated with S-type granite and migmatites, which are mainly localized at the southeastern part of the SCB (Wan et al., 2007; Charvet et al., 2010; Wang et al., 2014; Shu et al., 2015).

During the early Mesozoic, the SCB experienced a series of multi-direction subductions with its surrounding blocks and intracontinental deformation as well. The ca. 250-230 Ma collision of the Indochina block developed in its southwestern part along the

Jinshajiang-Songma-Songchay-Hainan suture and its possible eastward extension (JS-SMS-SCS in Fig. 1-4a; Lepvrier et al., 2004; Faure et al., 2014, 2016). In the north, the closure of the Paleo-Tethys Ocean was driven by the northward subduction of the Songpan-Ganzi remnant ocean along the Kunlun-Animaqin suture (AS in Fig. 1-4a; ca. 230-200 Ma; Harrowfield and Wilson, 2005). Eastwards, at 240-230 Ma, an intracontinental orogeny superimposed upon the Early Paleozoic Qinling-Dabie collision orogen (Fig. 1-4a; Mattauer et al., 1985; Xu et al., 2006). The northwestward subduction of the SCB under the Songpan-Ganzi block, around 240-200 Ma, gave rise to the Longmenshan thrust belt (LMS in Fig. 1-4a) in the northwest (Yan et al., 2011; Luo et al., 2014). Lastly, the Triassic intracontinental Xuefengshan belt occurred at ca. 245-215 Ma on the northwestern margin of the Cathaysia Block, but involved also a part of the SW margin of Yangtze and is represented by a series of NE-SW-striking and NW-verging folds and thrusts (XFS marked by light red color in Fig. 1-4a; Chu et al., 2012a, 2012b).



Figure 6-1. Intrusive contact between the Jurassic plutons and its wall rocks in the SCB. Detailed information of the contacts is listed in table 6-1.

The deformation produced by these multidirectional subductions and intracontinental tectonics are not only absorbed in the orogenic belts, but also inside of the Cathaysia Block due to its heterogeneity in composition and rigidity supported by widespread Triassic thermal tectonic ages within of the Cathaysia Block (*c.f.* Li et al., 2017 and references therein). In fact, the Cathaysia Block has been also called the “South China Fold Belt” (the SCFB in Fig. 1-4b; Huang, 1945).

6.3 Field and experimental results

6.3.1 Overview of the Jurassic plutons and their country rocks in the SCFB

According to our field investigations on 41 plutons and its country rocks, which were geochronologically and geochemically well-studied, in the Jurassic LGP across the SCFB (Fig. 1-4b), several general characteristics of these plutons and their country rocks can be described as follows:

(1) In the macroscopic view, the Jurassic plutons of the LGP are intruded in highly deformed rocks of the SCFB. The scattered distribution of the Jurassic plutons without regular cartographic distribution (Fig. 1-4) and the absence of large batholiths with size $> 10^4$ km³ rule out any apparent regional structural control;

(2) Significant Jurassic regional deformation is absent, and the pre-Jurassic folding and thrusting are concentrated along the northern, northwestern and southwestern borders of the Yangtze Craton as well as in the northwestern margin of the SCFB in the Xuefengshan belt (as marked by the light red color in Fig. 1-4b);

(3) Jurassic sedimentary rocks are rare, when exposed, their thickness is less than 2 km, with gently inclined strata unconformable covered by early Cretaceous strata (Shu et al., 2015);

(4) Few large-scale Jurassic basins can be found in the SCB, but in the northwest of the ancient Yangtze craton, i.e. the Sichuan basin (200×230 km²) in which Jurassic continental sediment thicknesses reaches to ca. 6 km (Fig. 1-4a; Meng et al., 2005);

(5) Metaluminous to weak peraluminous monzogranites are predominant with subordinate peraluminous plutons (Zhou et al., 2006; Li et al., 2009), but contemporaneous mafic magmatism is rare (Fig. 1-4a) (Li et al., 2003; He et al., 2010; Huang et al., 2015);

(6) At the scale of the granitic plutons, the most significant feature is that all of the forty-one observed Jurassic massifs show sharp contacts with their country rocks and the granite does not show any preferred mineral orientation (Fig. 6-1);

(7) A narrow contact metamorphic aureole with hornfels and marble is conspicuous, but lacks of ductile deformation and syn-kinematic metamorphism in both pluton and country rocks (Fig. 6-1; GPS of the observed contacts are enclosed in the Table 6-1).

6.3.2 Field observation and experimental analysis of the Jurassic Qitianling pluton

Among these 41 massifs, the representative late Jurassic Qitianling pluton is targeted in a detailed study as it has been well studied in geochemistry, petrology and chronology. This pluton is located at the NW margin of the SCFB (Figs. 6-1a and 6-4a) with a surface of ca. 530 km² and dated by zircon U-Pb ranging from 146 to 163 Ma with a peak age at ca. 155 Ma (Zhu et al., 2009). Three major facies of hornblende-biotite- and biotite-granite were identified, according to their mineral association and petrography. The country rocks of the Qitianling pluton consist of Carboniferous, Permian and Triassic limestone and sandstone with NE-SW striking folds (Fig. 6-2a) probably related to the late Triassic intracontinental shortening. A sharp and low dip-angle (< 30°) contact with Carboniferous limestone is observed on the border of the Qitianling pluton (Fig. 6-1a). According to our thin section observations, the granites show typical magmatic texture (Fig. 6-2b) and the Permian sandstone wall rocks show clastic texture (Fig. 6-2c). Furthermore, the evidence for significant ductile deformation along the contact surface between the pluton and the country rock, or a preferred orientation of minerals (biotite or feldspar) is absent in the contact zone.

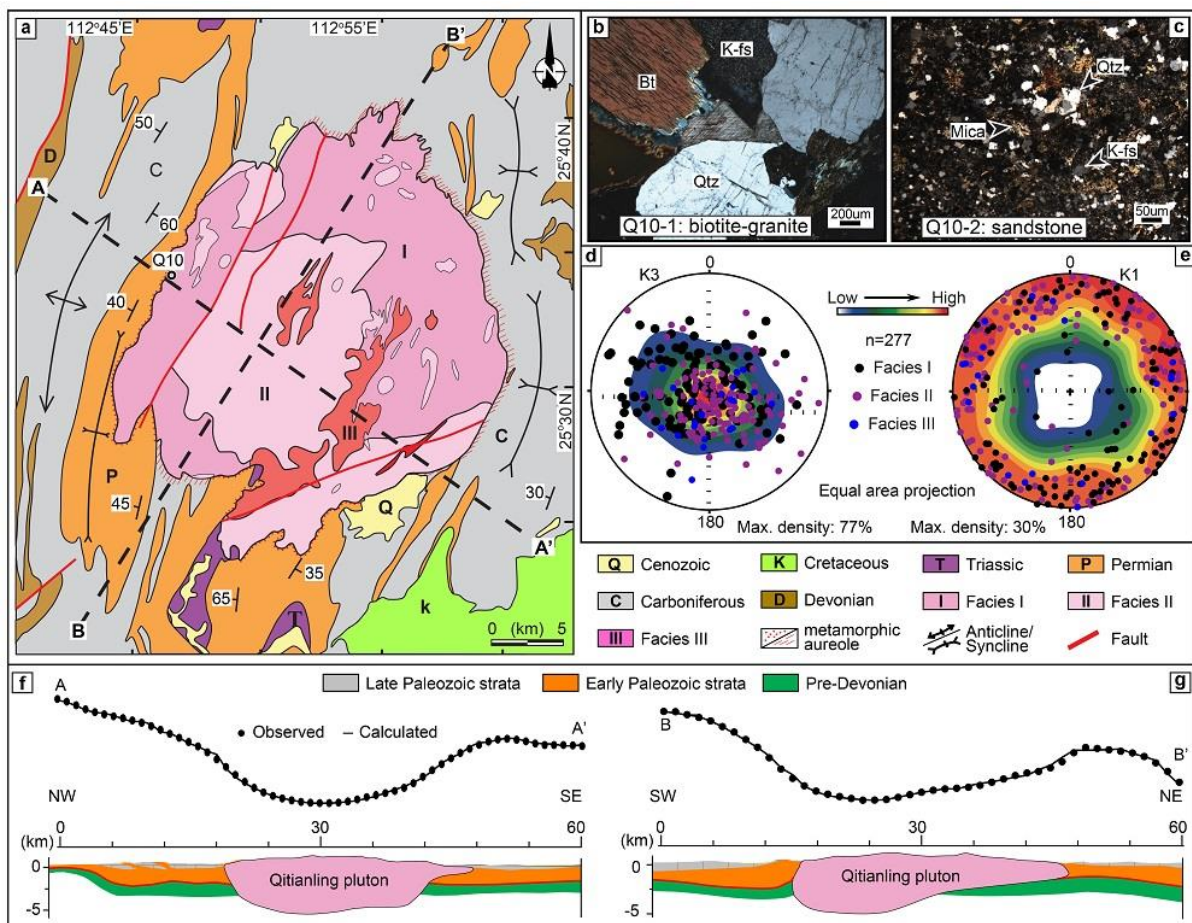


Figure 6-2. (a) Geological map of the Qitianling pluton with abbreviation for different strata: (b) and (c) thin section images of granite and wall rock, respectively, Bt=Biotite, Cal=Calcite, K-fs=K-feldspar and Qtz=Quartz. (d) and (e) stereographic plot showing the distributions of the pole of magnetic foliation and magnetic lineation, respectively. (h) and (g) two profiles of gravity modeling along the dash line in Fig. 6-2a.

AMS measurements were conducted on 277 cores of 44 sites collected from three facies of granites within a total elevation difference up to ca. 1 km and covering the Qitianling pluton. The AMS measurements present generally weak anisotropy degrees ($P_J < 1.08$), and well-grouped horizontal to sub-horizontal magnetic foliations (Fig. 6-2d) and randomly distributed magnetic lineations (Fig. 6-2e). Previous amphibole geobarometry study shows that the pressure for the Qitianling pluton emplacement is ca. 3.6 ± 0.9 kbar, suggesting a middle crust depths of ~ 9-12 km for the emplacement of the Qitianling pluton with geostatic gradient of 3 km/kbar. Our Bouguer gravity modeling suggests a lopolith-like geometry with thickness up to ~5-6 km. Therefore, the bottom of the Qitianling pluton may extend up to ca. 14-18 km and thermal condition of the country rock is estimated at ca. 400-550 °C with geothermal gradient of 30 °C/km. The ductile deformation of the country rock is possible to create the space for magma emplacement, with facilitation from additional thermal contribution of intruded magma. Moreover, our gravity modelling also reveals a symmetrical shape in the NW-SE direction (Fig. 6-2f) and gradually elongated and thinning from SW to NE for the Qitianling pluton, this SW-NE elongation is parallel with the regional structure system (Fig. 6-2g).

6.4 Discussion of the formation and geodynamic model of the Jurassic LGP in South China

6.4.1 Major geological features of Jurassic plutons and their incompatibilities with those predicted by the slab subduction model

According to our and previous observations and experimental data, we can summarize the Jurassic geological phenomena as following: (1) dominantly metaluminous to weak peraluminous granites with little basaltic and massive gabbro exposures; (2) weak Jurassic regional tectonics inside the SCFB but intensive magmatism; (3) widespread distribution of plutons; (4) weak interaction between the plutons and their country rocks; (5) emplacement duration as long as 40 Myrs. These evidences seem incompatible with the previously proposed geodynamic and tectonic models.

Previous geodynamic models for the Mesozoic magmatism in the SCB suggest a northwestward subduction of the Paleo-Pacific slab under the SCB with a change in the subduction angle since the Permian time, which would be characterized by a linear distribution of magmatism parallel to the subduction zone (Fig. 1-6; Zhou et al., 2000; Li and Li et al., 2007). The plate subduction models predict a southeastward age younging trend from the inland to current coastal zone. However, the recent geochronological studies show that the scattered distribution of Triassic and Jurassic pluton cover the entire SCFB (Fig. 1-4a). Moreover, other evidences related to the Jurassic subduction models, such as back-arc basins or trench-parallel magmatic arc, have not been observed yet (Chen et al 2008).

Table 6-1. The contact between the Jurassic pluton and its country rocks

| Site | GPS | | Pluton | Description of the contact |
|---------|--------------|---------------|--------------|---|
| | Latitude (N) | Longitude (E) | | |
| SC14141 | 25°32'12.88" | 112°53'53.58" | Qitianling | Sharp contact between coarse grained granite with amphibole (phase I) and medium grained granitic vein |
| SC14142 | 25°34'45.68" | 112°46'32.94" | Qitianling | Thin section of the undeformed Permian sandstone from the west contact of the Qitianling pluton |
| SC14148 | 25°12'48.23" | 111°53'40.45" | Huashan | Sharp contact between the sandstone and granite |
| SC14161 | 25°07'48.45" | 112°03'55.13" | Jingjiling | Contact between the coarse grained K-fs granite and fine grained granite |
| SC14162 | 25°07'48.46" | 112°03'55.14" | Jingjiling | Huge mafic enclave with mega-crystal of feldspar inside it. |
| SC14163 | 25°05'52.54" | 112°02'04.78" | Jingjiling | Bt-granite intruded in the Sinian metasedimentary rock |
| SC14165 | 25°15'48.57" | 112°07'38.54" | Jingjiling | North contact between granite and the sandstone |
| SC14166 | 25°23'55.21" | 112°35'29.67" | Xianghualing | Undeformed coarse grained two mica-granite |
| SC14168 | 24°36'35.13" | 111°28'47.60" | Huashan | The granite intruded in the undeformed and non-metamorphic sandstone, the occurrence of the contact is (235°, $\angle 15^\circ$) |
| SC14171 | 24°33'37.06" | 111°08'58.63" | Huashan | Granodiorite intruded by the pegmatite |
| SC14183 | 24°54'51.36" | 111°38'12.74" | Guposhan | Some small mafic enclaves can be found and weakly oriented megacrystal of K-feldspar (ca. 5cm) |
| SC1507 | 27°39'50.84" | 118°22'21.54" | Shibei | Undeformed coarse grained granite with mafic enclave and magma flow can be observed |
| SC1517 | 27°50'50.40" | 118°26'22.53" | Shibei | Granite with amphibole and many small sized mafic enclave (ca. 5-10cm) can be found and the enclaves are randomly distributed |
| SC1523 | 27°40'00.25" | 117°49'09.01" | Huangcun | Coarse grained biotite granite |

| | | | | |
|---------|--------------|---------------|-----------|---|
| SC1528 | 26°53'15.80" | 117°45'41.42" | Hecuokeng | In the contact region, the cataclasite are developed and filled by quartz vein |
| SC1530 | 26°49'16.30" | 117°47'53.86" | Hecuokeng | South contact of the pluton and the occurrence of the contact is (104°, $\angle 80^\circ$) |
| SC1534 | 26°30'35.54" | 118°15'54.46" | Zhouzhai | Coarse grained biotite granite |
| SC1535 | 25°54'38.44" | 117°18'27.45" | Gutian | Folded fine grained light yellow sandstone which considered as middle Jurassic stata |
| SC1552 | 25°38'40.46" | 116°48'32.01" | Gutian | unconformable contact between granite and cretaceous conglomerate |
| SC1556 | 25°27'24.26" | 116°47'14.66" | Gutian | contact between the pluton and carboniferous shcist |
| SC1562 | 25°03'22.64" | 116°07'50.24" | Wuping | Undeformed coarse grained granite without amp |
| SC1564 | 25°03'14.53" | 116°15'01.70" | Wuping | Contact between Devonian sandstone and granite, hornfacies sandstone, coarse granied granite with Qtz size at 0.5cm |
| SC15122 | 26°29'41.19" | 115°26'00.28" | Liangcun | Hornfels sandstone with fine graind two mica granite, but the muscovite is a secondary one |
| SC15123 | 26°23'34.33" | 115°39'32.00" | Jiangbei | Medium grained granite with vertical bedding of hornfels sandstone |
| SC15125 | 26°37'42.31" | 115°59'47.94" | Huangpi | exposed in a quarry with hornfels sandstone at the top of the pluton |
| SC15246 | 27°42'54.58" | 117°42'49.90" | Huangcun | Hornfels sandstone intruded by very fine grained granite |

Furthermore, the magmatism during the Triassic-Jurassic and Cretaceous epochs are geochemically different, and recent studies have concluded that the SCB underwent intracontinental compression (shortening) during the Triassic (Chu et al., 2012a) and extension (stretching) in the Cretaceous due to the subduction of the Pacific plate (Wei et al., 2014). This suggests that the mechanism of magma production during the Triassic and Jurassic may have been different from that during the Cretaceous, the latter is widely regarded as the product of subduction of the Pacific slab under the SCB. It follows that the geodynamic mechanism and tectonic setting, which produced the Jurassic plutons in the SCB still need to be worked out (Maruyama and Seno, 1986; Zhou et al., 2000; Lepvrier et al., 2004; Li and Li, 2007; Shu et al., 2009).

6.4.2 The genesis of the Jurassic magmatism of the LGP

The Jurassic LGP in the SCFB mainly consists of felsic plutons (Zhou et al., 2006). The epsilon Nd values of the Jurassic granitic plutons range from -16.4 to -3.4, indicating that the source of the magma is predominantly derived from the partially melted continental lower crust. However, some of the granites may represent fractionated mantle-derived melts, or a mixture between fractionated mantle-derived and crustally derived melts.

The partial melting mechanism of the lower continental crust enhanced by dehydration melting of hydrous minerals such as biotite and amphibole is due either to temperature increase, or decompression (Sawyer, 2011). It is commonly assumed that fluid-present partial melting is due to oceanic subduction, however, for the Jurassic LGP of SE China, the subduction model is incompatible with current observable geological phenomena and experimental data as documented above. Furthermore, the diagnostic features of decompression related structure, such as slab subduction paralleled basin-arc system and large scale normal fault, are absent. Therefore, we propose that the dehydration melting of hydrous metamorphic mafic or sedimentary rocks in the lower crust due to the increase of temperature is the potential genetic mechanism of the Jurassic LGP in the SCFB.

Temperature increase may result either from the thickening of continental crust due to the increase of radiogenic elements, or from mantle-derived mafic magma underplating in the lower crust. A thermal contribution from underplated mafic rock is supported by the local exposure of Jurassic gabbro and diorite (He et al., 2010, Yu et al., 2010; Fig. 1-4) However, as Hf and Nd isotopic studies indicate that the mantle magmatic contribution is limited, hence, we propose that the temperature increase in the lower crust of the SCFB was due to the crustal thickening with thermal contribution from underplated mafic rocks.

Due to the absence of evidence of Jurassic tectonic events in the interior of the SCFB, a thickened continental crust should be produced by pre-Jurassic tectonic events. Several lines of evidence support a crustal thickening by pre-Jurassic tectonics. First, as mentioned above, the SCB experienced multi-subductions with its surrounding blocks and intracontinental deformation during

the Triassic period (Fig. 1-4b). Second, Triassic peraluminous granitic plutons, which are interpreted as the products of partial melting of a thickened continental crust, show a wide distribution inside of the SCFB (Fig. 1-4b) (Tao et al., 2013; Zhu et al., 2013).

However, the large-scaled Triassic basin (Sichuan Basin) and intracontinental orogenic belts of Dabashan and Xuefengshan, are only developed in the border of the SCFB or in ancient suture (Fig. 1-4b). No Triassic-Jurassic basin-and-range system has been described inside of the SCFB area. These features are different from the basin-and-range system under the subduction setting which thickens the continental crust. For example, the Basin-and-Range province in western North America. We therefore further suggest that the crust of the SCFB was entirely thickened at the end of the Triassic and was characterized by a plateau-shaped topography with range belt only developed around the SCFB. This thickening mechanism may be due to the contrast between the Yangtze Craton with a rigid TGG basement, and the Cathaysia Block with a heterogeneous metasedimentary basement. The deformation produced by the Triassic multi-direction continental subductions around the SCB would be mainly concentrated in the less rigid Cathaysia Block. Therefore, thickening of its crust zone can be produced by the localized regional deformation.

Faure et al. (2016) have proposed a ca. 200 km crustal shortening in the Xuefengshan area, involving only the upper crust above a decollement layer. Assuming the thickness of the continental crust of the SCFB prior to this shortening about 30 km, and an average density values for the crust and lithospheric mantle at 2.6 g/cm³ and 3.3 g/cm³ respectively, we can estimate by Airy isostasy hypothesis that the crust was thickened to 37.5 km with a topographic elevation of ~1.6 km and a plateau root of 5.9 km (Fig. 6-2b).

The current width of the South China fold belt (the Cathaysia block) is about 800km wide. However, the width before the shortening is about 1000km. Assuming a 30km of the continental crustal thickness before the Triassic tectonics, 2.6 g/cm³ and 3.3 g/cm³ for the crust and mantle, respectively, taking *a* as the topographic elevation, *b* as the normal crustal thickness (30 km) and *c* as the topographic root, we may establish the following equation:

$$(a + b + c) * 2.6 = (b * 2.6) + (c * 3.0)$$

According to the volume conservation law, the crust may thicken from 30km to 37.5km. The detail results of calculation give *a* = 1.6 km, *c* = 5.9 km (Fig. 6-3b), and the crust is of 7.5 km thickened. So, the topography of the South China fold belt was uplifted by about 1 km in the elevation. Moreover, this topography presents a plateau shape as no large scaled Triassic and Jurassic basins can be found within this fold belt. Nevertheless, km-scaled thick sediments can be found in the northwestern side of the Cathaysia block and the southeastern side of the Sichuan basin.

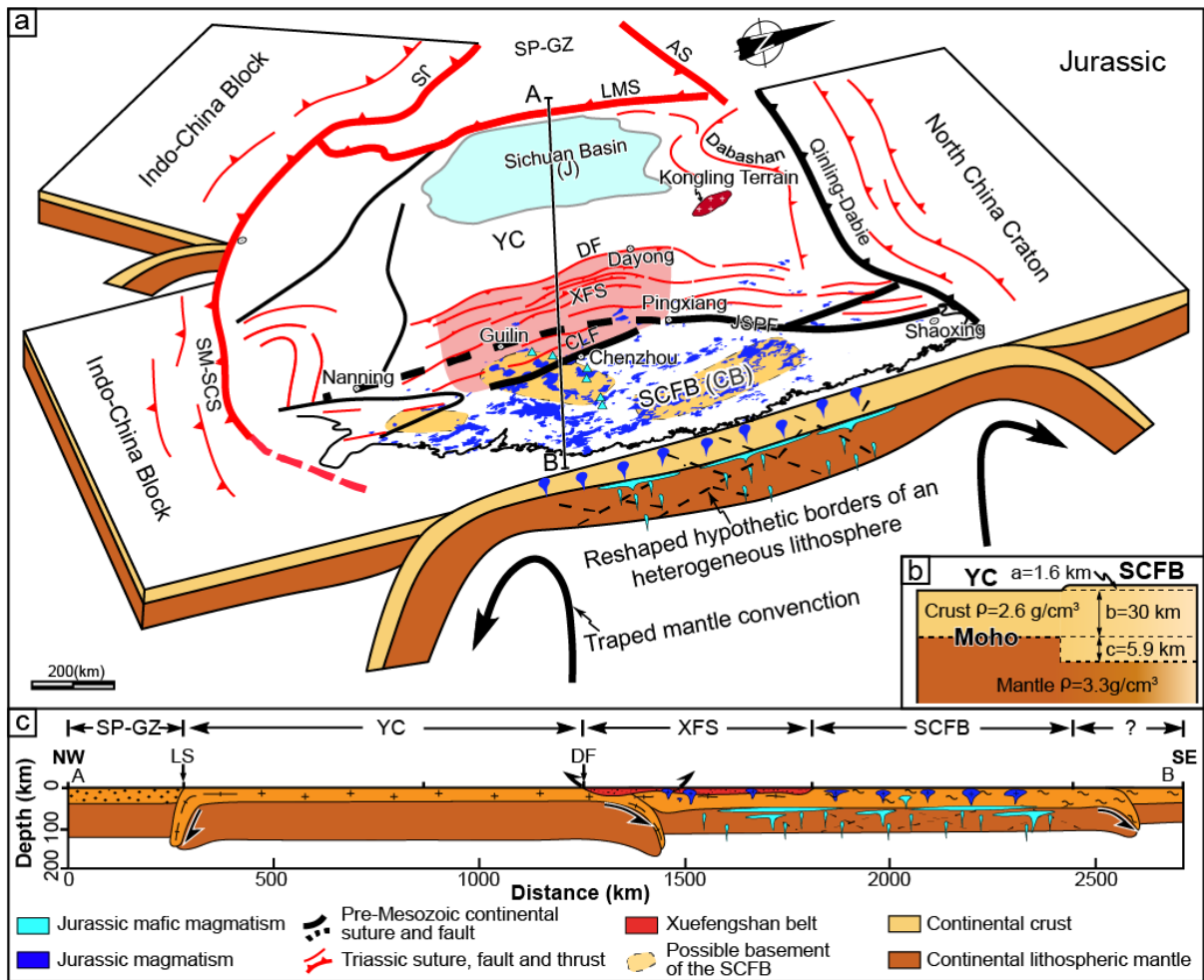


Figure 6-3. (a) Interpreted Jurassic schema of the SCB for the genesis of the magmatism. (b) The inserted scheme illustrates the thickening of the SCB according to Airy isostasy hypothesis. (c) Interpreted cross-section from Songpan-Ganzi to the SE coast of the SCB along the dash line AB in Fig. 6-3a, all the abbreviations are the same as those in Fig. 1-4.

The crustal thickening process would increase the pressure and temperature in the lower crust as well as the contact surface between the crust and the mantle. The lower part of the thickened continental crust will be more heated by the thermal conduction from the lithospheric mantle. According to Hu et al. (2000), the present thermal gradient for the intracontinental crust of the SCB was ca. 25 °C/km, which shows that the temperature at the bottom of the thickened continental crust (~37.5 km) may have reached up to ca. 950 °C, which is high enough to evoke the dehydration melting of the amphibolite in the lower continental crust to produce granitoid melts (Wolf and Wyllie, 1994).

The tectonic and geodynamic settings affect not only the magma genesis but also its emplacement process. Many studies of the pluton emplacement mechanism, including its duration, depth, petro and tectonic fabrics and pluton geometry, have proved to be a powerful tool to reveal the regional tectonic and geodynamic setting (Hutton, 1988; Paterson et al., 1989; Barbarin, 1990; Byerly et al., 2017 and references therein).

The duration of genesis of the Jurassic LGP in the SCB is ca. 40 Myrs (Fig. 1-4c), which is

longer than the current LIP, for example, the Emeishan mafic LIP (1-2 Myrs; Ali et al., 2005), the Sierra Madre Occidental silicic LIP (ca. 18 Myrs; Ferrari et al., 2002). The long genesis process for the SCFB LGP indicates a low magma production rate but long melting processes in the source region. For one single pluton, the duration of emplacement also ranges from 1 to 10 Myrs (Zhu et al., 2009), indicating that the plutons were constructed by multiple batches of magma, as the duration for one single magma batch to crystallize is usually shorter than several hundred thousand years according to the numerical modelling (e.g., Annen et al., 2015).

6.4.3 A tentative geodynamic model for the formation of the Jurassic LGP in the SCFB

As the Qitianling pluton presents common features with other 40 plutons that we observed in the field and analyzed in the laboratory and cover almost all the SCFB, we may generalize our interpretations to other Jurassic plutons in the SCFB. Figure 6-3a presents our Jurassic geodynamic interpretation on the formation of the LGP in the southeastern part of the SCB. The subduction of the SCB under its neighbouring blocks in the Triassic will mainly localize the deformation in the lower plate, i.e. the SCB, which will be thickened by multiple fold-and thrust belts controlled by variable convergence directions. Because of the low rigidity of the Cathaysia compared with the Yangtze Craton, this former block accommodated a large amount of deformation and its crust consequently thickened to form the SCFB. The scarcity of Jurassic sedimentation within the SCFB in contrast to the thick sediments in the surrounding Sichuan basin supports our interpretation that the SCFB was entirely thickened and uplifted with a plateau-shape topography and an elevation of ~1.6 km sustained by a root of ~5.9 km (Fig. 6-4b). This increased both pressure and temperature in the lower crust, and the contact surface between the mantle and the crust. Moreover, the thermal input from the mantle related to underplated mafic materials arising from the trapped convection asthenosphere mantle along the border of different blocks of the SCFB during the long decompression processes of the SCFB will enhance the partial melting of the lower continental crust of the SCFB.

6.5 Conclusions

With respect to the generally accepted mechanisms for the LIPs, i.e. contemporaneous plate tectonic and/or mantle convection driven mechanisms, the Jurassic LGP in the SCFB occurred tens millions of years later after the major Triassic tectonic event affecting this area. Though the Jurassic magmatism seems ultimately relating to a tectonic phase, the considerable “incubation time” between tectonic and magmatism makes the Jurassic LGP in southeastern of the SCB a rather unique occurrence of the random distribution, long duration and weak tectonism-magmatism interaction of the LGP in the SCFB, which seems satisfactorily explained by our model.

Furthermore, the topographic features and lack of synmagmatic tectonic events and large scaled basin-and-range system inside of the block do not favor the oceanic subduction model.

Altogether, the magma formation and its emplacement of the LGP in the SCFB are affected by the pre-magmatic ancient tectonic events in the SCB since the Precambrian and the crustal structure took important roles as well in the evolution of the Jurassic LGP from the melt generation in the lower crust to the emplacement in the middle crust.

Chapter 7. Discussion

7.1 The relationship between granite petrofabrics-pluton emplacement-tectonics

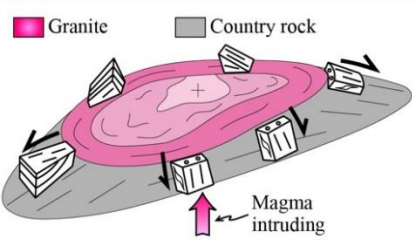
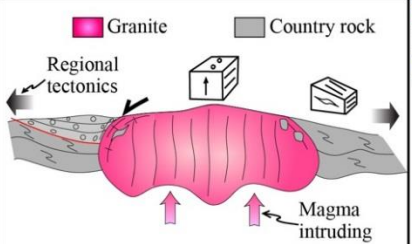
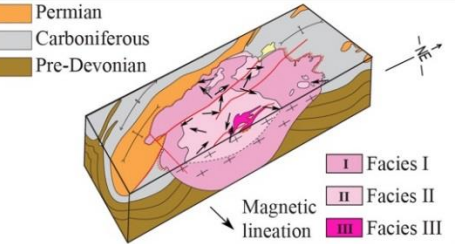
The relationship among granite petrofabrics, pluton emplacement and tectonics has long been studied. It is well acknowledged since the beginning of 19th century that granitic rocks exhibit planar and mineral preferred orientations, also called petrofabrics. Many studies aimed at relating these fabrics with magma mobility (flow) and or magma crystallization. Furthermore, different models have been proposed to solve the space problem related to pluton emplacement and give hints on its related tectonic regime (Fig. 1-3 and Table 7-1).

Thus, the question of the relationships between a pluton architecture, including its internal structure determined by petrofabrics, and its emplacement mechanism is one of the most disputed question. Concerning the petrofabrics of intrusive rocks, they are generally divided into two genetic groups, i.e. magmatic or tectonic related. Both of these two types of fabric can be used to reveal the magma emplacement process and the nature of regional tectonic regime, i.e. shortening (e.g. Brown and Solar, 1998; Lin et al., 2013), extension (e.g. Acocella, 2014), transpression settings (e.g. de Saint Blanquat, 1998), and non-tectonic emplacement (de Saint Blanquat et al et al., 2006; Byerly et al., 2017).

The magmatic fabric developed during the flowing or stationary cooling stage of the magma emplacement is considered as primary fabrics (Cruden, 1990; Stevenson et al., 2007). The tectonic fabrics may develop during or after the magma emplacement. Hence, the identification of the derivation of petrofabric of magmatic rocks, which is involved in or free from the regional tectonic regime, is pivotal for a pertinent interpretation of fabric measurements. Currently, the multidisciplinary methods are used to identify different fabrics of plutons, such as: i) field and microscopic observations of the structure and texture of country rocks (mostly in the thermal aureole), and plutons, ii) magnetic fabric measurement of the granite (e.g. de Saint Blanquat and Tikoff, 1997; Paterson et al., 1989; Byerly et al., 2017).

The early opinion suggested that the space for accommodating magma emplacement can be created by the magma itself or regional tectonics, thereby, the forceful and permissive models were proposed, respectively (e.g., Pitcher, 1979; Hutton, 1988; Petford et al., 2000; Stevenson, 2009). The classification of these two models depends on the contrast between the magma supply rate and regional tectonics, which control the space opening rate.

Table 7-1. Comparison of petrofabrics of different emplacement mechanisms

| Mechanism | | Forceful | Permissive (Passive or syntectonic) | ? (for the Qitianling pluton) |
|--|------------------|--|---|---|
| Features | |  |  |  |
| Sketch of the pluton, country rock and characteristics of emplacement | | | | |
| Mode of pluton building | | diapirism, ballooning | dyke accretion, cauldron subsidence | progressive downward accumulation |
| Deformation and fabric pattern | Wall rock | ductile deformation around the pluton and its aureole | ductile deformation by tectonics, brittle fracturing | sharp contact without deformation in neither wall rock nor pluton, narrow thermal aureole |
| | Pluton | concordant planar and linear fabrics between the pluton and wall rocks along the contact, dominated spherical or tabular body, usually at deep crust | preferred mineral orientation corresponding to the regional tectonic regime, deformation decrease from margin to center, elongated shape, usually shallow crust | horizontal foliation and scattered lineation without dominant direction, follow ancient structure geometry, unconstrained depth |
| Dynamics of pluton emplacement | | internal force (magma bouyancy) | external force (regional tectonics) | internal force (?) |
| Part of references | | Schuilng, 1962; Pitcher, 1983 Faure and Cottreau, 1988; Morgan et al., 2013. | Hutton, 1990; Stevenson, 2009; Nédélec and Bouchez, 2015; Wei et al., 2016. | This study |

The forceful model means that the magma supply rate is higher than the tectonic impelled space opening rate, on the contrary, the permissive model is proposed with the reverse of these two rates. Because the magma supply rates are usually orders of magnitude faster than the tectonic impelled space opening rates, especially when magma is emplaced as dikes, the upwelling of magma by the buoyancy force is currently considered as the major magma ascent way to transport magma from the source region to emplacement (Paterson and Tobisch, 1992). Therefore, the petrofabrics of the forcefully emplaced plutons, represented by the diapirism, ballooning and stoping, are yield due to the flow of the magma and interaction with the country rocks (Fig. 1-3). Nevertheless, the space for the emplacement of large scaled plutons cannot be created by the magma alone, as the internal force of the magma is not strong enough to break the rigid and cold crust and overcome the lithostatic pressure from the country rocks (Bunger and Cruden, 2011). Hence, premagmatic and synmagmatic tectonics are needed to deform and change the rheological condition of the country rocks or produce the space for syntectonic magma emplacement. Although the regional tectonic processes seem unable to produce a void that would facilitate magma emplacement, the effects of synmagmatic tectonics can be still recorded in the pluton, even under a low strain rate setting (Kruhl et al., 2007) and evidenced by different structures of wall rocks, geometry of pluton and intrusion related fabrics in the pluton and its wall rocks (Castro, 1987; Paterson et al., 1989; Barbarin, 1990). Here, we list some cases of tectonically related pluton emplacements.

7.1.1 Emplacement under a crustal shortening setting

Plutons emplaced under shortening setting (Fig. 7-1a; Lin et al., 2013 and references therein) are usually characterised by consistent fabrics in both plutons and country rocks. First, the magma intrudes more easily into the zone where the deviatoric stress is lower than the regional one, for instance, joint, schistosity and cleavage. Second, the long axis of a single igneous body is usually perpendicular to the maximum principal stress direction. Third, the foliation is often normal to regional tectonic regime, and more consistent than the lineations.

7.1.2 Emplacement under extensional setting

A regional extensional tectonic setting (Fig. 7-1b; Acocella, 2014 and references therein) is characterised by dominant normal faults with possibly subordinate strike-slip faults to accommodate the kinematic pattern. In surface, graben or half-graben filled by sedimentary basins are common. In the regional scale, the plutons are usually developed along a normal fault and the fabrics of plutons may be overprinted by regional tectonics, when the regional tectonics is long lasting enough. In the plate scale, the typical extensional setting, i.e. back-arc extensional area, are usually characterised by linearly distributed dykes, plutons and volcanics (Fig. 7-1b).

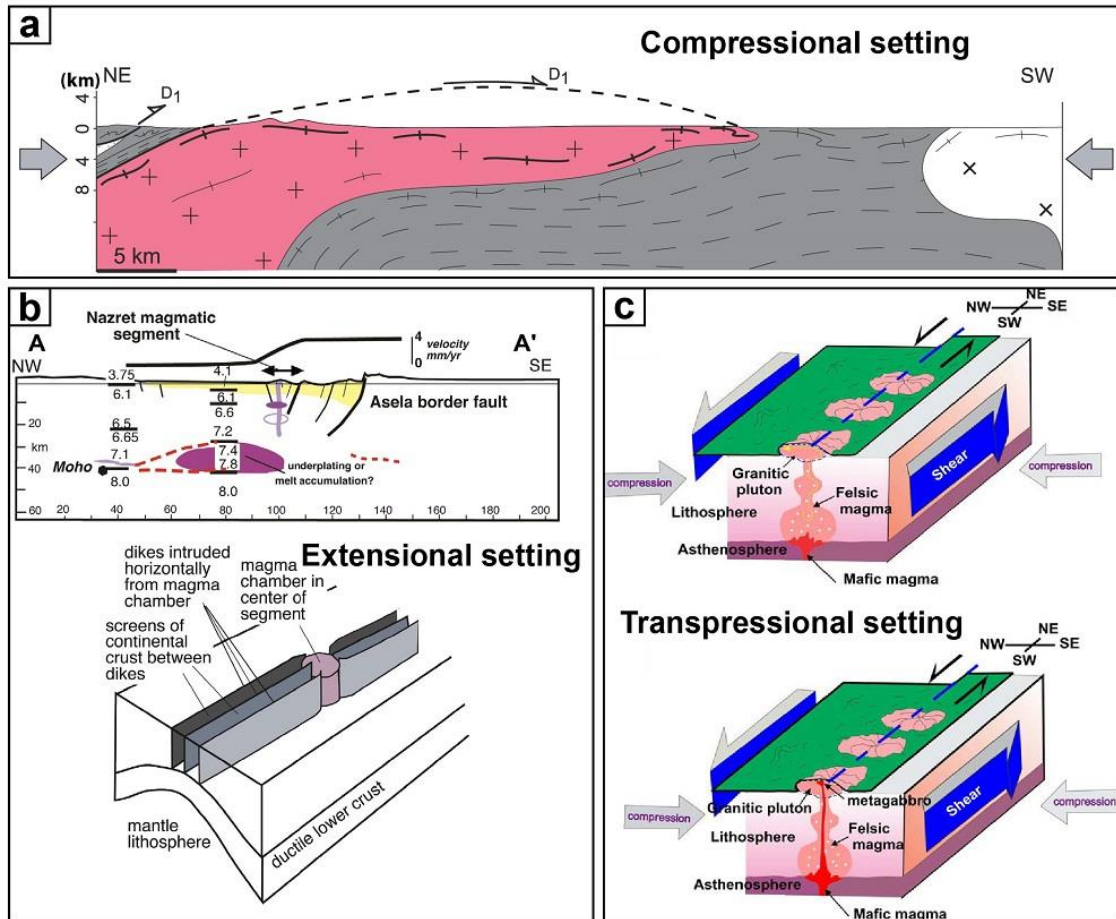


Figure 7-1. Magmatism developed in different tectonic settings. (a), (b) and (c) show magma emplaced at shortening (Lin et al., 2013), extension (Acocella, 2014) and transpression (Ntieche et al., 2017) setting, respectively.

7.1.3 Emplacement under transpressional setting

Magma intruded into the transpressional belt (Fig. 7-1c: Ntieche et al., 2017 and references therein) usually displays the dyke-shape body and incrementally develops, hence, the strong foliation and mylonitization of the igneous body with typical S-C fabric can be observed. Moreover, in the transpression zone, the kinematics of shear on the two sides of a releasing bend are in opposite directions.

Furthermore, the regional tectonics not only affect the emplacement stage, but also influence the entire magma evolution system, i.e. from its genesis (Barbarin, 1990; Wilson, 2007), segregation (Clemens and Petford, 1999; Rabinowicz and Vigneresse 2004;), ascent (Petford, 2000; Rosenberg, 2004) to emplacement (Hutton, 1988; Vigneresse, 1995; de Saint Blanquat et al., 2011). Thereby, the role of the regional tectonics on the magma evolution should be reconsidered.

7.2 Structural Characteristics of the Jurassic plutonism in South China

According to our field investigations on the forty-one Jurassic plutons with age ranging from ca.

180 Ma to ca. 150 Ma, and detailed multidisciplinary studies on two representative late Jurassic plutons, i.e. the Qitianling and Shibeai plutons, the Jurassic plutons in the South China Block present several characteristic features which are discussed below.

In the macroscopic view, the forty-one Jurassic plutons are characterised by an apparently random distribution without obviously tectonic control (Fig. 3-1), the contacts between the plutons and country rocks are sharp and lack of ductile deformation on both sides (Fig. 3-3, 4-3 and 6-3), narrow (usually less than 100 meters) and low grade metamorphic aureoles (hornfels facies) in the country rock are revealed.

In the microscopic view, the thin section observations show that the granites are characterised by typical magmatic texture with euhedral quartz, feldspar and biotite, and lack of deformation related textures, for instance, bulging, grain boundary migration and recrystallization, indicating that the pluton did not experienced synmagmatic and post-solidus tectonic influence, and the petrofabrics of granites are primary fabrics.

Detailed magnetic investigations on the Qitianling and Shibeai plutons show that the magnetic susceptibility is essentially carried by paramagnetic mineral and/or magnetite in pseudo single and multidomain (Fig. 3-6 and Fig. 4-4). The degree of anisotropy of the majority granitic specimens from these two plutons are lower than 1.12 (Unpublished data are reserved). The fabrics of the two plutons are characterised by oblate magnetic ellipsoid suggesting that the magnetic foliation is better developed than the linear one. However, the Qitianling pluton shows dominantly horizontal magnetic foliations with scatter horizontal to sub-horizontal lineations. The Shibeai pluton displays NE-SW orientated vertical magnetic foliations with variably plunging lineations in the south part of the pluton and gently tilted magnetic foliations in its northern part. The well developed horizontal to sub-horizontal foliation of the Qitianling pluton is almost parallel to the stratigraphic unconformity in the country rocks, and the NE-SW striking vertical foliation of the Shibeai pluton is consistent with the regional pre-Jurassic tectonic structures. Therefore, due to the lack of synmagmatic tectonics to control the magma emplacement, the structure of the country rocks seems to be the major factor controlling the geometric pattern of the magnetic fabrics in these two plutons.

The gravity modeling of the Qitianling pluton shows that the pluton has a lopolith-like geometry with probably pipe-like magma supply channels, however, the Shibeai pluton presents a lateral dike-accretion shape in the south and sub-horizontal magma sheets in the north.

Accordingly, we propose that the Qitianling pluton was constructed by the downward accumulation of magma sheets and floor sagging to accommodate the gradual emplacements of magma. However, the Shibeai pluton was probably built up by a lateral accretion of successive magma sheets with a dike-shape along fractures or preexisting cleavage in the highly deformed country rocks.

Our studies of the late Jurassic plutons in the South China Block present distinct features with respect to those accommodated by the forceful and syntectonic models (Table 7-1). Therefore, these two current models cannot satisfactorily explain what we observed in the Jurassic plutons in South China. Hence, according to our new multidisciplinary results and previous studies as well, we present our new understanding on the Jurassic magmatism in South China below.

7.3 New understanding on the Jurassic magmatism in South China

The Mesozoic magmatism is one of most important geological features for the South China Block characterised by its large surface (about 800 x 1500 km²; Fig. 1-4) and long duration (about 150 Myrs). Among the three periods, the Jurassic magmatism takes the most important place, at least for its surface cover (about 50%), with respect to that of Triassic and Cretaceous periods. Even still in debate, the general tectonic and geodynamic contexts for the Triassic (compression) and Cretaceous (extension) magmatism seem clear to the geoscience community. In other words, surface observations of plutons and country rocks, including the geology, petrology, geochronology, and geochemistry data fit well to the tectonic and geodynamic models proposed for the evolution of the SCB. On the contrary, the geodynamic interpretation of the Jurassic magmatism is not clearly understood. As mentioned in Chapter 6, the most popular model involving the Pacific Ocean subduction below the SCB cannot satisfactorily explain the surface geological observations in terms of lithology, geochronology and deformation (see Chapter 6 for the details). According to our field and laboratory observations on 41 Jurassic plutons covering almost the principal magmatic area in South China (Fig. 1-4) and previous results, we aim to propose a new model on the Jurassic magmatism in South China in terms of magma source, emplacement mechanism, and tectonic-geodynamic setting.

7.3.1 The source of the Jurassic magmatism in the South China Block

The magma source information is pivotal for the understanding of the magma emplacement, different sources imply different temperature, pressure and volatile component, which have crucial influence on the volume and viscosity of the melt, therefore, the transport behaviour of the magma will be different. The major geochemical data of bulk rock, e.g. the whole rock Neodymium (Nd), zircon Hafnium (Hf) and Oxygen-18 ($\delta^{18}O$) isotopic system, can help to reveal the source information of magma. Because of the low abundance and multi-source of the isotope and re-equalisation, the use and interpretation of the isotope information should be in caution. For granite, especially for the magma derived from a heterogeneous source region, a wide mixed isotopic value range will be acquired. The Jurassic granites from the representative Qitianling pluton show metaluminous features with A/CNK value between 0.9 and 1.1 (Zhou et al., 2006). The whole rock Nd values range from -16.4 to 3.4 with a mean value at -7.8, indicating a possible

complex source. Nevertheless, the majority source materials for the granites are probably derived from the partial melting of the continental crust (Shen et al., 2000).

The partial melting of the continental crust, depending on temperature, pressure and water content, is an efficient way to produce the magma in the lower continental crust (Skjerlie and Douce, 2002, Annen et al., 2006). The Triassic tectonic events, namely i) the collision between the Indochina block and South China Block in the southwest related to the closure of the S. branch of the Paleo-Tethys Ocean, ii) the intracontinental subduction in the Qinling-Dabie orogen in the north, with its westward extension in the Longmenshan in northwest, and iii) the Xuefengshan intracontinental orogen in the center of the SCB, yield the confining pressure to the South China Block. Moreover, due to the contrast in rigidity between the Yangtze Craton and Cathaysia Block, the regional stress will be essentially localized on the less rigid Cathaysia block, making the latter well deformed marked by its, numerous Cretaceous basins but rare Late Triassic and Jurassic ones, and various plutons with ages ranging from Middle Triassic to Late Cretaceous. The weak rigidity of the Cathaysia block is also proved by our paleomagnetic studies on the Qitianling and Shibeii plutons (see details in Chapter 5). Recent gravity and seismic investigations also support a homogenous basement for the Yangtze Craton and heterogeneous for the Cathaysia Block (Deng et al., 2014). As a consequence, the crust of the Cathaysia block will be significantly thickened (Fig. 6-3). The thickening of the Triassic continental crust of the Cathaysia Block is supported by intrusions of S-type granite.

Based on the field observation, Faure et al. (2016) have made a tectonic reconstitution on the Triassic intracontinental deformation and proposed a 200 km of crustal shortening in the Xuefengshan zone in the Cathaysia block. Accordingly, the corresponding crustal thickening may be quantitatively estimated with the Airy isostatic hypothesis. The actual width of the South China fold belt (the Cathaysia block) is about 800 km, while, the width before the shortening is about 1000 km. Assuming a 30 km of the continental crustal thickness before the Triassic tectonics, 2.6 g/cm³ and 3.3 g/cm³ for the crust and mantle, respectively, the crust may be thickened from 30 km to 37.5 km with a root of 5.9 km and a topography of about 1.6 km in the elevation (see Fig. 6-3c). Moreover, as no large scaled Triassic and Jurassic basins can be found within this Cathaysia block, probably due to the diffusion of deformation instead of its localisation along some major faults within the block, the topography was probably similar to a plateau. That is to say that the ancient Cathaysia block has been probably entirely uplifted. Nevertheless, the km-scaled thick sediments can be found in the northwestern side of the Cathaysia block corresponding to the southeastern part of the Sichuan basin.

Furthermore, the role of the underplating of the mantle cannot be ignored. The crustal thickening increases the mantle-crust contact surface, thus enhances thermal conduction. The thickened crust may also decrease the crustal thermal gradient and keep better the heat in the lower

crust. All of these support producing more Jurassic partial melting and then the remarkable Jurassic magmatism.

Though the Jurassic tectonic deformation in South China has been described (Dong et al., 2015 and references therein), the deformation occurred essentially in the surrounding zones of the ancient Cathaysia block, instead of in its interior. Moreover, the Jurassic deformation is much less intensive with respect Paleozoic and Triassic tectonics (Fig. 7-2), this is probably one of reasons why we did not observe any deformation on the contact between plutons and their country rocks of the plutons (Fig. 6-2 with details in Chapters 6). This tectonic quiet context during the Jurassic may suggest that the depression of the thickened crust lasted long time, and explain the reason why the process of partial melting took place during a long period.

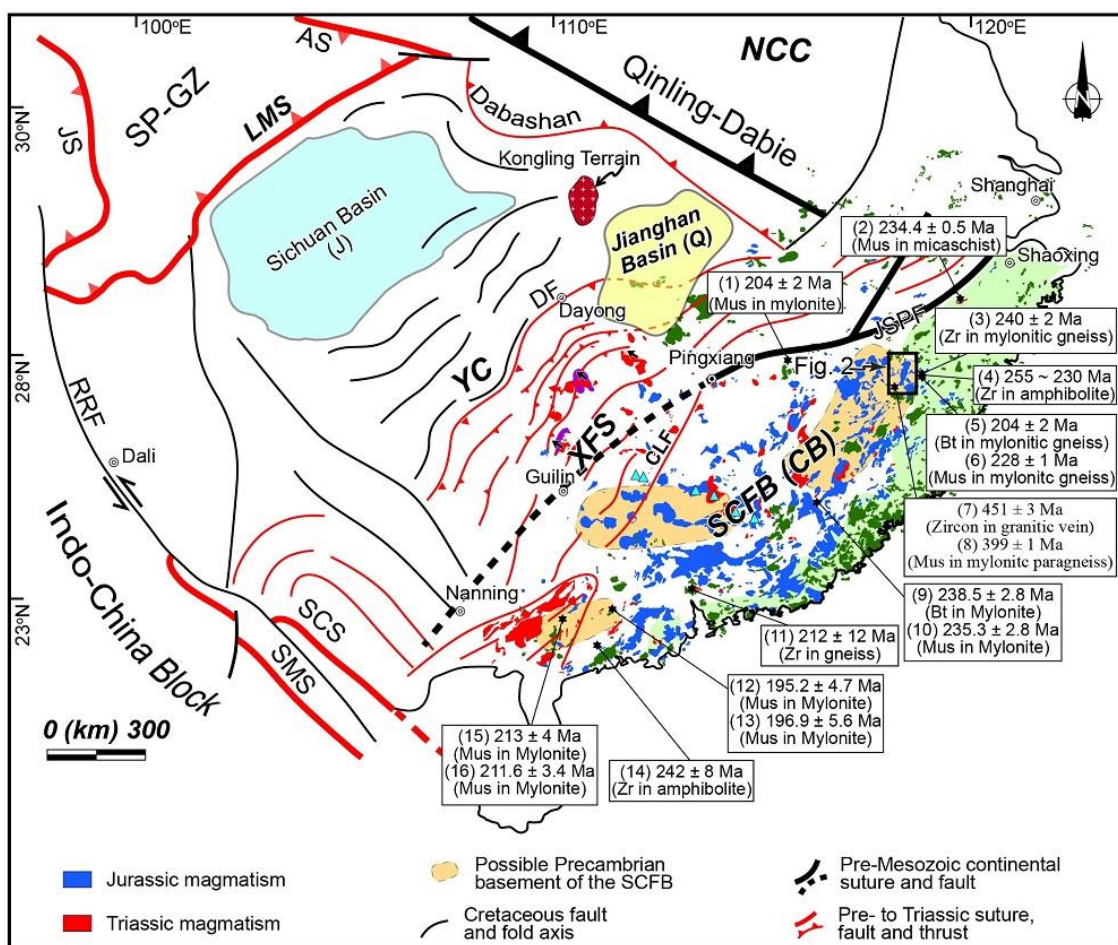


Figure 7-2. Sketch of the main geological units in China and tectonic framework of the South China Block with inserted Triassic thermal events records. The number inside of the bracket is corresponding to the references listed below: (1) and (2) Shu et al., 2015; (3), (4), (5), (6), (7) and (8) Xiang et al., 2008; Li et al., 2017; (9) and (10) Xu et al., 2011; (11) Wang et al., 2012; (12), (13), (15) and (16) Zhang and Cai, 2009; (14) Wan et al., 2010.

Briefly, the Jurassic magmatism in the South China Block is probably produced by the relatively

slow decompression of the thickened crust with an additional thermal conduction from the mantle, the melts due to the partial melting of the lower continental crust migrate upwards slowly to build plutons without visible deformation, i.e. without obvious tectonic control.

7.3.2 The emplacement mechanism of Jurassic plutons

The field and laboratory observations on the 41 Jurassic plutons (Fig. 1-4 and 6-3) show the absence of intrusion-related deformation in the plutons, even at their contacts with the country rocks. This suggests that the space required for magma emplacement developed without any ductile deformation. According to our field observations and laboratory analyses, and considering the state-of-the-art on the tectonic evolution of the South China Block, we propose one possible explanation to account for this phenomenon.

Firstly, as mentioned previously, all of our observations indicate that the Cathaysia block was devoid of internal deformation during the Jurassic. Without the assistance of regional tectonics to facilitate the magma emplacement, the buoyancy of magma should be the major force for magma upwelling due to its weak density with respect to its country rocks.

Secondly, the geochronological dating of the Jurassic plutons indicates a long duration of ca. 40 Myrs for the Jurassic magmatism (Zhou et al., 2006; 15 Ma to 20 Ma for the Qitianling pluton building; Zhu et al., 2009). The widely distributed and long lasting Jurassic mineralisation in the South China Block between 170-150Ma (Pirajno, 2013) also support a long duration for the Jurassic magma emplacement.

Thirdly, the Cathaysia Block or the South China fold belt, which is composed of several terranes, has experienced polyphased tectonics from the Neoproterozoic to late Early Mesozoic. This repeated deformation may reduce the rigidity of this zone and make it as a non-rigid block. In other words, it became so deformable that no any major structure controls the spatially continuity of deformation. Consequently, the South China Fold belt and the numerous faults may be considered as channels for magma upward migration. Besides, this may be also the reason why the pre-Jurassic basins in the Cathaysia Block are always small scale structures, while, a large scale Sichuan basin develops in the Yangtze Craton.

Lastly, when the Triassic collisional and intracontinental events ended up, the thickened continental crust of the South China fold belt began to be decompressed. This decompression triggered the partial melting of the continental crust giving rise to the Triassic per-aluminous plutons (Pedersen and Ro, 1992; Auzanneau et al., 2006). Moreover, with the polyphased deformation, water-rich sedimentary rocks accumulated in the fold belt, which may decrease the melting temperature and making partial melting easier (Sawyer et al., 2011). The decompression rate of the thickened continental crust is critical for our interpretation. Lacking immediate (Jurassic)

tectonic events the process could be long and slow, the partial melting might also take time to progressively migrate upwards to build plutons. Facilitated by the Pre-Jurassic structural heritage, a magma in a relatively small volume can make its upwelling by its own buoyancy and intrude into old structures. This seems well illustrated by the good coherences between (1) the sub-horizontal magnetic foliation of the lopolith-like Qitianling pluton and the same geometry of the unconformity in its country rocks (Figs. 3-8 and 3-9; see details in Chapter 3), and (2) the sub-vertical magnetic foliation of the dike-shape Shibeiputon and the similar geometry of folds in its country rocks (Figs. 4-9 and 4-10; see details in Chapter 4). In other words, the magma emplacement may be controlled by the structural heritage instead of syn-magmatic tectonics. Each pluton might be built up by the accumulation of numerous pulses in weak volume of each. As the volume of each intrusion is small, its thermal (aureole) and mechanical (deformation) effect on the country rocks will be weak. That would be the reason for the invisible deformation on the contact between the granite and country rocks with thin thermal aureole.

In brief, we can explain our general observations on the 41 Jurassic plutons and details ones on the two representative Qitianling and Shibeiputon by a derived model of diapirism: a slow decompression of the thickened crust makes producing partial melting, due to the pre-Jurassic structural heritage, the melt progressively migrates upwards by its buoyancy into ancient structures. The progressive and long accumulation of melt pulses in small volume produces little or no deformation effect on the country rocks and narrow thermal contacts between the plutons and their country rocks, in other words, the pluton is probably built up slowly without regional tectonic control.

7.3.3 Tectonic and geodynamic contexts of the Jurassic magmatism

The Mesozoic magmatism in South China can be divided into three parts in term of petrology and geochemistry, Triassic, Jurassic and Cretaceous. The Triassic granite is dominantly composed of peraluminous granitoids (> 60%), which is almost entirely produced by the partial melting of continental crust (Chappell and White, 2001). The Jurassic one principally consists of metaluminous to weak peraluminous with small proportion of mafic rock (Zhou et al., 2006; He et al., 2010). The Cretaceous granite essentially concerns granodiorite with important mantle input and associated with widely distributed volcanic rocks along the coast (Fig. 1-4). In term of deformation and tectonic context, the surface geology presents distinct phenomena for these three groups of granite. Numerous studies on the structural geology and geochronology show that the South China Block experienced a compressive tectonic during the Triassic, due to multidirectional subduction-collision, and a general extensional tectonics during the Cretaceous, due to the subduction of the Pacific Ocean under the South China Block. The magmatism, tectonics and their relationships for these two periods have been largely studied (e.g. Li, 2000; Chu et al., 2012a,

2012b; Song et al., 2015; Wei et al., 2016), moreover, it is out of the scope of this thesis, therefore, we will concentrate on the Jurassic magmatism in the southeastern part of the SCB (the ancient Cathaysia block).

As described above, according to the field and laboratory investigations, the intensity of the Jurassic tectonic is much less important with respect to the Triassic and Cretaceous ones, and its deformation is essentially found in the outer zone of the Cathaysia block surrounding the Sichuan basin (Fig. 1-4 and Fig. 7-2). No obvious Jurassic deformation can be found with few Jurassic sediments in the southwestern part of the Cathaysia block. Therefore, different from the Triassic and Cretaceous magmatism, the Jurassic one took place during a tectonically calm period, in other words, the Jurassic magmatism is a non-tectonic magmatism.

If the Mesozoic magmatism of South China can be considered as a Large Granite Province (LGP) according to its large extent and important magma volume, it seems to be an exceptional case with respect to the well-known ones, such as the plate tectonic-related Sierra Nevada in North America (Hofmann et al., 1997; Ferrari et al., 1999), the mantle-convection related Paraná flood-basalt in South America (Peate et al., 1990). Concerning the genesis of the magma, one magmatism links to one certain type of tectonics (general to the extension) or the mantle convection. However, the Mesozoic magmatism can be divided into three distinct periods with probably different causes. The Triassic and Cretaceous magmatism in South China link to two well distinct compressive and extensive tectonic settings, respectively. Moreover, it is difficult to category the more important Jurassic magmatism as no tectonic-related (such as back-arc and aligned distribution of plutons) and little mantle-related (mantle signature in the composition of magmatic rocks) features have been found. In term of the geological expression on surface, the characteristic phenomena observed in Jurassic plutons in South China cannot be compared to one or another of those well-known mechanisms. By synthesizing our new results from field and laboratory, the previous achievement, including essentially petrology, geochemistry and geochronology, as well as the knowledge on the tectonic evolution of the South China Block, we can summarize the new scenario of the Jurassic magmatism in South China as following. The ancient Cathaysia, i.e. the southeastern part of the South China Block and the zone where the Mesozoic Magmatism took place, was composed of several sub-blocks and has experienced several important tectonic events since its agglomeration with the Yangtze craton at the Neoproterozoic. It cannot be considered as a rigid block according to its widespread small-sized basins, plutons and faults, in other words, this block has been multiply deformed, fractured and presents a high lithological and structural heterogeneity. So, the Cathaysia block, or the South China Fold Belt (Huang, 1945), due to its lower rigidity with respect to the Yangtze craton, this belt has been thickened by the Triassic tectonics. The crustal thickening increases the pressure and temperature in the lower crust as well as the contacting surface with the mantle. With the increasing mantle thermal contribution (probably

essentially by conduction), after the Triassic compressive tectonics, the decompression of the thickened crust can trigger partial melting in the lower crust. Important volume of melt can be produced by the water content in the metasedimentary source rocks. The melt can use the pre-existing fractures and structures as its upwelling channels that may explain the distribution pattern of the Jurassic plutons: widespread without alignment neither the apparent control of major fault. Moreover, each pulse or batch of upwelling melt can be in relatively small volume as it does not need an important buoyancy to make its channel, in other words, the partial melting and its upwelling can take place in a small temporal shift, and one pulse or batch may follow another closely in time, that may explain why intrusion boundaries have been rarely observed within plutons. As no important Jurassic deformation has been observed in this belt, the Jurassic may be considered as a tectonically calm period. In this case, the procedure of depression - partial melting of the lower crust and - upwelling of melt may take long time. This may be the case for the Jurassic magmatism in South China which took about 40 Ma. If we summarize the mechanism of the Jurassic magmatism in few key words, they may be: crustal thickening during the Triassic tectonics, partial melting of a thickened crust, production of magma of high buoyancy and low viscosity, inheritance of pre-magmatic structures as magma channels and lack of significant of regional Jurassic tectonic in the SCB (Fig. 6-3).

Chapter 8. Conclusions and perspectives

8.1 Conclusions

The South China Block, located at the east of the Eurasia continent, is characterised by a widespread Triassic, Jurassic and Cretaceous magmatism. This study focused on the Jurassic plutons that mainly crop out in the southeastern part of the South China Block, i.e. the ancient Cathaysia Block or the South China Fold Belt. According to our field investigations on forty-one Jurassic plutons widely distributed in the SCFB area, and detailed multidisciplinary studies of two representative Jurassic plutons, i.e. the Qitianling and Shibeil plutons, to assess the relationship between the emplacement process and related tectonics, as well as geodynamic implications. Here, we present the conclusive results of our three studies and propose a tentative model that can adequately explain most of the geological phenomena, including previous geochemical and geochronological achievements.

(1) In the regional view, the Jurassic granitic plutons are widespread in the South China Fold Belt from the inland area to the coastal region without any particular geographic distribution. At the pluton scale, the plutons present irregular cartographic geometries, and the area of the majority of the plutons is less than 1000 km² without remarkable elongation.

(2) Lithologically, the Jurassic plutons are chemically metaluminous, or weakly peraluminous. A lower crustal material (i.e. TTG, or granulite facies metasediments) is inferred as the source materials. Locally, early to middle Jurassic gabbro and gabbro-diorite crop out in the central part of the SCFB. Thus the Jurassic granitoids are mainly derived from crustal sources. The small amount of the mafic rocks, obviously derived from a mantle source, suggests a thermal contribution from the mantle to trigger the crustal melting, but limited mantle materials were involved into the granitic magma system.

(3) The long duration (ca. 40 Myrs) of the Jurassic magmatism may be due to the low magma production rate, which is consistent with lack of the Jurassic regional tectonics to accelerate the production and emplacement of the melts derived from the lower continental crust.

(4) The country rocks have suffered from multiphases of tectonic events since the Neoproterozoic epoch, but no consistent regional structures of Jurassic age can be identified. For example, large scaled basins, subduction-parallel fold-fault system and arc related magmatic series.

(5) The Jurassic plutons in the South China Fold Belt are characterised by subsolidus magmatic texture, absence of well-organized preferred mineral orientation and post-solidus deformation in the

plutons. At outcrop scale, the granitic rocks have a mineral and magnetic fabric. This planar and linear preferred orientation, developed in subsolidus conditions, has a magmatic origin. However, at the scale of one pluton, post-solidus, or mylonitic fabrics are lacking, country rocks as well as their contacts with low grade thermal aureole in the country rocks. Detailed magnetic fabric studies of the Qitianling and Shibeijian Jurassic plutons show for each pluton a consistent magnetic foliation pattern but a large scattering of the magnetic lineation. Both pipe-like and dike-like feeders are identified by the gravity modeling. These new results suggest that the magma emplacement was probably controlled by the pre-Jurassic structure of the country rocks, instead of a synmagmatic tectonic regime.

Accordingly, all these newly obtained observations and experimental data are incompatible with the model of the continuous Pacific slab subduction to explain the Jurassic magmatism in the South China Block. Our results suggest that the Jurassic magmatism was produced during a tectonically quiet epoch. The partial melting of the thickened lower continental crust of the SCFB, due to the Middle Triassic continental collision between the SCB and the Indochina block, and the intracontinental tectonic events along the surrounding belts (Longmenshan, Dabashan) and within the South China Block in the Xuefengshan, might be considered as the major cause for the Jurassic magmatism. As the lack of Jurassic tectonics and the absence of the involving of mantle materials in large volume, the partial melting rate may be low and the magma makes its ascent due its low viscosity with respect to the country rocks, and its own buoyancy force through pre-Jurassic structures. Thus, the structural inheritance due to the multiple tectonic events that affected the SCB since the Neoproterozoic played an important role in the location of the Jurassic plutons.

8.2 Perspectives

Restore of the Jurassic geothermal state of the country rock will be done, combined with the parameter of the magma (Composition, Pressure, Temperature and Viscosity), which acquired by the experimental petrological work of another thesis on the Qitianling pluton, we can infer the thermal state and flexibility of the country rock to test the feasibility of our models for the magma emplacement. Furthermore, the numerical modelling of the formation and emplacement of the Jurassic magma in the SCB is needed in the future based on the abundant geochemical, geochronological and geophysical data of the Jurassic granites.

References

- Acocella, V. (2014). Structural control on magmatism along divergent and convergent plate boundaries: Overview, model, problems. *Earth-Science Reviews*, 136, 226-288.
- Ali, J. R., Thompson, G. M., Zhou, M. F., Song, X. (2005). Emeishan large igneous province, SW China. *Lithos*, 79(3), 475-489.
- Allibon, J., Bussy, F., Lewin, E., Darbellay, B. (2011). The tectonically controlled emplacement of a vertically sheeted gabbro-pyroxenite intrusion: feeder-zone of an ocean-island volcano (Fuerteventura, Canary Islands). *Tectonophysics*, 500(1), 78-97.
- An, M., Shi, Y. (2006). Lithospheric thickness of the Chinese continent. *Physics of the Earth and Planetary Interiors*, 159(3), 257-266.
- Annen, C., Sparks, R. S. J. (2002). Effects of repetitive emplacement of basaltic intrusions on thermal evolution and melt generation in the crust. *Earth and Planetary Science Letters*, 203(3), 937-955.
- Annen, C., J. Blundy, and R. Sparks (2006). The genesis of intermediate and silicic magmas in deep crustal hot zones, *Journal of Petrology*, 47(3), 505-539.
- Annen, C., Blundy, J. D., Leuthold, J., Sparks, R. S. J. (2015). Construction and evolution of igneous bodies: Towards an integrated perspective of crustal magmatism. *Lithos*, 230, 206-221.
- Aranguren, A., Cuevas, J., Tub , J.M., Romn-Berdiel, T., Casas-Sainz, A., Casas-Ponsati, A., (2003). Granite laccolith emplacement in the Iberian arc: AMS and gravity study of the La Tojiza pluton (NW Spain). *Journal of the Geological Society* 160, 435-445.
- Aspden, J. A., McCourt, W. J., Brook, M. (1987). Geometrical control of subduction-related magmatism: the Mesozoic and Cenozoic plutonic history of Western Colombia. *Journal of the Geological Society*, 144(6), 893-905.
- Bai, D.Y., Chen, J.C., Ma, T.Q and Wang, X.H (2005). Geochemical characteristics and tectonic setting of Qitianling A_Type granitic pluton in southeast Hunan, *Acta Petrologica et Mineralogica*, 24 (4), 255-272 (in Chinese with English abstract).
- Bain, A. A., A. Jellinek, and R. Wiebe (2013). Quantitative field constraints on the dynamics of silicic magma chamber rejuvenation and overturn, *Contributions to Mineralogy and Petrology*, 165(6), 1275-1294.
- Barbarin, B. (1990). Granitoids: main petrogenetic classifications in relation to origin and tectonic setting. *Geological Journal*, 25(3 - 4), 227-238.
- Barbarin, B. (1996). Genesis of the two main types of peraluminous granitoids. *Geology*, 24(4), 295-298.

- Barboni, M., Annen, C., Schoene, B. (2015). Evaluating the construction and evolution of upper crustal magma reservoirs with coupled U/Pb zircon geochronology and thermal modeling: A case study from the Mt. Capanne pluton (Elba, Italy). *Earth and Planetary Science Letters*, 432, 436-448.
- Barley, M. E., Pickard, A. L., Sylvester, P. J. (1997). Emplacement of a large igneous province as a possible cause of banded iron formation 2.45 billion years ago. *Nature*, 385(6611), 55.
- Bateman, R. (1984). On the role of diapirism in the, segregation, ascent and final emplacement of granitoid magmas. *Tectonophysics*, 110(3-4), 211-231.
- BGMRFJ, (1985). Bureau of Geology and Mineral Resources of Fujian Province (BGMRFJ) Regional Geology of the Jiangxi Province Geological Publishing House, Beijing (1985) 675 pp.
- BGMRHN (Bureau of Geology and Mineral Resources of Hunan Province), (1988). Regional Geology of Hunan Province. Geological Publishing House, Beijing, pp. 6–664 (in Chinese with English Abstract).
- Bird, P. (2003). An updated digital model of plate boundaries. *Geochemistry, Geophysics, Geosystems*, 4(3).
- Blundy, J. D., and C. J. Annen (2016). Crustal magmatic systems from the perspective of heat transfer, *Elements*, 12(2), 115-120.
- Borradaile, G. J., and B. Henry (1997). Tectonic applications of magnetic susceptibility and its anisotropy, *Earth-Science Reviews*, 42(1), 49-93, doi:[http://dx.doi.org/10.1016/S0012-8252\(96\)00044-X](http://dx.doi.org/10.1016/S0012-8252(96)00044-X).
- Borradaile, G. J., and J. S. Mothersill (1984), Coaxial deformed and magnetic fabrics without simply correlated magnitudes of principal values, *Physics of the Earth and Planetary Interiors*, 35(4), 294-300, doi:[https://doi.org/10.1016/0031-9201\(84\)90023-2](https://doi.org/10.1016/0031-9201(84)90023-2).
- Bouilhol, P., M. Schmidt, and J.-P. Burg (2015). Magma transfer and evolution in channels within the arc crust: the pyroxenitic feeder pipes of Sapat (Kohistan, Pakistan), *Journal of Petrology*, 56(7), 1309-1342.
- Brown, M., Solar, G. S. (1998). Granite ascent and emplacement during contractional deformation in convergent orogens. *Journal of Structural Geology*, 20(9), 1365-1393.
- Bunger, A. P., Cruden, A. R. (2011). Modeling the growth of laccoliths and large mafic sills: Role of magma body forces. *Journal of Geophysical Research: Solid Earth*, 116(B2).
- Burchardt, S. (2008). New insights into the mechanics of sill emplacement provided by field observations of the Njardvik Sill, Northeast Iceland. *Journal of Volcanology and Geothermal Research*, 173(3), 280-288.

- Burchardt, S. (2009). Mechanisms of magma emplacement in the upper crust (Doctoral dissertation, Niedersächsische Staats- und Universitätsbibliothek Göttingen).
- Burchardt, S., Walter, T. R. (2010). Propagation, linkage, and interaction of caldera ring-faults: comparison between analogue experiments and caldera collapse at Miyakejima, Japan, in 2000. *Bulletin of Volcanology*, 72(3), 297-308.
- Burchfiel B.C., Chen Z.L., Liu Y.P., Royden L.H., (1995). Tectonics of the Longmen Shan and adjacent regions, Central China. *International Geology Review*, 37(8): 661-735.
- Byerly, A., Tikoff, B., Kahn, M., Jicha, B., Gaschnig, R., Fayon, A. K. (2017). Internal fabrics of the Idaho batholith, USA. *Lithosphere*, 9(2), 283-298.
- Campbell, I. H., Griffiths, R. W. (1990). Implications of mantle plume structure for the evolution of flood basalts. *Earth and Planetary Science Letters*, 99(1-2), 79-93.
- Caricchi, L., Burlini, L., Ulmer, P., Gerya, T., Vassalli, M., Papale, P. (2007). Non-Newtonian rheology of crystal-bearing magmas and implications for magma ascent dynamics. *Earth and Planetary Science Letters*, 264(3), 402-419.
- Caricchi, L., C. Annen, J. Blundy, G. Simpson, and V. Pinel (2014). Frequency and magnitude of volcanic eruptions controlled by magma injection and buoyancy, *Nature Geoscience*, 7(2), 126.
- Castro, A. (1987). On granitoid emplacement and related structures. A review. *Geologische Rundschau*, 76(1), 101-124.
- Charvet, J., L. Shu, M. Faure, F. Choulet, B. Wang, H. Lu, and N. Le Breton (2010). Structural development of the Lower Paleozoic belt of South China: genesis of an intracontinental orogen, *Journal of Asian Earth Sciences*, 39(4), 309-330.
- Channell, J. E. T., McCabe, C. (1994). Comparison of magnetic hysteresis parameters of unremagnetized and remagnetized limestones. *Journal of Geophysical Research: Solid Earth*, 99(B3), 4613-4623.
- Charles, N., Augier, R., Gumiaux, C., Monié P., Chen, Y., Faure, M., Zhu, R. (2013). Timing, duration and role of magmatism in wide rift systems: Insights from the Jiaodong Peninsula (China, East Asia). *Gondwana Research*, 24(1), 412-428.
- Chen, J., and B.-m. Jahn (1998). Crustal evolution of southeastern China: Nd and Sr isotopic evidence, *Tectonophysics*, 284(1), 101-133, doi: [http://dx.doi.org/10.1016/S0040-1951\(97\)00186-8](http://dx.doi.org/10.1016/S0040-1951(97)00186-8).
- Chen, C.H., Lee, C.Y., Shinjo, R., (2008). Was there Jurassic paleo-Pacific subduction in South China?: Constraints from $^{40}\text{Ar}/^{39}\text{Ar}$ dating, elemental and Sr–Nd–Pb isotopic geochemistry of the Mesozoic basalts. *Lithos* 106, 83-92.
- Chu, Y., Faure, M., Lin, W., Wang, Q., Ji, W., (2012a). Tectonics of the Middle Triassic

-
- intracontinental Xuefengshan Belt, South China: new insights from structural and chronological constraints on the basal décollement zone. *International Journal of Earth Sciences* 101, 2125-2150.
- Chu, Y., Lin, W., Faure, M., Wang, Q., Ji, W., (2012b). Phanerozoic tectonothermal events of the Xuefengshan Belt, central South China: Implications from UPb age and LuHf determinations of granites. *Lithos* 150, 243-255.
- Clemens, J. D., Mawer, C. K. (1992). Granitic magma transport by fracture propagation. *Tectonophysics*, 204(3-4), 339-360.
- Clemens, J. D., Petford, N. (1999). Granitic melt viscosity and silicic magma dynamics in contrasting tectonic settings. *Journal of the Geological Society*, 156(6), 1057-1060.
- Clemens, J., I. Buick, and A. Kisters (2017). The Donkerhuk batholith, Namibia: A giant S-type granite emplaced in the mid crust, in a fore-arc setting, *Journal of the Geological Society*, 174(1). 157-169.
- Coleman, D. S., W. Gray, and A. F. Glazner (2004). Rethinking the emplacement and evolution of zoned plutons: Geochronologic evidence for incremental assembly of the Tuolumne Intrusive Suite, California, *Geology*, 32(5), 433, doi:10.1130/g20220.1.
- Corry, C. E. (1988). *Laccoliths: mechanics of emplacement and growth* (Vol. 220). Geological Society of America.
- Cruden, A. R. (1988). Deformation around a rising diapir modeled by creeping flow past a sphere. *Tectonics*, 7(5), 1091-1101.
- Cruden, A. R. (1990). Flow and fabric development during the diapiric rise of magma. *The Journal of Geology*, 98(5), 681-698.
- Cruden A R. (1998). On the emplacement of tabular granites (J). *Journal of the Geological Society-London*, 155(5): 853-862.
- Cruden, A. R., McCaffrey, K. J. W., Bungler, A. P. (2017). Geometric scaling of tabular igneous intrusions: Implications for emplacement and growth.
- Cui, J., Zhang, Y., Dong, S., Jahn, B. M., Xu, X., Ma, L. (2013). Zircon U–Pb geochronology of the Mesozoic metamorphic rocks and granitoids in the coastal tectonic zone of SE China: constraints on the timing of Late Mesozoic orogeny. *Journal of Asian Earth Sciences*, 62, 237-252.
- Currier, R. M., Forsythe, P., Grossmeier, C., Laliberte, M., Yagle, B. (2017). Experiments on the evolution of laccolith morphology in plan-view. *Journal of Volcanology and Geothermal Research*, 336, 155-167.
- Daly, R. A. (1903). The mechanics of igneous intrusion. *American Journal of Science*, (88),

269-298.

- Day, R., M. Fuller, and V. A. Schmidt (1977). Hysteresis properties of titanomagnetites: Grain-size and compositional dependence, *Physics of the Earth and Planetary Interiors*, 13(4), 260-267, doi:[http://dx.doi.org/10.1016/0031-9201\(77\)90108-X](http://dx.doi.org/10.1016/0031-9201(77)90108-X).
- Deniel, C., Vidal, P., Fernandez, A., Le Fort, P., and Peucat, J. J. (1987). Isotopic study of the Manaslu granite (Himalaya, Nepal): inferences on the age and source of Himalayan leucogranites. *Contributions to Mineralogy and Petrology*, 96(1), 78-92.
- de Saint Blanquat M, Tikoff B. (1997). Development of magmatic to solid-state fabrics during syntectonic emplacement of the Mono Creek Granite, Sierra Nevada Batholith [M]//Granite: from segregation of melt to emplacement fabrics. Springer Netherlands, 231-252.
- de Saint Blanquat, M., Tikoff, B., Teyssier, C., Vigneresse, J. L. (1998). Transpressional kinematics and magmatic arcs. *Geological Society, London, Special Publications*, 135(1), 327-340.
- de Saint Blanquat, M., Law, R.D., Bouchez, J.-L., Morgan, S.S., (2001). Internal structure and emplacement of the Papoose Flat pluton: An integrated structural, petrographic, and magnetic susceptibility study. *Geological Society of America Bulletin* 113, 976-995.
- de Saint Blanquat, M., Habert, G., Horsman, E., Morgan, S. S., Tikoff, B., Launeau, P., Gleizes, G. (2006). Mechanisms and duration of non-tectonically assisted magma emplacement in the upper crust: the Black Mesa pluton, Henry Mountains, Utah. *Tectonophysics*, 428 (1), 1-31.
- de Saint Blanquat, M., Horsman, E., Habert, G., Morgan, S., Vanderhaeghe, O., Law, R., Tikoff, B. (2011). Multiscale magmatic cyclicality, duration of pluton construction, and the paradoxical relationship between tectonism and plutonism in continental arcs. *Tectonophysics*, 500(1), 20-33.
- Chen W.F., Chen P.R., Zhou X.M., Huang H.Y., Ding X., Sun T., (2006). Single-zircon La-ICP-MS U-Pb Dating of the Yangmingshan Granitic Pluton in Hunan, South China and Its Petrogenetic Study. *Acta Geologica Sinica*, 80(7):1065-1077 (in Chinese with English abstract).
- Defant, M. J., Drummond, M. S. (1990). Derivation of some modern arc magmas by melting of young subducted lithosphere. *Nature*, 347(6294), 662-665.
- Deng X.G., Chen Z.G., Li X.H., Liu D.Y., (2004). SHRIMP U-Pb zircon dating of the Darongshan-Shiwandashan granitoid belt in southeastern Guangxi, China *Geological Review*, 50 (2004), pp. 427-432 (in Chinese with English abstract)
- Deng X.G., Li X.H., Liu Y.M., Huang G.F., Hou M.S., (2005). Geochemical characteristics of Qitianling granites and their implications for mineralisation. *Acta Petrologica et Mineralogica*, 24 (2): 93-102 (In Chinese with English abstract)
- Deng Y.F., Zhang Z.J., José B., Fan W.M., (2014). 3-D density structure under South China

-
- constrained by seismic velocity and gravity data. *Tectonophysics*, 627, 159-170.
- Dong Shuwen, Zhang Yueqiao, Long Changxing, Yang Zhenyu, Ji Qiang, Wang Tao, Chen Xuanhua, (2008). Jurassic tectonic revolution in China and new interpretation of the “Yanshan Movement”. *Acta Geologica Sinica (English edition)*, 82(2), 334-347.
- Dong, S., Zhang, Y., Zhang, F., Cui, J., Chen, X., Zhang, S., Huang, S. (2015). Late Jurassic–Early Cretaceous continental convergence and intracontinental orogenesis in East Asia: A synthesis of the Yanshan Revolution. *Journal of Asian Earth Sciences*, 114, 750-770.
- Duchesne, J. C. (1978). Quantitative modeling of Sr, Ca, Rb, and K in the Bjerkrem-Sogndal layered lopolith (SW Norway). *Contributions to Mineralogy and Petrology*, 66(2), 175-184.
- Dumond, G., A. S. Yoshinobu, and C. G. Barnes (2005). Midcrustal emplacement of the Sausfjellet pluton, central Norway: Ductile flow, stoping, and in situ assimilation, *Geological Society of America Bulletin*, 117(3-4), 383-395.
- Dunlop, D.J., Özdemir, Ö., (1997). *Rock Magnetism: Fundamentals and Frontiers*. Cambridge University Press, Cambridge (596 pp.).
- Dunlop, D. J. (2002). Theory and application of the Day plot (Mrs/Ms versus Hcr/Hc) 2. Application to data for rocks, sediments, and soils, *Journal of Geophysical Research: Solid Earth*, 107(B3), EPM 5-1-EPM 5-15, doi:10.1029/2001JB000487.
- Faure, M., Cottureau, N., (1988). Kinematic data on the emplacement of the Middle Carboniferous migmatitic dome in the Axial Zone of the Montagne Noire (Massif Central, France). *COMPTEs RENDUS DE L'ACADEMIE DES SCIENCES SERIE II* 307, 1787-1794.
- Faure, M., Pons, J., (1991). Crustal thinning recorded by the shape of the Namurian- Westphalian leucogranite in the Variscan belt of the northwest Massif Central, France *Geology* 19, 730-733.
- Faure M., Lin W., Shu L.S., Sun Y., Scharer U. (1999). Tectonics of the Dabieshan (eastern China) and possible exhumation mechanism of ultra-high-pressure rocks. *Terra Nova*, 11, 251-258.
- Faure, M., W. Lin, P. Monié and S. Meffre (2008). Palaeozoic collision between the North and South China blocks, Triassic intracontinental tectonics, and the problem of the ultrahigh-pressure metamorphism, *Comptes Rendus Geoscience*, 340(2), 139-150.
- Faure, M., Shu, L., Wang, B., Charvet, J., Choulet, F., Monié P. (2009). Intracontinental subduction: a possible mechanism for the Early Palaeozoic Orogen of SE China. *Terra Nova*, 21(5), 360-368.
- Faure, M., Lèpvrier, C., Van Nguyen, V., Van Vu, T., Lin, W., Chen, Z. (2014). The South China Block-Indochina collision: where, when, and how?. *Journal of Asian Earth Sciences*, 79, 260-274.
- Faure Michel, Wei Lin, Yang Chu, Claude Lèpvrier. (2016). Triassic tectonics of the southern

-
- margin of the South China Block. *C. R. Geoscience* 348 (2016) 5–14.
- Feng, Z., C. Wang, M. Zhang, and J. Liang (2012). Unusually dumbbell-shaped Guposhan–Huashan twin granite plutons in Nanling Range of south China: Discussion on their incremental emplacement and growth mechanism, *Journal of Asian Earth Sciences*, 48, 9-23.
- Ferrari, L., López - Martínez, M., Rosas - Elguera, J. (2002). Ignimbrite flare - up and deformation in the southern Sierra Madre Occidental, western Mexico: Implications for the late subduction history of the Farallon plate. *Tectonics*, 21(4).
- Fletcher, C. J., L. S. Chan, R. J. Sewell, S. D. G. Campbell, D. W. Davis, and J. Zhu (2004). Basement heterogeneity in the Cathaysia crustal block, southeast China, Geological Society, London, Special Publications, 226(1), 145-155.
- Fu Jian-ming, MA Chang-qian, XIE Cai-fu, ZHANG Ye-ming, PENG Song-bai (2004). Zircon SHRIMP dating of the Cailing granite on the eastern margin of the Qitianling granite, Hunan, South China, and its significance[J]. *Geology in China*, 31(1): 96-100(in Chinese with English abstract).
- Gao, S., J. Yang, L. Zhou, M. Li, Z. Hu, J. Guo, H. Yuan, H. Gong, G. Xiao, and J. Wei (2011). Age and growth of the Archean Kongling terrain, South China, with emphasis on 3.3 Ga granitoid gneisses, *Am. J. Sci.*, 311(2), 153-182, doi:10.2475/02.2011.03.
- Gilder, S. A., P. H. Leloup, V. Courtillot, Y. Chen, R. S. Coe, X. Zhao, W. Xiao, N. Halim, J.-P. Cogné and R. Zhu (1999), Tectonic evolution of the Tancheng-Lujiang (Tan-Lu) fault via Middle Triassic to Early Cenozoic paleomagnetic data, *Journal of Geophysical Research: Solid Earth*, 104(B7), 15365-15390, doi:10.1029/1999jb900123.
- Glazner, A. F., Bartley, J. M. (2006). Is stopping a volumetrically significant pluton emplacement process?. *Geological Society of America Bulletin*, 118(9-10), 1185-1195.
- Glazner, A. F. (2007). Thermal limitations on incorporation of wall rock into magma. *Geology*, 35(4), 319-322.
- Goodson, K. (2014). Penetrative Deformation of Dolostones during Contact Metamorphism and the Forceful Emplacement of the Tungstonia Granite, Kern Mountains, Nevada (Doctoral dissertation).
- Gradstein, F. M., Ogg, J. G., Schmitz, M., Ogg, G. (Eds.). (2012). *The geologic time scale*. elsevier.
- Gudmundsson, A. (1990). Emplacement of dikes, sills and crustal magma chambers at divergent plate boundaries. *Tectonophysics*, 176(3-4), 257-275.
- Gudmundsson, A. (2006). How local stresses control magma-chamber ruptures, dyke injections, and eruptions in composite volcanoes. *Earth-Science Reviews*, 79(1), 1-31.
- Gudmundsson, A. (2011). Deflection of dykes into sills at discontinuities and magma-chamber

- formation. *Tectonophysics*, 500(1), 50-64.
- Guo, L.Z., Shi, Y.S., Lu, H.F., (1989). The pre-Devonian tectonic patterns and evolution of South China. *Journal of Southeast Asian Earth Sciences*, 3: 87-93.
- Guo L., (2001). The plate tectonics of South China. Geological Publishing House Beijing.
- Guo F., Fan W., Li C., Zhao L., Li H., Yang J., (2012). Multi-stage crust–mantle interaction in SE China: temporal, thermal and compositional constraints from the Mesozoic felsic volcanic rocks in eastern Guangdong–Fujian provinces. *Lithos*, 150, pp. 62–84.
- Guo Y.Z. (2006). A Study on Magnetic Field Gradient Vector Structure Used to Locate Stannic Enrichment Ore Body in Qitianling Multi-metal Ore Area, South Hunan Province, *Acta Geologica Sinica*, 80 (10), 1553-1557 (in Chinese with English abstract).
- Hacker, B.R., Ratschbacher, L., Liou, J.G., (2004). Subduction, collision, and exhumation in the Qinling-Dabie Orogen. *Journal of the Geological Society London* 226, 157–175.
- Hammarstrom, J. M., and E. Zen (1986), Aluminum in hornblende: an empirical igneous geobarometer, *American Mineralogist*, 71(11-12), 1297-1313.
- Harrowfield, M. J. Wilson, C. J. L., (2005). Indosinian deformation of the Songpan Garz êFold Belt, northeast Tibetan Plateau. *Journal of Structural Geology* 27, 101-117, doi:<http://dx.doi.org/10.1016/j.jsg.2004.06.010>.
- He, B., Y.-G. Xu, and S. Paterson (2009). Magmatic diapirism of the Fangshan pluton, southwest of Beijing, China, *Journal of Structural Geology*, 31(6), 615-626.
- He, Z.Y., Xu, X.S., Niu, Y.L., (2010). Petrogenesis and tectonic significance of a Mesozoic granite–syenite–gabbro association from inland South China. *Lithos* 119, 621-641.
- Hedenquist, J. W., Lowenstern, J. B. (1994). The role of magmas in the formation of hydrothermal ore deposits. *Nature*, 370(6490), 519-527.
- Herrero-Bervera, E., Walker, G. P. L., Canon-Tapia, E., Garcia, M. O. (2001). Magnetic fabric and inferred flow direction of dikes, conesheets and sill swarms, Isle of Skye, Scotland. *Journal of Volcanology and Geothermal Research*, 106(3), 195-210.
- Hong D., Xie X., Zhang J., (1998). Deep structural setting of granitoids and their metallogeny in South China *Global Tecton. Metallog.*, 6: 181–186.
- Hollister, L. S., Grissom, G. C., Peters, E. K., Stowell, H. H., Sisson, V. B. (1987), Confirmation of the empirical correlation of Al in hornblende with pressure of solidification of calc-alkaline plutons. *American mineralogist*, 72(3-4), 231-239.
- Horsman, E., S. Morgan, M. de Saint-Blanquat, G. Habert, A. Nugent, R. A. Hunter, and B. Tikoff (2009). Emplacement and assembly of shallow intrusions from multiple magma pulses, Henry Mountains, Utah, *Earth and Environmental Science Transactions of the Royal Society of*

- Edinburgh, 100(1-2), 117-132.
- Horsman, E., B. Tikoff, and S. Morgan (2005). Emplacement-related fabric and multiple sheets in the Maiden Creek sill, Henry Mountains, Utah, USA, *Journal of Structural Geology*, 27(8), 1426-1444, doi:<http://dx.doi.org/10.1016/j.jsg.2005.03.003>.
- Hrouda F, Jelinek V., (1990). Resolution of ferrimagnetic and paramagnetic anisotropies in rocks, using combined low - field and high - field measurements[J]. *Geophysical Journal International*, 103(1): 75-84.
- Hsü, K. J., Li, J., Chen, H., Wang, Q., Sun, S., Şengör, A. M. C. (1990). Tectonics of South China: key to understanding West Pacific geology. *Tectonophysics*, 183(1-4). 9-39.
- Hu, S., He, L., Wang, J. (2000). Heat flow in the continental area of China: a new data set. *Earth and Planetary Science Letters*, 179(2), 407-419.
- Hu, R. Z., Zhou, M. F. (2012). Multiple Mesozoic mineralization events in South China—an introduction to the thematic issue. *Mineralium Deposita*, 47(6), 579-588.
- Hua, R., Chen, P., Zhang, W., Lu, J. (2005). Three large-scale metallogenic events related to the Yanshanian Period in Southern China. In *Mineral Deposit Research: Meeting the Global Challenge* (pp. 401-404). Springer Berlin Heidelberg.
- Huang, F., Scaillet, B., Wang, R., Erdmann, S., Chen, Y., Faure, M., Zhu, J. (2016). Experimental constraints on the Qitianling granite in south China: phase equilibria and petrogenetic implications. In *EGU General Assembly Conference Abstracts* (Vol. 18, p. 8972).
- Huang, H. Q., Li, X. H., Li, Z. X., Li, W. X. (2015). Formation of the Jurassic South China Large Granitic Province: insights from the genesis of the Jiufeng pluton. *Chemical Geology*, 401, 43-58.
- Huang, J. (1945). On Major Tectonic Forms of China, National Geological Survey of China under the Ministry of Economic Affairs.
- Huang, J.Q., (1977). The basic outline of China tectonics. *Acta Geol. Sin.* 52, 117–135.
- Huang X.L., Yu Y., Li J., Tong L.X., Chen L.L., (2013). Geochronology and Petrogenesis of the early Paleozoic I-type granite in the Taishan area, South China: Middle-lower crustal melting during orogenic collapse. *Lithos*, 177: 268-284.
- Huber, C., Bachmann, O., Dufek, J. (2011). Thermo-mechanical reactivation of locked crystal mushes: Melting-induced internal fracturing and assimilation processes in magmas. *Earth and Planetary Science Letters*, 304(3), 443-454.
- Humphreys, M. C., Menand, T., Blundy, J. D., Klimm, K. (2008). Magma ascent rates in explosive eruptions: constraints from H₂O diffusion in melt inclusions. *Earth and Planetary Science Letters*, 270(1), 25-40.

- HUPPERT, H. E., SPARKS, R. S. J. (1988). The generation of granitic magmas by intrusion of basalt into continental crust. *Journal of Petrology*, 29(3), 599-624.
- Hutton, D.H.W., (1988). Granite emplacement mechanisms and tectonic controls: inferences from deformation studies. *Earth and Environmental Science Transactions of the Royal Society of Edinburgh* 79, 245-255.
- Hutton, D. H. W., Dempster, T. J., Brown, P. E., Becker, S. D. (1990). A new mechanism of granite emplacement: intrusion in active extensional shear zones.
- Hutton, D. H. (1992). Granite sheeted complexes: evidence for the dyking ascent mechanism, *Geological Society of America Special Papers*, 272, 377-382.
- INGER, S., HARRIS, N. (1993). Geochemical constraints on leucogranite magmatism in the Langtang Valley, Nepal Himalaya. *Journal of Petrology*, 34(2), 345-368.
- Jiang, Y.H., Jiang, S.Y., Dai, B.Z., Liao, S.Y., Zhao, K.D., Ling, H.F., (2009). Middle to late Jurassic felsic and mafic magmatism in southern Hunan province, southeast China: Implications for a continental arc to rifting. *Lithos* 107, 185-204.
- Jiang, Y. H., Wang, G. C., Liu, Z., Ni, C. Y., Qing, L., Zhang, Q. (2015). Repeated slab advance–retreat of the Palaeo-Pacific plate underneath SE China. *International Geology Review*, 57(4), 472-491.
- John, B. E., and J. D. Blundy (1993). Emplacement-related deformation of granitoid magmas, southern Adamello Massif, Italy, *Geological Society of America Bulletin*, 105(12), 1517-1541.
- Kavanagh, J. L., Menand, T., Sparks, R. S. J. (2006). An experimental investigation of sill formation and propagation in layered elastic media. *Earth and Planetary Science Letters*, 245(3), 799-813.
- Knight Michael D. and Walker George P. L., (1988). Magma Flow Directions in Dikes of the Koolau Complex, Oahu, Determined From Magnetic Fabric Studies. *Journal of Geophysical Research*, 93 (B5), pp. 4301-4319.
- Kratinová Z., P. Závada, F. Hrouda, and K. Schulmann (2006). Non-scaled analogue modelling of AMS development during viscous flow: a simulation on diapir-like structures, *Tectonophysics*, 418(1), 51-61.
- Kruhl, J. H., S. Erdmann, and S. H. Büttner (2007). Brittle-ductile microfabrics in naturally deformed cordierite: Evidence for significant short-term strain-rate variations, *Journal of structural geology*, 29(2), 355-374.
- Lee, J. K., Williams, I. S., Ellis, D. J. (1997). Pb, U and Th diffusion in natural zircon. *Nature*, 390(6656), 159.
- Leloup, P. H., Lacassin, R., Tapponnier, P., Schärer, U., Zhong, D., Liu, X., Trinh, P. T. (1995). The Ailao Shan-Red River shear zone (Yunnan, China), Tertiary transform boundary of Indochina.

- Tectonophysics, 251(1), 3-84.
- Lepvrier, C., Maluski H., Tich, V.V., Leyreloup, A., Thi P.T., Vuong N.V. (2004). The Early Triassic Indosinian orogeny in Vietnam (Truong Son Belt and Kontum Massif); implications for the geodynamic evolution of Indochina. *Tectonophysics*, 393 (1-4): 87-118.
- Li, H., Y. Lu, D. Wang, Y. Chen, H. Yang, J. Guo, C. Xie, Y. Mei, L. Ma (2006). Dating of the rock-forming and ore-forming ages and their geological significances in the Furong Ore-field, Qitian Mountain, Hunan, *Geological Review*, 52 (1), 113-121 (in Chinese with English abstract).
- Li J.D., D.Y. Bai, G.Y. Wu, Q.J. Che, Y.R. Liu, T.Q. Ma (2005). Zircon SHRIMP dating of the Qitianling granite, Chenzhou, southern Hunan, and its geological significance. *Geological Bulletin of China*, 24 (5): 411-414 (in Chinese with English abstract).
- Li, J.H., Zhang, Y.Q., Dong, S.W., Johnston S.T., (2014). Cretaceous tectonic evolution of South China: A preliminary synthesis. *Earth-Science Reviews*, 134: 98-136.
- Li, J., Zhang, Y., Zhao, G., Johnston, S. T., Dong, S., Koppers, A., Xin, Y. (2017). New insights into Phanerozoic tectonics of South China: Early Paleozoic sinistral and Triassic dextral transpression in the east Wuyishan and Chencai domains, NE Cathaysia. *Tectonics*.
- Li, X.H. and McCulloch M.T. (1996). Secular variations in the Nd isotopic composition of the Neoproterozoic sediments from the southern margin of the Yangtze Block: evidence for a Proterozoic continental collision in southeastern China *Precambrian Res.*, 76: 67–76.
- Li, X.H., Zhao, J.X., McCulloch, M.T., Zhou, G., Xing, F., (1997). Geochemical and Sm-Nd isotopic study of Neoproterozoic ophiolites from southeastern China: Petrogenesis and tectonic implications. *Precambrian Res.*, 81, 129-144.
- Li, X.H., (2000). Cretaceous magmatism and lithospheric extension in Southeast China. *Journal of Asian Earth Sciences*, 18 (3): 293-305.
- Li, X.H., Li, Z.X., Ge, W.C., Zhou, H.W., Li, W.X., Liu, Y., Wingate, M.T.D., (2003a). Neoproterozoic granitoids in South China: crustal melting above a mantle plume at ca. 825Ma? *Precambrian Res.* 122, 45–83.
- Li, X.-H., W.-X. Li, Z.-X. Li, and Y. Liu (2008), 850–790 Ma bimodal volcanic and intrusive rocks in northern Zhejiang, South China: A major episode of continental rift magmatism during the breakup of Rodinia, *Lithos*, 102(1–2), 341-357, doi:<http://dx.doi.org/10.1016/j.lithos.2007.04.007>.
- Li, X., Li, W., Wang, X., Li, Q., Liu, Y., Tang, G. (2009). Role of mantle-derived magma in genesis of early Yanshanian granites in the Nanling Range, South China: in situ zircon Hf-O isotopic constraints. *Science in China Series D: Earth Sciences*, 52(9), 1262-1278.
- Li, Z.-X., Li, X.-H., (2007). Formation of the 1300-km-wide intracontinental orogen and

- postorogenic magmatic province in Mesozoic South China: A flat-slab subduction model. *Geology* 35, 179-182.
- Li, Z.X., Bogdanova, S.V., Collins, A.S., Davidson, A., Waele, B.D., Ernst, R.E., Fitzsimons, I.C.W., Fuck, R.A., Gladkochub, D.P., Jacobs, J., Karlstrom, K.E., Lu, S., Natapov, L.M., Pease, V., Pisarevsky, S.A., Thrane, K., Vernikovsky, V., (2008). Assembly, configuration, and break-up history of Rodinia: A synthesis. *Precambrian Research*, 160, 179-210.
- Lin, W., M. Faure, Q. Wang, P. Monié and D. Panis (2005). Triassic polyphase deformation in the Feidong-Zhangbaling Massif (eastern China) and its place in the collision between the North China and South China blocks, *Journal of Asian Earth Sciences*, 25(1), 121-136.
- Lin, W., Faure, M., Chen, Y., Ji, W., Wang, F., Wu, L., ... & Wang, Q. (2013). Late Mesozoic compressional to extensional tectonics in the Yiwulüshan massif, NE China and its bearing on the evolution of the Yinshan–Yanshan orogenic belt: Part I: Structural analyses and geochronological constraints. *Gondwana Research*, 23(1), 54-77.
- Ling H.F., Shen W.Z., Deng P., Jiang S.Y., Jiang Y.H., Qiu J.S., Huang G.L., Ye H.M., Tan Z.Z., (2005). Study of geochemistry and Petrogenesis of the Maofeng granite, northern Guangdong province. *Acta Petrologica Sinica*, 21(3): 677-687(In Chinese with English abstract).
- Liu, J., Tang, Y., Tran, M. D., Cao, S., Zhao, L., Zhang, Z., Chen, W. (2012). The nature of the Ailao Shan–Red River (ASRR) shear zone: constraints from structural, microstructural and fabric analyses of metamorphic rocks from the Diancang Shan, Ailao Shan and Day Nui Con Voi massifs. *Journal of Asian Earth Sciences*, 47, 231-251.
- Liu, R., Zhou, H.W., Zhang, L., Zhong, Z.Q., Zeng, W., Xiang, H., Jin, S., Lu, X.Q., Li, C.Z., (2010). Zircon U-Pb ages and Hf isotope compositions of the Mayuan migmatite complex, NW Fujian Province, Southeast China: Constraints on the timing and nature of a regional tectonothermal event associated with the Caledonian orogeny. *Lithos*, 119, 163-180.
- Liu, Q., Yu, J. H., Wang, Q., Su, B., Zhou, M. F., Xu, H., Cui, X. (2012). Ages and geochemistry of granites in the Pingtan–Dongshan Metamorphic Belt, Coastal South China: new constraints on Late Mesozoic magmatic evolution. *Lithos*, 150, 268-286.
- Lu, G., Zhao, L., Zheng, T., Kaus, B. J. (2014). Strong intracontinental lithospheric deformation in South China: Implications from seismic observations and geodynamic modeling. *Journal of Asian Earth Sciences*, 86, 106-116.
- Luo L., Qi J.F., Zhang M.Z., Wang K., Han Y.Z. (2014). Detrital zircon U–Pb ages of Late Triassic–Late Jurassic deposits in the western and northern Sichuan Basin margin: constraints on the foreland basin provenance and tectonic implications. *Int J Earth Sci (Geol Rundsch)* 103:1553–1568.

- Ma, X.Y and Wu, Z.W., (1981). Early tectonic evolution of China. *Precambrian Research* 14, 185–202.
- Maniar, P. D., Piccoli, P. M. (1989). Tectonic discrimination of granitoids. *Geological society of America bulletin*, 101(5), 635-643
- Mao, J.-W., Cheng, Y.-B., Chen, M.-H., Pirajno, F., (2013). Major types and time–space distribution of Mesozoic ore deposits in South China and their geodynamic settings. *Mineralium Deposita* 1–28.
- Martelet, G., J. Perrin, C. Truffert, and J. Deparis (2013). Fast mapping of magnetic basement depth, structure and nature using aeromagnetic and gravity data: combined methods and their application in the Paris Basin, *Geophysical Prospecting*, 61(4), 857-873, doi:10.1111/1365-2478.12024.
- Martín-Hernández, F., Lüneburg, C. M., Aubourg, C., Jackson, M. (2004). Magnetic fabric: methods and applications—an introduction. *Geological Society, London, Special Publications*, 238(1), 1-7.
- Maruyama, S., Send, T. (1986). Orogeny and relative plate motions: example of the Japanese Islands. *Tectonophysics*, 127(3-4), 305-329.
- Mathieu, L., De Vries, B. V. W., Holohan, E. P., Troll, V. R. (2008). Dykes, cups, saucers and sills: Analogue experiments on magma intrusion into brittle rocks. *Earth and Planetary Science Letters*, 271(1), 1-13.
- Matzel, J. E., Bowring, S. A., Miller, R. B. (2006). Time scales of pluton construction at differing crustal levels: Examples from the Mount Stuart and Tenpeak intrusions, North Cascades, Washington. *Geological Society of America Bulletin*, 118(11-12), 1412-1430.
- Mattauer, M., Matte, P., Malavieille, J., Tapponnier, P., Maluski, H., Ku, Z., Lu, Y., and Tang, Y., (1985). Tectonics of the Qinling Belt: Build-up and evolution of eastern Asia: *Nature*, 317: 496–500.
- McNulty, B. A., O. T. Tobisch, A. R. Cruden, and S. Gilder (2000). Multistage emplacement of the Mount Givens pluton, central Sierra Nevada batholith, California, *Geological Society of America Bulletin*, 112(1), 119-135.
- Menand, T., Phillips, J. C., Sparks, R. S. J. (2008). Circulation of bubbly magma and gas segregation within tunnels of the potential Yucca Mountain repository. *Bulletin of Volcanology*, 70(8), 947-960.
- Menand, T., de Saint-Blanquat, M., Annen, C. (2011). Emplacement of magma pulses and growth of magma bodies Emplacement of magma pulses and growth of magma bodies. *Tectonophysics*, 500(1-4), 1-2.

- Meng, Q.-R., Wang, E. Hu, J.-M., (2005). Mesozoic sedimentary evolution of the northwest Sichuan basin: Implication for continued clockwise rotation of the South China block. *Geological Society of America Bulletin* 117, 396, doi:10.1130/b25407.1.
- Merle, O., and Vendeville, B. (1995). Experimental modelling of thin-skinned shortening around magmatic intrusions. *Bulletin of Volcanology*, 57(1), 33-43.
- Metcalf, I. (2006). Palaeozoic and Mesozoic tectonic evolution and palaeogeography of East Asian crustal fragments: the Korean Peninsula in context. *Gondwana Research*, 9(1), 24-46.
- Morgan, S. S., R. D. Law, and M. W. Nyman (1998), Laccolith-like emplacement model for the Papoose Flat pluton based on porphyroblast-matrix analysis, *Geological Society of America Bulletin*, 110(1), 96-110.
- Morgan, S., Jones, R., Conner, J., Student, J., Schaner, M., Horsman, E., de Saint Blanquat, M. (2017). Magma sheets defined with magnetic susceptibility in the Maiden Creek sill, Henry Mountains, Utah, USA. *Geology*, 45(7), 599-602.
- Mourtada-Bonnefoi, C. C., Laporte, D. (2004). Kinetics of bubble nucleation in a rhyolitic melt: an experimental study of the effect of ascent rate. *Earth and Planetary Science Letters*, 218(3), 521-537.
- Moyen, J. F., Martin, H., Jayananda, M., Auvray, B. (2003). Late Archaean granites: a typology based on the Dharwar Craton (India). *Precambrian Research*, 127(1), 103-123.
- Morgan, J. McGovern, P. J. (2005). Discrete element simulations of gravitational volcanic deformation: 1. Deformation structures and geometries. *Journal of Geophysical Research: Solid Earth*, 110(B5).
- Morgan, S., Law, R., de Saint Blanquat, M., (2013). Forceful emplacement of the Eureka Valley–Joshua Flat–Beer Creek composite pluton into a structural basin in eastern California; internal structure and wall rock deformation. *Tectonophysics* 608, 753-773.
- Náđđec, A., Bouchez, J. and Bowden, P. (2015). *Granites*. Oxford University Press. New York.
- Ni, N., N. Chen, J. Chen, and M. Liu (2016). Integrating WorldView-2 imagery and terrestrial LiDAR point clouds to extract dyke swarm geometry: Implications for magma emplacement mechanisms, *Journal of Volcanology and Geothermal Research*, 310, 1-11.
- Ntieche, B., Mohan, M. R., Amidou, M. (2017). Granitoids of the Magba shear zone, West Cameroon, Central Africa: Evidences for emplacement under transpressive tectonic regime. *Journal of the Geological Society of India*, 89(1), 33-46.
- O'Driscoll, B., Troll, V. R., Reavy, R. J., Turner, P. (2006). The Great Eucrite intrusion of Ardnamurchan, Scotland: Reevaluating the ring-dike concept. *Geology*, 34(3), 189-192.
- Passchier, C. W., and R. A. Trouw (1998). Deformation Mechanisms, in *Microtectonics*, edited, pp.

-
- 25-56, Springer.
- Paterson S R, Vernon R H, Tobisch O T., (1989). A review of criteria for the identification of magmatic and tectonic foliations in granitoids[J]. *Journal of structural geology*, 11(3): 349-363.
- Paterson, S. R., Tobisch, O. T. (1992). Rates of processes in magmatic arcs: implications for the timing and nature of pluton emplacement and wall rock deformation. *Journal of Structural Geology*, 14(3), 291-300.
- Paterson, S.R., Vernon, R.H., (1995). Bursting the bubble of ballooning plutons: A return to nested diapirs emplaced by multiple processes. *Geological Society of America Bulletin* 107, 1356-1380.
- Paterson, S. R., Pignotta, G. S., Farris, D., Memeti, V., Miller, R. B., Vernon, R. H., Žák, J. (2008). Is stopping a volumetrically significant pluton emplacement process?: Discussion. *Geological Society of America Bulletin*, 120(7-8), 1075-1079.
- Paterson, S. R. (2009). Magmatic tubes, pipes, troughs, diapirs, and plumes: Late-stage convective instabilities resulting in compositional diversity and permeable networks in crystal-rich magmas of the Tuolumne batholith, Sierra Nevada, California. *Geosphere*, 5(6), 496-527.
- Pearce, J. A., Peate, D. W. (1995). Tectonic implications of the composition of volcanic arc magmas. *Annual Review of Earth and Planetary Sciences*, 23(1), 251-285.
- Petford, N., Cruden, A.R., McCaffrey, K.J.W., Vigneresse, J.L., (2000). Granite magma formation, transport and emplacement in the Earth's crust. *Nature* 408, 669-673.
- Pitcher, W.S., (1979). The nature, ascent and emplacement of granitic magmas. *Journal of the Geological Society* 136, 627-662.
- Pitcher, W. S. (1983). Granite type and tectonic environment. *Mountain building processes*, 19, 40.
- Potro, R., M. D éz, J. Blundy, A. G. Camacho, and J. Gottsmann (2013). Diapiric ascent of silicic magma beneath the Bolivian Altiplano, *Geophysical Research Letters*, 40(10), 2044-2048.
- Qiu, Y.M., Gao, S., McNaughton, N.J., Groves, D.I., Ling, W.L., (2000). First evidence of > 3.2 Ga continental crust in the Yangtze craton of south China and its implications for Archean crustal evolution and Phanerozoic tectonics. *Geology* 28, 11–14.
- D RAFF, A. R. T. H. U. R., Mason, R. G. (1961). Magnetic survey off the west coast of North America, 40 N. latitude to 52 N. latitude. *Geological Society of America Bulletin*, 72(8), 1267-1270.
- Rabinowicz, M., Vigneresse, J. L. (2004). Melt segregation under compaction and shear channeling: Application to granitic magma segregation in a continental crust. *Journal of Geophysical Research: Solid Earth*, 109(B4).
- Ragan, D. M. (2009). *Structural geology: an introduction to geometrical techniques*. Cambridge

- University Press.
- Ren, J.S., Chen, T., (1989). Tectonic evolution of the continental lithosphere in eastern China and adjacent areas. *Journal of Southeast Asian Earth Sciences*, 3: 17-27.
- Ren J.S., Wang Z.X., Chen B.W., Jiang C.F., Niu B.G., Li J., Xie G.G., He Z.J., Liu Z.G. (1999). *The Tectonics of China from a Global View Geological Publishing House, Beijing* 32 pp.
- Ren, J., Tamaki, K., Li, S., Junxia, Z. (2002). Late Mesozoic and Cenozoic rifting and its dynamic setting in Eastern China and adjacent areas. *Tectonophysics*, 344(3), 175-205.
- Richards, M. A., Duncan, R. A., Courtillot, V. E. (1989). Flood basalts and hot-spot tracks: plume heads and tails. *Science*, 246 (4926), 103-107.
- Roberts, J. L. (1970). The intrusion of magma into brittle rocks. *Mechanism of igneous intrusion*, 2, 287-338.
- Rochette, P., Jackson, M., Aubourg, C., (1992). Rock magnetism and the interpretation of anisotropy of magnetic susceptibility. *Reviews of Geophysics* 30, 209-226.
- Roger F., Jolivet M., Malavielle J., (2008). Tectonic evolution of the Triassic fold belts of Tibet. *Comptes Rendus Geoscience* 340, 180–189.
- Roger F., Jolivet M., Malavielle J. (2010). The tectonic evolution of the Songpan-Garzê (North Tibet) and adjacent areas from Proterozoic to Present: A synthesis. *Journal of Asian Earth Sciences*, 39(4) : 254-269.
- Roig, J. Y., Faure, M., Truffert, C. (1998). Folding and granite emplacement inferred from structural, strain, TEM and gravimetric analyses: the case study of the Tulle antiform, SW French Massif Central. *Journal of Structural Geology*, 20(9), 1169-1189.
- Roman, A., Jaupart, C. (2016). The fate of mafic and ultramafic intrusions in the continental crust. *Earth and Planetary Science Letters*, 453, 131-140.
- Romer, R. L., Förster, H. J., Breitzkreuz, C. (2001). Intracontinental extensional magmatism with a subduction fingerprint: the late Carboniferous Halle Volcanic Complex (Germany). *Contributions to Mineralogy and Petrology*, 141(2), 201-221.
- Rosenberg, C. L. (2004). Shear zones and magma ascent: a model based on a review of the Tertiary magmatism in the Alps. *Tectonics*, 23(3).
- Rubin, A. M. (1993). On the thermal viability of dikes leaving magma chambers. *Geophysical Research Letters*, 20(4), 257-260.
- Runcorn, S. T. (1973). Implications of continental drift to the earth sciences (No. 550.3 TAR).
- Rutherford, M. J. (2008). Magma ascent rates. *Reviews in Mineralogy and Geochemistry*, 69(1), 241-271.
- Sawyer, E. W., Cesare, B., Brown, M. (2011). When the continental crust melts. *Elements*, 7(4),

-
- 229-234.
- Scaillet, B., Holtz, F., Pichavant, M., and Schmidt, M. (1996). Viscosity of Himalayan leucogranites: Implications for mechanisms of granitic magma ascent. *Journal of Geophysical Research: Solid Earth*, 101(B12), 27691-27699.
- Scaillet, B., Pêcher, A., Rochette, P., and Champenois, M. (1995). The Gangotri granite (Garhwal Himalaya): laccolithic emplacement in an extending collisional belt. *Journal of Geophysical Research: Solid Earth*, 100(B1), 585-607.
- Scaillet, B., and Searle, M. P. (2006). Mechanisms and timescales of felsic magma segregation, ascent and emplacement in the Himalaya. Geological Society, London, Special Publications, 268(1), 293-308.
- Schulling, R., (1962). On petrology, age and structure of the Menderes migmatite complex (SW-Turkey). *Bulletin of the Mineral Research and Exploration Institute of Turkey* 58, 71-84.
- Schofield, N. J., D. J. Brown, C. Magee, and C. T. Stevenson (2012). Sill morphology and comparison of brittle and non-brittle emplacement mechanisms, *Journal of the Geological Society*, 169(2), 127-141.
- Shu, L., X. Zhou, P. Deng, B. Wang, S.-Y. Jiang, J. Yu, and X. Zhao (2009). Mesozoic tectonic evolution of the Southeast China Block: new insights from basin analysis, *Journal of Asian Earth Sciences*, 34(3). 376-391
- Shu, L.-S., M. Faure, J.-H. Yu, and B.-M. Jahn (2011a). Geochronological and geochemical features of the Cathaysia block (South China): New evidence for the Neoproterozoic breakup of Rodinia, *Precambrian Research*, 187(3-4). 263-276, doi:<http://dx.doi.org/10.1016/j.precamres.2011.03.003>.
- Shu, X.J., Wang, X.L., Sun, T., Xu, X., Dai, M.N., (2011a). Trace elements, U–Pb ages and Hf isotopes of zircons from Mesozoic granites in the western Nanling Range, South China: Implications for petrogenesis and W–Sn mineralization. *Lithos* 127, 468-482.
- Shu, L.S (2012). An analysis of principal features of tectonic evolution in South China Block. *Geological Bulletin of China*, 31 (7): 1035-1053.
- Shu L.S., Wang B., Cawood P.A., Santosh M., Xu Z.Q. (2015). Early Paleozoic and Early Mesozoic intraplate tectonic and magmatic events in the Cathaysia Block, south China. *Tectonics*, 34 (2015), pp. 1600–1621.
- Skjerlie, K. P., PATIÑO DOUCE, A. E. (2002). The fluid-absent partial melting of a zoisite-bearing quartz eclogite from 1·0 to 3·2 GPa; Implications for melting in thickened continental crust and for subduction-zone processes. *Journal of Petrology*, 43(2), 291-314.
- Sparks, R. S. J., Marshall, L. A. (1986). Thermal and mechanical constraints on mixing between

-
- mafic and silicic magmas. *Journal of Volcanology and Geothermal Research*, 29(1-4), 99-124.
- Stevenson, C. T., Owens, W. H., Hutton, D. H., Hood, D. N., Meighan, I. G. (2007). Laccolithic, as opposed to cauldron subsidence, emplacement of the Eastern Mourne pluton, N. Ireland: evidence from anisotropy of magnetic susceptibility. *Journal of the Geological Society*, 164(1), 99-110.
- Stevenson, C., (2009). The relationship between forceful and passive emplacement: The interplay between tectonic strain and magma supply in the Rosses Granitic Complex, NW Ireland. *Journal of Structural Geology* 31, 270-287.
- Suk, D., Halgedahl, S. L. (1996). Hysteresis properties of magnetic spherules and whole rock specimens from some Paleozoic platform carbonate rocks. *Journal of Geophysical Research: Solid Earth*, 101(B11), 25053-25075.
- Sylvester, A. G., Ortel, G., Nelson, C. A., Christie, J. M. (1978). Papoose Flat pluton: A granitic blister in the Inyo Mountains, California. *Geological Society of America Bulletin*, 89(8), 1205-1219.
- Talbot, J. Y., Chen, Y., Faure, M. (2005). A magnetic fabric study of the Aigoual–Saint Guiral–Liron granite pluton (French Massif Central) and relationships with its associated dikes. *Journal of Geophysical Research: Solid Earth*, 110(B12).
- Tao, J., Li, W., Li, X., Cen, T. (2013). Petrogenesis of early Yanshanian highly evolved granites in the Longyuanba area, southern Jiangxi Province: Evidence from zircon U-Pb dating, Hf-O isotope and whole-rock geochemistry. *Science China Earth Sciences*, 56(6), 922-939.
- Talbot, J. Y., Martelet, G., Courrioux, G., Chen, Y., Faure, M. (2004). Emplacement in an extensional setting of the Mont Lozère–Borne granitic complex (SE France) inferred from comprehensive AMS, structural and gravity studies. *Journal of Structural Geology*, 26(1), 11-28.
- Tarling, D., and F. Hrouda (1993). *Magnetic anisotropy of rocks*, Springer Science & Business Media.
- Tatsumi, Y., Hamilton, D. L., Nesbitt, R. W. (1986). Chemical characteristics of fluid phase released from a subducted lithosphere and origin of arc magmas: evidence from high-pressure experiments and natural rocks. *Journal of Volcanology and Geothermal Research*, 29(1-4), 293-309.
- Taylor, S. R., McLennan, S. M. (1995). The geochemical evolution of the continental crust. *Reviews of Geophysics*, 33(2), 241-265.
- Thompson, J. F. H., Sillitoe, R. H., Baker, T., Lang, J. R., Mortensen, J. K. (1999). Intrusion-related gold deposits associated with tungsten-tin provinces. *Mineralium Deposita*, 34(4), 323-334.

- Tikoff, B., de Saint Blanquat, M., Teyssier, C. (1999). Translation and the resolution of the pluton space problem. *Journal of Structural Geology*, 21(8), 1109-1117.
- Van der Pluijm, B. A., and Marshak, S. (2004), *Earth structure*. New York.
- Vanko, D. A., Bishop, F. C. (1982). Occurrence and origin of marialitic scapolite in the Humboldt Lopolith, NW Nevada. *Contributions to Mineralogy and Petrology*, 81(4), 277-289.
- Vigneresse, J. L. (1990), Use and misuse of geophysical data to determine the shape at depth of granitic intrusions. *Geol. J.*, 25: 249-260. doi:10.1002/gj.3350250308.
- Vigneresse, J.L., (1995). Control of granite emplacement by regional deformation. *Tectonophysics* 249 (3-4), 173-186.
- Wan, Y., D. Liu, M. Xu, J. Zhuang, B. Song, Y. Shi, and L. Du (2007). SHRIMP U–Pb zircon geochronology and geochemistry of metavolcanic and metasedimentary rocks in Northwestern Fujian, Cathaysia block, China: Tectonic implications and the need to redefine lithostratigraphic units, *Gondwana Research*, 12(1–2), 166-183, doi:http://dx.doi.org/10.1016/j.gr.2006.10.016.
- Wan, Y., Liu, D., Wilde, S. A., Cao, J., Chen, B., Dong, C., Du, L. (2010). Evolution of the Yunkai Terrane, South China: evidence from SHRIMP zircon U–Pb dating, geochemistry and Nd isotope. *Journal of Asian Earth Sciences*, 37(2), 140-153.
- Wang, B., Shu, L., Faure, M., Jahn, B. M., Lo, C. H., Charvet, J., Liu, H. (2014). Phanerozoic Multistage Tectonic Rejuvenation of the Continental Crust of the Cathaysia Block: Insights from Structural Investigations and Combined Zircon U-Pb and Mica $^{40}\text{Ar}/^{39}\text{Ar}$ Geochronology of the Granitoids in Southern Jiangxi Province. *The Journal of Geology*, 122(3), 309-328.
- Wang D., Zheng J.P., Ma Q., Griffin W.L., Zhao H., Wong J. (2013a). Early Paleozoic crustal anatexis in the intraplate Wuyi-Yunkai orogen, South China. *Lithos*, 175-176: 124-145.
- Wang, F. Y., Ling, M. X., Ding, X., Hu, Y. H., Zhou, J. B., Yang, X. Y., Sun, W. (2011). Mesozoic large magmatic events and mineralization in SE China: oblique subduction of the Pacific plate. *International Geology Review*, 53(5-6), 704-726.
- Wang, G. C., Jiang, Y. H., Liu, Z., Ni, C. Y., Qing, L., Zhang, Q., Zhu, S. Q. (2016). Multiple origins for the Middle Jurassic to Early Cretaceous high-K calc-alkaline I-type granites in northwestern Fujian province, SE China and tectonic implications. *Lithos*, 246, 197-211.
- Wang J., Li Z.X., (2003a). History of Neoproterozoic rift basins in South China: implications for Rodinia break-up. *Precambrian Research*, 122 (1-4): 141-158.
- Wang L., Long W.G., Zhou D., (2013b). Zircon LA-ICP-MS U-Pb age of Caledonian granites from Precambrian basement in Yunkai area and its geological implications[J]. *Geology in China*,

- 40(4): 1016-1029(in Chinese with English abstract).
- Wang, Q., Xu, J. F., Jian, P., Bao, Z. W., Zhao, Z. H., Li, C. F., Ma, J. L. (2005). Petrogenesis of adakitic porphyries in an extensional tectonic setting, Dexing, South China: implications for the genesis of porphyry copper mineralization. *Journal of Petrology*, 47(1), 119-144.
- Wang Q., Wyman D.A., Xu J.F., Zhao Z.H., Jian P., Xiong X.L., Bao Z.W., Li C.F., Bai Z.H., (2006). Petrogenesis of Cretaceous adakitic and shoshonitic igneous rocks in the Luzong area, Anhui Province (eastern China): Implications for geodynamics and Cu–Au mineralization. *Lithos*, 89 (3-4): 424-446.
- Wang, X. L., Zhou, J. C., Griffin, W. A., Wang, R. C., Qiu, J. S., O'reilly, S. Y., Zhang, G. L. (2007). Detrital zircon geochronology of Precambrian basement sequences in the Jiangnan orogen: dating the assembly of the Yangtze and Cathaysia Blocks. *Precambrian Research*, 159(1), 117-131.
- Wang, Y., W. Fan, M. Sun, X. Liang, Y. Zhang, and T. Peng (2007). Geochronological, geochemical and geothermal constraints on petrogenesis of the Indosinian peraluminous granites in the South China Block: A case study in the Hunan Province, *Lithos*, 96(3-4), 475-502, doi:10.1016/j.lithos.2006.11.010.
- Wang, Y., F. Zhang, W. Fan, G. Zhang, S. Chen, P. A. Cawood, and A. Zhang (2010). Tectonic setting of the South China Block in the early Paleozoic: Resolving intracontinental and ocean closure models from detrital zircon U - Pb geochronology, *Tectonics*, 29(6).
- Wang, Y., Wu, C., Zhang, A., Fan, W., Zhang, Y., Zhang, Y., Yin, C. (2012). Kwangsian and Indosinian reworking of the eastern South China Block: constraints on zircon U–Pb geochronology and metamorphism of amphibolites and granulites. *Lithos*, 150, 227-242.
- Wang, Y., Fan, W., Zhang, G., Zhang, Y. (2013c). Phanerozoic tectonics of the South China Block: key observations and controversies. *Gondwana Research*, 23(4), 1273-1305.
- Wegener, A. (1912). Die entstehung der kontinente. *Geologische Rundschau*, 3(4), 276-292.
- Wei, W., Chen, Y., Faure, M., Shi, Y.H., Martelet, G., Hou, Q.L., Lin, W., Le Breton, N., Wang, Q.C., (2014). A multidisciplinary study on the emplacement mechanism of the Qingyang–Jiuhua Massif in Southeast China and its tectonic bearings. Part I: Structural geology, AMS and paleomagnetism. *Journal of Asian Earth Sciences* 86, 76-93.
- Wei, W., Chen, Y., Faure, M., Martelet, G., Lin, W., Wang, Q., Yan, Q., Hou, Q., (2016). An early extensional event of the South China Block during the Late Mesozoic recorded by the emplacement of the Late Jurassic syntectonic Hengshan Composite Granitic Massif (Hunan, SE China). *Tectonophysics* 672–673, 50-67.
- Weinberg, R. F. (1999). Mesoscale pervasive felsic magma migration: alternatives to dyking. *Lithos*, 44(1-2), 127

- 46(3), 393-410.
- Wilson, B. M. (2007). *Igneous petrogenesis a global tectonic approach*. Springer Science & Business Media.
- Wolf, M. B., Wyllie, P. J. (1994). Dehydration-melting of amphibolite at 10 kbar: the effects of temperature and time. *Contributions to Mineralogy and Petrology*, 115(4), 369-383.
- Xiang, H., Zhang, L., Zhou, H., Zhong, Z., Zeng, W., Liu, R., Jin, S. (2008). U-Pb zircon geochronology and Hf isotope study of metamorphosed basic-ultrabasic rocks from metamorphic basement in southwestern Zhejiang: The response of the Cathaysia Block to Indosinian orogenic event. *Science in China Series D: Earth Sciences*, 51(6), 788-800.
- Xie Douke, Ma Rongsheng, Zhang Yushen. (1996) *The Crust Growth and Mantle Plume Tectonics of South China Continent*[M]. Beijing: Geological Press, 1996.
- Xie, L., R.-C. Wang, J. Chen, and J.-C. Zhu (2010). Mineralogical evidence for magmatic and hydrothermal processes in the Qitianling oxidized tin-bearing granite (Hunan, South China): EMP and (MC)-LA-ICPMS investigations of three types of titanite, *Chemical Geology*, 276(1-2), 53-68, doi:10.1016/j.chemgeo.2010.05.020.
- Xu J.F., Shinjo R., Defant M.J., Wang Q., Rapp R.P. (2002). Origin of Mesozoic adakitic intrusive rocks in the Ningzhen area of east China: Partial melting of delaminated lower continental crust? *Geology*, 30 (12): 1111-1114.
- Xu X.S., O'Reilly, S.Y., Griffin W.L., Deng P., Pearson, N.J., (2005). Relict Proterozoic basement in the Nanling Mountains (SE China) and its tectonothermal overprinting. *Tectonics* 24.
- Xu, X. B., Zhang, Y. Q., Shu, L. S., Jia, D. (2011). La-ICP-MS U-Pb and $^{40}\text{Ar}/^{39}\text{Ar}$ geochronology of the sheared metamorphic rocks in the Wuyishan: Constraints on the timing of Early Paleozoic and Early Mesozoic tectono-thermal events in SE China. *Tectonophysics*, 501(1), 71-86.
- Xu, Y. G., He, B., Chung, S. L., Menzies, M. A., Frey, F. A. (2004). Geologic, geochemical, and geophysical consequences of plume involvement in the Emeishan flood-basalt province. *Geology*, 32(10), 917-920.
- Xu Z Q, Zeng L S, Liu F L. (2006). Polyphase subduction and exhumation of the Sulu high-pressure-ultrahigh-pressure metamorphic terrane. *Geol Soc Am Spec Paper*, , 403: 93—113.
- Yan, D.P., Zhou, M.F., Song, H.L., Wang, X.W., Malpas, J., (2003). Origin and tectonic significance of a Mesozoic multi-layer over-thrust system within the Yangtze Block (South China). *Tectonophysics*, 361, 239-254.
- Yan, D.P., Zhou, M.F., Li, S.B., Wei, G.Q., (2011). Structural and geochronological constraints on

- the Mesozoic-Cenozoic tectonic evolution of the Longmenshan thrust belt, eastern Tibetan Plateau. *Tectonics*, vol. 30, TC6005.
- Yu, J., O'Reilly, Y.S., Wang, L., Griffin, W.L., Jiang, S., Wang, Y., Xu, X., (2007). Finding of ancient materials in Cathaysia and implication for the formation of Precambrian crust. *Chinese Science Bulletin* 52, 11–18.
- Yu, J.-H., Wang, L.-J., Griffin, W.L., O'Reilly, S.Y., Zhang, M., Li, C.-Z., Shu, L.-S., (2009). A Paleoproterozoic orogeny recorded in a long-lived cratonic remnant (Wuyishan terrane), eastern Cathaysia Block, China. *Precambrian Research* 174, 347–363.
- Yu, J. H., O'Reilly, S. Y., Wang, L., Griffin, W. L., Zhou, M. F., Zhang, M., Shu, L. (2010). Components and episodic growth of Precambrian crust in the Cathaysia Block, South China: evidence from U–Pb ages and Hf isotopes of zircons in Neoproterozoic sediments. *Precambrian Research*, 181(1), 97-114.
- Yu, J.H., O'Reilly, S.Y., Zhou, M.F., Griffin, W.L., Wang, L.J., (2012). U–Pb geochronology and Hf–Nd isotopic geochemistry of the Badu Complex, Southeastern China: Implications for the Precambrian crustal evolution and paleogeography of the Cathaysia Block. *Precambrian Research*, 222-223, 424-449.
- Žák, J., Paterson, S. R., Memeti, V. (2007). Four magmatic fabrics in the Tuolumne batholith, central Sierra Nevada, California (USA): implications for interpreting fabric patterns in plutons and evolution of magma chambers in the upper crust. *Geological Society of America Bulletin*, 119(1-2), 184-201.
- Zhang, G., A. Guo, Y. Wang, S. Li, Y. Dong, S. Liu, D. He, S. Cheng, R. Lu, and A. Yao (2013). Tectonics of South China continent and its implications, *Science China Earth Sciences*, 56(11), 1804-1828.
- Zhang, K. J., Cai, J. X. (2009). NE–SW-trending Hepu–Hetai dextral shear zone in southern China: penetration of the Yunkai Promontory of South China into Indochina. *Journal of Structural Geology*, 31(7), 737-748.
- Zhang, Q., (2013) A discussion on Mesozoic large-scale magmatism and felsic large igneous province in eastern China. *Acta Petrologica et Mineralogica*, 32(4): 557-564.
- Zhang, Y., Yang, J.H., Sun, J.F., Zhang, J.H., Chen, J.Y., Li, X.H., (2015). Petrogenesis of Jurassic fractionated I-type granites in Southeast China: Constraints from whole-rock geochemical and zircon U-Pb and Hf-O isotopes. *Journal of Asian Earth Sciences* 111, 268-283.
- Zhao, G., Cawood, P. A. (1999). Tectonothermal evolution of the Mayuan Assemblage in the Cathaysia Block; implications for Neoproterozoic collision-related assembly of the South China Craton. *American Journal of Science*, 299(4), 309-339.

- Zhao G.C. and Cawood P.A. (2012). Precambrian geology of China. *Precambrian Research*, 222-223: 13-54.
- Zhao, K.-D., S.-Y. Jiang, Y.-H. Jiang, and D.-Y. Liu (2006). SHRIMP U-Pb dating of the Furong unit of Qitianling granite from southeast Hunan province and their implications, *Acta Petrologica Sinica*, 22 (10), 2611-2616 (in Chinese with English abstract).
- Zhao, K.-D., S.-Y. Jiang, Y.-H. Jiang, and R.-C. Wang (2005). Mineral chemistry of the Qitianling granitoid and the Furong tin oredeposit in Hunan Province, South China, *European Journal of Mineralogy*, 17(4), 635.
- Zheng, Y.F, Zhang, S.B, Zhao, Z.F, Wu, Y.B, Li, X.H, Li, Z.X, Wu, F.Y. (2007). Contrasting zircon Hf and O isotopes in the two episodes of Neoproterozoic granitoids in South China: Implications for growth and reworking of continental crust. *Lithos*, 96: 127-150.
- Zheng, Y.-F., R.-X. Wu, Y.-B. Wu, S.-B. Zhang, H. Yuan, and F.-Y. Wu (2008). Rift melting of juvenile arc-derived crust: Geochemical evidence from Neoproterozoic volcanic and granitic rocks in the Jiangnan Orogen, South China, *Precambrian Research*, 163(3-4), 351-383, doi:<https://doi.org/10.1016/j.precamres.2008.01.004>.
- Zhou, X. M., Li, W. X. (2000). Origin of Late Mesozoic igneous rocks in Southeastern China: implications for lithosphere subduction and underplating of mafic magmas. *Tectonophysics*, 326(3), 269-287.
- Zhou, X.M., Sun, Tao., Shen, W.Z., Shu, L.S., Niu, Y.L., (2006). Petrogenesis of Mesozoic granitoids and volcanic rocks in South China: A response to tectonic evolution. *Episodes* 29, 26-33.
- Zhou XY, Yu JH, Wang YJ, Shen LW and Zhang CH. (2015). Composition and formation of the basement metamorphic rocks in Yunkai terrane, western Guangdong Province, South China. *Acta Petrologica Sinica*, 31(3): 855-882.
- Zhu, J., G. Huang, P. Zhang, F. Li, B. Rao (2003). On the emplacement age and material sources for the granites of Cailing superunit, Qitianling pluton, south Hunan Province, *Geological Review*, 49(3), 245-252 (in Chinese with English abstract).
- Zhu, J., H. Zhang, C.F. Xie, P.H. Zhang, C. Yang (2005). Zircon SHRIMP U-Pb geochronology, petrology and geochemistry of the Zhujianshui granite, Qitianling pluton, Southern Hunan Province, *Geological Journal of China Universities*, 11(3), 335-342 (in Chinese with English abstract).
- Zhu, J., R.-C. Wang, P.-H. Zhang, C.-F. Xie, W.-L. Zhang, K.-D. Zhao, L. Xie, C. Yang, X.-D. Che, A.-P. Yu, L.-B. Wang (2009). Zircon U-Pb geochronological framework of Qitianling granite batholith, middle part of Nanling Range, South China, *Science in China Series D: Earth*

- Sciences, 52(9), 1279-1294, doi:10.1007/s11430-009-0154-4.
- Zhu, K.Y., Li, Z.X., Xu, X.S., Wilde, S. A., (2013). Late Triassic melting of a thickened crust in southeastern China: Evidence for flat-slab subduction of the Paleo-Pacific plate. *Journal of Asian Earth Sciences*, 74, 265-279.
- Zhu, K.Y., Li, Z.X., Xu, X.S., Wilde, S.A., Chen, H.L., (2016). Early Mesozoic ferroan (A-type) and magnesian granitoids in eastern South China: Tracing the influence of flat-slab subduction at the western Pacific margin. *Lithos*, 240-243: 371-381.
- Zhu Rixiang, Yang Zhenyu, Wu Hanning, Ma Xinghua, Huang Baochun, Meng Zifang, Fang Dajun, (1998). Paleomagnetic constraints on the tectonic history of the major blocks of China during the Phanerozoic. *Science in China Series D: Earth Sciences*, 41, 1-19.

Supplementary materials

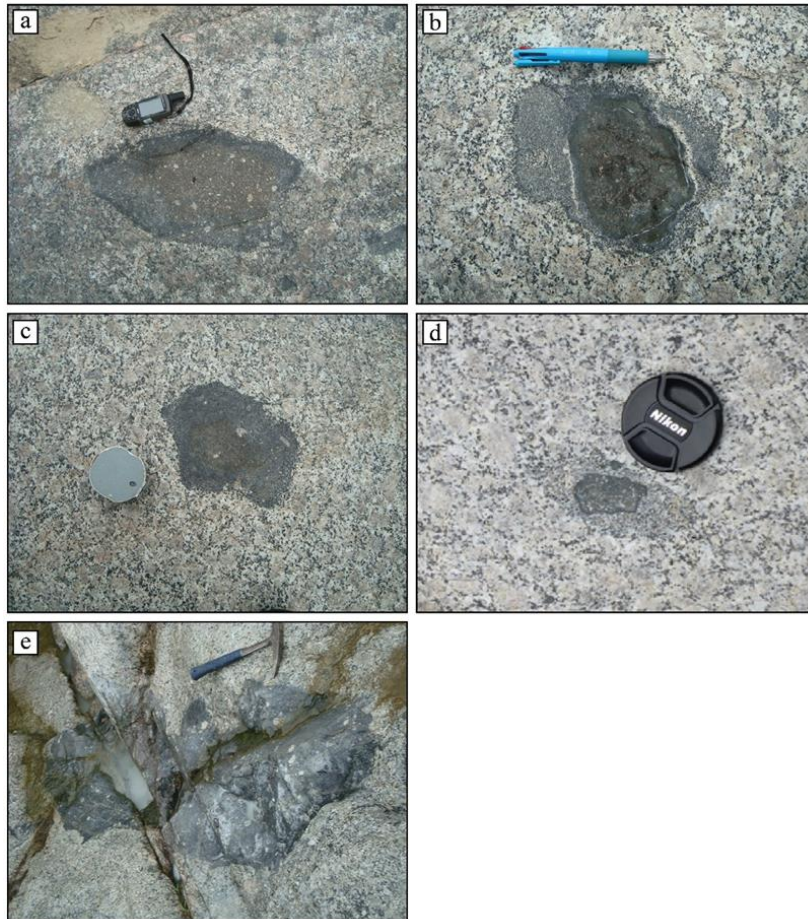


Figure S1. The mafic-granitoid enclaves in facies I granite of the Qitianling pluton.

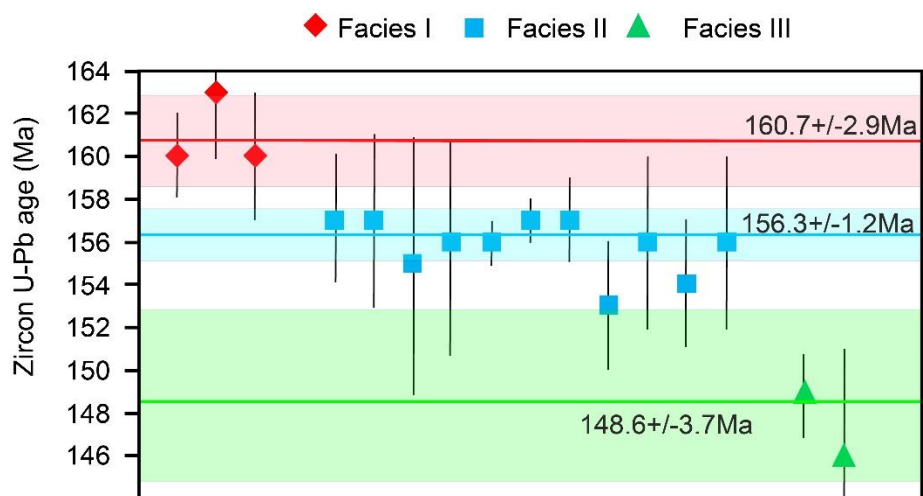


Figure S2. The SHRIMP zircon U-Pb age data of the Qitianling pluton, detailed data information are listed in Table S4.

Table S1. Sampling sites, measured density values, and site-mean AMS measurement results for the Qitianling pluton.

| Site | Geographic coordinates | | Alt. (m) | n | Litho. | Density (g/m ³) | Km (10 ⁻⁶ SI) | P _J | T | Site mean AMS results | | | |
|------|------------------------|----------|----------|----|--------|-----------------------------|--------------------------|----------------|-------|-----------------------|---------------------------|--------------------|---------------------------|
| | Lat.(°N) | Lon.(°E) | | | | | | | | K ₁ | α ₉₅ (max/min) | K ₃ | α ₉₅ (max/min) |
| | | | | | | | | | | Dec (°)/ Inc(°) | (°) | Dec (°)/ Inc(°) | (°) |
| 1 | 25.65 | 112.94 | 530 | 5 | BG* | 2.6 | 3630 | 1.06 | 0.24 | 233.2/20.7 | 25.1/0.2 | 110.9/54.7 | 7.3/2.3 |
| 2 | 25.55 | 112.98 | 397 | 8 | BG | 2.68 | 7230 | 1.05 | 0.34 | 329.5/6.1 | 35.5/5.9 | 226.4/64.7 | 14.1/2.7 |
| 3-1 | 25.55 | 112.99 | 342 | 7 | ME* | 2.83 | 24500 | 1.04 | 0.21 | 163.3/19.8 | 12.6/7.1 | 269.3/37.4 | 15.1/4.7 |
| 3-2 | 25.55 | 112.99 | 342 | 6 | BG | 2.83 | 6740 | 1.03 | 0.32 | 174.6/16.6 | 28.2/12.5 | 276.8/35.1 | 16.3/10.8 |
| 4 | 25.54 | 112.97 | 504 | 6 | PG* | 2.58 | 2610 | 1.08 | 0.71 | 108.4/48.0 | 31.0/8.0 | 303.0/41.1 | 9.3/7.7 |
| 5 | 25.54 | 112.96 | 578 | 8 | FM* | 2.61 | 2680 | 1.06 | 0.88 | 107.9/8.9 | 65.2/17.3 | 341.1/75.4 | 18.3/17.2 |
| 6 | 25.54 | 112.95 | 682 | 7 | BG | 2.58 | 4770 | 1.07 | 0.58 | 198.0/2.3 | 9.7/6.2 | 296.8/75.5 | 7.9/5.3 |
| 7 | 25.55 | 112.94 | 725 | 7 | BG | 2.62 | 272 | 1.02 | 0.82 | 274.7/42.1 | 74.4/16.9 | 89.6/47.8 | 49.1/17.5 |
| 8 | 25.54 | 112.92 | 766 | 7 | BG | 2.61 | 80.6 | 1.02 | 0.79 | 302.4/7.9 | 60.7/9.1 | 200.2/56.8 | 9.3/8.0 |
| 9 | 25.54 | 112.9 | 741 | 9 | BG | 2.56 | 141 | 1.02 | -0.35 | 53.7/10.1 | 28.5/12.6 | 201.5/78.1 | 38.2/14.4 |
| 10 | 25.58 | 112.78 | 403 | 5 | BG | 2.7 | 1190 | 1.1 | -0.2 | 136.4/47.5 | 16.9/7.3 | 316.1/42.5 | 47.7/14.8 |
| 11 | 25.58 | 112.79 | 440 | 5 | BG | 2.64 | 9040 | 1.05 | 0.7 | 245.3/18.5 | 29.4/8.4 | 113.7/63.3 | 24.9/15.4 |
| 12 | 25.57 | 112.79 | 470 | 8 | BG | 2.67 | 18700 | 1.04 | 0.51 | 283.7/15.8 | 37.5/6.6 | 125.4/73.1 | 13.7/7.2 |
| 13 | 25.57 | 112.8 | 508 | 6 | BG | 2.61 | 535 | 1.02 | 0.27 | 139.7/16.9 | 27.8/9.9 | 3.4/67.8 | 20.9/8.4 |
| 14 | 25.57 | 112.81 | 556 | 8 | BG | 2.63 | 1980 | 1.03 | 0.21 | 58.8/18.4 | 40.0/6.4 | 227.2/71.3 | 7.3/3.2 |
| 15 | 25.56 | 112.82 | 627 | 7 | BG | 2.6 | 133 | 1.01 | 0.21 | 354.6/8.0 | 35.4/6.7 | 97.6/58.2 | 41.9/5.6 |
| 16 | 25.56 | 112.83 | 802 | 6 | FM | 2.56 | 133 | 1.02 | 0.03 | 337.0/14.2 | 18.3/10.9 | 234.3/40.8 | 17.2/9.3 |
| 17 | 25.55 | 112.82 | 730 | 5 | PG | 2.57 | 109 | 1.01 | 0.01 | 43.7/25.7 | 12.7/5.6 | 212.8/63.9 | 34.3/8.8 |
| 18 | 25.54 | 112.83 | 962 | 7 | BG | 2.6 | 115 | 1.01 | 0.53 | 324.5/8.6 | 40.2/22.8 | 68.8/58.4 | 24.0/12.3 |
| 19 | 25.54 | 112.84 | 1092 | 5 | BG | 2.68 | 994 | 1.03 | 0.68 | 170.7/0.8 | 35.0/13.2 | 78.4/71.8 | 24.6/14.2 |
| 20 | 25.53 | 112.84 | 1186 | 10 | BG | 2.69 | 3100 | 1.03 | 0.13 | 334.2/14.0 | 71.1/11.8 | 157.7/75.9 | 23.0/8.7 |

| | | | | | | | | | | | | | |
|-------|-------|--------|------|---|------|------|------|------|-------|------------|-----------|------------|-----------|
| 21 | 25.51 | 112.81 | 993 | 7 | BG | 2.67 | 4610 | 1.04 | 0.19 | 290.8/17.3 | 39.8/9.6 | 149.5/68.2 | 11.0/5.1 |
| 22 | 25.52 | 112.79 | 862 | 5 | PG | 2.57 | 149 | 1.01 | -0.44 | 224.9/53.7 | 39.8/11.4 | 77.8/31.7 | 56.6/8.8 |
| 23* | 25.6 | 112.84 | 997 | 6 | BG | 2.62 | 237 | 1.01 | 0.05 | 80.4/21.7 | 30.0/9.8 | 184.7/31.7 | 31.3/11.5 |
| 24* | 25.6 | 112.84 | 968 | 8 | BG | 2.57 | 161 | 1.02 | 0.76 | 26.3/16.1 | 62.5/18.9 | 117.4/3.9 | 22.9/9.1 |
| 25 | 25.59 | 112.83 | 891 | 5 | PG | 2.65 | 2420 | 1.02 | -0.03 | 122.2/13.7 | 20.0/7.4 | 345.3/71.5 | 29.0/9.6 |
| 26 | 25.58 | 112.84 | 813 | 7 | BG | 2.69 | 7340 | 1.05 | 0.54 | 104.3/2.4 | 60.8/5.6 | 225.7/85.5 | 6.8/4.9 |
| 27* | 25.57 | 112.82 | 648 | 5 | BG | 2.63 | 272 | 1.01 | -0.43 | 166.1/11.2 | 6.9/4.6 | 75.4/3.6 | 32.1/3.1 |
| 28 | 25.56 | 112.82 | 601 | 5 | BG | 2.47 | 173 | 1.02 | -0.03 | 1.8/0.7 | 39.5/4.3 | 117.4/88.3 | 31.4/8.9 |
| 29 | 25.51 | 112.85 | 1356 | 6 | BG | 2.59 | 2390 | 1.06 | 0.39 | 247.2/1.7 | 41.6/9.5 | 151.9/72.3 | 10.6/7.0 |
| 30 | 25.5 | 112.86 | 1250 | 5 | BG | 2.65 | 1170 | 1.21 | 0.77 | 315.0/31.7 | 73.3/2.8 | 91/49.3 | 23.9/8.3 |
| 31 | 25.48 | 112.82 | 870 | 8 | BG | 2.66 | 9560 | 1.05 | 0.22 | 47.6/4.5 | 26.7/7.3 | 173.2/82.3 | 10.1/4.1 |
| 32 | 25.47 | 112.81 | 791 | 7 | BG | 2.67 | 1810 | 1.03 | 0.31 | 100.0/0.1 | 51.0/7.3 | 190.9/83.7 | 11.9/7.2 |
| 33 | 25.46 | 112.81 | 705 | 6 | BG | 2.66 | 1430 | 1.05 | 0.52 | 198.7/15.1 | 37.9/9.3 | 11.6/74.8 | 14.2/8.8 |
| 34 | 25.45 | 112.8 | 554 | 5 | BG | 2.67 | 1300 | 1.04 | 0.55 | 331.8/10.9 | 51.1/4.3 | 99.8/72.6 | 14.3/7.5 |
| 35 | 25.45 | 112.8 | 554 | 5 | FBG* | 2.66 | 606 | 1.04 | 0.49 | 77.5/4.5 | 20.5/13.2 | 251.7/85.5 | 14.0/2.7 |
| 36 | 25.45 | 112.8 | 554 | 7 | BG | 2.69 | 3070 | 1.05 | 0.11 | 173.8/15.0 | 30.0/8.5 | 15.0/74.0 | 12.8/3.4 |
| 37 | 25.47 | 112.85 | 988 | 7 | BG | 2.61 | 3130 | 1.03 | 0.08 | 34.1/20.6 | 12.1/10.4 | 132.2/20.5 | 28.7/9.7 |
| 38* | 25.46 | 112.86 | 997 | 6 | BG | 2.6 | 804 | 1.02 | -0.64 | 29.6/25.3 | 22.9/6.2 | 291.0/17.6 | 71.1/9.3 |
| 39 | 25.46 | 112.86 | 968 | 7 | BG | 2.63 | 753 | 1.08 | -0.14 | 271.9/18.0 | 26.6/15.4 | 133.9/66.5 | 26.0/8.6 |
| 40 | 25.44 | 112.85 | 891 | 5 | BG | 2.63 | 90.8 | 1.01 | 0.58 | 178.6/7.2 | 52.6/14.4 | 345.8/82.7 | 33.8/4.6 |
| 41 | 25.44 | 112.86 | 813 | 5 | BG | 2.55 | 79.9 | 1.01 | 0.58 | 317.6/5.0 | 55.4/10.6 | 195.7/80.5 | 22.9/14.0 |
| 42 | 25.5 | 112.92 | 797 | 6 | BG | 2.61 | 161 | 1.03 | 0.54 | 90.7/12.4 | 59.2/32.1 | 270.3/77.6 | 44.5/22.3 |
| 43* | 25.49 | 112.92 | 729 | 5 | BG | 2.54 | 168 | 1.03 | 0.67 | 99.1/69.7 | 23.9/5.6 | 249.4/17.8 | 10.4/6.6 |
| 44-1 | 25.48 | 112.92 | 645 | 5 | BG | 2.58 | 892 | 1.05 | 0.66 | 135.2/2.3 | 46.5/15.1 | 233.3/73.8 | 16.0/12.4 |
| 44-2* | 25.48 | 112.92 | 645 | 5 | PG | 2.58 | 190 | 1.01 | -0.08 | 355.0/9.4 | 24.3/8.5 | 264.2/4.9 | 36.6/7.6 |
| 45 | 25.47 | 112.93 | 562 | 7 | BG | 2.62 | 1900 | 1.07 | 0.05 | 18.4/30.9 | 52.7/13.2 | 145.7/45.3 | 18.3/14.6 |
| 46* | 25.46 | 112.94 | 544 | 5 | PG | 2.61 | 151 | 1.01 | 0.33 | 213.1/12.8 | 66.3/14.7 | 116.8/25.9 | 21.9/12.6 |

| | | | | | | | | | | | | | |
|-----|-------|--------|------|---|----|------|------|------|-------|------------|-----------|------------|-----------|
| 47 | 25.45 | 112.94 | 516 | 8 | BG | 2.64 | 2180 | 1.07 | -0.13 | 311.2/1.1 | 23.9/9.8 | 218.1/69.8 | 22.6/10.8 |
| 48 | 25.45 | 112.94 | 434 | 6 | BG | 2.61 | 153 | 1.06 | 0.62 | 86.0/7.9 | 28.1/11.8 | 323.7/75.5 | 12.9/8.4 |
| 49 | 25.45 | 112.94 | 434 | 6 | BG | 2.57 | 151 | 1.05 | 0.55 | 129.9/5.9 | 26.7/2.5 | 311.6/84.1 | 14.8/2.0 |
| 50 | 25.5 | 112.93 | 971 | 7 | BG | 2.61 | 56.8 | 1.03 | 0.64 | 31.1/19.2 | 34.5/16.0 | 163.7/62.8 | 34.4/10.1 |
| 51 | 25.5 | 112.91 | 906 | 5 | BG | 2.59 | 177 | 1.02 | 0.13 | 0/26.3 | 50.6/32.5 | 172.3/63.5 | 36.1/3.8 |
| 52* | 25.5 | 112.9 | 959 | 5 | BG | 2.59 | 124 | 1.03 | 0.08 | 258.4/59.4 | 26.4/7.1 | 143.0/14.2 | 20.9/6.9 |
| 53* | 25.51 | 112.89 | 1124 | 6 | BG | 2.48 | 105 | 1.02 | 0.66 | 160.9/11.3 | 12.3/5.8 | 254.3/16.5 | 7.9/2.9 |

Note:

- (1) Site: sampling site, Lat.: Latitude, Lon.: Longitude, Alt.: Altitude, n: number of specimen at sampling site;
- (2) Litho.: Lithology, BG: biotite granite, ME: mafic enclave, PG: porphyritic granite, FM: fine grained monzogranite, FBG: fine grained biotite granite;
- (3) Km: bulk magnetic susceptibility PJ: degree of susceptibility anisotropy, T: shape parameter of the AMS ellipsoid, K1: Magnetic lineation, K3: The pole of the magnetic foliation, Inc.: Inclination, Dec.: Declination, α_{95} (max/min): the long and short axes of the confidence ellipsoid at 95% level.
- (4) *sampling site close to fault. The dark-grey, light grey and unfilled lines representing the data of facies I, facies II and facies III, respectively.
- (5) Formulae to calculate the AMS parameters: $Km = (K1+K2+K3)/3$, $PJ = \exp \{ \sqrt{2((n1-n)^2+(n2-n)^2+(n3-n)^2)} \}$, $T = (2n2-n1-n3)/(n1-n3)$, the n1, n2 and n3 is the natural logarithm normed K1, K2 and K3 susceptibilities, respectively.

Table S2. Density of the granite of the Qitianling pluton.

| Sample No. | Density (g/cm³) | Sample No. | Density (g/cm³) | Sample No. | Density (g/cm³) |
|-------------------|-----------------------------------|-------------------|-----------------------------------|-------------------|-----------------------------------|
| 01-101A | 2.60 | 19-222 | 2.68 | 37-339 | 2.61 |
| 02-105 | 2.68 | 20-228A | 2.69 | 38-348 | 2.60 |
| 03-122A | 2.83 | 21-236 | 2.67 | 39-354 | 2.63 |
| 04-127B | 2.58 | 22-240A | 2.57 | 40-355B | 2.63 |
| 05-132B | 2.61 | 23-247 | 2.62 | 41-361 | 2.55 |
| 06-138A | 2.58 | 24-257 | 2.57 | 42-369B | 2.61 |
| 07-144A | 2.62 | 25-259 | 2.65 | 43-377A | 2.54 |
| 08-151A | 2.61 | 26-266A | 2.69 | 44-383B | 2.58 |
| 09-162 | 2.56 | 27-273A | 2.63 | 45-390B | 2.62 |
| 10-167 | 2.70 | 28-280 | 2.47 | 46-395A | 2.61 |
| 11-175 | 2.64 | 29-286 | 2.59 | 47-403B | 2.64 |
| 12-180 | 2.67 | 30-291 | 2.65 | 48-404 | 2.61 |
| 13-184A | 2.61 | 31-299 | 2.66 | 49-580 | 2.57 |
| 14-193 | 2.63 | 32-305A | 2.67 | 50-584A | 2.61 |
| 15-200A | 2.60 | 33-311 | 2.66 | 51-595 | 2.59 |
| 16-207A | 2.56 | 34-319A | 2.67 | 52-601 | 2.59 |
| 17-209 | 2.57 | 35-324 | 2.66 | 53-609A | 2.48 |
| 18-218A | 2.60 | 36-336B | 2.69 | Average | 2.62 |

Table S3. Density and thickness of country rocks of the Qitianling pluton area.

| Age | Lithology | Density (g/cm³) | Thickness | |
|-----------------|---------------------------------|-----------------------------------|------------------|----------------|
| | | | Min. (m) | Max.(m) |
| Cretaceous | Sandstone, conglomerate | 2.53 | 227 | 2983 |
| Jurassic | Sandstone, conglomerate | 2.55 | 701 | 1200 |
| Triassic | Muddy limestone | 2.68 | 85 | 400 |
| Permian | Sandstone, siltstone, limestone | 2.63 | 260 | 1900 |
| Carboniferous | Limestone, muddy sandstone | 2.81-2.73 | 500 | 2000 |
| Devonian | Sandstone, limestone, dolomite | 2.68 | 600 | 2000 |
| Silurian | Sandstone | 2.64 | 730 | 4000 |
| Ordovician | Black chert, slate | 2.68 | 300 | 3400 |
| Cambrian | Sandstone, slate | 2.7 | 580 | 4000 |
| Neoproterozoic | Chert, sandy slate | 2.71 | 3300 | 4800 |
| Mesoproterozoic | Genesis | 2.8 | | 25000 |

Table S4. SHRIMP zircon U-Pb age dating results.

| Number | Facies | Lithology | Age | Spots/ MSWD | Data source |
|--------|--------|-----------------------------------|-------------|----------------|------------------|
| D220-1 | I | Med-grain porphyr Hbl-Bt granite | 160 \pm 2 | 5 (2) | Fu et al., 2004 |
| QT-87 | I | Med-grain porphyr Bt granite | 160 \pm 3 | 12 (3.8) | Zhu et al., 2005 |
| QT-85 | I | Fine-grain Bt-granite | 163 \pm 3 | 9 (0.75) | Zhu et al., 2009 |
| YC-1 | II | Med-grain porphyr Hbl-Bt granite | 157 \pm 2 | 7 (1.3) | Li et al., 2005 |
| QT-72 | II | Med-grain porphyr (Hbl)Bt granite | 157 \pm 3 | 9 (0.68) | Zhu et al., 2009 |
| QT-94 | II | Med-fine-grain porphyr Bt granite | 157 \pm 4 | 6 (4.6) | Zhu et al., 2009 |
| FB13 | II | (Hbl) Bt-granite | 155 \pm 6 | 9 (1.13) | Zhu et al., 2009 |
| FB12 | II | (Hbl) Bt-granite | 156 \pm 5 | 12 (1.14) | Zhu et al., 2009 |
| FR-43 | II | (Hbl) Bt-granite | 156 \pm 1 | 10 (1.7) | Zhu et al., 2009 |
| FR-63 | II | (Hbl) Bt-granite | 157 \pm 1 | 11 (1.7) | Zhu et al., 2009 |
| QT-65 | II | Med-fine-grain Bt granite | 153 \pm 3 | 11 (0.7) | Zhu et al., 2009 |
| QT-55 | II | Med-grain porphyr Bt granite | 156 \pm 4 | 11 (2.1) | Zhu et al., 2009 |
| QT-34 | II | Fine-grain Bt-granite | 154 \pm 3 | 7 (1.17) | Zhu et al., 2009 |
| QT-96 | II | Fine-grain Bt-granite | 156 \pm 4 | 9 (6) | Zhu et al., 2009 |
| QT-66 | III | fine-grain porphyr Bt-granite | 149 \pm 2 | 7 (0.98) | Zhu et al., 2009 |
| D212 | III | granite porphyry | 146 \pm 5 | 11 (1.76) | Li et al., 2006 |

Note: Lines filled by light grey representing the age data which may reset by post-solidus thermal fluids. Detailed references information are listed in the main paper.